Summer 8-14-2015

Functional characterization of the roles of endocytic recycling regulator EHD1 using in vivo and in vitro analyses

Priyanka Arya
University of Nebraska Medical Center

Functional Characterization of the roles of Endocytic Recycling Regulator EHD1 using in vivo and in vitro analyses

by

Priyanka Arya

A DISSERTATION

Presented to the Faculty of
The University of Nebraska Graduate College
in Partial Fulfillment of the Requirements
for the Degree of Doctor of Philosophy

Genetics, Cell Biology & Anatomy
Graduate Program

Under the Supervision of Professor Hamid Band

University of Nebraska Medical Center
Omaha, Nebraska

August, 2015

Supervisory Committee:

Venkatesh Govindarajan, Ph.D.

Karen Gould, Ph.D.

Andrew Dudley, Ph.D.

David Li, Ph.D.

Acknowledgements

First and foremost, I would like to express my sincere appreciation and gratitude to my advisor Dr. Hamid Band for sharing his expertise, valuable guidance and encouragement over the last five years. His support, attention and invaluable feedback have been instrumental to the success of my work. I have a great deal of admiration for his ability to foster a culture of continuous learning and creativity within his laboratory. My research work experience was truly enriched by the depth of Dr. Band's research acumen and his leadership qualities. Dr. Band demonstrates genuine concern for the development of his students and enables growth by supporting their career interests. I have been a proud beneficiary of his support and direction in my ongoing pursuit for a career in clinical genetics.

I wish to extend my deepest gratitude to Dr. Venkatesh Govindarajan, Dr. Andrew Dudley, Dr. Karen Gould and Dr. David Li for serving on my supervisory committee. I am extremely fortunate to have been associated with this consortium of intellectuals who have helped me continually refine my research work by challenging the fact finding process and helping me stay on course with the core objectives of my research. The results of my research work would have been half as efficacious without the critical inputs and commitment from this committee. I would like to especially thank Dr. Venkatesh Govindarajan for introducing me to several key techniques used throughout this study. I have gained immensely from my interactions with him over the years and I truly appreciate his commitment despite his demanding schedule.

I would like to acknowledge Dr. Mark Rainey's contributions in laying down the genesis of my project. In the short time we worked together, he was able to train me on certain foundational aspects of mouse embryonic development. I would like to extend special thanks to Dr. Manju George for having shared a number of ideas and suggestions that stemmed from her experience as a post-doctorate in the laboratory.

Next, I would like to thank Dr. Amarnath Natarajan for teaching me key aspects of chemical biology. The studies described in chapter 4 would not have been possible without the help of Dr. Amarnath Natarajan, Dr. Nicholas Palermo, Dr. Babu Guda, Simarjeet Negi, Dr. Jamie Arnst and Dr. David Kelly. I would also like to offer my special thanks to Dr. Woo-

Yang Kim for being a great teacher and helping me with the neural stem cell project. Even though the project had to be discontinued due to certain technical challenges, the concepts and skills I developed during this work will remain valuable.

My acknowledgements would be incomplete without the mention of Dr. Bhavana Dave, Dr. Tanner Hagelstrom and Michelle Hess from the human genetics laboratory at the Munroe Meyer Institute. I am extremely privileged to be have been taught and mentored by them. I consider their career trajectory and experiences to be a great source of encouragement and their continued support and input integral to shaping my career in clinical genetics.In the same vein I would also like to thank Dr. Vimla Band and Dr. Shantaram Joshi for their wise counsel and support over the years. I would also like to take this opportunity to thank to my previous mentors Dr. Narayan Jayasuryan and Dr. ShriKrishna Isloor for introducing me to the world of research. The projects I carried out in their laboratories laid a strong foundation for me to pursue a graduate career. I am thankful to all the faculty members, staff and students of the Department of Genetics, Cell Biology and Anatomy who have continually demonstrated respect, diversity and inclusion towards each other no matter how challenging the situation was. I am proud to be a pedigree of this work culture characterized by collaboration and cohesiveness.

My time spent in the laboratory would have been half as exciting and memorable without the camaraderie I shared over years with some of the former and current members of the laboratory. I would like to thank each and every member of Dr. Band's laboratory that I have had the pleasure of working with. I would like to thank my dear friends Dr. Prasanta Dash, Dr. Bhopal Mohapatra, Alex Moffitt, Aditya Bele, Eric Tom and many others for being an unswerving support system and making my life so much more enjoyable in Omaha.

This journey would not have been possible without the support of my family. I would like to take this opportunity to extend my heartfelt appreciation to my parents- Manglesh and Kewal Krishan Arya and sisters- Alka and Anu Arya, for their constant encouragement throughout this pursuit and inspiring me to follow my dreams. My father especially, for believing in me and teaching me that through hard work and determination, anything is possible. Last but not the least, I would also like to thank my husband Ramya Pattnaik, for I would not be where I am without his unconditional love and support throughout the years.

Functional Characterization of the roles of Endocytic Recycling Regulator EHD1 using in vivo and in vitro analyses

Priyanka Arya, Ph.D.

University of Nebraska Medical Center, 2015

Supervisor: Hamid Band, M.D., Ph.D.

Endocytic recycling is a fundamental cellular process that allows the precise regulation of the membrane components and receptors at the cell surface. Recent studies have established that the C-terminal Eps15 homology domain-containing (EHD) proteins function as key regulators of this process. Four highly-conserved members of the EHD protein family in mammals, EHD1-EHD4, play shared as well as unique roles in endocytic trafficking. Studies presented here demonstrate a critical role of EHD1 in the normal ocular development in mice. *Ehd1* knockout mice generated in our laboratory displayed gross ocular phenotypes including the anophthalmia, microphthalmia, and congenital cataracts. Hematoxylin and eosin (H&E) staining revealed defects in the *Ehd1* mutant mice that included smaller lens, lack of lens, and persistence of the lens-stalk and hyaloid vasculature. By deleting *Ehd1* specifically in the lens (*Ehd1 CKO*), my studies provide evidence that EHD1 expression in the lens precursor cells within the surface ectoderm is necessary for the normal lens development. *Ehd1 CKO* mice recapitulated the major ocular phenotypes of the *Ehd1-null* mice, and exhibited reduced proliferation and increased cell death within the lens epithelium as well as a disorganized corneal endothelium. These data suggest the important roles of EHD1 in the overall process of eye development.

EHD proteins are characterized by the presence of a C-terminal Eps15 homology (EH) domain. EH-domains are known to mediate interactions with proteins containing sequences with core Asn-Pro-Phe (NPF), Asp-Pro-Phe (DPF) or Gly-Pro-Phe (GPF) tri-peptide motifs. Such interactions are thought to facilitate EHD protein functions, but only a small number of such partners has been identified. To identify novel EH domain-NPF mediated interaction partners, I carried out a proteome-wide bioinformatics analysis to categorize proteins that possess single or multiple putative EH domain-binding motifs and generated a 9-mer peptide library corresponding to motifs containing the N/D/G-P-F sequence together with 6 C-terminal residues found in known EHD protein interaction partners as well as a subset of the previously uncharacterized proteins identified by the bioinformatics analysis selected based on their potential roles in endocytic traffic and related cellular processes. I developed a quantitative high-throughput fluorescence polarization-based competition assay using the EH domain of EHD1 as a prototype and a fluorescent peptide corresponding to a known EHD1 binding motif on MICAL-L1 protein. Using this assay, and the unlabeled peptides in the library in a competition assay, I determined the interaction affinities of the putative peptide motifs for binding to the EH domain of EHD1. This approach helped identify a large number of new EHD interacting partners of which selected candidates were validated using a GST-EH domain pull-down assay. These studies helped markedly expand the potential EHD protein interactome, and implicate the newly identified candidates in multiple cellular functions of EHD1 and potentially other family members.

Table of Contents

List of figures

Chapter 1

Chapter 2

Chapter 3

Chapter 4

List of Tables

Chapter 2

Chapter 3

Chapter 4

Abbreviations

ADP	Adenosine-5’-diphosphate
AGFGs	Arf-GAP domain and FG repeat-containing protein family
ak	aphakia gene
ADP	Adenosine-5’-diphosphate
Arf	ADP-ribosylation factor
ATP	Adenosine-5’-triphosphate
ATPase	ATP hydrolysis enzyme
BMPs	Bone morphogenetic proteins
BSA	Bovine serum albumin
BrdU	5-bromo-2’-deoxyuridine
$Ca_v1.2$	L-type Ca-channel type 1.2
CC	Coiled-coil domain
CCP	Clathrin-coated pit
CCV	Clathrin-coated vesicles
cDNA	Complementary DNA
CDH23	Cadherin 23
CELSR	Cadherin epidermal growth factor laminin G seven-pass G-type receptors
CIMPR	Cation-independent mannose 6-phosphate receptor
Cre	Cre recombinase
C-terminal	At the carboxyl-terminus
DMEM	Dulbecco’s Modified Eagle Medium
DMSO	Dimethyl sulfoxide
DNA	Deoxyribonucleic acid
DnaJs	DNAJ homolog subfamily members
DPF	Aspartate-Proline-Phenylalanine
dyl	Dysgenetic lens mice
ECM	Extracellular matrix

EDTA	Ethylenediaminetetraacetic acid
EE	Early endosome
EEA1	Early endosomal antigen-1
EHBP1	EH domain binding protein 1
EH-domain	Eps15 homology domain
EHD	C-terminal Eps 15 homology domain containing protein
Ehd1 CKO	*Ehd1* conditional knockout mice
Ehd1-het	*Ehd1* heterozygous
Ehd1-null	*Ehd1* homozygous null
Ehd1-WT	*Ehd1* wildtype
EM	Electron microscopy
Eps15	Epidermal growth factor substrate 15
ER	Endoplasmic reticulum
ERC	Endocytic recycling compartment
FBS	Fetal bovine serum
GPF	Glycine-proline-phenylalanine
GTP	Guanosine triphosphate
GTPase	GTP hydrolysis enzyme
Fer1L5	Fer-1-like-5
FGFR	Fibroblast growth factor (FGF) receptor
Floxed (fl)	Flanked by loxP sites
5FU	5-fluoro-5’-deoxyuridine
FP	Fluorescence polarization
Fz	Frizzled receptors
GDP	Guanosine-5’-diphosphate
GFP	Green fluorescent protein
GLUT4	Glucose transporter 4
GST	Glutathione S-transferase
GTP	Guanosine-5’-transferase
h	hour
H&E	hematoxylin and eosin

het	heterozygous
HEK 293	Human embryonic kidney (HEK) 293 cells
HEPES	4-(2-hydroxyethyl)-1-piperazineethanesulfonic acid
HMG	high-mobility group
HRP	Horseradish peroxidase
Hs	*Homo sapiens*
Hsp70	70 kilodalton heat shock proteins
IF	Immunofluorescence
IGF-1R	Insulin-like growth factor receptor 1
IP	Immunoprecipitation
IPTG	Isopropyl β-D-1thiogalactopyranoside
K_d	Dissociation constant
kDa	KiloDalton
KEGG	Kyoto Encyclopedia of Genes and Genomes
K_i	Inhibition constant
LDL	Low-density lipoprotein
LE	Late endosome
Lrp	low-density lipoprotein-related protein
MICAL-L1	Molecule Interacting with CasL-like 1
MSR	Minimum Significant ratio
min	minute
N-terminal	At the amine-terminus
NCX	Na/Ca exchanger
NBF	Neutral-buffered formalin
NgCAM	L1/neuron-glia cell adhesion molecule
NIH	National Institute of Health
NPF motif	Asparagine-proline-phenyalanine motif
nm	nanometer
NMJ	Neuromuscular junction
NMR	Nuclear magnetic resonance
NPF	Asparagine-proline-phenylalanine

OCH	Outer hair cell library
OV	Optic vesicle
PLE	Presumptive lens ectoderm
PBS	Phosphate-buffered saline
PCR	Polymerase chain reaction
PM	Plasma membrane
Rab	Ras-like in rat brain
Rab11-FIP2	Rab11 family-interacting protein
RE	Recycling endosomes
Rme-1	Receptor-mediated endocytosis protein 1
RNA	Ribonucleic acid
RPE	Retinal pigmented epithelium
RTK	Receptor tyrosine kinases
KCa2.3	Small conductance Ca^{2+}-activated K^{+} Channel protein
SiRNA	Small interfering RNA
SDS-PAGE	Sodium dodecyl sulfate-polyacrylamide gel electrophoresis
SCAMPs	Secretory carrier-associated membrane proteins
sFGFR	secreted FGF receptor
SH3 domain	Src homology 3 domain
SNP	Single nucleotide polymorphism
SNX	Sorting nexins
$t_{1/2}$	Half-life
TBST	Tris-buffered saline with Tween-20
TfR	Transferrin receptor
TGN	Trans-Golgi network
TF	Total fluorescence
Tris	Tris (hydroxymethyl) aminomethane
TUNEL	Terminal deoxynucleotidyl transferase (TdT)-mediated deoxyuridine triphosphate nick end labeling
TX-100	Triton X-100
UniProtKB	UniProt knowledgebase

WB	Western blot
WHO	World Health Organization
WT	Wildtype
Y2H	Yeast two-hybrid system

Chapter 1: Introduction

1. The endocytic trafficking

1.1 Overview

The plasma membrane (PM) is the outermost surface of a cell that acts a protective barrier and provides a platform for a cell to communicate with other cells and its environment. The composition of this lipid bilayer is tightly regulated by the entry and exit of various molecules in order to generate appropriate responses within a cell. Endocytosis refers to the process of internalization of extracellular material, ligands, plasma membrane lipids and integral proteins into the cell (Mukherjee et al., 1997). Exocytosis on the other hand is a cellular process by which newly synthesized or internalized lipids and proteins are delivered back to the PM. All material entering the cell converges upon a common sorting station known as the sorting endosome or early endosome (EE) (Figure 1.1). The receptors and other protein components are either recycled back to the PM, routed towards the lysosomes for degradation or targeted to the trans-Golgi network (TGN). Receptors can undergo recycling to the PM via the fast recycling pathway or through the slow recycling pathway (Figure 1.1). While most components of the internalized cargoes including several receptors, proteins and lipids are recycled back to the PM, ligands and certain signaling receptors are delivered to the late endosomes (LE) and lysosomes for degradation (Figure 1.1) (G. J. Doherty and McMahon, 2009).

1.2 Routes of internalization into the cell

There are various routes of endocytic uptake into the cell, which can be broadly divided into clathrin-mediated endocytosis (CME) and clathrin-independent endocytosis (CIE). CIE is further divided into caveolin-mediated endocytosis and clathrin and caveolin-independent endocytosis (Mayor and Pagano, 2007)(Figure 1.2).

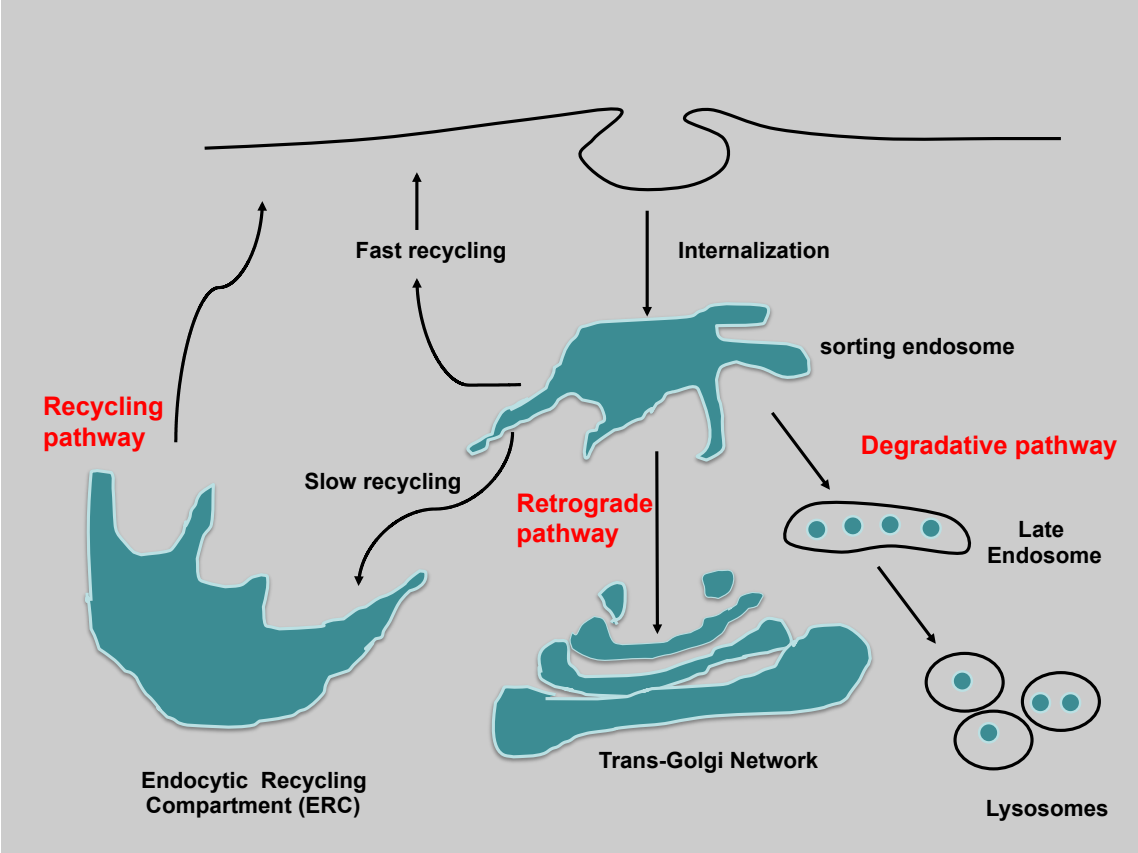

Figure 1.1 Endocytic trafficking pathways: Following internalization the cargo components merge at a common location known as the early endosomal (EE) compartment. Trafficking routes from the EE include recycling back to the plasma membrane via a fast recycling or through a slow recycling pathway that involves an endocytic recycling compartment (ERC), lysosomal degradation by delivery to the late endosome (LE), or retrograde transport to the trans-Golgi network (TGN).

endocytosis (CIE). CIE is further divided into caveolin-mediated endocytosis and clathrin and caveolin-independent endocytosis (Mayor and Pagano, 2007)(Figure 1.2).

CME is the best-characterized endocytic route for the entry of molecules into the cells. Clathrin is identified as being the major protein making the lattice-like coat around vesicles. During CME, cargo receptors are internalized into clathrin-coated pits (CCPs) followed by invagination and pinching off from the PM to generate clathrin-coated vesicles (CCVs). A wide variety of adapters (such as adapter protein 2 (AP2)) and accessory proteins present in the cells bind to conserved sequences on the cytosolic tails of cargo receptors, recruit clathrin to the PM and promote clathrin polymerization into curved lattices that drive membrane deformation. The final step of CCV formation is mediated by the recruitment of GTPase protein dynamin, which results in membrane scission (Mukherjee et al., 1997). After membrane scission, the clathrin coat is disassembled. Transferrin receptor (TfR) is a classic example of a receptor internalized through CME.

Apart from CME, cargo proteins undergo endocytosis by CIE. Caveolae-mediated endocytosis is an example of one such mechanism. Cargoes including SV40 virions, cholera toxin B subunit (CTxB) and glycosylphosphatidylionositol (GPI)-linked proteins are internalized in caveolin-positive structures (G. J. Doherty and McMahon, 2009; Parton et al., 1994). Caveolin binds to glycophospholipids and this leads to formation of flask-shaped invaginations called caveolae. In addition to these pathways, recent studies have described endocytic mechanisms independent of clathrin and caveolin, including RhoA, Flotillins, Arf6 or cdc42-dependent internalization mechanisms.

Recent studies have reported that the same ligand-receptor complex can be internalized by different mechanisms and generate profoundly different biological responses.

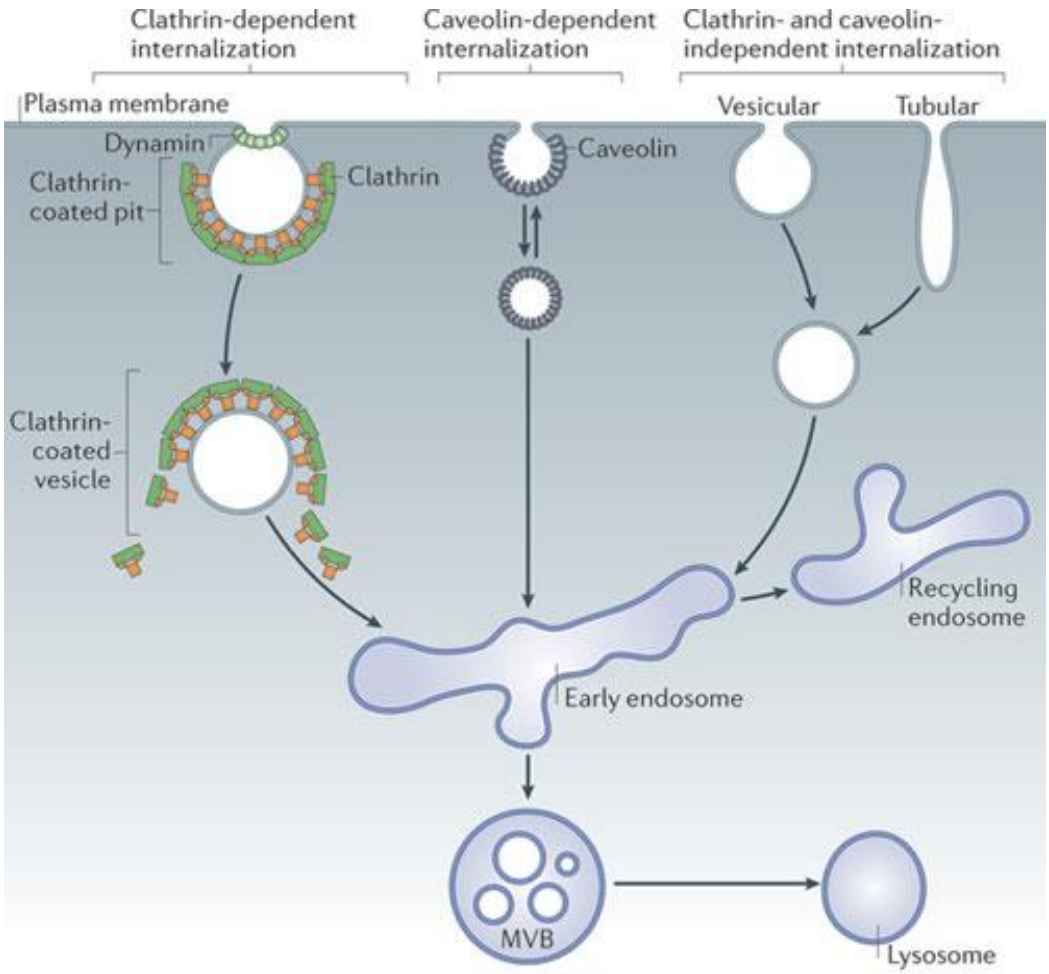

Figure 1.2 Routes of endocytosis: There are multiple pathways of endocytosis into cells; for example, clathrin-dependent, caveolin-dependent and clathrin- and caveolin-independent internalization. Internalized cargo is trafficked into endosomes, where it is sorted either back to the surface of the cell or into other compartments (multivesicular bodies (MVBs) and lysosomes for degradation. Image used with permission and modified from (McMahon and Boucrot, 2011).

For example, epidermal growth factor (EGF) receptor (EGFR), under low ligand concentration is internalized predominantly by CME and does not undergo degradation, but is rather recycled to the cell surface to maintain sustained signaling (Sigismund et al., 2008) Conversely, at higher EGF concentration, EGFRs internalized through clathrin-independent mechanisms are targeted to late endosomes/lysosomes for degradation.

1.2 Endocytic compartments

Regardless of the mode of internalization, most cargo proteins are first delivered to a common intracellular compartment known as sorting endosome or the early endosome (EE). Once inside an EE, the cargo is sorted to subdomains that are either thin tubular extensions or large vesicles. The primary function of this highly dynamic structure is to target molecules to their correct destinations. From the EE, the cargo is directed to three known destinations: the PM, the LE and the endocytic recycling complex (ERC). The intraluminal acidic pH (~6.3-6.8) within a sorting endosome causes conformational changes in proteins leading to ligand release from their receptors. The uncoupling of receptors from their associated ligands is the first step in the process of endocytic sorting (Maxfield and McGraw, 2004). As a result of sorting endosome maturation, soluble molecules including proteins and lipids, are delivered to the LE. While the maturing sorting endosome moves to the center of the cell, most recycled molecules are removed rapidly and effectively (Figure 1.3). For instance, the cargo that clusters in tubular membranes primarily undergoes recycling whereas the large vesicles are sorted to the degradation pathway. Since the surface-area-to volume ratio of tubules is greater than that of vesicles, receptors and other membrane proteins are concentrated in this region (Maxfield and McGraw, 2004). From the sorting endosomes, there are two main routes back to the cell surface. Recycling molecules are sorted into newly formed extensive tubular membranes. These tubular membranes facilitate receptor recycling to the PM through the ‘fast’ recycling pathway or through the ‘slow’ recycling

pathway (Daro et al., 1996). In the fast recycling pathway, the receptors are directly targeted to the cell surface from the EE. However, in the slow recycling pathway, the majority of recycling receptors are first trafficked to the endocytic recycling compartment (ERC) where they proceed by a 'slow –recycling' route to reach the PM. Recycling kinetics studies of canonical recycling receptors (e.g. TfR) have confirmed the existence of a faster route ($t_{1/2}$ = 5 min) and a slower route ($t_{1/2}$ = 15-30 min) for recycling (Daro et al., 1996).

In addition to its roles as a sorting endosome for the recycling and degradative pathways, the EEs also serve as a connecting point between the endocytic and biosynthetic routes. The EEs gradually matures to become the LE that matures to become lysosome by fusing to an existing lysosome. While the formation of endosomal tubular structures facilitate recycling, retromer-mediated tabulation is used for retrograde trafficking from EE to the *trans*-Golgi network (TGN)(Lu and Hong, 2014). Retromer is a hetero-pentameric complex consisting of two sub-complexes: the membrane associating SNX (sorting nexins) dimer and a cargo selection trimer consisting of vacuolar protein sorting (Vps) including Vps26, Vps29 and Vps35 (Bonifacino and Hurley, 2008). The cargo selection trimer directly binds to sorting motifs in the cytoplasmic domain of cargos. The SNX proteins comprise a PX domain that binds phosphoinositides, such as PI(3)P and PI(3,5)P_2. SNX proteins also contain curvature sensing Bin-Amphiphysin-Rvs (BAR) domain that facilitates the retromer-regulated formation of tubular membrane structures necessary for retrograde transport (Bonifacino and Hurley, 2008).

The ERC is a long-lived collection of tubular organelles that are associated with microtubules. The distribution of ERC is condensed around the microtubule organizing center (e.g in Chinese hamster ovarian (CHO) cells) but in other cells, ERC tubules are distributed throughout the cytoplasm. Transport from ERC requires the formation of transport intermediates that can be either vesicles or tubules. Glucose transporter 4 (GLUT4) is a recycling protein expressed in muscle and adipose tissues that catalyzes the

transport of glucose across the PM (Foley et al., 2011). Under resting state, the GLUT4 transporter has an intracellular distribution but is translocated to the PM in response to insulin. GLUT4 follows an endocytic itinerary that is very similar to that of TfR. A single molecule of GLUT4 transporter undergoes multiple rounds of recycling before being targeted for degradation. In the presence of insulin, most of the GLUT4 can be found in the compartments that also contain TfR. However, in the absence of insulin, GLUT4 is transported from the ERC to a compartment known as insulin-responsive compartment (IRC). Under low insulin concentration, GLUT4 is equally distributed between the ERC and IRC. Thus, the ERC/endosomes are not only involved in the sorting of GLUT4 to the insulin-regulated pathway, but are also a reservoir for insulin-recruited GLUT4 (Foley et al., 2011).

2. Regulators of endocytic trafficking

2.1 Ras superfamily of Rab GTPase proteins

In recent years, great strides have been made in identifying the molecular machinery that regulates membrane trafficking pathways. Endocytic transport is a highly regulated process consisting of a series of fission and fusion events. Molecular regulators of endocytic trafficking include an array of Rab proteins together with their effectors and other interaction partners. Rab proteins are small (21 – 25 kDa) monomeric GTPases that constitute the largest of the Ras superfamily. Rab GTPases are implicated in endocytic regulatory functions by mediating vesicle formation, intracellular transport, vesicle tethering/docking, and membrane fusion (Stenmark, 2012). The Rab-GTPase family consists of 11 members in yeast, 29 members in *C. elegans* and 70 different proteins in humans. Rab-proteins function as Guanosine triphosphate (GTP)-binding molecular switches that alternate between two conformational states: the GTP-bound ‘on’ form and guanosine diphosphate (GDP)-bound ‘off’ form. Rab proteins are localized to the membranes of distinct transport vesicles and to their specific target compartments (Grosshans et al., 2006). The functions of Rab GTPases

show the versatility of these molecular switches at various stages of endocytic trafficking. For example, Rab5 serves as a meditator of trafficking from the PM to the EE compartment, while Rab7 is associated with degradative compartment and serves as a marker for LE; Rab4, Rab11 and Rab35 mediate recycling events (Bottger et al., 1996; Bucci et al., 1992; Feng et al., 1995). Among the recycling regulators, Rab4 and Rab35 control the fast recycling route from the EEs and REs directly back to the PM, whereas Rab11 controls recycling through the ERC (Sonnichsen et al., 2000). Rab9 is involved in transport from EEs to the TGN (Figure 1.3). Under steady state, Rab proteins accumulate at their target compartment and thus have been used as markers for different organelles. Studies have shown that EEs and recycling endosomes (REs) comprise of multiple combinations of Rab4, Rab5 and Rab11 domains that are highly dynamic, but maintain their distinct Rab identity. The spatial segregation of Rab molecules to distinct membrane domains, in part, is mediated by Rab effector proteins (de Renzis et al., 2002). The accurate regulation of Rab recruitment and release from specific subdomains is critical for organelle biogenesis and transport of cargos along the endocytic pathways.

2.2 EH domain containing proteins and their functions

Among several other proteins involved in the overall process of endocytosis, Eps15 homology (EH) proteins play a key role to link different components of the endocytic machinery. The EH proteins are defined by the presence of one to three copies of the EH domain, an evolutionary conserved protein-protein interaction endocytic machinery. The EH proteins are defined by the presence of one to three copies of the EH domain, an evolutionary conserved protein-protein interaction module present from yeast to mammals (Miliaras and Wendland, 2004). The EH domain (70-100 amino acids long) derives its name from Eps15 (EGFR-phosphorylated substrate protein 15) protein, a motif present in three

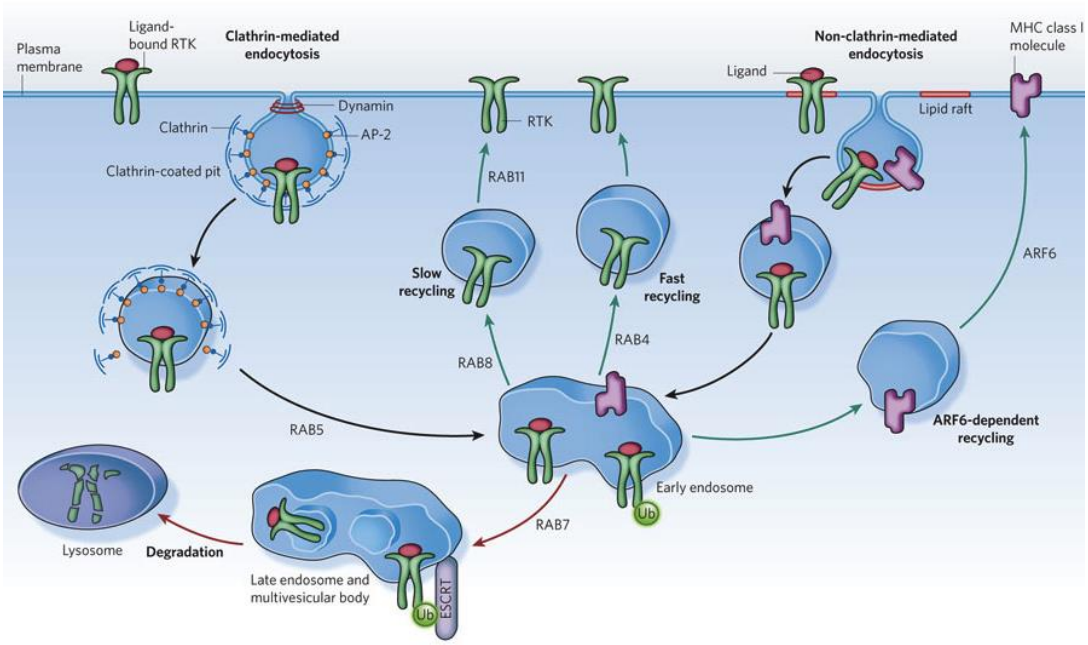

Figure 1.3 Endocytic trafficking of signalling receptors: Signalling receptors (for example receptor tyrosine kinases (RTKs)) are mainly internalized through clathrin-mediated endocytosis (left). In this pathway of endocytosis, ligand binding accelerates the recruitment of receptors to clathrin (present in clathrin-coated pits) through adaptors, such as AP-2. Clathrin then polymerizes, and this drives the invagination of the pit, which is eventually released into the cytoplasm through the action of the GTPase dynamin. There are many forms of non-clathrin-mediated endocytosis (right), which, in some cases, depends on plasma-membrane microdomains enriched in particular lipids (known as lipid rafts). After internalization, by either clathrin-mediated endocytosis or non-clathrin-mediated endocytosis, receptors are routed to early endosomes. Trafficking in the endosomal compartment is controlled by small GTP-binding proteins of the RAB and ARF (ADP-ribosylation factor) families. From the early endosome, cargo is either recycled to the plasma membrane (green arrows) or degraded (red arrows). Cargo can be recycled through a fast recycling route (which depends on RAB4) or a slow recycling route (which depends on the combined action of RAB8 and RAB11). In addition, proteins that have been internalized by non-clathrin-mediated endocytosis, such as major histocompatibility complex (MHC) class I molecules, can be recycled to the plasma membrane through ARF6-dependent pathways. Cargo can also be trafficked through a RAB7-dependent, degradative route, through late endosomes and multivesicular bodies, and then lysosomes. Image used with permission and modified from (Scita and Di Fiore, 2010).

copies at the N-termini of the endocytic proteins Eps15 and Eps15R (Eps15 Related)(Wong et al., 1995). Structurally, the EH domain is composed of two closely associated helix-loop-helix motifs, also called EF-hands, connected by a short antiparallel β-sheet. Most EH domains bind preferentially to the Asparagine-Proline-Phenylalanine (NPF) tri-peptide motifs found in other EH-binding proteins. The binding pocket for the NPF motif is formed by the Leu 155, Leu 165, and Trp 169 residues (in the second EH domain of Eps15), and the latter two residues are conserved in more than 95% of EH domains of other proteins. Mutations of Leu 165 and Trp 169 into Ala lead to complete loss of binding to NPF-containing proteins (Paoluzi et al., 1998). EH proteins are thought to function as scaffolding proteins that link the endocytic machinery to actin, ubiquitin and lipid phosphatases, and are also implicated in the regulation of protein transport/sorting and membrane trafficking.

Eps15 and Eps15R proteins exhibit a nearly identical domain organization consisting of three N-terminal EH domains, a central coiled-coil domain, and a C-terminal region rich in Aspartate-Proline-Phenylalanine (DPF) repeats. Studies have established a role of Eps15 and Eps15R in receptor-mediated endocytosis. Eps15/Eps15R regulate receptor (including TfR and EGFR) internalization through clathrin-coated pits. Eps15 (and Eps15R) binds to AP-2 adaptor protein, and other proteins involved in endocytosis and/or synaptic vesicle recycling such as Synaptojanin1 and Epsin (Benmerah et al., 1998). Eps15 has also been shown to co-localize with markers of the plasma membrane clathrin-coated pits and vesicles. Electron microscopy studies have provided evidence of Eps15 localization at the rim of the budding coated pits, suggesting a role for Eps15 in clathrin-mediated endocytosis (Confalonieri and Di Fiore, 2002).

In humans, 11 EH-containing proteins have been identified that have been categorized into five families: Eps15s (Eps15 and Eps15R), Intersectins (INTS1 and INTS2), RalBP1-associated Eps-homology domain proteins (Reps1 and Reps2), γ-synergin and Eps15 homology domain containing proteins (EHD1, EHD2, EHD3 and EHD4) (Figure 1.4). (Polo et al., 2003). Studies presented in this dissertation are focused towards the EHD family of endocytic proteins.

3. Structure and functions of EHD proteins

3.1 Domain architecture and structure of EHD proteins

The gene encoding the mammalian C-terminal EHD protein, EHD1, was first identified in the year 1999 using chromosome mapping studies (Haider et al., 1999; Mintz et al., 1999). Subsequently, EHD2, EHD3, and EHD4, three other paralogs of the EHD protein family, were identified and their expression analysis in various human tissues was characterized (Pohl et al., 2000). Shortly after, in 2001, two reports suggested a role of EHD1 and its *Ceanorhabditis elegans* (*C. elegans*) ortholog, Receptor-Mediated Endocytosis (RME-1), in mediating recycling of receptors from the ERC to the PM, thus implicating a role for this family in membrane trafficking (B. Grant et al., 2001; Lin et al., 2001).

In mammalian cells, EHD protein family includes four highly homologous paralogs consisting of: EHD1, EHD2, EHD3 and EHD4. In contrast, invertebrates including *C. elegans* and *Drosophila melanogaster* possess a single EHD family ortholog. EHD proteins are highly conserved through evolution and display a high level of amino acid sequence identity with one another (approximately 70-80% with the mammalian paralogs). *C.elegans* RME-1, shares 67% identity with EHD1 over its entire length. Within the EHD family, EHD1 and EHD3 are the most closely related with 86.5% identity in their overall amino acid sequence (Naslavsky and Caplan, 2011).

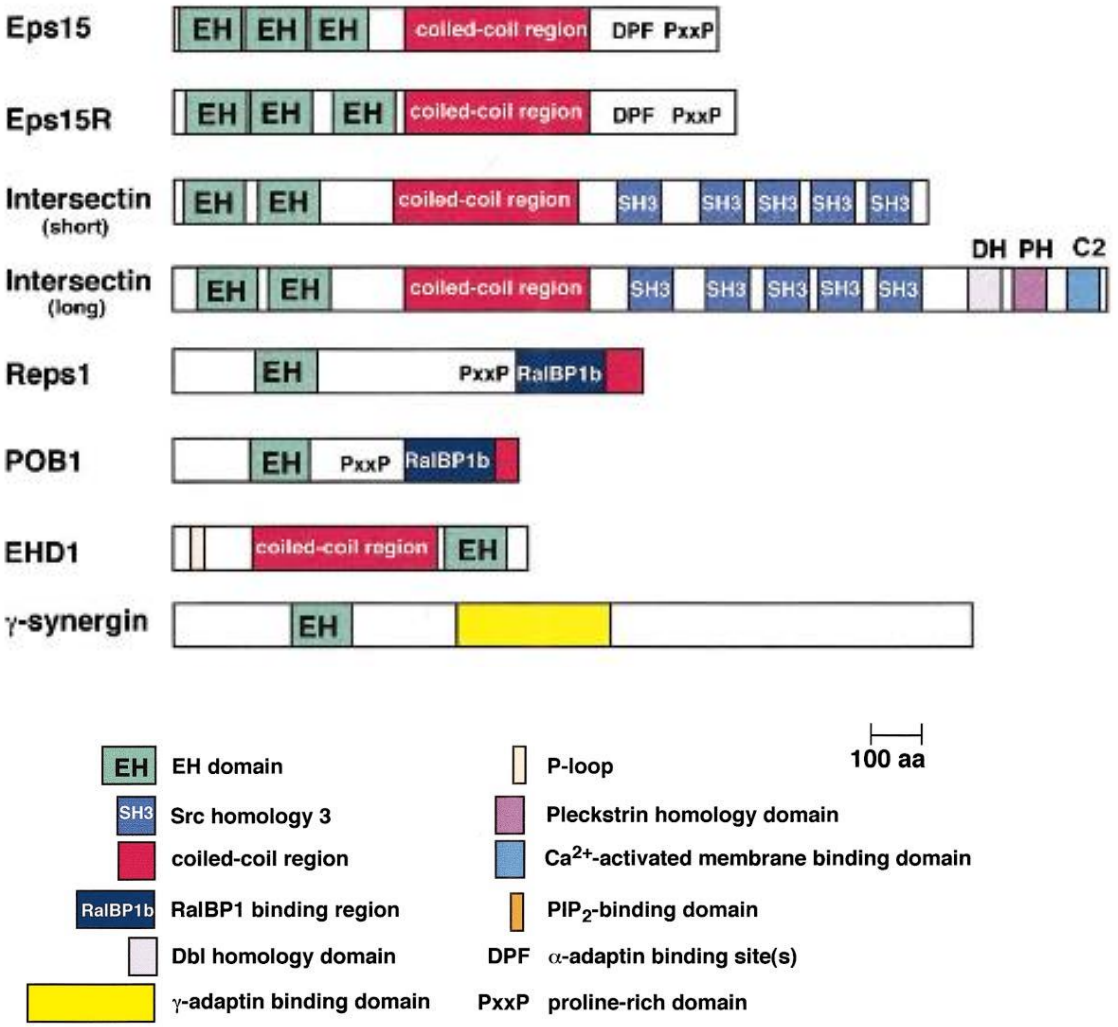

Figure 1.4 The architecture of EH domain-containing proteins: The organization and domain structure of EH domain-containing proteins in humans. Image used with permission and modified from (Santolini et al., 1999).

The domain architecture of EHD proteins consist of an N-terminal nucleotide binding domain (G-domain), a linker region followed by a central coiled-coil domain that generates a lipid binding surface, and a characteristic EH domain localized to the C-terminus of the protein (Figure 1.5 a). The elucidation of solution structure of EH domain of EHD1 (Kieken et al., 2007) and crystal structure of the full-length mouse EHD2 (Daumke et al., 2007) have greatly contributed to our understanding of the function of these domains in EHD proteins.

Based on the crystal structure of EHD2, EHD proteins contain an N-terminal nucleotide-binding G domain but exhibit preference for ATP binding over GTP (k_m of 80 μm for ATP vs. no detectable K_m for GTP-binding) (Daumke et al., 2007; Lee et al., 2005). The G domain retains its nomenclature based on its three-dimensional structural similarity to the G-domain of Dynamin. A dominant negative mutation of RME-1 identified in the initial *C. elegans* genetic screen yolk protein uptake defective mutants was found in the conserved nucleotide-binding domain (G65R). Whereas, the localization of wild-type RME-1 was observed in the cytoplasm and on the endosomal membranes, the G65R mutant protein was mislocalized and found predominantly in the cytoplasm, indicating the importance of the G-domain in targeting the protein to the membrane (Caplan et al., 2002a; Lin et al., 2001). The G-domain also contains a highly conserved hydrophobic interface that serves as a dimerization platform. EHD2 protein crystallizes as a homo-dimer; the G-domain along with the helical domain adopts a scissor-shaped conformation, such that the C-termini of the two monomers cross each other, orienting the EH-domains in line with the G-domains of the opposing monomers (Figure 1.5 b). The EH-domain of EHD2 was similar in structure to the previously solved EH domain (EH-2) of Eps15 (de Beer et al., 1998) and to the EH domain of EHD1 (Kieken et al., 2007). The EH domain of EHD2 consists of two closely packed perpendicular EF-hands connected by a short antiparallel β–sheet and a Ca^{2+} ion bound to the second EF hand (de Beer et al., 1998).

A

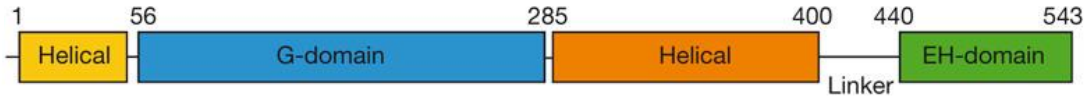

B

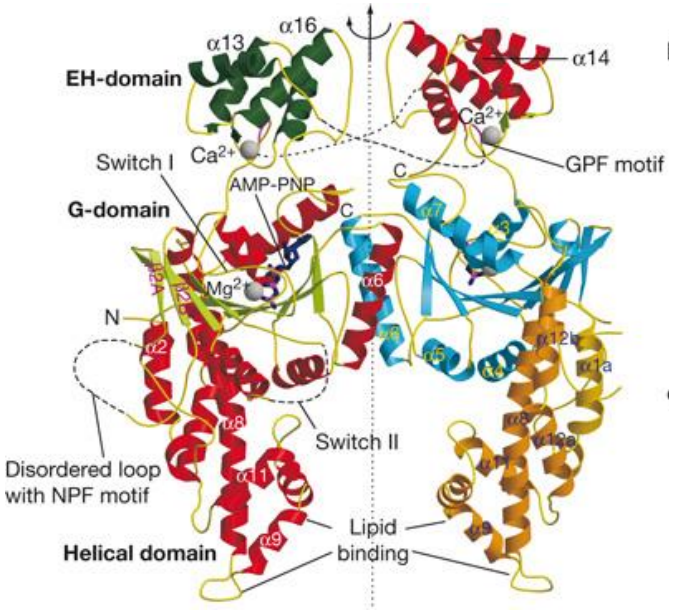

Figure 1.5 A: Domain structure of EHD proteins (numbering from mouse EHD2 amino acids). **B**: Ribbon-type presentation of the EHD2 dimer. One molecule is coloured according to the secondary structure (helices in red, -strands in green) and the other according to the domain structure. GPF and NPF motifs are indicated. Image used with permission and modified from (Daumke et al., 2007).

3.2 EH-domain interaction with NPF motifs

The coordinate actions of EHD proteins are primarily mediated by their EH-domain interaction with partners containing asparagine-proline-phenylalanine (NPF) motifs. Although, there are hundreds of proteins containing one or more NPF motifs, EH domains exhibit selectivity and specificity for binding. So far, more than 25 different direct and indirect interaction partners have been identified for the EHD proteins (Naslavsky and Caplan, 2011). Several of these interaction partners have already been implicated at distinct steps in the process of endocytosis. While the mode of interaction is not completely characterized for all the partners, the vast majority of EHD protein-protein interactions are mediated through the EH-NPF motif binding. The binding of EHD proteins to Rab4/Rab5 effector Rabenosyn-5 (Naslavsky et al., 2004), Rab11 effector Rab11-Fip2 (Naslavsky et al., 2006a), Syndapins (Braun et al., 2005), SNARE protein SNAP29 (Xu et al., 2004), Myoferlin (K. R. Doherty et al., 2008), fer-1-like-5 (Fer1L5) (Posey et al., 2011), MICAL-L1 (Giridharan et al., 2013; Sharma et al., 2009) and Numb (C. A. Smith et al., 2004) is mediated by one or more NPF motifs present in these proteins. Rabensoyn-5, Rab11-Fip2, Rabankyrin-5 and MICAL-L1 are all Rab effectors and it is the EH-NPF interaction through with EHD proteins cross talk with various Rab proteins. The functional relevance for the EH domain was demonstrated in *C.elegans* wherein a mutation near the EH domain of RME-1 resulted in reduction in yolk protein uptake in the oocytes. The mutant protein was locked on the endosomal membranes in contrast to the cytoplasmic localization of the wild type RME-1 protein (B. Grant et al., 2001).

So far, the solution structure of N-terminal EH domain proteins including, three Eps15 EH-domains, POB1, and Reps1 have been solved (Santolini et al., 1999). The structure of the Eps15 EH2 domain demonstrated that the NPF residues fit into the hydrophobic pocket on the surface of the EH domain through their type I β-turn confirmation (de Beer et al., 1998). A highly conserved tryptophan residue in the EH domain interacts

with the asparagine residue of NPF and the hydrophobic phenylalanine functions as an anchor for the NPF motif.

The NMR structure of the human EH domain of EHD1 (Glu401-Glu534) was solved recently by Kieken et al.(Kieken et al., 2007). The overall structure of EH -domain of EHD1 protein exhibits structural resemblance to the previously solved crystal structure to the N-terminal EH domains, consisting of two helix-loop-helix motifs connected by a short antiparallel β-sheets between the loops followed by a proline rich C-terminal tail. EH-domain of EHD1 shares 49.5% overall structural similarity to the EH2 domain of Eps15.

The EH domain of EHDs differ from that of N-terminal EH domain-containing proteins based on the presence of a highly positive charged surface (Kieken et al., 2007). N-terminal EH domain proteins, including Eps15 and Intersectin, have an overall negatively charged surface area. Paoluzi et al. have demonstrated that the first and third EH domains of Eps15R prefer binding to peptides that contain arginine following the NPF motif (Paoluzi et al., 1998). Consistent with the positive charged surface of the EH domains of EHD proteins, the vast majority of EHD interaction partners contain acidic residues following the NPF motif. A mechanistic explanation for this binding was demonstrated by the NMR solution structure of the EH domain of EHD1 in complex with MICAL-L1 peptide (NPFEEEEED) indicating that the first two glutamate residues flanking the NPF lie in a favorable position to form salt bridges with lysine residue within the EH-domain. To demonstrate the contribution of negatively-charged residue following the NPF motif, Henry et al. (G. D. Henry et al., 2010) utilized biophysical approaches to measure the interaction energetics of EH domain of EHD1 with peptides derived from two well characterized EHD binding partners: Rabensoyn5 (Ac-GPSLNPFDEED) and Rab11-Fip2 (Ac-YESTNPFTAK). The study supports the notion that negatively charged residues following the NPF motif contribute to binding. Using an extended interaction motif (NPF-DE-DE-DE), this study also predicted new interaction partners.

Utilizing an unbiased bioinformatics-based in silico approach I have categorized all human and mouse proteins in the Uniprot database (using the verified proteins in the Ensembl database) to organize mammalian proteins with potential EH domain interaction motifs. I have designed multiple extended motifs to predict novel interaction partners following which we created a peptide library to confirm EH-NPF interaction in a biophysical assay. The details of this work will be described in Chapter 4 of this dissertation.

3.3 EH domain-independent EHD interactions

Even though the vast majority of EHD protein interactions are mediated via EH domain-NPF motif sequence binding, there exist several EHD interactions that are either uncharacterized or are mediated through a different domain present in the EHD proteins. For instance, a yeast two-hybrid library screen using human heart cDNA-encoded proteins for interaction with Ankyrin-B (a protein important for membrane targeting and stability of membrane ion channels, transporters etc.) as a bait identified EHD3 protein as a potential interacting candidate (Gudmundsson et al., 2010). In vitro studies confirmed the ankyrin-B/EHD3 interaction using radiolabeled EHD3 with Glutathione S-transferase (GST)-ankyrin B. The association was also observed with other EHD proteins including EHD1, EHD2 and EHD4. Furthermore, ankyrin-B membrane binding domain was demonstrated to directly associate with EHD proteins through their coiled-coil domain whereas the N-terminal region, G-domain and EH-domain lacked ankyrin-binding activity (Gudmundsson et al., 2010).

Another screen utilizing a membrane-based yeast two-hybrid screen of an outer hair cell (OCH) cDNA library with Cadherin 23 (CDH23) (a transmembrane protein localized near the tips of hair cell stereocilia in the inner ear) as the bait identified EHD4 as a potential interacting partner (Sengupta et al., 2009).

Further studies demonstrated distinct EHD4/CDH23 plasma membrane co-localization in the hair cells. In addition, co-immunoprecipitation experiments confirmed that

EHD4 binds to CDH23, and that this interaction is mediated through the EH domain. The interaction is abolished when the EH domain was deleted suggesting the binding is unlikely to be mediated by other domain of EHD4. CHD23 protein does not contain any NPF motifs suggesting that EHD4 EH domain binds through a non-NPF motif (Sengupta et al., 2009). My studies described in Chapter 4 have identified a single GPF/DPF motif in CDH23 protein.

As described in section 1.3, the retromer complex comprises of two sub-complexes: the vacuolar protein sorting 35/29/26 sub-complex that binds cargo and the sorting nexin (SNX)1/2 sub-complex that tubulates endosomal membranes. The retromer complex is required for the endosomal-to Golgi retrieval of the cation-independent mannose 6-phosphate receptor (CIMPR). Using a proteomic approach utilizing a transgenic mouse cell line that has lost the retromer function by deletion of VPS26 gene, protein profiles of endosomally enriched membranes were prepared and compared to the wild-type cell lines (Gokool et al., 2007). Mass spectrometry identified EHD1 as one of the proteins with elevated expression levels in the VPS-null cell line. EHD1 interaction with retromer was determined by immunoprecipitation experiments and it was determined that this interaction is independent of the EH domain of EHD1 or the NPF motif present in the VPS35 protein (Gokool et al., 2007).

Small conductance (KCa2.3) Ca^{2+}-activated K^+ Channel protein plays a critical role in maintaining vascular tone and in blood pressure regulation. KCa2.3 is rapidly endocytosed and recycled back to the PM. KCa2.3 immunoprecipitates with EHD1 and Rab35 (a fast endocytic recycling protein) and this association is critical to the proper sorting of the channel protein into the recycling pathway. EHD1 was demonstrated to associate through the N-terminus of KCa2.3, the exact motif within the associating partner or the domain requirement for EHD1 is not fully characterized (Gao et al., 2010). It is interesting to note that KCa2.3 protein does contain a conserved NPF motif (Chapter 4). EHD1 has also been shown to interact with Insulin-like growth factor 1 receptor (IGF-1R) but the associating

motif/domain remains uncharacterized at this point (Rotem-Yehudar et al., 2001). It is highly plausible that EHD proteins interact with these proteins through a linker protein or that the interactions are highly dynamic in fashion.

3.4 In vitro functional roles of EHD proteins

Despite the high level of sequence homology between the four EHD paralogs, these proteins mediate distinct as well as shared roles in regulating endocytic trafficking (George et al., 2007). The best-characterized member of the family, EHD1 is localized to the tubular and vesicular membranes of the ERC (Caplan et al., 2002b) where it mediates receptor recycling back to the PM (Figure 1.6). The EH domain of EHD1 is responsible for its tubular localization since mutation of lysine 483 residue within the EH domain affects EHD1 binding to lipids and also abrogates its tubular localization (Naslavsky et al., 2007). EHD1 has been attributed to the recycling of a number of receptors including TfR (internalized through clathrin dependent pathway) as well as Major histocompatibility complex class I (MHC-I) and β-integrins (clathrin independent pathway) (Caplan et al., 2002b; Jovic et al., 2007; Lin et al., 2001). The knockdown of EHD1 impairs exit of TfR and MHC-I from the ERC and causes accumulation within this compartment. Since these studies it has been reported that EHD1 mediates receptor recycling of a growing list of receptors including the cystic fibrosis transmembrane conductance regulator (Picciano et al., 2003), the insulin-responsive glucose transporter (GLUT4) (GuilhermeSorianoFurcinitti et al., 2004), α-amino-3-hydroxy-5-methyl-4-isoxazoleproprionic acid (AMPA) type glutamate receptors (Park et al., 2004), MHC-II molecules (Walseng et al., 2008), the hyperpolarization-activated cyclic nucleotide-gated (HCN) ion channel family members HCN1, HCN2 and HCN4 (Hardel et al., 2008), G-protein-activated inwardly rectifying potassium channels (Chung et al., 2009) and the KCa2.3 (Gao et al., 2010). Aside from its role in recycling, EHD1 also regulates internalization of the low-density lipoprotein (LDL) receptor (Naslavsky et al., 2007) and

L1/neuron-glia cell adhesion molecule (NgCAM) in neuronal cells (Yap et al., 2010), and regulates IGF-1R signaling (Rotem-Yehudar et al., 2001). EHD1 associates with retromer complex and facilitate retrograde transport from endosomes to the Golgi and stabilizes tubules containing sorting nexin 1 (Gokool et al., 2007). EHD1 also plays a key role in the transport of receptors from EE to ERC based on its localization at the peripheral endosomes and its functional relationship with Rab35 (Sato et al., 2008) and connecdenn (Allaire et al., 2010).

EHD2, the least homologous member, exhibits ~70% amino acid sequence identity with other EHDs. EHD2 demonstrates strong evidence for homo-oligomerization in contrast to other EHDs that form hetero-oligomers. EHD2 is the only protein within the family whose complete crystal structure has been solved (Daumke et al., 2007). EHD2 regulates TfR and GLUT4 internalization in adipocytes through its EH domain interaction with EH-domain-binding protein (EHBP1) (Guilherme et al., 2004) that link clathrin-mediated endocytosis to the actin cytoskeleton (GuilhermeSorianoBose et al., 2004). EHD2 was also shown to interact with the clathrin adaptor complex protein subunits of AP-1 and AP-2 (Park et al., 2004). EHD2 overexpression with either the wild type EHD2 or EHD2ΔEH impairs transferrin internalization. George et al. (George et al., 2007) provided evidence that EHD2 can play redundant functional roles with EHD1 in regulating TfR recycling from ERC and in complementing the *C. elegans rme-1* mutant phenotype (Figure 1.6). EHD2 interacts with Myoferlin, (a membrane-anchored, C2 domain-containing protein that is highly expressed in fusing myoblasts) via the EH-NPF motif (K. R. Doherty et al., 2008).

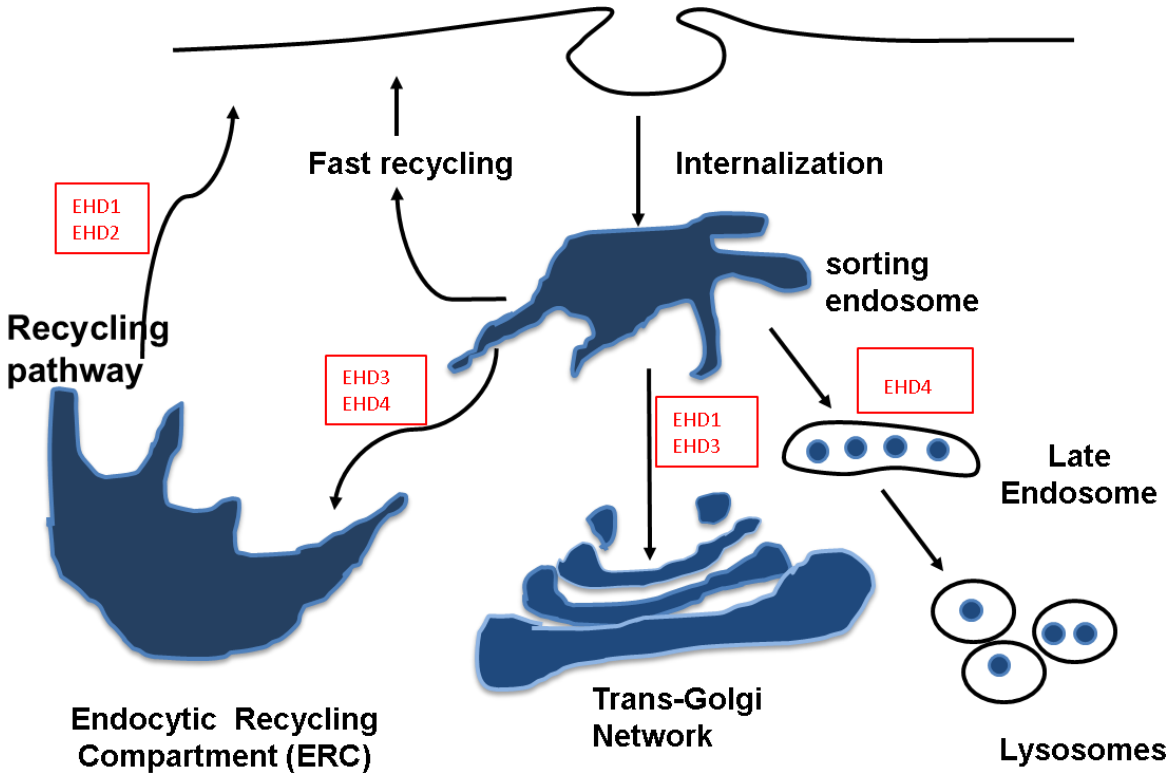

Figure 1.6 Schematic depicting the proposed roles for EHD proteins during endocytic transport.

Recent studies have suggested varied functions of EHD2 in regulating sarcolemmal repair (Marg et al., 2012), myoblast fusion (K. R. Doherty et al., 2008; Posey et al., 2011) control of Rac1 (Benjamin et al., 2011) , and actin cytoskeleton (Stoeber et al., 2012), and the organization of caveolar structure underneath the PM (Moren et al., 2012; Stoeber et al., 2012).

EHD3 exhibits the highest sequence identity with EHD1 (~85%) and regulates transport from early endosome to ERC and to the TGN (Figure 1.6). Yeast two-hybrid analysis and immunoprecipitation of overexpressed EHDs have suggested EHD3 interaction with EHD1 (Galperin et al., 2002; George et al., 2007; Naslavsky et al., 2006a). Although overexpressed EHD1 and EHD3 co-localize, EHD3 primarily acts upstream of EHD1 and does not appear to play a primary role in regulating exit from the ERC to the PM. RNAi mediated knockdown of EHD3 results in impaired transport causing cargo accumulation in the EE (Naslavsky et al., 2006a). EHD3 along with other family members directly interacts with ankyrin-B and EHD3-deficient cardiomyocytes display selective loss of Na/Ca exchanger expression and function (Gudmundsson et al., 2010). EHD3 also binds to Rab effectors, including Rab11-Fip2, Rabenosyn-5 and MICAL-L1 (Naslavsky et al., 2006a; Naslavsky et al., 2006b; Sharma et al., 2009).

EHD4 localizes to Rab5- and EEA1-positive EEs and regulates receptor transport from EE to LE as well as to the ERC (Figure 1.6). (Sharma et al., 2008). EHD4 (also known as pincher) has been shown to be involved in the internalization of nerve growth factor receptor (TrkA and TrkB)(Shao et al., 2002). TrkA protein contains two NPF motifs, however, a direct association of EHD4 with TrkA has not been characterized. EHD4 co-operates as a hetero-oligomer partner with EHD1 in the control of NgCAM trafficking in neuronal cells (Yap et al., 2010). EHD4 also interacts with the NPF-containing cell-fate determinant adaptor protein Numb.

3.5 In vivo functional roles of EHD proteins

Initial evidence for a role of EHD proteins in controlling endocytic receptor recycling was provided by *C. elegans* genetic screens for receptor-mediated endocytosis (*rme*) mutants, which identified RME-1 (Human EHD1 ortholog), followed by functional studies in Chinese hamster ovary (CHO) cells. RME-1 mutants were defective for yolk receptor recycling and showed basolaterally-accumulated endocytosed fluid phase endocytic markers in grossly enlarged endosomes (B. Grant et al., 2001). Furthermore, by using a dominant-negative approach, the role of EHD1 in the regulation of TfR recycling from the endocytic recycling compartment to the PM was illustrated in CHO cells (Lin et al., 2001). In *Drosophila melanogaster,* the single EHD1 ortholog, Past1, is ubiquitously expressed during early embryogenesis and is capable of binding to the adaptor protein Numb (C. A. Smith et al., 2004). *Past1* deletion led to premature death of the adult flies and their infertility suggesting a role of Past1 in germline development and survival of adult fly (Olswang-Kutz et al., 2009).

EHD1 expression is reported in the testis, kidney, heart, spleen, brain, and in specific retinal layers (George et al., 2007; Mintz et al., 1999). The first study to study the in vivo biological functions of EHD proteins in a mammalian system was published by Rapaport et al. wherein they deleted EHD1 in the mouse (Rapaport et al., 2006). *Ehd1-null* (Horowitz lab) mice thus generated appeared healthy, had a normal life span and displayed no histological abnormalities; however mouse embryonic fibroblasts (MEFs) derived from these animals exhibit recycling defects (Jovic et al., 2007; Naslavsky et al., 2007; Rapaport et al., 2006). Strikingly, by utilizing a different targeting strategy and different mouse strains, Rainey et al. showed that *Ehd1-null* (Band lab) mice exhibit overt phenotypes (Rainey et al., 2010). *Ehd1-null* (Band lab) mice on a mixed 129S;B6 background are born at sub-Mendelian ratios, exhibit male infertility (consistent with the fly phenotypes) due to spermatogenesis defects and a proportion of these mice display ocular phenotypes. Work

described in Chapter 3 characterizes the ocular defects observed in *Ehd1-null* (Band lab) mice in greater details. On further backcrossing this strain to a C57BL/6J background, we observed embryonic lethality wherein mutant embryos die at mid-gestation period (manuscript under review). These results indicate that loss of *Ehd1* leads to partial or complete lethality based on the mouse background and imply an important role of EHD1 for embryonic viability, growth, ocular development and fertility of mice. In addition, *Ehd1-null* (Band lab) mice display smaller muscles and myofibers, and loss of EHD1 results in overgrowth of T-tubules with excess vesicle accumulation in skeletal muscle (Posey et al., 2014). Furthermore, EHD1 and EHD4 proteins were observed to localize to the primary synaptic clefts of the neuromuscular junction (NMJ). However, *Ehd1-null* (Band lab) mice display normal NMJ morphology and muscle functions, concomitant with de novo localization of otherwise cytosolic EHD4 to NMJ, suggesting functional compensation by other EHD paralogs (Mate et al., 2012).

In mice, EHD2 expression is observed in lungs, heart, spleen, brain, and mammary gland (George et al., 2007). The biological roles of EHD2 are somewhat unclear owing to the fact that a knockout mouse model is still unavailable. Our laboratory has taken a lead in this aspect and *Ehd2-null* mice have been generated recently in our laboratory and are being characterized. EHD2 interacts with Myoferlin and Fer1L5, and knockdown of EHD2 leads to impaired myoblast fusion (K. R. Doherty et al., 2008; Posey et al., 2011). Future studies will assess if EHD2 protein displays functional redundancy with other EHD proteins or has a central role in tissues of interest where it exhibits the greatest expression levels.

The highest EHD3 protein expression is observed in mouse kidneys, liver, heart, spleen and brain (George et al., 2007; Gudmundsson et al., 2010; Patrakka et al., 2007). Within kidneys, EHD3 is predominantly expressed in the glomerular endothelial cells. *Ehd3* null mice however displayed no gross renal structural or functional abnormalities. Notably, *Ehd3* deletion resulted in marked increase in EHD4 expression in glomerular endothelial

cells. Combined *Ehd3/4* deletion unleashed dramatic pathology and resulted in death of DKO mice within 3-24 weeks of age. DKO mice displayed small, pale kidneys, severe proteinuria, and displayed lesions characteristic of thrombotic microangiopathy (George et al., 2011). EHD3 along with other EHD proteins is expressed in cardiac muscle and EHD3 plays an indispensable role in proper trafficking of the Na/Ca exchanger (NCX) to the myocyte cell membrane through its association with ankyrin-B (Gudmundsson et al., 2010). The first link between EHD3 protein and cardiovascular disease was provided recently where EHD3 and NCX levels were consistently increased in heart failure models (Curran et al., 2014). These examples illustrate the significance of EHD proteins especially that of EHD3 in human pathological conditions.

Ehd4-null mice generated by targeting Exon 1 were born at expected Mendelian ratios and were viable; however, male mice showed smaller testis. Despite the slight reduction in sperm count and smaller testis size in *Ehd4-null*, the mutants were able to sire pups, albeit the brood size was smaller (George et al., 2010). EHD4 expression is temporally regulated during testis development, being high at pre-puberty phase but reduced in the adult mice. In contrast, EHD1 expression is low during pre-puberty but higher at puberty. EHD1 and EHD4 are thus important for fertility and testis size, respectively (George et al., 2010; Rainey et al., 2010). As, *Ehd1/Ehd4* DKO animals are never born, conditional deletion of these genes using testis specific cre lines should help answer questions related to their specific and redundant functions in testis development. Apart from its role in testis development, EHD4 mRNA expression is observed in mouse cochlea where it interacts with Cadherin 23, a transmembrane protein localized at the tips of hair cell stereocilia. Functional redundancy with EHD1 in cochleal tissue leading to compensatory increase in EHD1 expression levels may account for the absence of hearing defect in *Ehd4-null* mice (Sengupta et al., 2009).

4. Ocular development in mice

4.1 Overview

The eye is essentially a highly specialized extension of the brain with two primary functions: image formation and image processing. The vertebrate eye is derived from two distinct tissue layers: the optic vesicle (derived from the forebrain neural epithelium) and the overlying ectoderm of the head. In the 1890's German scientist, Hans Spemann began tissue ablation and transplantation experiments in the amphibian embryos to test the hypothesis that lens formation was dependent on contact between the two layers. Spemann used a hot needle to destroy the optic vesicle before its association with the overlying ectoderm. The results demonstrated that neither the lens nor the retina developed on the manipulated side, suggesting that an interaction with eye tissue is required for vertebrate lens formation (Spemann, 1901). Spemann thus provided experimental results to prove that proper development of lens required input from the optic vesicle; it remained unclear whether the optic vesicle was sufficient to induce a lens. In 1904, Warren Lewis performed tissue recombination experiments by transplanting an optic vesicle under the flank ectoderm in frog embryos and found that an ectopic lens formed in the transplanted region (Lewis WH, 1904). These results suggested that stimuli from the optic vesicle were sufficient to induce lens formation in embryonic ectoderm. It was however, discovered within few years that structures bearing some resemblance to lenses can develop in the absence of optic vesicles (Saha et al., 1989). Using a lineage tracing technique, Grainger and colleagues revealed the flaw in Lewis's experimental design where contaminating donor cells carried along with the transplanted optic vesicle were responsible for the lens formation in flank regions (Grainger et al., 1988). In recent years, Grainger's group has further provided evidence that lens development is a successive process that begins prior to the contact of the ectoderm with the optic vesicle and identified a key role for the anterior neural plate as an early inducer of lens ectoderm

(Grainger, 1992; J. J. Henry and Grainger, 1987). These classical embryological experiments form an important basis as we try to further understand the molecular details of these processes.

4.2 Lens development in mice

The lens is a fairly simple organ system consisting of only two types of cells: the proliferative lens epithelial cells, and the differentiated fiber cells (Lovicu and McAvoy, 2005). The vertebrate eye develops from the surface ectoderm, the optic vesicle (a lateral evagination from the wall of the diencephalon), and the surrounding mesenchyme. Eye development in mice begins during late gastrulation at embryonic day 9.5 (E9.5), when neuroepithelium derived from the diencephalon evaginates to form the bilateral optic vesicle (OV). The physical association between the OV with a layer of surface epithelium termed presumptive lens ectoderm (PLE) marks early stages of lens morphogenesis. Once in close proximity, cytoplasmic extensions extend between the two tissue layers. Shortly after the physical contact is established, lens ectoderm undergoes thickening, forming the lens placode (Chow and Lang, 2001; Lang, 2004) (Figure 1.9). Ocular abnormalities including anophthalmia (absence of the globe), microphthalmia (reduced size of the globe) result if the cells of the lens placode either exhibit reduced proliferation or increased apoptosis. For example, Pax6 insufficiency results in proliferation defects in the lens placode resulting in smaller lens vesicles (van Raamsdonk and Tilghman, 2000). Six3 inactivation in the lens placode results in increased apoptosis (Liu et al., 2006; Yamada et al., 2003).

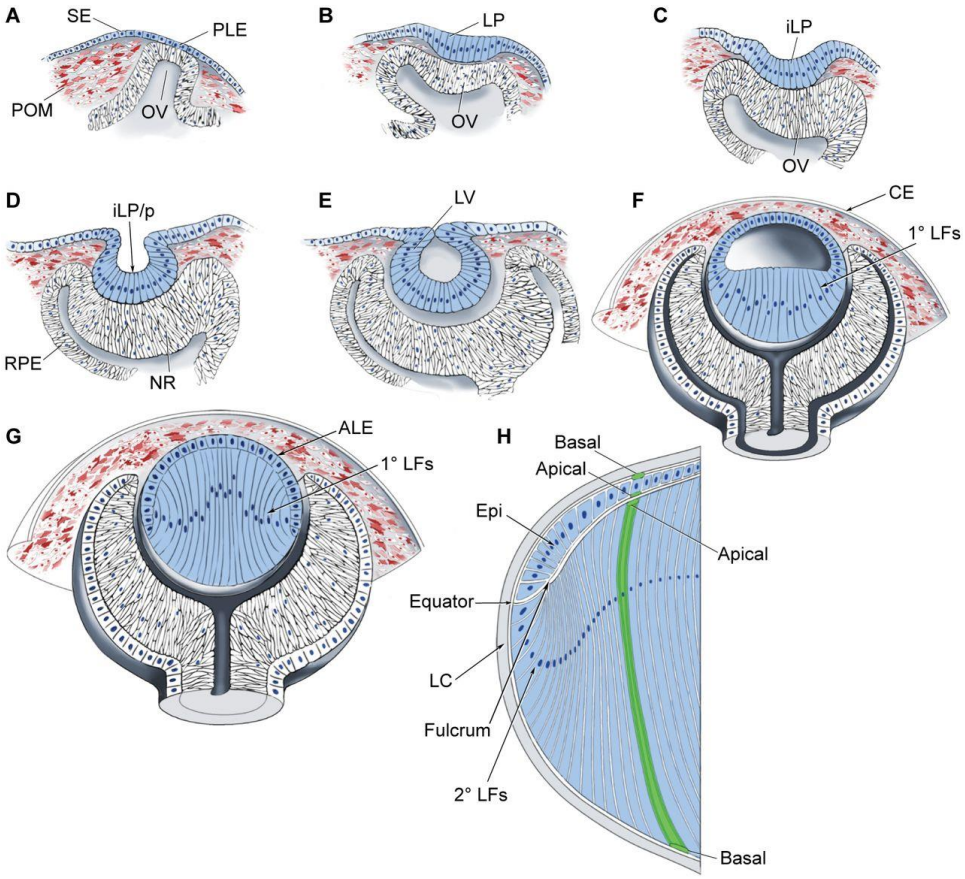

Figure 1.7 Stages of lens formation in mouse embryos: (A) E9.0, prospective lens ectoderm. (B) E9.5, lens placode. (C) E10, invaginating lens placode. (D) E10.5, invaginating lens placode to lens pit. (E) E11, open lens vesicle. (F) E12.5, primary lens fiber cell differentiation. (G) E13.5-E14.5, completion of primary lens fiber cell elongation to secondary lens fiber cell formation. (H) Lens growth and secondary lens fiber cell differentiation in adult ocular lens. The apical-basal polarity of lens epithelial and fiber cells is indicated. ALE, anterior lens epithelium; CE, corneal epithelium; iLP, invaginating lens placode; iLP/p, invaginating lens placode/lens pit; LC, lens capsule; Epi, lens epithelium; LP, lens placode; NR, neuroretina; OV, optic vesicle; POM, periocular mesenchyme; 1° and 2° LFs, primary and secondary lens fibers; PLE, prospective lens ectoderm; RPE, retinal pigmented epithelium; SE, surface ectoderm. Image used with permission and modified from (Cvekl and Ashery-Padan, 2014).

The lens placode and the underlying optic vesicle invaginates in concert to form the lens pit and optic cup, respectively. Subsequently, the lens pit deepens and folds to form the lens vesicle while the surface ectoderm closes over it leaving a narrow transitory structure known as lens stalk (Figure 1.7). The lens stalk eventually degenerates, separating the lens vesicle. The incomplete separation of the lens vesicle from the surface ectoderm results in a common developmental abnormality known as persistence of lens stalk. A number of genes including AP-2α (Pontoriero et al., 2008), β-catenin (A. N. Smith et al., 2005), Foxe3 (Brownell et al., 2000), N-cadherin (van Raamsdonk and Tilghman, 2000), Ndst1 (Pan et al., 2006) and Pax6 (Baulmann et al., 2002) are critical players for lens placodal invagination, lens vesicle formation and its separation from the ectoderm. At E13.5, the surface ectoderm adjacent to the lens vesicle differentiates into the corneal epithelium while the lens vesicle differentiates into the lens. The next step involves the differentiation of two forms of cells within the lens vesicle: the anterior vesicle cells giving rise to a sheet of cuboidal epithelial cells whereas the posterior lens vesicle cells elongate to form the primary fibers that fill up the lumen of the vesicle. From this stage onwards, the lens grows rapidly by cell proliferation and differentiation. Proliferation is restricted to the epithelium and greatest activity is seen in a region just above the lens equator known as the germinative zone. At the germinative zone, adjacent epithelial cells move closer to the lens equator where they withdraw from the cell cycle, elongate and differentiate into fiber cells (Cvekl and Ashery-Padan, 2014) (Figure 1.7). Thus, new fibre cells are added continuously to the fiber mass throughout life. Both primary and secondary fibres permanently withdraw from the cell cycle and eventually degenerate all intracellular organelles. These changes are characterized by the appearance of several specific (α, β, γ) crystallin proteins (X. Wang et al., 2004). The lens maintains a distinct polarity with its anterior surface retaining proliferative capacity whereas the posterior fiber cells undergoing terminal differentiation. The influence of ocular environment on lens

growth and polarity was demonstrated by lens inversion experiments (Coulombre and Coulombre, 1963). The experiment involved removal of the embryonic chick lens, which was inverted so that the lens epithelium now faced the vitreous and neural retina instead of the aqueous humor. In this new environment, the lens epithelial cells facing the vitreous elongated and differentiated to form lens fiber mass, while a new epithelium layer formed over the former posterior side of the lens. These experiments led to the conclusion that factors present in the vitreous humor promote fiber cell differentiation, whereas the aqueous environment promotes lens maintenance and growth (Lovicu and McAvoy, 2005). This phenomenon was later reproduced in mice (Yamamoto, 1976).

Within the optic cup, the inner layer forms the neural retina, whereas the cells in the outer layer form the melanin-producing retinal pigment epithelium (RPE). The cells of the inner layer proliferate and form a variety of glia, ganglion neurons, interneurons and light-sensitive photoreceptor neurons. Together, these cells form the neural retina. The optic stalk connects the eye to the brain (Figure 1.7). The axons of the retinal ganglion cells meet at the base of the eye and travel down to the optic stalk to form the optic nerve, which carries electrical impulses to the visual area of the brain.

4.3 Corneal structure and early development in mice

The cornea is a highly specialized structure that plays an important role in the maintenance of transparency and acts as a barrier against pathogens and environmental challenges. The cornea consists of five layers: the corneal epithelium, the Bowman's membrane, the corneal stroma, the Descemet's membrane and the corneal endothelium. The corneal epithelium consists of non-keratinized stratified squamous epithelium, and is continuous with the conjuctival epithelium. Corneal epithelium has a remarkable regenerative capacity owing to the stem cells that reside at the corneo-scleral limbus region. The Bowman's membrane consists of a random fibrillar network of type-I collagen fibrils.

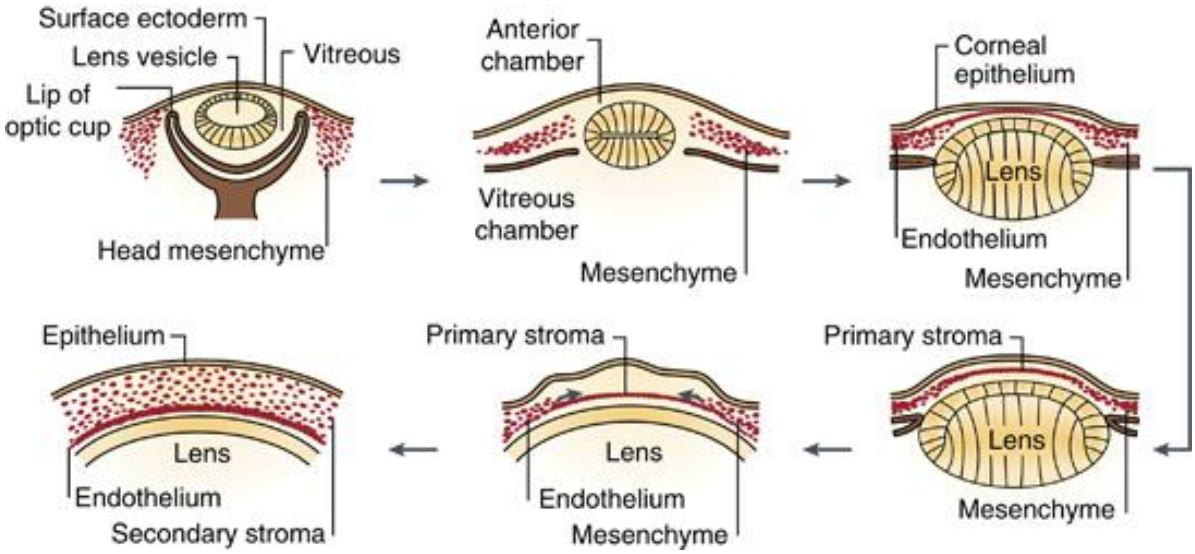

Figure 1.8 Corneal development: The cornea begins to develop when the surface ectoderm closes after the formation of the lens vesicle and its detachment from the surface ectoderm. Mesenchymal cells (neural crest cells) invade the cornea and form the corneal stroma after condensation Image used with permission from (Zavala et al., 2013)

Beneath the Bowman's membrane is the stroma made up of water and collagen, constituting 90 percent of the corneal thickness (Graw, 2003). The Descemet's membrane is a specialized basal lamina underneath the corneal stroma and is produced by the corneal endothelium. This membrane serves as a protective barrier against infection and injuries. The corneal endothelium is characterized by a single layer of flattened cells that forms a boundary between the corneal stroma and the anterior chamber. Two important functions carried out by corneal endothelial cells are to maintain corneal transparency by regulating corneal hydration and to permit the passage of nutrients from the aqueous humor. The corneal endothelium cells mediate these functions by forming "leaky" junctions to allow nutrients to enter the stroma and counterbalance of the inward fluid flow by the presence of NA^{+}/K^{+}-ATPase and bicarbonate-dependent Mg^{2+}-ATPase "pumps"(Joyce, 2003).

The corneal morphogenesis involves differentiation of cells from the surface ectoderm, and the migration of mesoderm and mesenchymal cells of the neural crest origin. The ectodermal cells differentiate to give rise to a multilayered structure (consisting of corneal and conjuctival epithelia) in response to stimulation from the lens vesicle. In mouse embryos, corneal endothelium and stroma is derived from a single wave of migration of neural crest cells, which invade the primary stroma and form both the corneal stroma and endothelium (Figure 1.8). These mesenchymal cells secrete collagen type I and hyaluronidase, which cause the stroma to shrink to ultimately become a transparent cornea (Kidson et al., 1999).

4.4 Transcription factors involved in lens development

Grainger and colleagues have defined at least four stages that correspond to early tissue interactions during lens induction: a) a period of lens-forming competence in the mid/late gastrula ectoderm (Servetnick and Grainger, 1991); b) the acquisition of a lens-forming bias throughout the head ectoderm during neurulation; c) the specification of lens

fate towards the end of neurulation; and d) the lens differentiation that continues throughout life (Grainger, 1992).

Of the several master control genes that direct distinct pathways of development and differentiation in a mammalian system, Pax6 functions as a critical regulator gene in eye development (Ashery-Padan and Gruss, 2001). Pax6 is a member of the Pax family transcription factors that contain a paired domain and a homeodomain (Walther and Gruss, 1991).

In vertebrates, Pax6 expression is first observed in the anterior neural plate region that gives rise to retina, and at a later point in the head surface ectoderm that forms the lens. The expression level of Pax6 increases in the lens placode after its contact with the optic vesicle. Pax6 expression is required for lens induction and also for the activation of crystallin expression later in lens development (Duncan et al., 1998). The correct dosage of Pax6 is essential for normal eye development. In mice, *Pax6* heterozygotes have *small eye* phenotype whereas homozygous mutants have only remnants of ocular tissue and die shortly after birth (Glaser et al., 1992; Hill et al., 1991). In addition, overexpression of *Pax6* leads to severe eye abnormalities (Schedl et al., 1996a). In humans, homozygous loss of Pax6 function causes aniridia and affects all expressing tissues and is neonatal lethal.

FoxE3 is a transcription factor of the forkhead class that has been shown genetically to be downstream of Pax6 in lens development. In humans, mutations in *FoxE3* are associated with anterior segment ocular dysgenesis and Peters' anomaly (Blixt et al., 2000; Medina-Martinez and Jamrich, 2007). The dysgenetic lens (dyl) mice carry mutations in *FoxE3* where failure of lens vesicle closure and separation as well as reduced proliferation in lens epithelial cells is seen (Brownell et al., 2000). During lens differentiation, FoxE3 mutants do not lose their fiber cell nuclei and the lens develops cataracts.

Sox2 is a high-mobility group (HMG) DNA binding domain transcription factor related to the sex-determining factor Sry. *Sox2* and other family members Sox1 and Sox3 have

been implicated in lens development based on their expression patterns (Kamachi et al., 1998). The sox2 proteins form a complex with Pax6 protein to stimulate transcription by binding to the δ-crystallin enhancer sequences (Kamachi et al., 2001). In humans, an estimated 4-20% cases of anophthalmia and microphthalmia are caused by mutations or deletion in the *Sox2* gene (Schneider et al., 2009).

Prox1 is a vertebrate homolog of the Drosophila homeodomain protein *prospero* (Tomarev et al., 1998). Prox1 is expressed in the presumptive lens and retina from an early stage of mouse eye development. Prox1 expression is initially localized to the cytoplasm of the lens placodal cells and then is seen in the nuclei of the posterior cells that give rise to the primary fibers. In a mature lens, Prox1 exhibits nuclear localization in newly differentiating lens fiber cells whereas epithelial cells maintain Prox1 expression mainly in the cytoplasm. *Prox1-null* mice revealed fiber cell differentiation defects suggesting its requirement in this process (Wigle et al., 1999).

The Pitx family consists of a paired-like class of homeobox transcription factors. Pitx2 and Pitx3 are expressed in developing eye tissues including the cornea, lens and retina. In humans, mutations in Pitx3 cause anterior segment mesenchymal dysgenesis. The aphakia (ak) gene is a natural mutant of Pitx3. In ak mice, the developing lens vesicle fails to form the lens epithelium and fiber cells, and ultimately degenerates (Grimm et al., 1998; Medina-Martinez et al., 2009). The *ak/ak* mice have an ocular phenotype similar to *dyl* mice, suggesting an involvement of both (*Pitx3* and *Foxe3*) genes in the same pathway.

Additional transcription factors critical for normal lens development are *Mab21l1*, *L-Maf*, *MafB* and *c-Maf* (basic-leucine zipper domain). *Mab21l1*-knockout mice form a thickened lens placode which fails to invaginate due to defective cell proliferation (Yamada et al., 2003). *Maf* genes bind to a cis-regulatory motif common among the crystallin genes and are involved in lens differentiation.

4.5 Signaling pathways regulating lens development

Bone morphogenetic proteins (BMPs): BMPs are secreted proteins that constitute the largest subfamily within the transforming growth factor-β (TGF-β) family of growth factors. BMPs play a key role in early lens development. *Bmp4* and *Bmp7* are expressed in overlapping expression patterns in early eye tissues. (Dudley and Robertson, 1997; Furuta and Hogan, 1998). *Bmp7* deletion in mice results in variably-penetrant phenotypes that ranges from mild microphthalmia to anophthalmia (Dudley et al., 1995) depending on the mouse strain background (Wawersik et al., 1999). Even though *Bmp4*-null embryos do not survive past E10.5, lens formation from the presumptive lens ectoderm from these mutants can be rescued by recombining them in explant cultures with optic vesicles derived from wild type mice. However, recombinant Bmp4 was insufficient to rescue lens formation when the presumptive lens ectodermal tissue from *Bmp4* mutant embryos was explanted. This finding suggested that Bmp4 functions in lens formation by promoting the production of an inducer by the optic vesicle rather than by acting directly on the ectoderm (Furuta and Hogan, 1998). It is now suggested that Bmp4 functions together with Sox2 in a parallel branch of the lens induction pathway. Even though Bmp4 and Bmp7 exhibit overlapping expression in the ocular tissue, the two proteins play non-redundant roles in early eye development. Beebe et al demonstrated that targeted deletion of BMP receptor (Bmpr1a/ Alk3) in the lens results in smaller lenses with thinner epithelium, with highly vacuolated fiber cells (D. Beebe et al., 2004; Rajagopal et al., 2009). Acvr1 (Alk2) deletion resulted in smaller lenses, decreased placodal proliferation, abnormal cell cycle exit and epithelial and fiber cell apoptosis (Rajagopal et al., 2009). Double deletion of Bmpr1a together with Acvr1 prevented lens induction and lens ectoderm cells failed to reorganize the actin cytoskeleton to their apical ends at the onset of invagination (Rajagopal et al., 2009). In addition, in vitro experiments have shown that primary lens fiber cell elongation is suppressed in the presence of noggin

(a Bmp ligand binding inhibitor) demonstrating the requirement of BMP signaling for primary lens fiber cell development (Faber et al., 2002).

Fibroblast growth factor (FGF) receptor signaling: FGFR signaling plays a key role at multiple stages of lens development, including lens induction, lens cell proliferation and survival, and fiber cell differentiation. Mammals contain four FGFR tyrosine kinase genes (FGFR1-4), all of which are expressed in the vertebrate lenses in distinctive spatio-temporal patterns (de Iongh et al., 1996; de Iongh et al., 1997). Of the known 22 FGF genes, at least 13 are expressed in the eye (Robinson, 2006). Binding of FGFs induces FGFR dimerization that results in transphosphorylation and activation of the cytoplasmic domains of the receptor that initiates intracellular signal transduction cascades (Figure 1.9).

Experiments in rat explant cultures have shown that the distinct polarity of lens may be determined by a FGF gradient (Chamberlain and McAvoy, 1987). It was shown that low concentration of FGF2 promotes lens epithelial proliferation whereas high concentration induces fiber cell differentiation. This fits well with the fact that vitreous humor (which bathes the lens fiber cells) but not aqueous (which bathes the lens epithelium) can induce fiber cell differentiation in rat explant cultures (Lovicu et al., 2011). Further studies to support the role for FGF in fiber differentiation have come from transgenic mouse studies involving overexpression of a truncated FGF receptor that acted in a dominant-negative manner (Stolen and Griep, 2000) or by the overexpression of a secreted FGF receptor (sFGFR3), which led to fiber cell differentiation inhibition in vivo (Govindarajan and Overbeek, 2001).

Expression of a kinase-deleted form of FGF receptor-1 in the lens placode caused reduced levels of Pax6 and resulted in smaller lenses (Faber et al., 2001). In 2006, Pan et al. demonstrated that deletion of heparan sulfate biosynthetic gene Ndst1 (a co-factor for FGF receptor activation) disrupted lens and optic vesicle formation (Pan et al., 2006). Mutation of critical amino acids in *Frs2α,* an adapter protein that participates in FGF receptor signaling led to disruption of optic vesicle and lens formation (Gotoh et al., 2004).

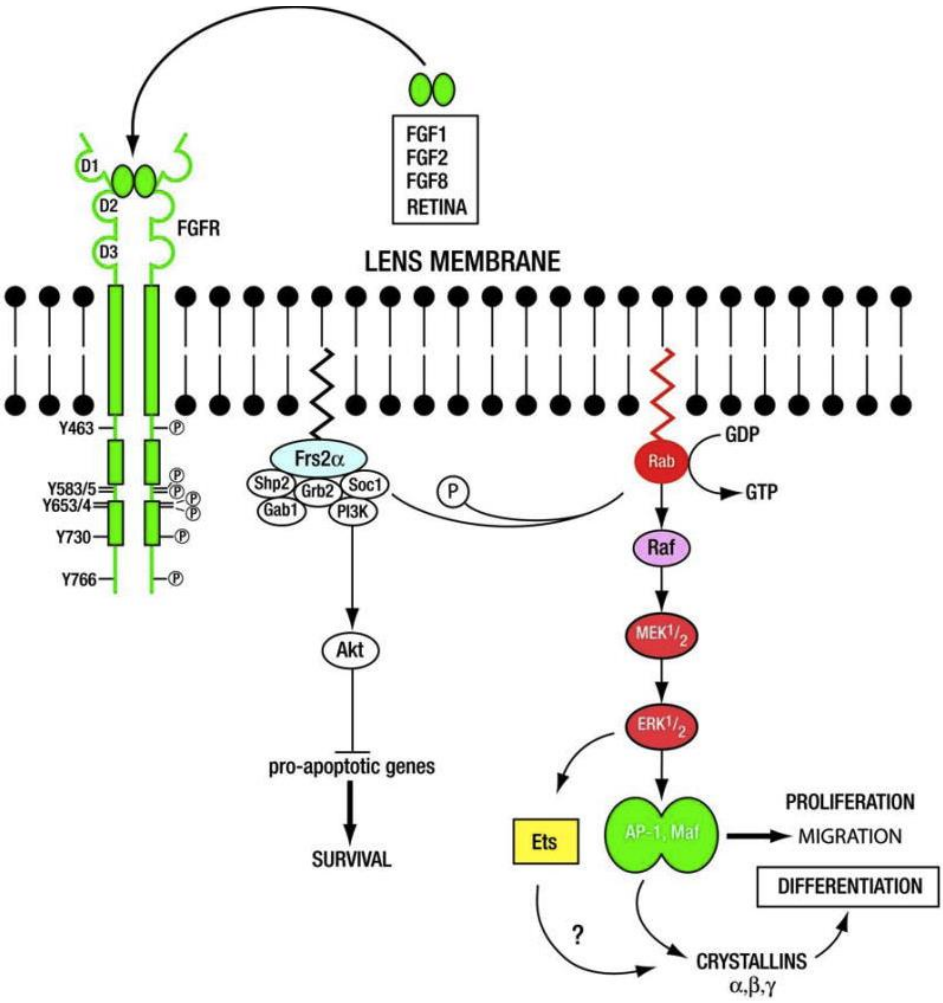

Figure 1.9 Schematic diagram of FGF signaling in lens differentiation: FGF binding to the outside of FGFR induces FGFR dimerization, receptor autophosphorylation followed by phosphorylation of the lipid-anchored docking protein Frs2α. Tyrosine-phosphorylated Frs2α serves as a focal protein for a multiprotein complex assembly that signals via two branches of FGF signaling, PI3K/Akt and FGF/MAPK. Image used with permission and modified from (Cvekl and Duncan, 2007).

Loss of *Frs2α* in the lens caused significant apoptosis and decreased phosphorylation of both Erk1/2 and Akt (Madakashira et al., 2012). Conditional deletion of *fgfr2* led to increased apoptosis and eventually resulted in lens degeneration (Garcia et al., 2005; Garcia et al., 2011). Double deletion of *fgfr1* and *fgfr2* in the lens placode ablates lens formation. Similarly, lens specific deletion of *fgfr1*, *fgfr2*, and *fgfr3* led to increased apoptosis and failure of specific deletion of *fgfr1*, *fgfr2*, and *fgfr3* led to increased apoptosis and failure of primary and secondary fiber cell differentiation (Zhao et al., 2008).

Wnt-signaling in lens development: Wnt pathway components, including Wnt ligands, Frizzled (Fz) receptors, low-density lipoprotein-related protein (Lrp) 5/6 co-receptors, and anatagonists (Dkk, Sfrps), are all expressed in developing eyes. These include Fz receptors (1-10) and 19 known Wnt ligands. Signaling by Wnts and Fz receptors has been categorized into canonical (Wnt/β-catenin), non-canonical (Wnt/planar-cell polarity (PCP)) and Wnt/Ca^{2+} pathways. Transgenic mice that overexpress constitutively-active β-catenin in the presumptive lens ectoderm showed inhibition of lens induction (A. N. Smith et al., 2005). In β-catenin-knockout mice, even though lens placode formed normally the lens formation was aberrant (Kreslova et al., 2007). Also, mice with a mutation in Lrp6 (co-receptor for Fz receptor) show aberrant lens development with major defects in lens epithelial differentiation (Stump et al., 2003). Wnt/PCP pathway plays a critical role in developmental pathways that involve cytoskeletal remodeling. Non-canonical Wnt signaling has been suggested to have a role in fiber cell differentiation. For example, inhibition of Rho GTPase activity both in lens epithelial cells and fiber cells disrupts β-catenin-based adherens junctions leading to abnormal cytoskeletal organization and impaired fiber cell morphology (Maddala et al., 2004; Maddala et al., 2008).

Notch Signaling: Notch signaling pathway (which includes receptors *Notch1-4* and ligands *Deltalike1,3,4* and *Jag1,2*) regulates cell fate determination during development. Multiple Notch pathway genes, including *Notch1*, *Notch2*, *Notch3*, *Jag1*, *Dll1*, *Rbpj* (DNA binding

protein) and the effector *Hes1* are expressed in the developing mouse eyes (Le et al., 2009; Rowan et al., 2008). Several studies have indicated a role for Notch signaling in fiber cell differentiation. Deletion of *Jag1* from presumptive lens ectoderm resulted in severe lens growth and fiber cell differentiation defects. Similar to *Jag1* mutants, *Notch2* mediated functions are essential for lens development and differentiation (Saravanamuthu et al., 2012).

4.6 Conclusions

Congenital eye malformations that lead to anophthalmia (no eye), microphthalmia (small eye) (anophthalmia or microphthalmia are seen in 1-3 live births per 10,000), aniridia (absent or partial iris), and congenital cataracts (1-6 per 10,000 births) adversely affect the sight of approximately 1.4 million children of the world population (http://www.who.int/blindness/causes/priority/en/index3.html). According to the latest assessment by the World Health Organization (WHO), cataract is responsible for 51% cases of world blindness affecting 20 million people worldwide (http://www.who.int/blindness/causes/priority/en/index1.html). Recent advances in molecular genetic techniques have led to the identification of various signaling pathways, hierarchy of transcription factors and complex patterns of gene expression required during the early embryonic eye development. These findings have contributed immensely to our understanding of eye diseases, accurate diagnosis and improved therapeutic strategies.

Prior to our studies it was unknown whether *Ehd1* gene has a role in ocular development. A previous study from our group first reported the presence of ocular phenotypes in *Ehd1-null* mice but did not describe these phenotypes in detail (Rainey et al., 2010). In Chapter 3 of this thesis, I have characterized the *Ehd1* null mouse model to decipher functional roles of EHD1 in eye development, and have provided evidence to support its role in the process mammalian lens development. The germ-line deletion model,

together with the lens-specific deletion model, I have established could potentially serve as a unique model to investigate the lens morphogenesis, pathogenesis of cataracts and screen for drugs to slow or prevent cataractogenesis.

Chapter 2: Materials and Methods

5.1. Materials & Methods for experiments in Chapter 3

5.1.1. Mouse models and genotyping

Ehd1$^{flox/flox}$ mice, carrying the floxed *Ehd1* allele in which exon 1 is flanked by loxP sites, and germline knockout mice (*Ehd1-null*) derived from *Ehd1*$^{flox/flox}$ mice have been described previously (Rainey et al., 2010). *Ehd1-null* mice were maintained on mixed 129;B6 background. Single nucleotide polymorphism (SNP) analysis (DartMouse, Lebanon, NH) revealed these to have ~70% contribution from the C57Bl/6 genome (Figure 2.1). *Ehd1-WT* (wild type), *Ehd1-het* (heterozygous), and *Ehd1-null* (homozygous null) mice were generated by mating *Ehd1-het* mice. Breeders were maintained on high-fat chow (# 2019, Harlan Laboratories Inc., Madison, WI). Genomic DNA was extracted from embryonic yolk sacs or adult tail tips with proteinase K digestion, isopropanol precipitation and used for genotyping as described previously (Rainey et al., 2010). To conditionally delete *Ehd1* in the lens, *Ehd1*$^{flox/flox}$ mice (backcrossed more than 6 generations into C57BL/6J, and 98% C57Bl/6 by DartMouse SNP typing) were crossed with *Le-Cre* transgenic mice (maintained in a hemizygous manner on an FVB/N background), which expresses Cre recombinase from a Pax6 promoter active in the lens-forming ectoderm by day E9.0 (Ashery-Padan et al., 2000). Subsequent back-cross to *Ehd1*$^{flox/flox}$ mice generated the *Ehd1*$^{flox/flox}$*;Le-Cre* genotype referred to as conditional knockout (CKO) mice. *Ehd1*$^{flox/flox}$ mice without the *Le-Cre* served as controls. To confirm *Le-Cre*-mediated deletion in the lens, genomic DNA samples were isolated from P0/P1 micro-dissected lenses from control and test pups and subjected to PCR analysis using *Ehd1*-specific primer pairs as described previously (Rainey et al., 2010). Embryos/mice were genotyped for the presence of *Le-Cre* transgene using the primer set 5'-GCATTACCGGTCGATGCAACGAGTGATGAG-3' and 5'-GAGTGAACGAACCTGGTCGAAATCAGTGCG-3'. All animal studies were approved by the Institutional Animal Care and Use Committee (# 07-061-FC12). Animals were treated

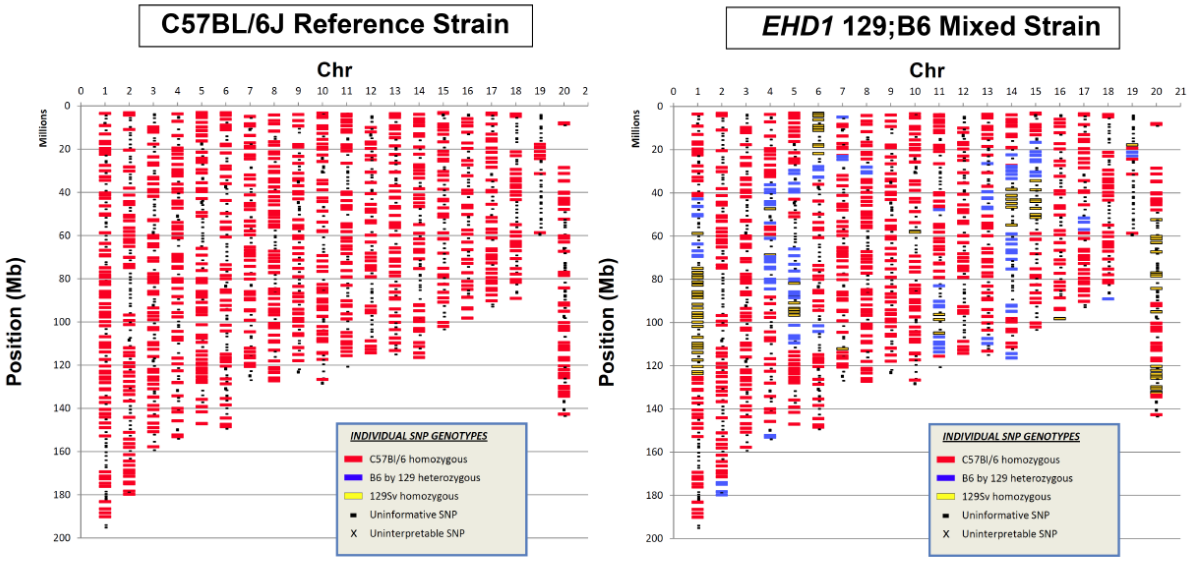

Figure 2.1 Genotyping analysis of EHD1 WT and Null 129;B6 mice in comparison to the Jackson Laboratory C57BL/6J reference strain was carried out by DartMouse, Lebanon, NH using 1449 SNP Illumina bead Chip. Each SNP output is color coded, e.g red represents C57Bl/6, blue represents heterozygous (B6 x 129), and yellow represents 129Sv. All analyzed mice (WT or *Ehd1-null*) correspond to approximately mid-70% C57BL/6 background.

humanely in accordance with the University of Nebraska Medical Center and the National Institute of Health (NIH) guidelines for the Care and the Use of Laboratory Animals.

5.1.2. Histology and Immunohistochemistry

For timed-pregnancy experiments, matings were set up in the evenings, and vaginal plugs were detected the following morning. The noon of the day of vaginal plug detection was considered E0.5. Pregnant dams were euthanized by CO_2 asphyxiation at the indicated time points and embryos were removed by hysterectomy. Embryonic yolk sacs were collected and used for genotyping, as described above. Embryos were fixed at 4°C in 10% neutral-buffered formalin (NBF) for 3 to 12 hours, transferred to 70% ethanol prior to paraffin embedding and sectioned at 4-6 μm. Sections were stained with hematoxylin and eosin (H&E), and micrographs were captured using a Leica microscope or with an iScan Coreo Slide Scanner of the iScan Image Viewer (Roche) (at a resolution of 0.2325 micron per pixel) at the UNMC Tissue Sciences Facility. The total lens epithelial cell count was determined by counting hematoxylin-stained nuclei from serial sections of WT or *Ehd1 CKO* embryonic lenses using ImageJ software. Briefly, a line was drawn on 40x sagittal sections to demarcate the equatorial region where epithelial cells began to elongate and epithelial cells within this region were counted.

The following mouse monoclonal antibodies were used in immunofluorescence (IF) staining: anti-γ-Tubulin Clone GTU-88 (T5326; Sigma-Aldrich Corp, St. Louis, MO), anti-ZO-1 (1A12) (339100; Invitrogen, Camarillo, CA), anti-Bromodeoxyuridine (BrdU) Clone Bu20a (M0744; Dako, Carpinteria, CA), anti-α-Catenin (610193), anti-N-Cadherin (610920), anti-β-Catenin (610153) and anti-E-cadherin (610181) (all from BD-Transduction laboratories, Franklin Lakes, NJ). Rabbit polyclonal or monoclonal antibodies used were: anti-GFP (2555, Cell Signaling Technology, Beverly, MA), anti-Pax6 (PRB-278P; Covance, Princeton, NJ), anti-Pax-2 (71-6000; Invitrogen, Camarillo, CA), anti-keratin 12 (KAL-KR074, TransGenic

Inc; Japan); anti-Prox1 (AB5475) and anti-Sox2 (AB5603) (from Millipore Corp., Massachusetts, MA); anti-γ-crystallin (a gift from Dr. Samuel Zigler, The Johns Hopkins University, School of Medicine, Baltimore, MD)(Russell et al., 1984); anti-alpha A Crystallin (ab5595) (Abcam Inc., Cambridge, MA); anti-β-crystallin (FL-252) (sc-22745; Santa Cruz Biotechnology, Dallas, Texas). Affinity-purified rabbit polyclonal anti-EHD1, rabbit anti-EHD2, anti-EHD3 and anti-EHD4 antisera were generated as described previously (George et al., 2007; George et al., 2010; George et al., 2011; Gudmundsson et al., 2010; Mate et al., 2012; Rainey et al., 2010).

For antibody staining, rehydrated tissue sections were boiled in antigen unmasking solution (H-3300, Vector Laboratories, Burlingame, CA) in a microwave for 20 min, slides were cooled, washed once in PBS, and blocked in heat-inactivated 10% Fetal Bovine Serum (SH30910.03, HyClone Laboratories, Logan, UT) for one hour at room temperature (RT). Primary antibodies diluted in blocking buffer were added overnight at 4°C (except EHD antibody staining, which was done at RT for an hour), slides were washed 3 times with PBS followed by incubation with Alexa Fluor 488 or 594-conjugated donkey anti-rabbit or anti-mouse secondary antibodies (1:200; Invitrogen, Carlsbad, CA) for one hour at RT in the dark. For negative controls, sections were incubated in the blocking buffer without the primary antibody. Nuclei were visualized with DAPI in antifade mounting medium (ProLong® Gold Antifade mountant, Invitrogen, Carlsbad, CA). Fluorescent images were captured on a Zeiss LSM-710 confocal microscope. Tiled images under 20x and 40x objectives were captured for embryonic eyes with 10% overlap and processed using the Zeiss Zen 2010 stitching software to merge into a single image. Images were processed using Adobe Photoshop CC software. For presentation, signal intensities were adjusted equally for brightness and contrast between control and test images.

5.1.3. BrdU and TUNEL labeling

Pregnant dams were injected intraperitoneally with 150 mg/kg of body weight of 10 mg/ml BrdU (5-bromo-2'-deoxyuridine) (Sigma-Aldrich, St. Louis, MO) and 1 mg/ml 5FU (5-fluoro-5'-deoxyuridine) (Sigma-Aldrich, St. Louis, MO) and sacrificed an hour later. Staining was performed on paraffin-embedded serial sections of embryo eyes using mouse anti-BrdU antibody. Images were captured with MagnaFire imaging software using Nikon Eclipse E600 Fluorescent microscope fitted with an Optronics camera. Cell proliferation was quantified by calculating the percentage of nuclei that were BrdU positive in a given section.

Terminal deoxynucleotidyl transferase (TdT)-mediated deoxyuridine triphosphate nick end labeling (TUNEL) assay, was performed on deparaffinized sections according to the manufacturer's instructions (Roche, Indianapolis, IN). Label solution without TdT was used as a negative control. Sections treated with DNase I (3 U/ml), to induce DNA strand breaks, served as positive controls. Slides were mounted with ProLong® mounting medium. TUNEL-positive cells were detected and quantified as with BrdU staining.

5.1.4. Statistical analysis

Serial sections from a minimum of four different embryos from at least three litters per time point were analyzed (N, number of embryos). Unpaired Student's t-test was used to analyze the significance of differences between experimental groups. Data are presented as mean ± standard error of the mean with $P \leq 0.05$ deemed significant.

5.2. Materials & Methods for studies described in Chapter 4

5.2.1. Bioinformatics analysis and peptide library synthesis

Sequence motifs that could predict potential interaction partners of EH domains of the Eps 15 homology domain containing (EHD) proteins were designed by expanding on

motifs characterized in previous studies (de Beer et al., 2000). In total, 99 different sequence combinations were used as query motifs, where the core sequence was one of the following: aspartate-proline-phenylalanine (DPF), glycine-proline-phenylalanine (GPF) or asparagine-proline-phenylalanine (NPF). The core motifs were extended by including aspartate, glutamate, serine or lysine residues at the +1, +2, +3 and +4 positions, to yield permutations of D/G/N-P-F-D/E/S/K-D/E/S/K-D/E/S/K-D/E/S/K, substituting a single amino acid residue at a time. Using this *in silico* approach we generated a query set of 99 potential motifs (Table 2.1). The entire human proteome representing verified non-redundant protein entries were queried using UniProt knowledgebase (UniProtKB)/Swiss-Prot database. The search identified 2793 distinct proteins as potential binding partners containing one or more motifs corresponding to various search sequences (Appendix A). Of these, 403 proteins contained multiple (at least two) motifs. Within this short list of 403 candidate proteins, we used search parameters to remove the majority of secreted proteins, and extracellular or trans-membrane regions of transmembrane proteins. The subcellular location of proteins was predicted using the ngLOC tool (King et al., 2012). Following this, the identified proteins were functionally classified using the Kyoto Encyclopedia of Genes and Genomes (KEGG) pathway analysis for the most relevant processes such as vesicular trafficking, membrane transport, actin cytoskeleton, and developmental pathways including Dorso-ventral axis formation, Axon guidance. The final set of proteins was short-listed based on their functional relevance and the presence of two or more motifs. The motifs that were C-terminal and ended before the +6 sequence were eliminated. Repeated motif sequences identified in different proteins were also excluded. The resulting list included 137 candidate proteins, of which eight are known EHD1 interactor partners (Naslavsky and Caplan, 2011)(Appendix B). A library of 9-mer peptides corresponding to individual motifs within these proteins was generated by peptide synthesis, as described below.

DPF motifs	GPF motifs	NPF motifs
DPFDDDD	GPFDDDD	NPFDDDD
DPFDDDE	GPFDDDE	NPFDDDE
DPFDDED	GPFDDED	NPFDDED
DPFDDEE	GPFDDEE	NPFDDEE
DPFDEDD	GPFDEDD	NPFDEDD
DPFDEDE	GPFDEDE	NPFDEDE
DPFDEED	GPFDEED	NPFDEED
DPFDEEE	GPFDEEE	NPFDEEE
DPFEDDD	GPFEDDD	NPFEDDD
DPFEDDE	GPFEDDE	NPFEDDE
DPFEDED	GPFEDED	NPFEDED
DPFEDEE	GPFEDEE	NPFEDEE
DPFEEDD	GPFEEDD	NPFEEDD
DPFEEDE	GPFEEDE	NPFEEDE
DPFEEED	GPFEEED	NPFEEED
DPFEEEE	GPFEEEE	NPFEEEE
DPFKKKK	GPFKKKK	NPFKKKK
DPFKKKS	GPFKKKS	NPFKKKS
DPFKKSK	GPFKKSK	NPFKKSK
DPFKKSS	GPFKKSS	NPFKKSS
DPFKSKK	GPFKSKK	NPFKSKK
DPFKSKS	GPFKSKS	NPFKSKS
DPFKSSK	GPFKSSK	NPFKSSK
DPFKSSS	GPFKSSS	NPFKSSS
DPFSKKK	GPFSKKK	NPFSKKK
DPFSKKS	GPFSKKS	NPFSKKS
DPFSKSK	GPFSKSK	NPFSKSK
DPFSKSS	GPFSKSS	NPFSKSS
DPFSSKK	GPFSSKK	NPFSSKK
DPFSSKS	GPFSSKS	NPFSSKS
DPFSSSK	GPFSSSK	NPFSSSK
DPFSSSS	GPFSSSS	NPFSSSS

Table 2.1 List of extended interaction motifs for EHD proteins. 99 motifs were generated in different combinations, where the primary sequence of interest was one of the following: aspartate-proline-phenylalanine (DPF), glycine-proline-phenylalanine (GPF), or asparagine-proline-phenylalanine (NPF). The primary motifs were extended by adding either aspartate (D)/glutamate(E) or serine(S)/lysine(K) amino acids at the +1, +2, +3 and +4 positions, such that the length of the motif can now be extended to seven amino acids. Only a single amino acid residue was changed at a time to create an extended arm of the motif.

Peptide sequences FITC-βA-NPFEEEEED-[OH] (referred to as NPF1), –[H]-G-NPFEEEEED-[OH] (referred to as NPF2), and -[H]-G-APAEEEEED-[OH] (referred to as APA3) (Table 2.2) were synthesized and purified by the Tufts University peptide synthesis Core facility, Boston, MA, and used to establish the binding and competition assays. The unlabeled peptide library consisting of 333 (9-mer) peptides was synthesized by ChinaPeptides Co., Ltd. (Shanghai, China). All peptides were purified to ≥ 95% purity by high-performance liquid chromatography (HPLC) and confirmed by MassSpec analysis (Appendix C). The peptides were dissolved in dimethyl sulfoxide (DMSO) to prepare stock solutions.

5.2.2. Constructs

GFP-Rabenosyn-5 (#37538), pcDNA5 DNAJA2-GFP (#19492) and pGEX6P1-EHD1-438-534 (#36459) (referred to as EH1-A) (Table 2.3) constructs were obtained from Addgene (Cambridge, MA). The sequence encoding the EH-domain (residues 400-535) of human EHD1 (referred to as EH1-B) (Table 2.3) was polymerase chain reaction (PCR) amplified from the pGEX4T2-EHD1 full-length vector using the primer pairs, EH1-ERIF: 5'-TCGCCCGGAATTCTCGGTGTGGAGGAGTCCCTG-3' & EH1-XHOR1: 5'-CGATGCGGCCGCTCGAGTTCACTCATGTCTGCG-3', purified using the illustraGFX PCR DNA and Gel Band purification kit (28-9034-70, GE Healthcare Life Sciences, Pittsburgh, PA), restriction-digested with EcoR1 (R3101S) and Xho1 (R0146S) enzymes (New England BioLabs Inc., Ipswich, MA) and gel-purified followed by sub-cloning into the bacterial expression vector pGEX4T2 (28-9545-50, GE Healthcare Life Sciences, Pittsburgh, PA). Positive clones were selected based on their ability to code for a GST fusion protein of the expected size and sequence verified using the primer set pGEXFwd: 5'-CCGGGAGCTGCATGTGTCAGAGG-3' and pGEXRev: 5'-GGGCTGGCAAGCCACGTTTGGTG-3' at the UNMC sequencing core. Full-length

pGEX4T2-EHD1 plasmid was subjected to site directed mutagenesis to mutate Tryptophan 485 residue into Alanine (W485A) by using QuickChange site-directed mutagenesis kit (Stratagene, La Jolla, CA). Subsequently, the sequences within this construct encoding the EHD1 EH domain (amino acids 400-535) with a W485A mutation (referred to as EH1-B-W485A) (Table 2.3) were sub-cloned into pGEX4T2 vector, as described above.

5.2.3. Protein expression and purification

Bacteria were grown overnight in a starter culture at 37°C with 250 rpm. The following morning, the cultures were diluted at a 1:10 ratio and incubated in a shaker incubator until the A_{600} reached 0.6-0.8. At this point, 1mM isopropyl 1-thio-β-D-galactopyranoside (IPTG) (I2481C100, Gold BioTechnology, Inc., St. Louis, MO) was added and cultures were grown for another 4 hours. The bacteria were pelleted at 3500 g for 20 min at 4^{o}C. The pellet was resuspended in 50 mM Tris, pH 7.5 containing 2mg/ml Lysozyme, 150 mM NaCl, 0.5% Triton X-100, 1mM dithiothreitol (DTT) and 1mM phenylmethylsulfonyl fluoride (PMSF). Cells were sonicated using a probe sonicator (Sonic Dismembrator, Model 100, Fisher Scientific) at a pulse setting of 8, twice for 30 sec each. Bacterial lysate was spun down at 25,000 rpm at 4°C for 30 min. The supernatant was incubated with glutathione sepharose 4B beads (17-0756-01, GE Healthcare Life Sciences, Pittsburgh, PA) for 2 h in a rotary shaker at 4°C. Glutathione beads were washed 3 times with buffer containing 20 mM HEPES, pH 7.6, 150 mM NaCl, 1mM DTT, and 1 mM PMSF and then transferred to a poly-prep chromatography column (731-1550, Bio-Rad, Hercules, CA). Proteins were eluted with 10 mM reduced glutathione in 50 mM Tris, pH 7.5. Purified proteins were dialyzed for a minimum of 4 hours using 10 KDa cut off Slide-A-Lyzer dialysis cassette (66810, Thermo Scientific, Rockford, IL) against the dialysis buffer (20mM HEPES, pH 7.6; 50 mM NaCl, 1mM DTT). Dialyzed proteins were quantified using Pierce BCA Protein Assay (23225, Thermo Scientific, Rockford, IL) and stored at -80 degrees with 10%

Peptide	Sequence	Label
NPF1	FITC-βA-NPFEEEEED-[OH]	FITC
NPF2	-[H]-G-NPFEEEEED-[OH]	None
APA3	-[H]-G-APAEEEEED-[OH]	None

Note: FITC, Fluorescein isothiocyanate

Table 2.2 Peptides used in the study

Construct	Sequence	Vector
EH1-A	EHD1-438-534	pGEX6P1
EH1-B	EHD1-400-535	pGEX4T2
EH1-B-W485A	EHD1-400-535	pGEX4T2

Table 2.3 EH domain constructs used in the study

glycerol added. Purified GST-fusion proteins were run on 10% SDS PAGE and stained with Commassie brilliant blue to visualize protein bands.

5.2.4. Fluorescence Polarization (FP) assays

All FP measurements were performed in 384-well, low-volume, black round-bottom polystyrene NBS microplates (Corning). For each reaction, the total volume was set at 20 µl and the assay buffer consisted of 1X PBS. The polarization values were measured at an excitation wavelength of 485 nm and emission wavelength of 583 nm using a Spectramax M5 plate reader (Molecular Devices, Sunnyvale, CA). The plates were incubated at room temperature and FP was measured at 5, 15, 30, and 60 min after the addition of the fluorescent peptide probe. No difference in the data values was detected between 5 and 60 min. The 5 min data points were fitted and IC_{50} values were estimated using standard non-linear regression on SigmaPlot 11.0.

5.2.5. Fluorescence polarization binding assays and K_d value estimation

To each well, 10 µl of 100 nM FITC labeled NPF1 peptide and 10 µl of increasing concentrations of GST fusion proteins of the EH domain of EHD1, EH1-A, EH1-B or EH1-B W485A (~9 nM - 130 µM) in assay buffer consisting of 1X PBS were added. GST alone (purified from pGEX4T2 vector) was used as a control. The assay plates were read as described above. The K_d values were derived from first principles, and calculated using non-linear regression on SigmaPlot 11.0.

5.2.6. Fluorescence polarization competition assays and K_i value determination

To each well, 5 µl of increasing concentrations of unlabeled NPF2 or APA3 peptides (0-500 µM) and 15 µl of EH1-A, EH1-B, EH1-B W485A or GST proteins (at a final concentration of 10 µM) together with FITC-NPF1 (at a final concentration of 100 nM) were

added. The assay plates were read as described above. The K_i values for peptide competition were determined using the Coleska-Wang equation (Nikolovska-Coleska et al., 2004).

5.2.7. Assay development and optimization for high-throughput screening

DMSO Tolerance: Increasing concentrations of DMSO (0, 2.5%, 5%, 10%, 20%) were added to each well to obtain a final concentration of 10 µM GST-EH1 and 100 nM of FITC-NPF1. Total fluorescence and FP measurements were carried out immediately after setting-up the reaction. No deviation in fluorescence signal was observed for up to 10% DMSO concentrations (Figure 4.6, Chapter 4) and a final concentration of 5% DMSO was selected for the screen.

Peptide library plate setup: The 333 lyophilized peptides in the EHD interaction peptide library were individually dissolved in DMSO at a concentration of 100 mM. Subsequently, 100 µl working stocks of 15 mM concentration of each peptide were added from A2- H11 (for a total of 80 peptides) to individual wells of a 96-well plate (Master plate) (Figure 2.2). The first column consisted of 100 µl of 15 mM concentration of FITC-NPF1 peptide. The last column consisted of only DMSO. From this master plate, 25 µl per well (including NPF1 and DMSO) was transferred sequentially using a Biomek FX liquid handling system to create four daughter plates. One plate (Test plate) was used for the assay and rest of the plates were sealed and stored at -80°C. A 6 µl aliquot of each peptide was transferred from the test plate to fill each quadrant of a 384-well plate resulting in four peptide well replicates per plate. Serial dilution of peptides was carried out to obtain a range of final peptide concentrations between 500 µM and 7.75 µM in 5% DMSO/PBS. Subsequently, master mix containing 10 µM EH1-A protein together with 100 nM FITC-NPF1 was added to each

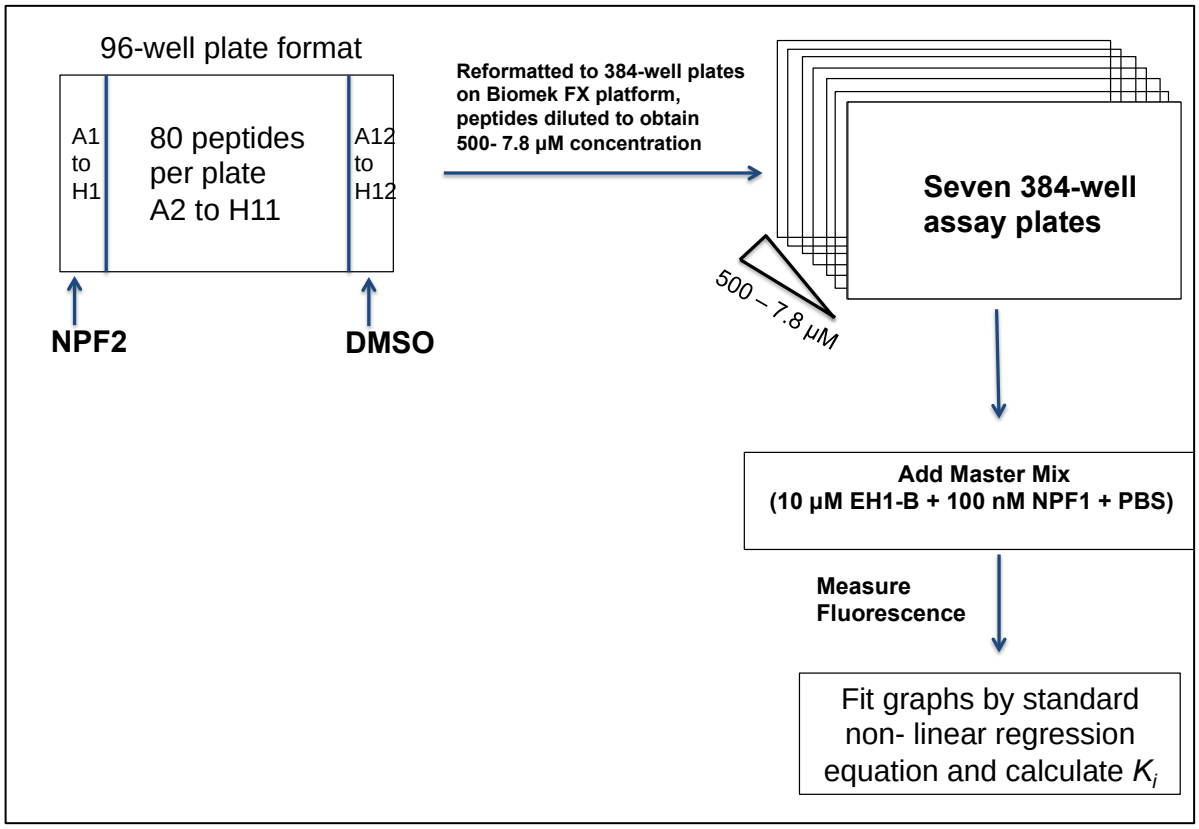

Figure 2.2 Schematic describing qHTS assay design.

diluted peptide plate. Total fluorescence and FP measurements were carried out immediately after setting-up the reaction.

5.2.8. Computational analysis

Three crystal structures of EHD1 in complex with peptides (pdb ids; 2KFF, 2KFG, 2KFH) were obtained from the Protein Data Bank (Jovic, 2009). These structures were imported into Molegro Virtual Docker and the peptide-binding cavity was identified using the software's built-in ray tracer. Each peptide was docked to the target molecule five times, using 3000 genetic algorithm iterations to account for the large size of the ligands. The PLANTS scoring function was used because it is optimized for docking peptides. Peptides were rank-ordered by Molegro re-rank score.

5.2.9. Cell lines and transfection methods

Human embryonic kidney (HEK) 293 cells were maintained in Dulbecco's Modified Eagle Medium (DMEM) (11965-092, Gibco/Life Technologies, Grand Island, NY) supplemented with 10% fetal bovine serum (10437-028, Gibco/Life Technologies, Grand Island, NY). Cells were seeded at a density of 1 X 10^6 per P100 plate for 12 hours, transfected with 5 µg plasmid DNA for 6 hours using the calcium phosphate (Sigma-Aldrich, St. Louis, MO) co-precipitation method. Cells were washed and fresh media was added. Cell lysates were prepared after 60 hours.

5.2.10. Antibodies and other reagents

The following antibodies were used in this study: rabbit anti-green fluorescence protein (GFP) (2555, Cell Signaling Technology, Beverly, MA). Affinity-purified rabbit polyclonal anti-EHD1, and rabbit anti-EHD2, anti-EHD3 and anti-EHD4 antisera were used as described previously (Rainey et al., 2010).

5.2.11. Immunoblotting and pull-down assays

For Immunoprecipitation, HEK293 cells were transiently transfected with different GFP-tagged constructs in P100 dishes. Cells were grown for additional 60 h, harvested and lysed overnight at 4°C in 1 ml/plate lysis buffer containing 50 mM Tris, pH 7.5, 150 mM NaCl, 0.5% Triton X-100 (wt/vol), 1mM sodium orthovanadate, 10mM sodium fluoride and 0.5 mM PMSF. Cell lysate was centrifuged at 14,000 rpm to pellet the insoluble material and protein concentration was determined by using the BCA reagent according to the manufacturer's directions. One milligram of total cell lysate protein was incubated with 30 ug of GST-EH1 proteins bound to glutathione beads. After 3 h incubation at 4°C, the beads were washed six times in lysis buffer (described above) and bound proteins eluted in boiling SDS-Laemmli sample buffer. Proteins were separated by 9% SDS-PAGE, transferred to PVDF membranes (IPVH00010, Miilipore, Billerica, MA) and immunoblotted with an anti-GFP antibody overnight at 4°C. Bound antibodies were visualized with horseradish peroxidase (HRP)-conjugated protein A (10-1023, Life Technologies, Grand Island, NY) using the ECL detection system (PI-32106, Thermo Scientific, Rockford, IL).

5.2.12. Yeast two-hybrid screen

Y2H screen was carried out by Proteinlinks, San Diego, CA. 0.36×10^7 and 0.8×10^7 Hela cDNA clones were screened in separate two screens. Four verified clones were confirmed from twelve initially positive clones ($URA3^+LacZ^+$). The verified clones were sequenced using the primer set: 5'-GGTTTTCATGAAATTGAAGCGGATG-3' and 5'-CTTTTCGTAAATTTCTGGCAAGGTAG-3'.

Chapter 3: EHD1 is required for ocular lens development

6. Introduction

Endocytic traffic represents a fundamental cellular process conserved in most eukaryotes (Maxfield and McGraw, 2004). Cell biological studies have demonstrated that cell surface receptors as well as membrane lipids are constantly internalized at rates determined by cellular activities such as uptake of nutrients, stimulation by extracellular ligands as well as uptake of particulate materials (B. D. Grant and Donaldson, 2009). Internalized receptors may be targeted for degradation in the lysosomes, often depending on the stimulating ligands, or recycled back to the cell surface together with membrane lipid components. The process of endocytic recycling is also used adaptively to orchestrate trans-cellular transport processes and selective localization of surface lipids and receptors to specific membrane domains in polarized cells (Scita and Di Fiore, 2010). The recycling pathway also appears to play an important role in a variety of other cell biological processes such as membrane repair, cytokinesis (Montagnac et al., 2008), cell migration (Jones et al., 2006) and developmental patterning (Bokel and Brand, 2014).

C-terminal Eps15 homology domain-containing (EHD) proteins are a recently described family of endocytic recycling regulatory proteins (B. D. Grant and Caplan, 2008). The role of EHD proteins in endocytic traffic was first revealed through identification of *rme-1* (*receptor-mediated endocytosis 1*) mutant in *C. elegans*, which impaired the yolk protein transport across the intestinal epithelium into coelom (Lin et al., 2001). Cell biological studies demonstrated that RME-1 as well as a human ortholog EHD1 localized to an endocytic recycling compartment and EHD function was required for transferrin recycling and retrograde transport of a reporter protein to the trans-Golgi network(George et al., 2007; B. Grant et al., 2001; Lin et al., 2001). Mammals express four highly homologous EHD proteins (EHD1-4). EHD1 has been most extensively studied in cellular models and shown to be required for endocytic recycling of a number of other cell surface receptors, including transferrin receptor (Lin et al., 2001), MHC-I (Caplan et al., 2002b), MHC-II molecules

(Walseng et al., 2008), β1-integrin (Scheiblin et al., 2014) and GLUT4 glucose transporter (Guilherme et al., 2004).

All four EHD proteins contain an N-terminal ATPase/GTPase domain that controls membrane binding and oligomerization, a central coiled-coiled domain that mediates homo- and hetero-oligomerization, and a characteristic C-terminal EH domain that mediates interactions with proteins containing Asn-Pro-Phe (NPF) or related tri-peptide motifs (de Beer et al., 2000; B. D. Grant and Caplan, 2008; Kieken et al., 2007; Kieken et al., 2010). Biochemically, EHD proteins are thought to facilitate membrane tubulation and scission to facilitate vesicle budding and transport in the recycling pathway (Daumke et al., 2007). Crystal structure of EHD2 revealed it to be a dimer and it is presumed that other family members adopt a similar conformation (Daumke et al., 2007). EHD proteins form homo- or hetero-dimers, thought to facilitate EHD function (Daumke et al., 2007; Lee et al., 2005; Naslavsky and Caplan, 2011). Consistent with their structural relatedness, reconstitution of rme-1 mutant worms with each of the four human EHD proteins led to restoration of function (George et al., 2007).

In vitro studies have suggested that EHD3 and EHD4 mediate early steps of membrane-associated receptor recycling whereas EHD1 and EHD2 regulate later steps (George et al., 2007; Sharma et al., 2008). Several lines of evidence point to unique functional roles of individual EHD proteins, despite their structural similarities. EHD protein expression in mammalian tissues shows discrete patterns and distinct family members predominate within the different cell types found in complex tissues. Loss of one family member can trigger compensatory increase of another, but this too appears to differ with cell/tissue compartments (George et al., 2011; Rainey et al., 2010). Biochemical studies also indicate that individual EHD proteins may preferentially dimerize with distinct family members (Lee et al., 2005). Thus, it is likely that individual EHD proteins serve distinct physiological roles despite their shared biochemical mechanisms.

In order to define the biological roles of mammalian EHD family proteins, we and others have generated mouse gene deletion models. These models reveal unique as well as redundant roles of EHD proteins in vivo. *EHD1* deletion exhibits a strain-dependent phenotype. *Ehd1* mutant mice on 129Sv/Ev or Swiss Webster background appeared normal (Rapaport et al., 2006). In contrast, *Ehd1-null* mice on a mixed 129/B6 background exhibit pre-natal lethality, reduced size and male infertility (Rainey et al., 2010). Further studies indicated that *Ehd1-null* mice exhibit smaller muscle fibers, consistent with a role of EHD1 in myocytes proliferation and fusion (Posey et al., 2014).

Deletion of *Ehd3* or *Ehd4* has no apparent impact on prenatal mouse development but *Ehd4–null* male mice exhibited smaller testes and reduced fertility (George et al., 2010; George et al., 2011). Further studies of *Ehd3-null* mice have revealed cardiac abnormalities including arrhythmias and blunted response to adrenergic stimulation together, with reduced expression of Na/Ca exchanger (NCX1), L-type Ca-channel type 1.2 ($Ca_v1.2$) and associated functions (Curran et al., 2014; Gudmundsson et al., 2010). Notably, mice with combined *Ehd3* and *Ehd4* resulted in high pre- and peri-natal mortality, with surviving animals exhibiting severe renal thrombotic microangiopathy and death due to renal failure (George et al., 2011). These initial studies support the approach of using knockout models to define specific as well as redundant biological roles of the EHD family of endocytic regulators.

Previously, we noted that *Ehd1-null* mice on 129/B6 background exhibited ocular abnormalities, but these were not characterized in any detail (Rainey et al., 2010). Here, I provide evidence that EHD1 is required for the development of ocular lens and cornea. My studies show that *Ehd1-null* mice display pleiotropic ocular phenotypes, including anophthalmia, aphakia, microphthalmia and congenital cataracts. Importantly, conditional deletion of *Ehd1* in the presumptive lens ectodermal cells recapitulated the lenticular phenotypes observed in *Ehd1-null* mice, and also resulted in corneal endothelial

differentiation defects. The ocular phenotypes caused by the loss of a single regulator of endocytic recycling, *Ehd1,* provides a novel model system to elucidate mechanistic links between surface receptor recycling and control of cellular processes that ensure orderly development of the compartments of mammalian eye.

7. Results:

7.1 *Ehd1-null* mice exhibit ocular abnormalities

As described previously (Rainey et al., 2010) , *Ehd1-null* mice on a mixed 129/B6 background are born at sub-Mendelian ratios and males were infertile due to defects in spermatogenesis. Close examination of adult *Ehd1-null* mice revealed a range of ocular defects, including microphthalmia, congenital cataracts, and anophthalmia (Figure 3.1A, panels b-d) that were not seen in wildtype control mice (Figure 3.1A, panel a). Approximately 56% of individual eyes in adult (6 weeks or older) *Ehd1-null* mice displayed these defects, with cataracts being the most common defect (Table 3.1). To assess whether ocular defects were present in *Ehd1-null* mice during embryonic ocular development, WT and *Ehd1-null* embryos were collected between embryonic (E) days E10.5-E18.5 and eye and lens morphologies were analyzed. Visual examination of whole embryos at E14.5 revealed pleiotropic ocular defects in *Ehd1-null* embryos (Figure 3.1A, panels f-h, arrowheads), similar to those seen in adult mice, but not in wildtype controls (Fig 3.1A, panel e, arrow). Hematoxylin and eosin (H&E) staining of sections of embryonic ocular tissues revealed defects in *Ehd1-null* embryos as early as E10.5. At this age, the lens pit appeared smaller and misshapen (Figure 3.1B, panels b & c, arrowheads) compared to wildtype controls (Figure 3.1B, panel a, arrows). Histological analysis of E12.5, E14.5, and E16.5 embryos also revealed smaller lenses, and frequent persistence of the lens stalk (Figure 3.1B, panels e, e', h, h', k arrowheads) and hyaloid vasculature (Figure 3.1B, panels h, k open arrowheads) (42.8% of embryos analyzed) (n=21). In the remaining *Ehd1-null* embryos (57.1%), the lens was absent (aphakia) and the retina misfolded (Figure 3.1B, panels f, f', i, i', l, see asterisk) in contrast to controls (Figure 3.1B, panels d, d', g, g', j) (n=26). Persistent lens stalk and hyaloid vasculature was also seen in some of the *Ehd1-het* embryos (Figure 3.3). At post-natal day 10 (P10), control eyes consisted of a well-formed lens with an

overlying cornea and a laminated retina (Figure 3.1B, panels m, m'). In contrast, *Ehd1-null* mice of the same age exhibited eyes phenotypes ranging from a near normal lens, cornea and retina (Figure 3.1B, panels n, n') to absent lens and misfolded retina (Figure 3.1B, panel o, o', see asterisk). Together, these results indicated that EHD1 is necessary for proper differentiation of ocular tissues including the lens, cornea and retina. In this report, I have focused on the impact of *Ehd1* deletion on lens and corneal development. The effects of *Ehd1* loss on retinal development will be described separately.

7.2 EHD1 is expressed in the developing eye

I carried out immunofluorescence studies to assess endogenous expression of EHD1 protein in ocular tissues. EHD1 expression was localized in the apical junctions of epithelial cells lining the lens pit, and in the underlying optic vesicle at E10.5 (Figure 3.3A); EHD1 staining partly colocalized with the adherens junctional marker, E-cadherin (Figure 3.3B), as seen in merged images (Figure 3.3C, arrows). At E12.5, EHD1 was localized to the sub-membranous region of epithelial cells in the lens vesicle, especially under the apical surface (Figure 3.3G, I). At E14.5, EHD1 expression was seen in the lens epithelial and fiber cells, the peri-ocular mesenchymal cells that would form the future corneal stroma and endothelial layers (Figure 3.3M, O). Expression of EHD1 was detectable in the lens, corneal and conjunctival epithelial cells at E16.5 (Figure 3.3U, W). In late postnatal eyes, EHD1 was also expressed in the ganglion cell layer and the outer and inner nuclear layers of the neural retina (data not shown), consistent with a previous report (Rapaport et al., 2006). Loss of EHD1 expression in *Ehd1-null* embryos was confirmed by immunofluorescence (Figure 3.3D, F, J, L, P, R, X, Z, arrowheads). These results correlated the ocular phenotypes seen in *Ehd1-null* embryos with loss of EHD1 expression in these tissues.

Our previous studies have demonstrated that deletion of individual EHD family members often results in the up-regulation of other family members in various organ

systems compensating for the loss of function of the deleted gene (George et al., 2010; George et al., 2011; Gudmundsson et al., 2010; Rainey et al., 2010). To assess if the loss of EHD1 expression in ocular tissues led to up-regulation of expression of other EHD proteins, I examined the expression levels of EHD2, EHD3 and EHD4 in ocular tissues of *Ehd1-null* and WT mice. At E12.5, the highest EHD2 expression within the eye was seen in the surface ectoderm (Figure 3.4A, arrows), blood vessels in the vitreous (Figure 3.4A, arrows), and in RPE cells surrounding the neural retina in WT (not shown) as well as in *Ehd1-null* embryos (Figure 3.4B arrowheads). At E16.5, EHD2 was expression was observed in the corneal and eyelid epithelium (Figure 3.4C, arrows) in WT and *Ehd1-null* eyes (Figure 3.4D, arrowheads). Ubiquitous expression of EHD3 and EHD4 was seen in all ocular tissues at E12.5 and at E16.5 (Figure 3.4E, G and I, K, arrows). EHD2 and EHD3 expression in *Ehd1-null* ocular tissues remained unaltered (Figure 3.4F, H and J, L, arrowheads). EHD4 expression, though unaltered in the *Ehd1-null* embryos at E12.5 (Figure 3.4J), was reduced in the lens epithelial cells (Figure 3.4L, arrowheads). These results suggested that, a) EHD proteins show overlapping expression patterns during early ocular development and b) the lack of compensatory upregulation of EHD2-4 expression in *Ehd1-null* eyes suggest unique functions of EHD1 in regulating eye development. It should be noted that *Ehd3-null* or *Ehd4-null* embryos do not show any ocular abnormalities.

As lens development was altered in *Ehd1-null* embryos, I performed immunofluorescence (IF) studies to assess the expression of two genes critical for early lens differentiation in these mutants. The paired domain and homeodomain-containing transcription factor Pax6 and the high mobility group (HMG) domain transcription factor Sox2 are required for specification of lens ectodermal precursors (Ashery-Padan and Gruss, 2001; Ogino et al., 2012). Heterozygous mutations in Pax6 gene are associated with ocular abnormalities including *Aniridia* and Peter's anomaly in humans (Glaser et al., 1994), and *Small eye* phenotype in mice and rats (Hill et al., 1991; Hogan et al., 1986). In addition,

Pax6 overexpression or loss-of-function mutations results in microphthalmia or anophthalmia (Schedl et al., 1996b). Sox2 mutations in humans result in severe anophthalmia and microphthalmia (Fantes et al., 2003; Hagstrom et al., 2005). Conditional deletion of *Sox2* results in a failure of lens vesicle formation, with reduced expression of β-crystallin and Prox1 expression. In *Ehd1-null* eyes, Pax6 and Sox2 expression and localization were comparable to WT controls (Figure 3.5). These results indicated that the lens developmental defects seen in the *Ehd1-null* lenses were not due to altered Pax6 or Sox2 expression.

7.3 Conditional deletion of EHD1 in the lens leads to microphthalmia and cataracts

Embryonic eye development in mice begins during late gastrulation at E9.5, when neuroepithelium derived from the diencephalon evaginates bilaterally to form the optic vesicle (OV). The OV makes contact with a layer of surface epithelium termed presumptive lens ectoderm (PLE): this ectoderm thickens to form the lens placode. As the OV and surface epithelium associate closely through the formation of cytoplasmic extensions, inductive signaling between them shapes each other's subsequent development (Robinson, 2006). In the *Ehd1-null* mice, EHD1 expression is lost not only in the lens but also in surrounding ocular tissues such as optic vesicle (and later retina) that are necessary for early lens differentiation. Therefore, in order to determine whether alterations in lenticular development in *Ehd1-null* mice is due to loss of EHD1 in the lens, I generated conditional knockout mice with *Ehd1* deleted in the lens. Mating the $Ehd1^{flox/flox}$ mice (Rainey et al., 2010) to the *Le-Cre* transgenic mice allowed us to conditionally delete *Ehd1 (CKO)* in the lens and ocular surface epithelial cells (cornea, conjunctiva, eyelids) (Ashery-Padan et al., 2000) (Figure 3.6A). The GFP reporter within the *Le-Cre* transgene, which served as a surrogate for Cre expression, was expressed at E11.5 in the lens vesicle in *Ehd1 CKO* (Figure 3.6C). PCR analysis of tail DNA also confirmed the genotypes of the *Ehd1 CKO* and

control mice (data not shown). *Ehd1 CKO* mice were born at the expected Mendelian ratios. Immunofluorescence studies showed the loss of EHD1 expression in the lens, cornea and conjunctival epithelial cells but not in the optic cup or retina of *Ehd1 CKO* embryos (Figure 3.6E, G, I, arrowheads) compared to control embryos (Figure 3.6D, F, H, arrows) directly correlating Cre expression with loss of EHD1 expression.

Similar to *Ehd1-null* mice, adult Ehd1 CKO (6 weeks or older) mice also displayed microphthalmia and cataracts (Figure 3.7). Nearly 80% of *Ehd1 CKO* animals exhibited ocular phenotypes with microphthalmia (41.6%) and cataracts (23.2%) and microphthalmia together with cataracts (15.5%) (Table 3.2). Interestingly, though the proportion of mice with ocular abnormalities was higher in the *Ehd1 CKO* compared to whole body *Ehd1-null* mice, the *CKO* mice exhibited a less severe phenotype and anophthalmia was not observed in *Ehd1 CKO* mice. These results support a lens-intrinsic role for *Ehd1*, but also suggest that loss of *Ehd1* in non-lens tissues enhances the severity of lens defects seen in whole body *Ehd1-null* mice. Overall, these results confirm the requirement of *Ehd1* for early lens development. Since *Ehd1 CKO* mice recapitulated the major lens phenotypes observed in *Ehd1-null* mice further cellular and molecular characterization were carried out using these mice.

7.4 Histological characterization of defective lens development in *EHD1 CKO* mice

Histological examination of H&E sections revealed alterations in the development of *Ehd1 CKO* lenses (Figure 3.8A, panels a - i'). At E10.5, the lens ectoderm in control embryos had invaginated to form the lens pit (Figure 3.8A, panel a, arrow), which had deepened to form a lens vesicle by day E11.5. The lens pit and vesicle, though smaller, were still seen at similar ages in the *Ehd1 CKO* embryo (Figure 3.8A, panel b, arrowhead), suggesting that *Ehd1* deletion does not affect lens induction, invagination or vesicle formation. At E12.5 and E14.5, *Ehd1 CKO* lenses retained their normal polarity and

architecture (Figure 3.8A, panels d, f), but were smaller than in control animals (Figure 3.8A, panels c, e). The lens phenotypes in *Ehd1 CKO* eyes were accentuated by E16.5 (Figure 3.8A, panels h, h', i, i',); the overall lens size was reduced, the epithelial layer of lenses was invariably thinner with sparse cells (Figure 3.8A, panels i, i', open arrowheads) (Figure 3.9) and the corneal endothelium was absent (Figure 3.8A, panels i, i', arrowheads). A small proportion (21.4%, n=14 at E16.5) of *Ehd1 CKO* embryos also exhibited the persistence of lens stalks (data not shown). Six months old adult *Ehd1 CKO* mice exhibited highly vacuolated lenses (Figure 3.8A, panels k, l) in contrast to control (Figure 3.8A, panel j). Thus, impaired lens development seen in *Ehd1 CKO* mice reflects a requirement of EHD1 during early lens development. As expected, retinal development appeared unaltered in *Ehd1 CKO* eyes at all stages examined.

During normal eye development, the lens grows by a coordinated balance between lens epithelial cell proliferation and fiber cell differentiation. In response to an inductive signal from the retina, lens epithelial cells near the equator withdraw from the cell cycle, elongate and differentiate as secondary lens fiber cells. This anterior-posterior polarity of the lens is maintained throughout life (Robinson, 2006). In order to determine whether *Ehd1 CKO* lenses remained smaller as a consequence of reduced lens epithelial number, I compared the lens epithelial cell counts between *Ehd1 CKO* and control (*Ehd1*$^{flox/flox}$) lenses. In control eyes, the epithelial cell numbers steadily increased from E12.5 to E16.5; and were 69.6 ± 4.7, 135.6 ± 6.1 and 186.7 ± 9.4 cells at E12.5, E14.5 and E16.5, respectively ($n \leq 4$). In contrast, the epithelial cell numbers at these stages were 61.3 ± 3.7, 87.1 ± 18.7 and 79.7 ± 2.7 indicating that the lens growth was significantly reduced in *Ehd1 CKO* lenses ($n \leq 5$)(Figure 3.8B). In order to assess whether reduced lens epithelial cell number in *Ehd1 CKO* eyes is due to reduced cell proliferation, I performed BrdU incorporation studies. These studies revealed a reduction in BrdU incorporation in *Ehd1 CKO* mice compared to controls at E12.5 ($p < 0.01$) but not at E14.5 or E16.5 (Figure 3.8C). These results suggested that

the reduced lens size in *Ehd1 CKO* embryos could be, at least in part, due to reduced lens epithelial cell proliferation.

In order to determine if reduced lens epithelial cell number in *Ehd1 CKO* embryos may be due to defects in lens epithelial viability, I performed a TUNEL assay (Figure 3.10). An increase in the number of TUNEL-positive nuclei was seen in *Ehd1 CKO* lenses when compared to controls at E10.5, E12.5, E14.5 and E16.5 (Figure 3.10 A-J). These results suggest that EHD1 is also required for cell survival during early lens development. Together, my results suggest that the smaller lenses seen in *Ehd1 CKO* embryos likely arise from a combination of reduced proliferation and increased death of lens epithelial cells.

7.5 Aberrant lens epithelial cell polarity but normal fiber cell differentiation in *Ehd1 CKO* embryonic lenses

To assess if the *Ehd1 CKO* lens epithelial cells retained lens epithelial cell characteristics, expression of key epithelial cell polarity markers was examined. In the mature lens, the adherens junctional protein E-cadherin is expressed on the baso-lateral surfaces of lens epithelial cells but not in lens fiber cells. N-cadherin expression, on the other hand, is present both in the lens epithelium and fiber cells (Pontoriero et al., 2009). Immunofluorescence analyses revealed that E-cadherin expression was modestly reduced in the lens epithelial cells of *Ehd1 CKO* embryos (Figure 3.11B, D, arrowheads) at E16.5, but its membrane localization within the cells remained unaffected. N-cadherin expression pattern and localization remained unchanged in *Ehd1 CKO* vs. control embryonic lenses (Figure 3.12). The tight junction marker ZO-1 is expressed in tight junctions near the apical surface of lens epithelial cells and elongating fiber cells. ZO-1 staining and gamma-tubulin puncta define the normally formed interface between lens epithelial and fiber cells (Sugiyama et al., 2009). This interface was much shorter and irregular in the *Ehd1 CKO*

embryonic lenses (Figure 3.11F, H, arrowheads), suggesting a defect in the lens epithelial fiber interface.

Lens fiber cell differentiation is accomplished by proliferating lens epithelial cells giving rise to secondary fiber cells, a process characterized by temporally and spatially regulated expression of crystallins (Cvekl and Duncan, 2007). To determine if the secondary fiber cell differentiation was aberrant, I assessed the expression of lens specific crystallins by immunofluorescence. No discernable differences between control and *Ehd1 CKO* embryonic lenses were observed in the expression pattern of α, β and γ- crystallin proteins at day E16.5 (Figure 3.13). These results indicate that EHD1, though required for lens epithelial proliferation and survival, appears to be dispensable for crystallin expression.

7.6 EHD1 deletion in the lens results in aberrant corneal endothelial differentiation

During mouse embryonic development, corneal endothelium is derived from migrating peri-ocular mesenchymal cells of neural crest and mesodermal origins (Kao et al., 2008). Absence of corneal endothelium was a consistent phenotype seen in *Ehd1 CKO* eyes. To further investigate the alterations in corneal development, I performed a series of immunofluorescence analyses (Figure 3.14A-J). Expression of Keratin 12 (K12), a marker of early corneal epithelial differentiation, was unaltered in *Ehd1 CKO* (Figure 3.14B), suggesting that EHD1 is not necessary for early corneal differentiation. Though a proper corneal endothelium had not formed in *Ehd1 CKO* eyes, the disorganized group of mesenchymal cells seen anterior to the lens expressed N-cadherin (Figure 3.14D, F, arrowheads). Expression of ZO-1, a critical component of tight junctional complexes, was discontinuous and reduced in the anterior chamber of *Ehd1 CKO* (Figure 3.14H, J, arrowheads) compared to control embryos (Figure 3.14G, I, arrowheads) at E16.5. These results suggest that extra-ocular mesenchymal cells that form the corneal endothelial layer

failed to develop tight junctions with their neighboring cells, which in turn suggested a failure of the transition from mesenchymal to epithelial state in *Ehd1 CKO* lenses.

8. Discussion

Endocytic traffic is a key biological process in all eukaryotes. Yet little is known about the physiological roles of endocytic pathways, in particular the recycling arm of endocytic traffic, in regulating tissue morphogenesis in mammals. Endocytic recycling plays an essential role in efficient retrieval, polarization and maintenance of membrane receptors following endocytic internalization (G. J. Doherty and McMahon, 2009). The physiological roles of the recently identified EHD family of endocytic regulators are just beginning to be elucidated. Here, by deleting the EHD family member *Ehd1* in the murine germline and in the lens, I demonstrate that EHD1 is a required regulator of lens development in mice. My studies show that a significant proportion of germline *Ehd1-null* mice display marked ocular abnormalities. These phenotypes included anophthalmia, aphakia, microphthalmia and congenital cataracts. These defects were evident by weaning age and persisted throughout life. To our knowledge, this is the first report implicating an endocytic trafficking protein in ocular development.

EHD1 expression was seen in the lens, retina and ocular surface epithelia including the cornea and conjunctiva. The other family proteins, EHD2-4 showed overlapping expression with EHD1 in ocular tissues. EHD proteins are highly similar in structure and exhibit shared as well as unique functions (George et al., 2007) and loss of one EHD family member is usually compensated by upregulation of another (George et al., 2010; George et al., 2011; Mate et al., 2012; Sengupta et al., 2009). Since only about half of *Ehd1-null* animals showed eye phenotypes, I first examined if other EHD family members compensated for loss of EHD1. However, my results did not reveal any increases in EHD2, EHD3, or EHD4 expression even in severely affected *Ehd1-null* eyes. Consistent with a lack of compensation by family members, germline deletion of *Ehd3* or *Ehd4* did not produce any apparent ocular abnormalities (George et al., 2011)(the impact of *Ehd2* deletion has not been determined to date). In contrast, *Ehd1* deletion produces dramatic eye phenotypes that

appear very early during embryogenesis and persist throughout life. Altogether, these results suggest that EHD1 plays a dominant role in ocular development, and EHD2-4 expression is insufficient to compensate for the loss of EHD1. It remains possible however that EHD family members, or alternate endocytic pathway regulators, do provide redundancy accounting for apparently normal ocular development in a subset of *Ehd1-null* and *Ehd1 CKO* mice and the strain-dependence of *Ehd1-null* phenotype.

A lens intrinsic role for EHD1

As germline deletion of *Ehd1* exhibited multiple defects including high pre-natal mortality (Rainey et al., 2010), I considered the possibility that ocular abnormalities observed in these mutants could be a secondary consequence of loss of *Ehd1* in other tissues that help regulate eye development. Additionally, even within ocular tissues, development is intimately linked to reciprocal signaling between various compartments, such as those between the developing lens, ocular mesenchyme and optic vesicle (Cvekl and Ashery-Padan, 2014; Donner et al., 2006; Lang, 2004). To test this possibility, I deleted *Ehd1* in cells derived from the ocular surface ectoderm such as lens, corneal and conjuctival epithelial cells. As expected, other alterations seen in the germline deletion of *Ehd1* such as male sterility and embryonic lethality were absent in *Ehd1 CKO* mice. The *Ehd1 CKO* mice recapitulated the lenticular abnormalities such as microphthalmia and cataracts (anophthalmia was distinctly absent) seen in the *Ehd1-null* mice. These results point to a lens-intrinsic role of *Ehd1*. Ocular phenotypes were evident at birth and became more pronounced by the weaning age. Although milder compared to those in *Ehd1-null* mice, the ocular phenotypes in *Ehd1 CKO* mice were observed at a higher frequency (135 out of 168 eyes analyzed in *Ehd1 CKO* vs. 119 out of 212 eyes analyzed in *Ehd1-null*). One reason for the increased severity of ocular phenotypes in *Ehd1-null* mice could be the loss of EHD1 in the retina and in peri-ocular mesenchymal cells. Another reason could be differences in

genetic background between *Ehd1 CKO* (129.B6.FVB) and *Ehd1-null* (129.B6) mice. Consistent with this possibility is the result that knockout mice enriched for 129Sv/Ev and Swiss Webster background were apparently normal (Rapaport et al., 2006) whereas *Ehd1-null* mice on 129.B6 background exhibit marked developmental defects, including reduced pre-natal viability, small size, male infertility and ocular defects (Rainey et al., 2010). It should be noted that the two possibilities i.e. lens-intrinsic role for *Ehd1* and influence of genetic background are not mutually exclusive.

EHD1 and lens growth

Though smaller lens pits and vesicles were seen in the *Ehd1 mutants*, the fact that lenses do form suggest that *Ehd1* is dispensable for initial stages of lens development including lens induction, placode formation and initiation of lens invagination. However, invagination, though initiated, is not completed in *Ehd1 mutants* as the lens vesicle fails to separate from the overlying ectoderm. Though observed in a number of mutants (Chen et al., 2008; Kuracha et al., 2011; Pontoriero et al., 2008) lens vesicle detachment is a poorly understood phenomenon. Interestingly, in spite of the persistence of the lens stalks, the lens epithelial cells in these mutants retain the ability to initiate fiber differentiation and primary and secondary fiber cells form appropriately suggesting that *Ehd1* is dispensable for fiber differentiation.

Ehd1 CKO also showed a reduction in E-cadherin expression and aberrant ZO-1 distribution in the lens epithelial compartment. The defective ZO-1 localization and reduced E-cadherin expression indicates altered apico-basal polarity of lens epithelial cells in *Ehd1 CKO* mice, suggesting a role for EHD1 in maintaining lens epithelial cell polarity. These alterations could be a consequence of increased lens epithelial apoptosis. However, we cannot rule out a direct role for *Ehd1* in regulation of E-cadherin and ZO-1. At the lens epithelial- fiber interface, endocytic structures have been noted by electron microscopy (EM)

in the avian lens (Bassnett et al., 1994). While nothing is known about endocytic traffic of ZO-1 or other tight junction proteins in the lens, recent studies in other cell line models reveal an important role of endocytic recycling of other tight junction proteins claudin-1 and claudin-2 in maintaining apico-basal polarity (Dukes et al., 2011; Fletcher et al., 2014; Heller et al., 2010). Thus, EHD1 may regulate endocytic recycling of tight junction proteins. Future studies will explore if EHD1, either directly or through its interacting partners, regulates the endocytic recycling of E-cadherin or ZO-1, or their associated proteins, in the lens epithelium.

My results suggest that the main function of *Ehd1* in lens development is regulation of lens epithelial survival and viability. *Ehd1 mutant* lens epithelial cells show a significantly higher rate of apoptosis. How EHD1 might regulate cell survival and proliferation is not known, but a number of key cell surface receptors that regulate cell proliferation and survival in the lens epithelium are either known e.g. IGF1-R and *β1*-integrin (Jovic et al., 2007; Rotem-Yehudar et al., 2001) or are potential targets of EHD1 including FGF and BMP receptors. For instance, fibroblast growth factor (FGF) receptor signaling is required for lens epithelial and fiber cell survival (Zhao et al., 2008). Loss of BMPR1a leads to increased apoptosis of lens placodal cells (Rajagopal et al., 2009). IGF1R is widely expressed in the germinative and transitional zones in the lens, and in the developing retina, iris, ciliary body and cornea (Xie et al., 2007). Transgenic mice with overexpressed insulin or IGF-1 show altered lens growth, and fiber cell differentiation defects (Xie et al., 2007). *β1-integrin CKO* in the lens show disorganized lens epithelium and increased epithelial cell death (Simirskii et al., 2007). Future studies will assess if EHD1 regulates these receptors or others that control cell proliferation, survival and epithelial remodeling during lens development.

EHD1 and corneal development

In addition to lens defects in *EHD1 CKO* mice, I observed profound alterations in corneal endothelial differentiation. Normal corneal endothelial layer exhibits regularly-spaced tight junctions and adherens junctions that are recognized by staining for ZO-1 and N, or E-cadherin, respectively.

In contrast to control embryos, the cells lining the inner surface of corneal stroma in *Ehd1 CKO* embryos failed to form proper junctional complexes, which is evident by the absence of ZO-1 staining of these cells. N-cadherin expression was seen in multiple cell layers in the *Ehd1 CKO* compared to a single layer in control mice. These alterations reflect the failure of the mesenchymal corneal endothelial precursors to convert to an epithelial identity with apico-basal polarity. Though we cannot rule out the possibility of a direct role for *Ehd1* in regulating corneal endothelial differentiation, it is likely that altered corneal endothelial differentiation is due to loss of *Ehd1* in adjacent ocular tissues such as the lens and /or in the corneal epithelial cells. EHD1 expression in the corneal endothelial precursors was unaltered in the *Ehd1 CKO* as the Cre recombinase is not expressed in these cells. Signals from the lens are known to regulate N-cadherin expression in avian eyes (D. C. Beebe and Coats, 2000). In addition, ablation of lens in mice inhibits corneal endothelial formation (Zhang et al., 2007). The lens thus serves as a critical signaling center that orchestrates overall development of the corneal endothelium and the stroma (Gage and Zacharias, 2009). A more direct impact of EHD1 in corneal endothelium will be of considerable interest given the ion and water transport functions of this cell layer. The corneal endothelial cells help maintain hydration and in turn, corneal transparency by the expression of Na^+/K^+-ATPase and bicarbonate-dependent Mg^{2+}-ATPase pumps (Bonanno, 2012; Srinivas, 2010). Notably, EHD proteins associate with ankyrin proteins to regulate membrane targeting and stability of membrane ion channels in cardiomyocytes, and lack of

EHD3 expression impairs the expression and function of Na/Ca exchanger (NCX) in these cells (Curran et al., 2014; Gudmundsson et al., 2010).

In conclusion, my studies using germline and conditional knockouts of *Ehd1* provide evidence for a novel role of the endocytic recycling pathway in regulating key ocular developmental decisions during mouse lens development. Further studies using this model should help delineate how the basic process of endocytic recycling is intertwined with cell-cell interaction and signaling pathways to regulate developmental decisions in the mammalian eye.

.

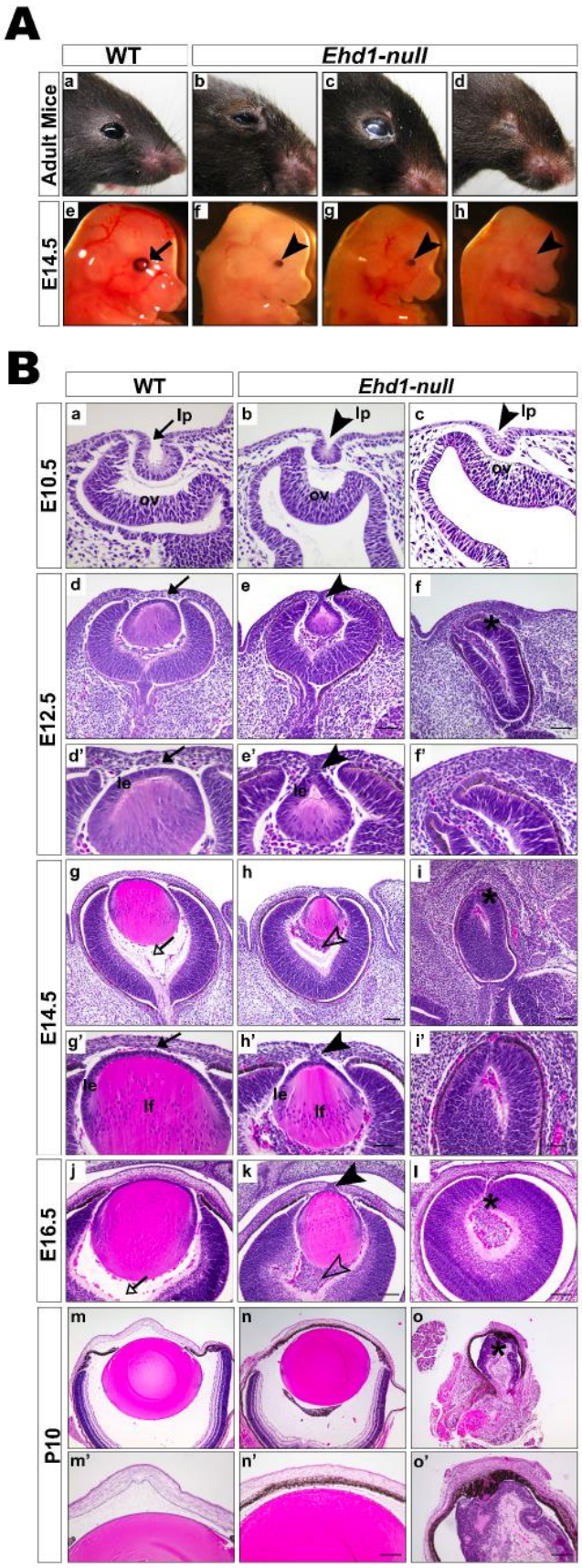
A
WT
Ehd1-null
Adult Mice
E14.5
a
b
c
d
e
f
g
h
B
WT
Ehd1-null
E10.5
E12.5
E14.5
E16.5
P10
lp
ov
le
lf
a
b
c
d
e
f
d'
e'
f'
g
h
i
g'
h'
i'
j
k
l
m
n
o
m'
n'
o'

Figure 3.1 Defective ocular development in *Ehd1-null* mice. 1A: Gross anatomical or histological features of eye structures of *Ehd1-null* adult mice (b, c, d) and E14.5 embryos (f, g, h) were compared to control adult mice (a) and embryos (e). Shown are examples of microphthalmia (b), cataract (c) and anophthalmia (d) in *Ehd1-null* mice. At embryonic day E14.5, smaller eyes and irregular retinal-pigmented epithelium (RPE) are visible in *Ehd1-null* embryos (f, g, h) compared to littermate wild type control (e). **1B:** Histological analyses of formalin-fixed, paraffin-embedded sections depicting examples of: smaller lens pits in *Ehd1-null* (b, c) compared to WT (a) at E10.5; and lens stalk persistence (e, e' h, h', k, arrowheads), hyaloid vasculature persistence (e, e', h, h', k, open arrowheads), aphakia (f, f', i, i', l, asterisk) in *Ehd1-null* compared to WT controls (d, d' g, g' j, arrows) at E12.5, E14.5, E16.5; normal architecture of the lens and the retina with a smaller lens (n, n') and a severely malformed residual eye in *Ehd1-null* mice (o, o', asterisk) at P10 vs. a well-formed lens, cornea and distinct lamination of neural retina in WT eyes (m, m'). Abbreviations: lp, lens pit; ov, optic vesicle; le, lens epithelium; lf, lens fiber cells. Scale bars are 50 μm in panels (a, b, c, d', e', f', g', h', i'), 100 μm in panels (d, e, f, j, k, l, m', n', o') and 200 μm in panels (g, h, i, m, n, o).

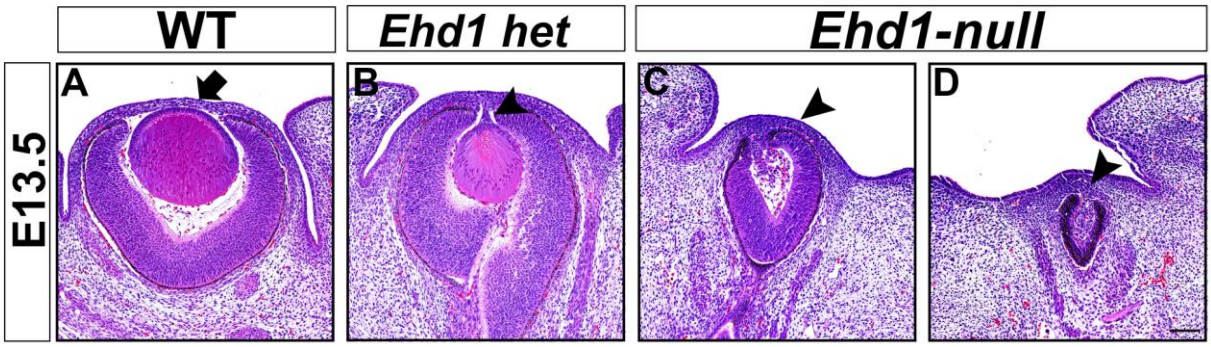

Figure 3.2 Paraffin embedded sections of embryonic eyes from E13.5 WT (A), Ehd1 Het (B), *Ehd1-null* (C, D) were stained with H&E. EHD1 Het embryos occasionally displayed lens stalk phenotype (arrowhead). *Ehd1-null* eyes exhibit residual retinal structures in panel C, D (arrowheads) as compared to WT littermate controls. Scale bar is 100 μm.

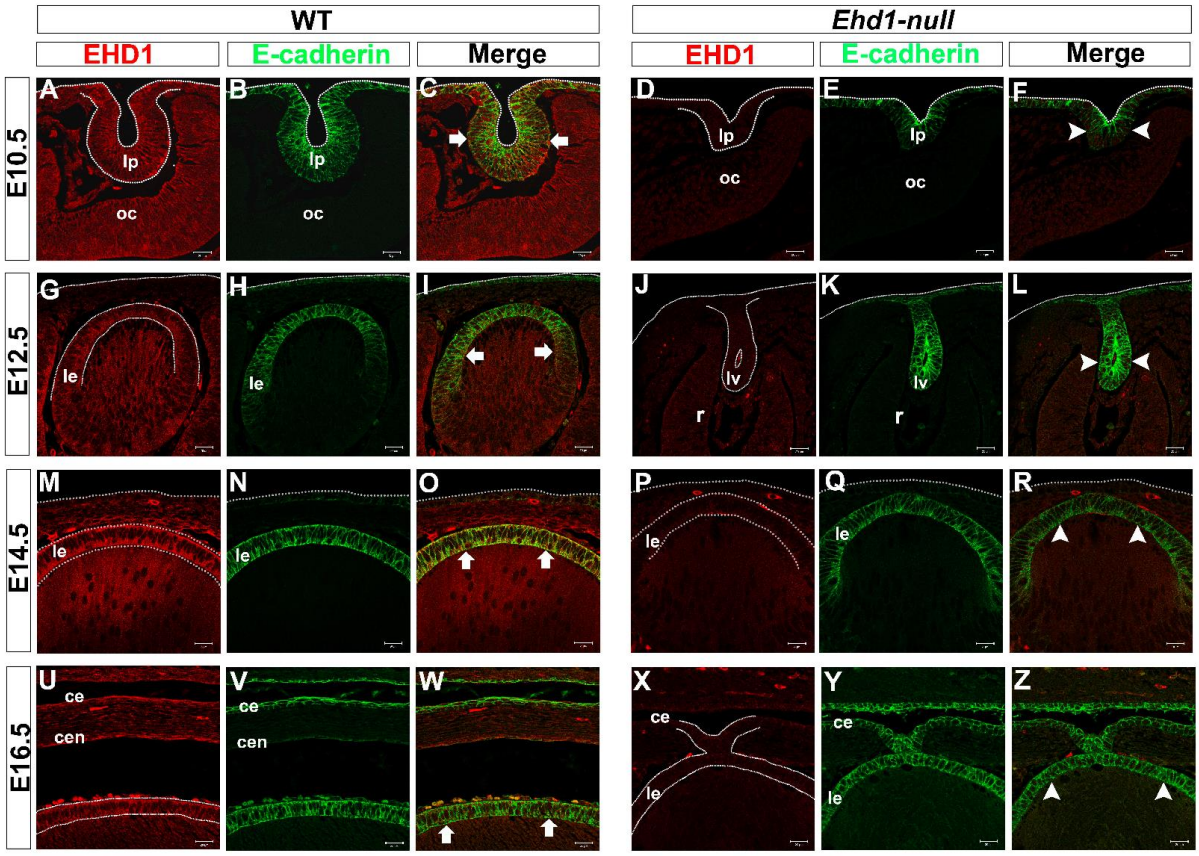

Figure 3.3 EHD1 expression during mouse eye development. Formalin-fixed, paraffin-embedded 4 µm thick eye tissue sections, at the indicated embryonic time points, were stained with anti-EHD1 (red) and anti-E-cadherin (green) antibodies and visualized by confocal fluorescence microscopy. In control embryos, EHD1 expression is observed in the lens pit and the underlying optic cup at E10.5 (A, C); in the surface ectoderm, the epithelial cells and the underlying optic cup (G, I) at E12.5; in the overlying ectoderm and the lens epithelial cells (M, O) at E14.5 and in the eyelids, the corneal epithelium, corneal stroma and the lens epithelium (U, W) at E16.5. Colocalization (yellow) is observed along the cells of the lens pit (C, arrows) and the lens epithelium (I, O, W, arrows) in control embryos. EHD1 staining is not observed in *Ehd1-null* at E10.5 (D, F), at E12.5 (J, L), E14.5 (P, R) and E16.5 (X, Z). E-cadherin colocalization with EHD1 is not observed in *Ehd1-null* embryos (F, L, Z, arrowheads). The dotted line demarcates the lens pit, the surface ectoderm and the lens epithelium. Abbreviations: lp, lens pit; oc, optic cup; lv, lens vesicle; r, retina; le, lens epithelium; ce, corneal epithelium. Scale bar is 20 µm.

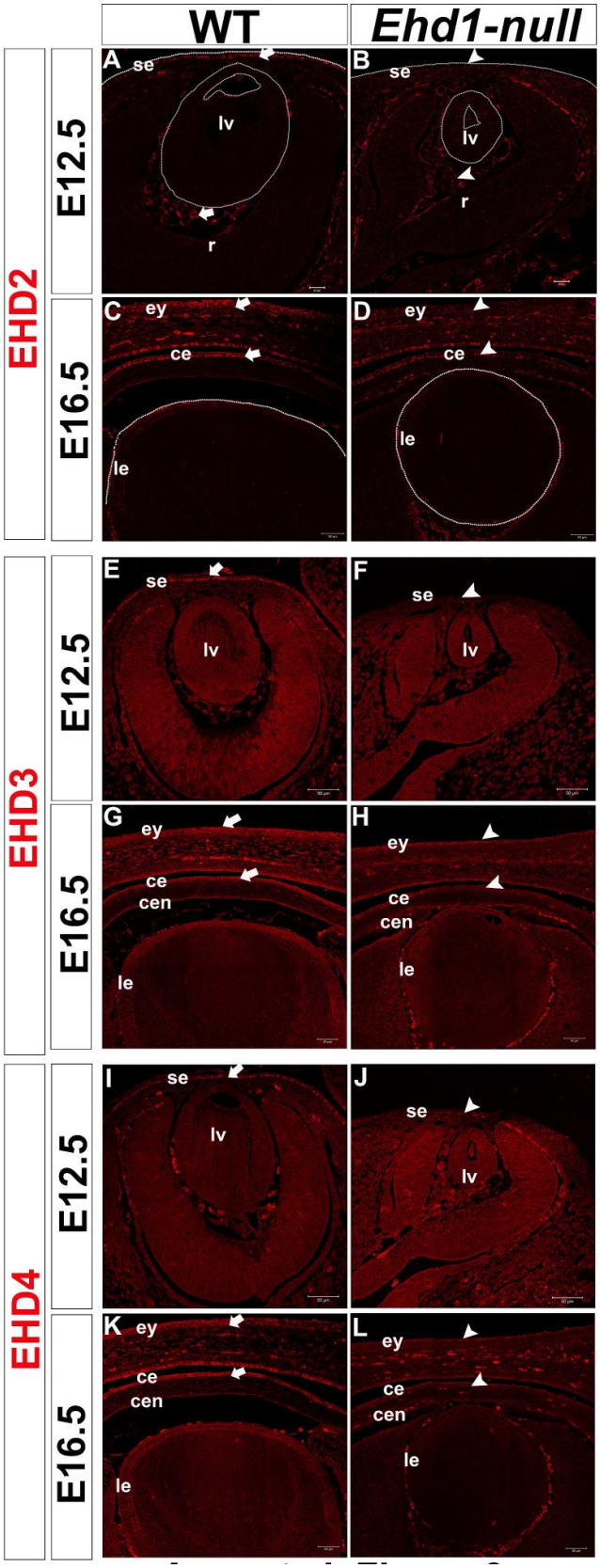
WT
Ehd1-null
EHD2
EHD3
EHD4
E12.5
E16.5
A
B
C
D
E
F
G
H
I
J
K
L
se
lv
r
ey
ce
le
cen

Figure 3.4 Expression of EHD family members is not altered in developing eyes of *Ehd1-null* mice. Formalin-fixed, paraffin-embedded tissue sections, at the indicated embryonic time points, were stained with anti-EHD2, anti-EHD3, anti-EHD4 antibodies and visualized by confocal fluorescence microscopy. In control embryos, EHD2 expression is observed in the surface ectoderm (A, arrows), blood vessels of the vitreous (A, arrows) at E10.5 and in the eyelids (C, arrows), the corneal epithelium (C, arrows) at E16.5. EHD2 expression pattern in *Ehd1-null* embryos (B, D, arrowheads) is comparable to that in controls. EHD3 expression is observed in: the overlying surface ectoderm of WT (E, arrow) and *Ehd1-null* embryos (F, arrowheads) at E12.5, and in the eyelids, the corneal epithelium, the lens epithelium and surrounding mesenchymal tissues of WT (G, arrows) and *Ehd1-null* eyes (H, arrowheads). Similarly, EHD4 expression is seen in: the surface ectoderm and optic vesicle of WT (I, arrow) and *Ehd1-null* embryos (J, arrowhead) and in the eyelids, corneal epithelium and in the lens epithelium at E16.5 in WT (K, arrow) and *Ehd1-null* (L, arrowheads). Abbreviations: se, surface ectoderm; lv, lens vesicle; r, retina; ey, eyelids; le, lens epithelium; ce, corneal epithelium; cen, corneal endothelium. Scale bar is 20 μm in panels A, B and 50 μm in the remaining panels.

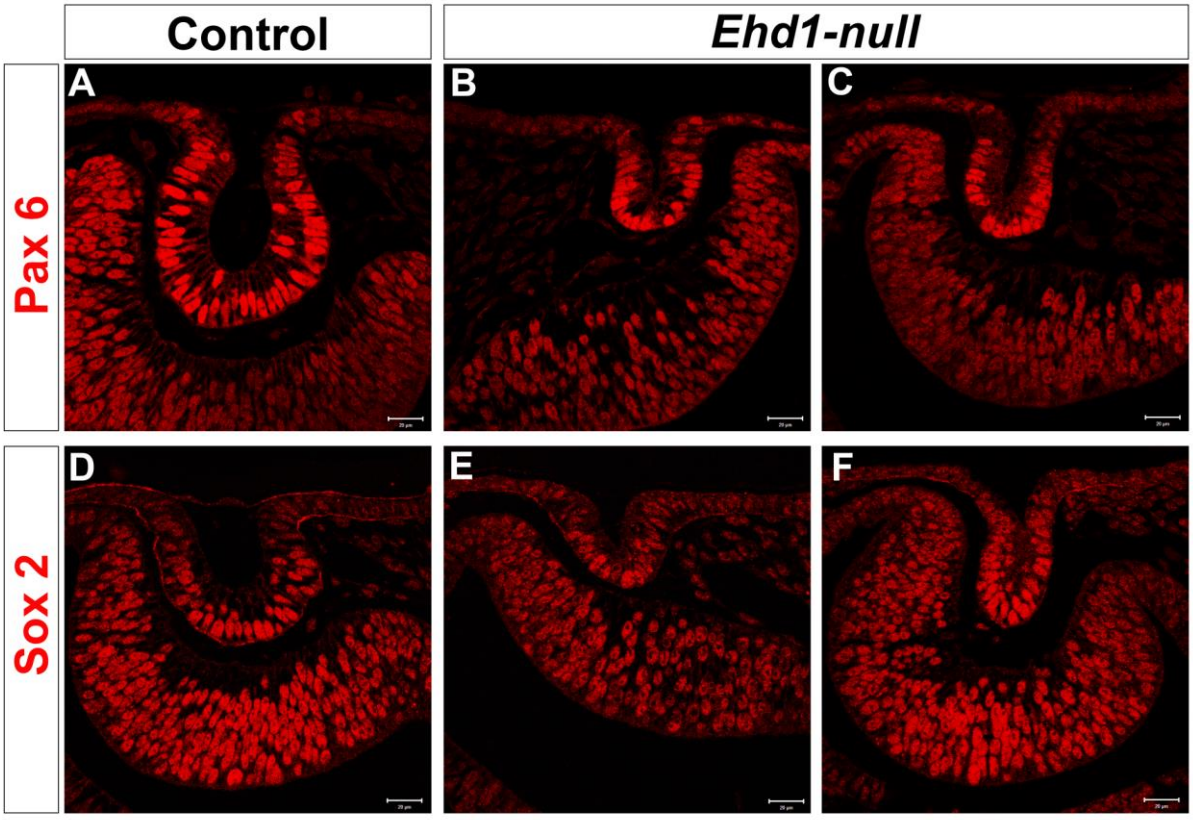

Figure 3.5 Lens specification and induction markers are unaltered in *Ehd1-null* embryos. Pax6 (A-C) and Sox2 (D-E) expression was determined on paraffin embedded sections from eyes of E10.5 WT and *Ehd1-null* embryos. Pax6 staining was observed in the invaginating lens placode and in the optic vesicle. The expression remained unaltered in the *Ehd1–null* (B-C) as compared to control (A) embryos. Similarly, the lens specification marker Sox2 staining was comparable in embryonic eyes of *Ehd1-null* (E-F) to controls (D). Two representative images with varying degree of lens placodal invagination in *Ehd1-null* embryos is depicted. Scale bar is 20 μm.

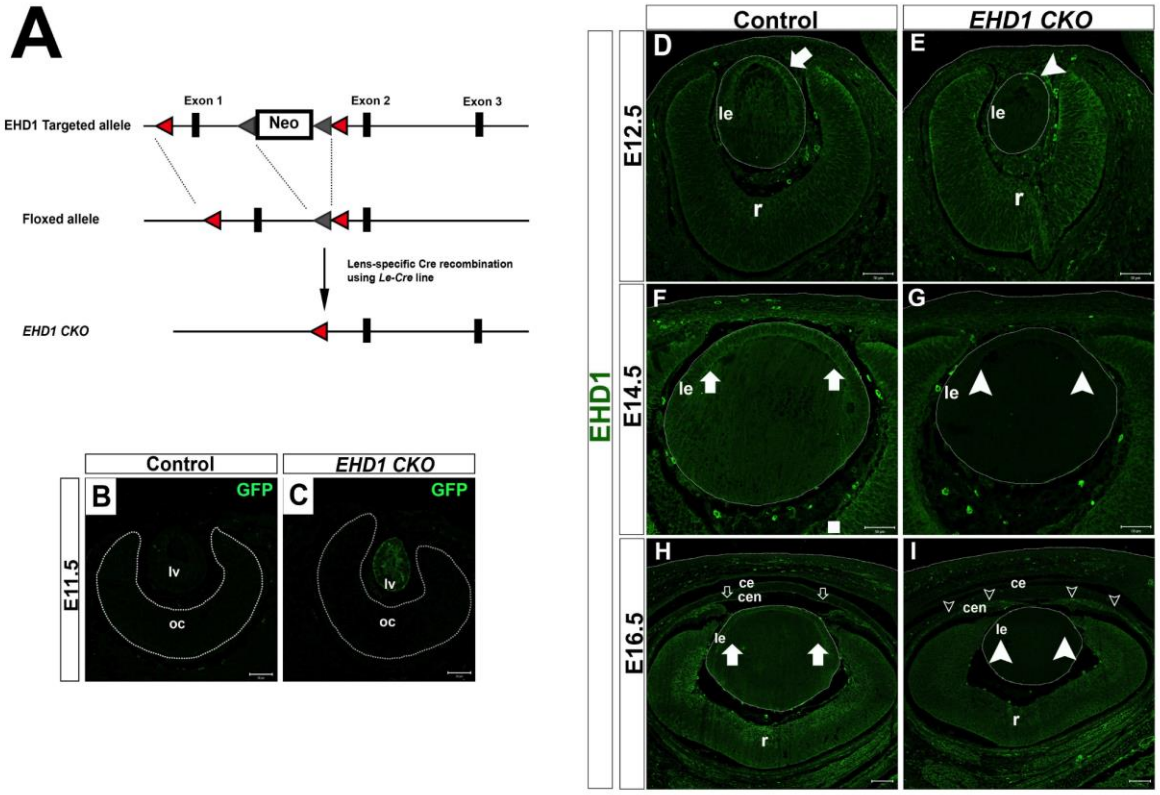

Figure 3.6 Conditional deletion of *Ehd1* in the mouse lens. A: Schematic of the floxed *Ehd1* allele with a Neo cassette surrounded by FRT recombination sites (grey triangles) and loxP recombination sites surrounding exon 1 (red triangles) (top), floxed allele after genetic transgenic FLP recombinase-mediated removal of the Neo cassette (middle) and the mutant allele lacking exon 1 sequences (called *Ehd1 CKO*) expected to be generated upon *Le-Cre* driven Cre recombinase expression (bottom). **B, C:** Formalin-fixed paraffin-embedded sections of E11.5 embryonic eyes of control (B; floxed mice lacking *Le-Cre*) or *Ehd1 CKO* mice (C) were subjected to staining with anti-GFP antibody (green) followed by confocal imaging. Lens-specific expression of GFP in *Ehd1 CKO* mice confirms the specificity of *Le-Cre* transgene in our stocks. **D-I:** Control sections (D, F, H) or *Ehd1 CKO* (E, G, I) embryonic eyes at the indicated ages were stained with an anti-EHD1 antibody and analyzed by confocal microscopy. Loss of EHD1 staining is seen specifically in the developing lens in *Ehd1 CKO* embryos (E, G, I, arrowheads) while staining in retina is intact and comparable to that in control embryos (D, F, H). EHD1 expression is also retained in the neural crest derived corneal endothelial cells as seen in E16.5 *Ehd1 CKO* (I, open arrowheads) vs. control (H, open arrows) embryos. A dotted line demarcates the lens boundary in panels D, E, F, G, H, I. Abbreviations: le, lens epithelium; r, retina; ce, corneal epithelium; cen, corneal endothelium. Scale bar is 50 μm in panels B-G and 100 μm in panels H, I.

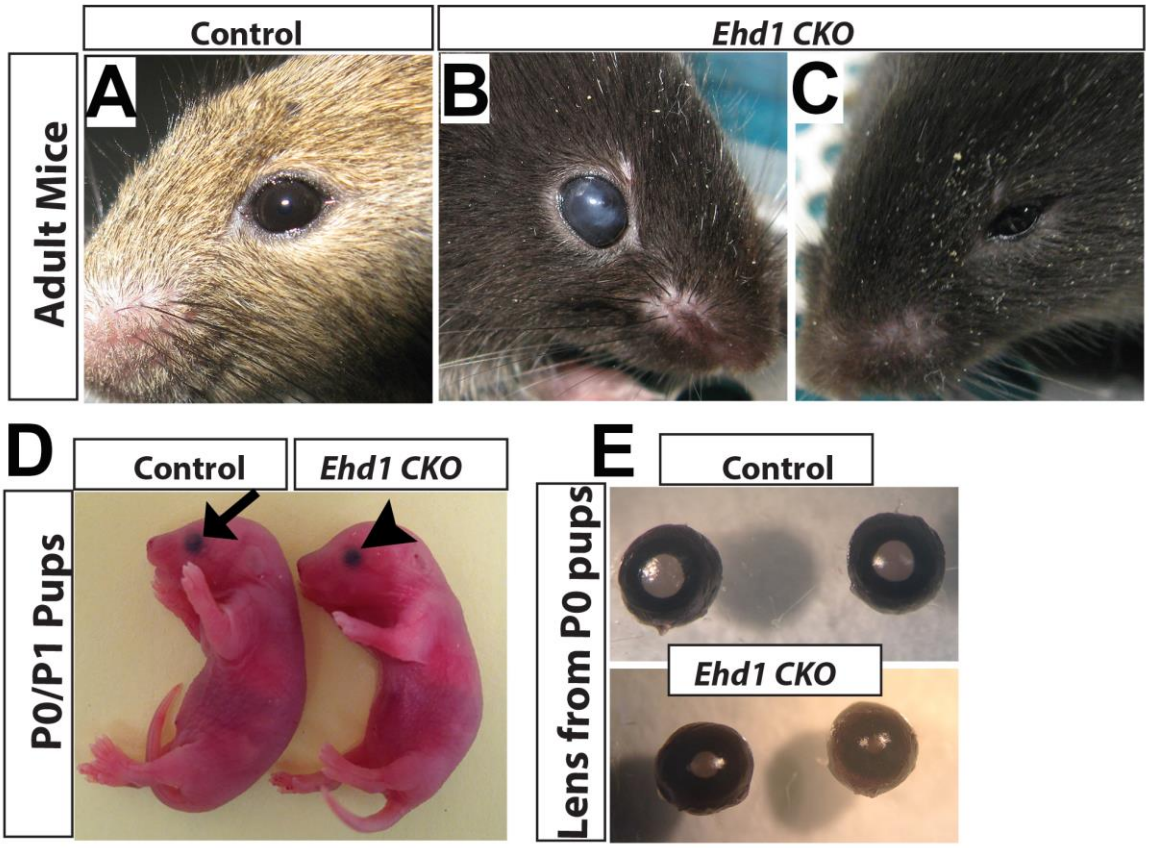

Figure 3.7 *Ehd1 CKO* mice possess ocular defects. 6-week-old mice were photographed to depict ocular defects including microphthalmia (C), cataract (B) in *Ehd1 CKO* mice compared to controls (A). At birth, *Ehd1 CKO* pups were grossly similar in size and weight as compared to control pups; however the lens defects were prominent in the mutant pups. (Panel C; right vs left). Eyes were removed from P0 pups and images were captured under a dissection microscope. *Ehd1 CKO* eyeballs.

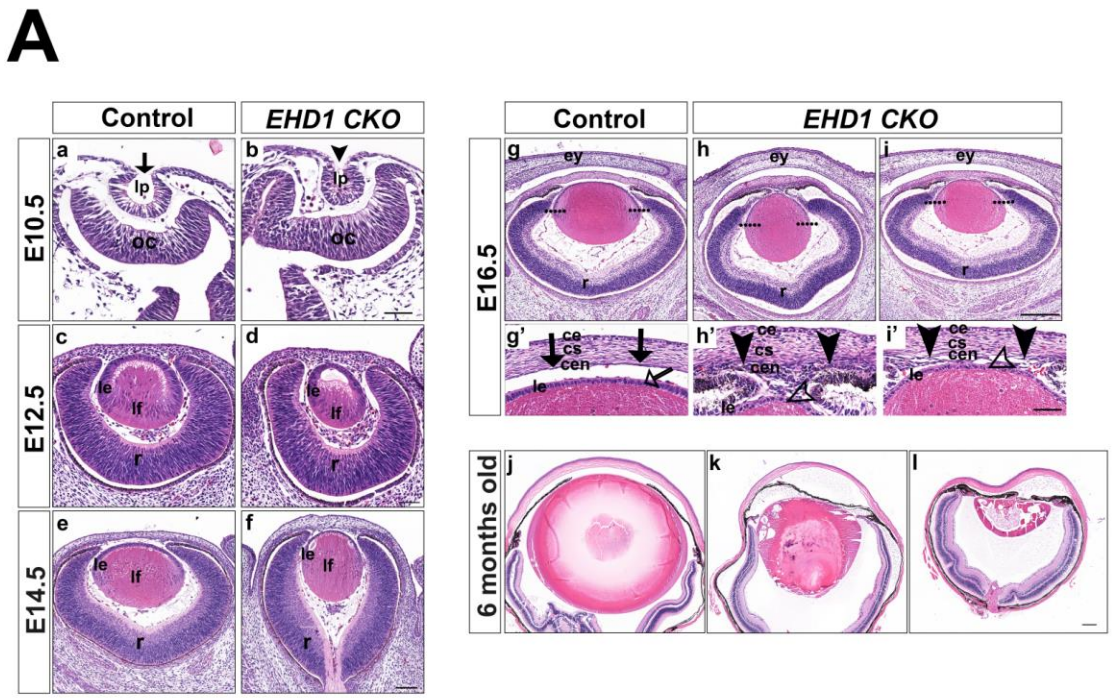
A
Control
EHD1 CKO
E10.5
E12.5
E14.5
E16.5
6 months old
lp
oc
le
lf
r
ey
ce
cs
cen

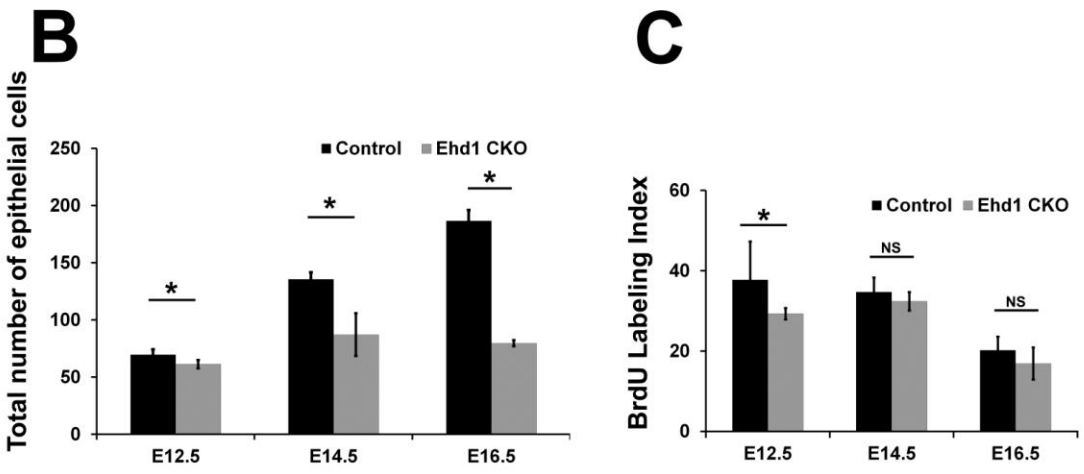
B
Total number of epithelial cells
Control
Ehd1 CKO
250
200
150
100
50
0
E12.5
E14.5
E16.5
*

C
BrdU Labeling Index
Control
Ehd1 CKO
60
40
20
0
E12.5
E14.5
E16.5
*
NS

Figure 3.8 Lens development defects in *Ehd1 CKO* mice. A: H & E sections of embryonic (a-i') or 6-month old (j-l) eyes from control (a, c, e, g, g', j, j) or *Ehd1 CKO* mice (b, d, f, h, i, h', I', k, l) at E10.5 (a, b), E12.5 (c, d), E14.5 (e, f), E16.5 (g-i) and 6-months of age (j-l). Smaller lens pit in E10.5 *Ehd1 CKO* (b, arrowhead) compared to control (a, arrow) embryo is indicated. Smaller lenses are seen in *Ehd1 CKO* embryos at E12.5 (d), E14.5 (f) and E16.5 (h, I, h', I'). At E16.5, *Ehd1 CKO* embryonic lenses show lens epithelial thinning, aberrant epithelial cell shape (open arrowheads), and absence of corneal endothelium (downward arrowheads). The dotted lines on two sides of lens in panels g-i represents the equator region. g', h', i' panels are higher magnification images of segments from g, h and i panels, respectively. Scale bar is 100 μm. B: Lens epithelial cell numbers in control (black bars) and *Ehd1 CKO* eyes (grey bars) at E12.5, E14.5, E16.5 were quantified and performed as described in Methods. Error bars indicate SEM. *$p < 0.001$ C: BrdU positive lens epithelial cell nuclei were counted in control and *Ehd1 CKO* embryos at E12.5, E14.5 and E16.5. *$p < 0.01$. NS, not significant. Abbreviations: lp, lens pit; oc, optic cup; le, lens epithelium; lf, lens fiber cells; r, retina; ey, eyelids; ce, corneal epithelium; cs, corneal stroma; cen, corneal endothelium.

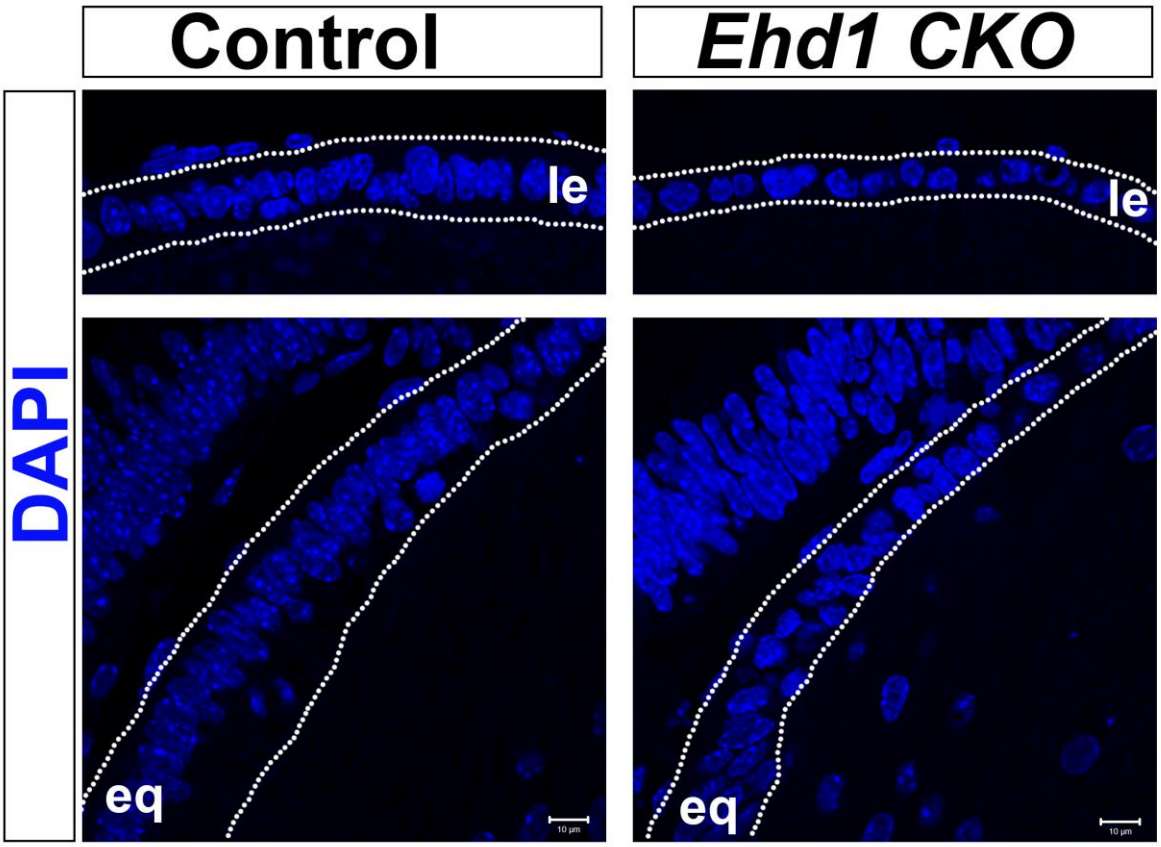

Figure 3.9 *Ehd1 CKO* mice exhibit lens epithelial defects. Representative images of control (left panel) vs *Ehd1 CKO* (right panel) illustrating the thinner central epithelium, equator region with sparse nuclei in mutant embryos at E16.5. Abbreviations: le, lens epithelium; eq, lens equator region. Scale bar is 10 μm.

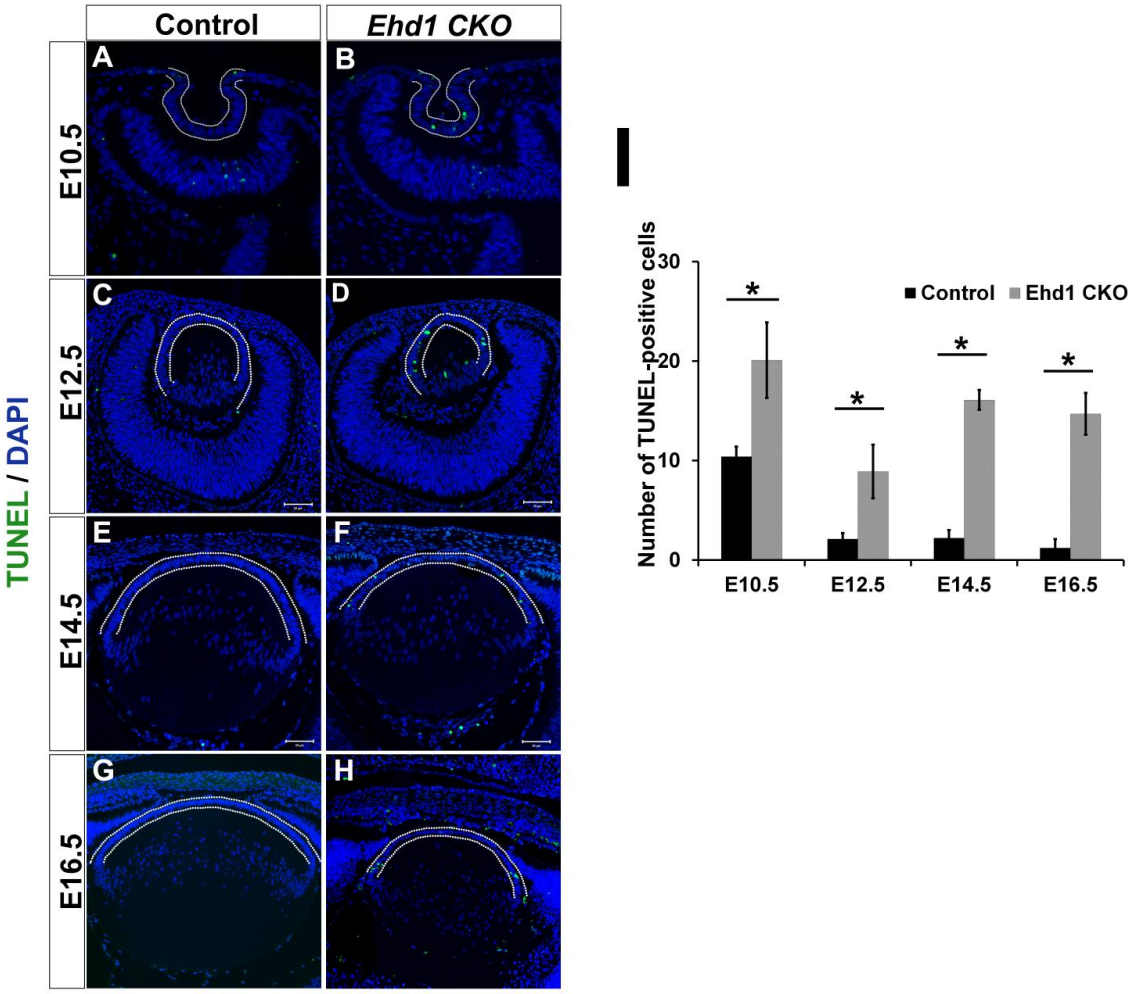

Figure 3.10 EHD1 is required for Cell Survival. A-H: Immunofluorescence staining revealed by TUNEL (terminal deoxynucleotidyl transferase-mediated deoxyuridinetriphosphate nick end-labeling) assay in embryonic sections from control (A, C, E, G) and *Ehd1 CKO* (B, D, F, H) at E10.5 (A, B), E12.5 (C, D), E14.5 (E, F), and E16.5 (G, H). Nuclei are stained blue with DAPI. Increased apoptotic cells (green) are detected in *Ehd1 CKO* mouse lens epithelium. Dotted white lines demarcate the lens region used for the analysis **I-J:** Quantification data from counting of TUNEL-positive nuclei in control and *EHD1 CKO* lenses.*p < 0.01;.n= number of embryos analyzed. Scale bar is 50 μm.

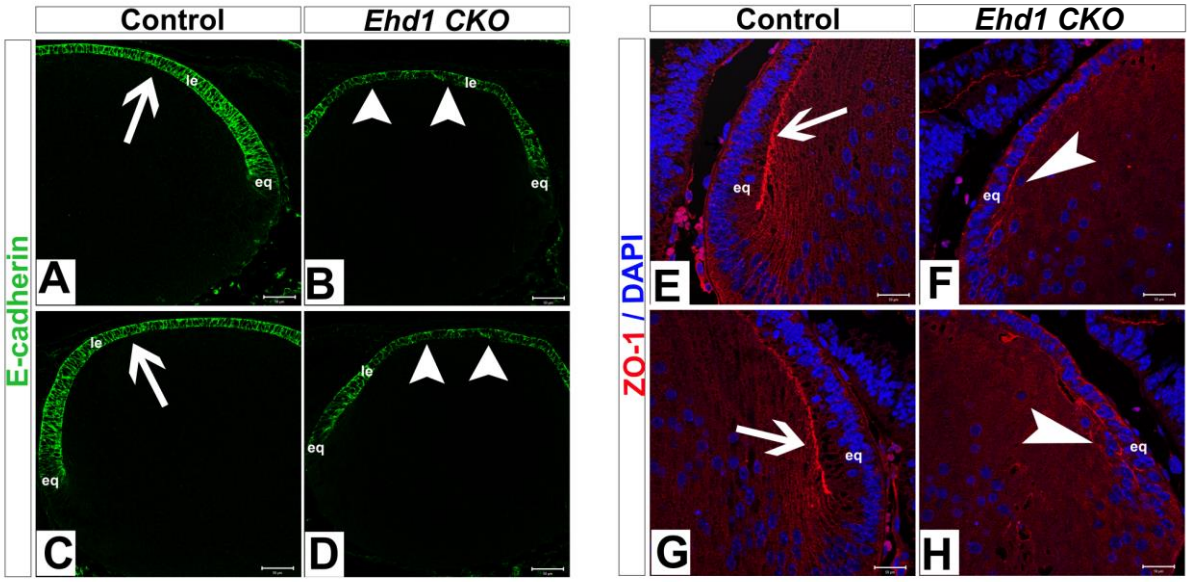

Figure 3.11 Altered expression of junctional proteins in *Ehd1 CKO* mice. Formalin fixed paraffin embedded tissue sections from E16.5 are stained for anti-E-cadherin (green) (A-D) and ZO-1 (red) (E-H) antibodies and subjected to confocal fluorescence microscopy. Nuclei are stained blue with DAPI. **A-D:** Normal pattern of expression is evident in control lens (A, C) whereas in the *Ehd1 CKO*, E-cadherin expression is dramatically reduced (B, D). **E-H:** ZO-1 expression is irregular and disrupted at the apical lens epithelial junctions in *Ehd1 CKO* mice (F, H) in contrast to the littermate controls (E, G). Abbreviations: eq, lens equator; le, lens epithelium. Scale bar is 50 μm.

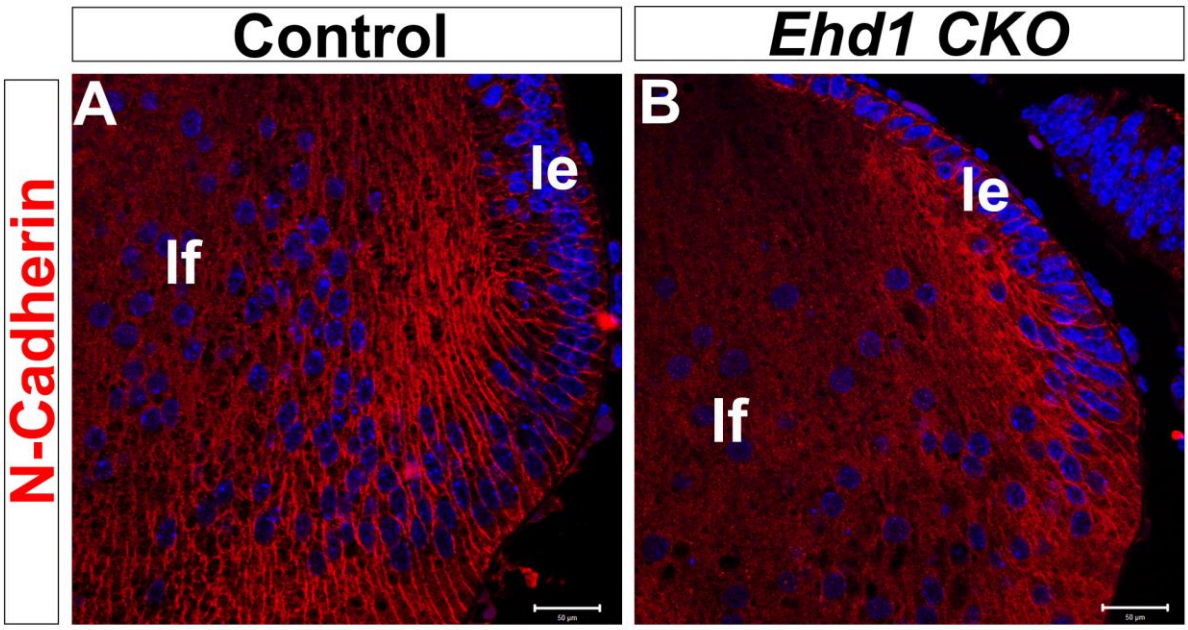

Figure 3.12 Junctional protein N-cadherin expression is unaltered in *Ehd1 CKO* mice. N-cadherin expression is observed in the lens epithelial and fiber cells of control (A) and *Ehd1 CKO* (B) at E16.5. Abbreviations: le, lens epithelium; lf, lens fiber cells. Scale bar is 50 μm.

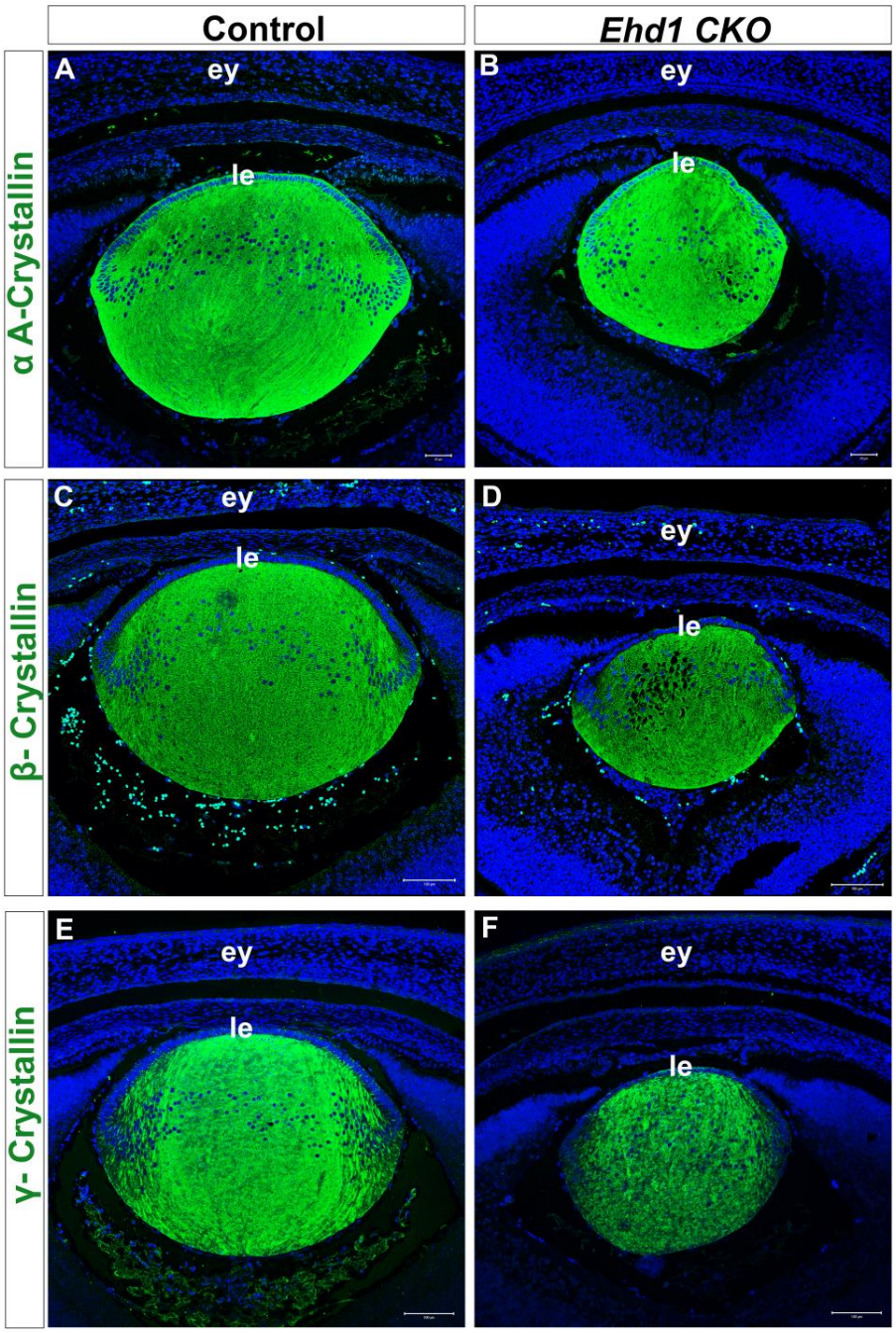

Figure 3.13 Analysis of fiber cell differentiation marker expression in *Ehd1 CKO* shows little to no change. Paraffin embedded sections of E16.5 control (A, C, E) and *Ehd1 CKO* (B, D, F) were immunostained with antibodies against αA-, β-, γ-crystallin. Similar expression pattern is observed for these antibodies in *Ehd1 CKO* lenses as compared to controls. Abbreviations: le, lens epithelium; ey, eyelids. Scale bar is 50 μm (A, B), 100 μm (C-F).

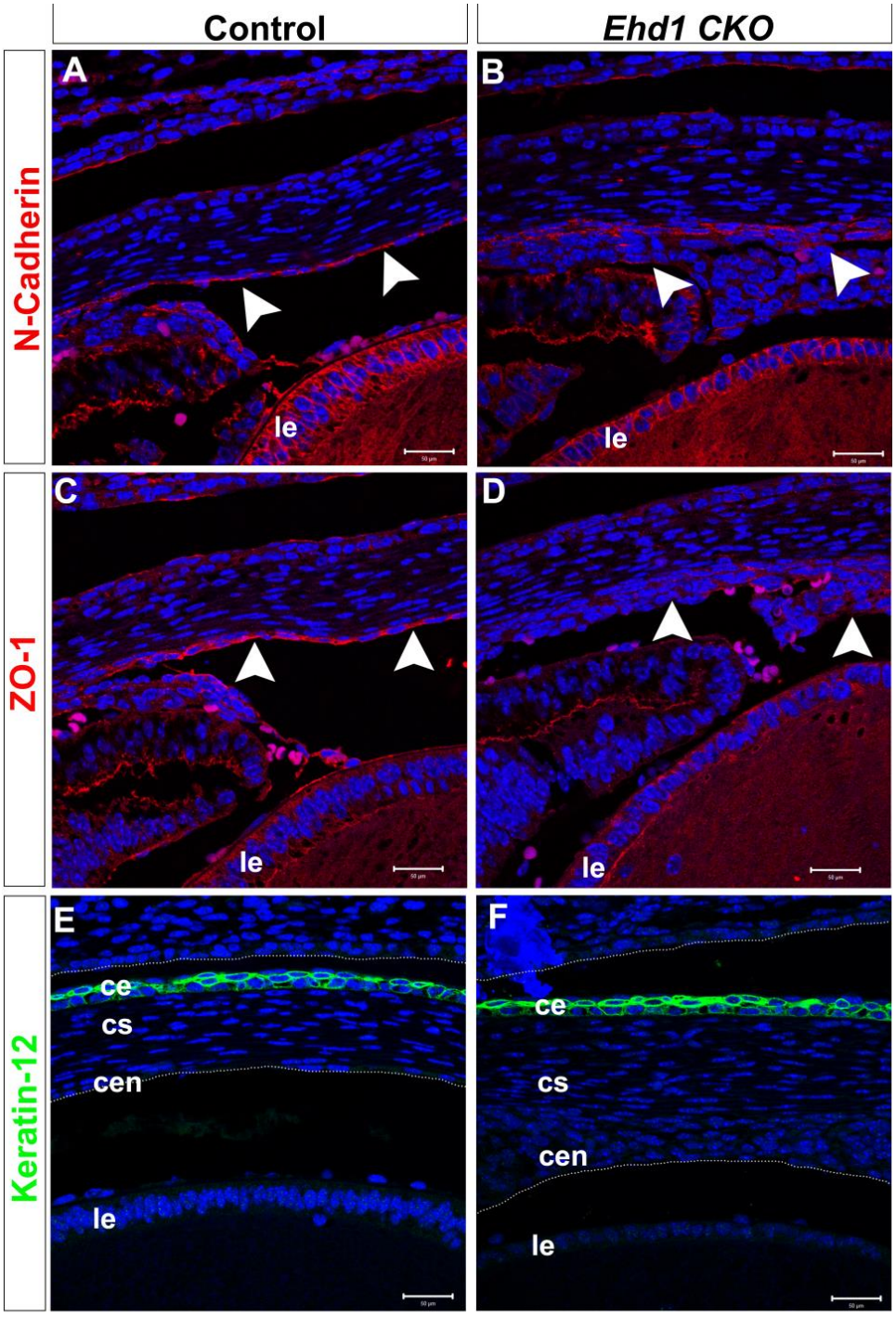
Control
Ehd1 CKO
N-Cadherin
ZO-1
Keratin-12
A
B
C
D
E
F
le
ce
cs
cen

Figure 3.14 Corneal endothelium differentiation defects in *Ehd1 CKO* mice. Formalin fixed paraffin embedded tissue sections from E16.5 were stained with anti-N-cadherin (A-B), anti- ZO-1 (C, D) and anti-Keratin-12 (K-12) (E, F) antibodies in *Ehd1 CKO* and littermate controls. **A-B:** N-cadherin expression is localized to the corneal endothelial layer in controls in the anterior chamber (A, arrowheads). N-cadherin expression was seen in a cluster of cells that accumulate anterior to the lens in the *Ehd1 CKO* eyes (B, arrowheads). **C-D:** ZO-1 expression is almost completely lost from the anterior segment and corneal endothelium (D, arrowheads) in contrast to the control (C, arrowheads). **E-F:** In control cornea (A), K-12 is expressed in corneal epithelial cells. K-12 expression is maintained in *Ehd1 CKO* eyes (B). Scale bar is 50 μm.

	Microphthalmia	Cataracts	Microphthalmia + Cataracts	Anophthalmia	Normal
No. of eyes analyzed (%)	12 (5.7%)	55 (26%)	11 (5.2%)	41 (19.3%)	93 (43.8%)

Table 3.1 Summary of prevalence of ocular phenotypes in *Ehd1-null* mice. New-born pups were examined at weaning age to determine the range of ocular defects and tabulated under microphthalmia (small eye), anophthalmia (absence of eye) and cataracts (cloudiness of eye). Individual eyes were accounted for tabulation.

	Microphthalmia	Cataracts	Microphthalmia + Cataracts	Normal
No. of eyes analyzed (%)	70 (41.7)	39 (23.2)	26 (15.5)	33 (19.6)

Table 3.2 Summary of prevalence of ocular phenotypes in *EHD1 CKO* mice. New-born pups were examined at weaning age to determine the range of ocular defects and tabulated under microphthalmia (small eye) and cataracts (cloudiness of eye). Individual eyes were accounted for tabulation.

Chapter 4: Bioinformatics coupled with a high throughput screen identifies novel binding partners for EHD1 protein

10. Introduction

Endocytic recycling is a vital cellular process that ensures the display of membrane receptors on the cell surface at precise levels and within correct subdomains; such regulation is essential for correct cell-cell and cell-environment communication. Members of the C-terminal Eps15-Homology Domain-containing (EHD) protein family serve as critical regulators of endocytic recycling. EHD proteins include four highly homologous members in mammals, EHD 1-4, that play shared as well as unique roles in the endocytic recycling pathway. The EHD paralogs exhibit remarkable sequence identity among the family members (70-87% identical), with EHD1 and EHD3 being the most closely related (B. D. Grant and Caplan, 2008). *In vitro* studies have demonstrated that EHD3 and EHD4 mediate early steps of membrane-associated receptor recycling whereas EHD1 and EHD2 regulate later steps (George et al., 2007; Naslavsky and Caplan, 2011). EHD1 is the best characterized among the four members and regulates the membrane trafficking of transferrin receptor, MHC-I protein, MHC-II protein, β1 integrin, GLUT4 glucose transporter and others. All EHD proteins contain three highly related functional domains: an N-terminal ATPase/GTPase that controls membrane binding and oligomerization, a central coiled-coiled domain that mediates homo- and hetero-oligomerization amongst family members and a characteristic Eps15 Homology (EH) domain localized to the C-terminus of the proteins (Daumke et al., 2007).

The EH domain is an evolutionary conserved recognition module that was first identified as a repeated domain in the N-terminus of the endocytic adapter protein known as epidermal growth factor (EGF) receptor tyrosine kinase substrate (Eps15) (Fazioli et al., 1993). EH domains are present in species as diverse as yeast to higher metazoans such as nematodes, insects and mammals (Confalonieri and Di Fiore, 2002). The EH domain is an approximately 100 amino acids protein-protein interaction module that facilitates interaction

to target proteins. Phage display assays have determined that EH domains bind to proteins containing asparagine-proline-phenylalanine (NPF) tri-peptide motifs (Salcini et al., 1997).

The first structure of an EH domain (Eps15 EH2), solved by NMR studies, revealed the presence of two closely related helix-loop-helix motifs, also called EF hands, connected by a short antiparallel β-sheet (de Beer et al., 2000). Since then, structures of several EH domains have been solved including the EHD proteins. The structure for human EHD1 EH domain and the crystal structure of human EHD2 have demonstrated the basic conservation of the EH domain features seen in previously solved N-terminus EH proteins but with potential differences in surface charge (Kieken et al., 2007). NMR spectroscopy studies have identified that the NPF residues adopt a conformation similar to the type I β-turn motif and completely embed in a hydrophobic domain within the EH domain. The asparagine residue of the NPF motif is capable of tightly interacting with a conserved tryptophan residue within the EH domain (de Beer et al., 1998; de Beer et al., 2000). Mutation of this conserved tryptophan residue impairs EH-NPF interaction (de Beer et al., 1998). The EH domain found in EHD proteins differs from that of N-terminal EH proteins by a highly positive electrostatic surface potential that exhibits preference for acidic residues following the NPF motif in interacting proteins.

EHD proteins mediate several of their receptor recycling functions by intimately binding to endocytic regulatory proteins. Recent studies have identified approximately 25 such direct or indirect interaction partners. Even though the exact mode of interaction is not known in all the cases, the great majority of these interactions are mediated via the EH-NPF binding. The binding of EHD proteins to Rab4/Rab5 effector Rabenosyn-5 (Naslavsky et al., 2004); Rab11 effector Rab11-Fip2 (Naslavsky et al., 2006b); PACSIN/syndapin I and II (Braun et al., 2005); SNARE protein SNAP29/GS32 (Xu et al., 2004); MICAL-L1 (Sharma et al., 2009); a cell fate specification protein Numb (C. A. Smith et al., 2004); EHBP1 (Guilherme et al., 2004); and Myoferlin (K. R. Doherty et al., 2008) is mediated by one or

more NPF motifs present in these proteins. Interestingly, the consensus NPF motifs of these proteins have acidic residues at +1, +2 and +3 positions.

Previous studies have commented on the presence of hundreds of NPF-containing proteins in the *C. elegans* proteome (B. D. Grant and Caplan, 2008). However, our current knowledge is limited to a handful of interaction partners known so far. Since the majority of EHD protein functions and sites of action are dependent on their protein-protein interaction module, we have synthesized a peptide library to detect novel interaction partners of EHD1 using a fluorescence polarization (FP) based quantitative high-throughput assay (qHTS). In order to design an exhaustive target list we have extended the motif search to include aspartate-proline-phenylalanine (DPF) and glutamate-proline-phenylalanine (GPF) motifs that have been previously known to bind the EH domains (Kieken et al., 2010).

My studies describe the development and optimization of a competitive qHTS screen using GST fused-EH domain of EHD1 protein. I report the identification and validation of several new interaction partners of EHD1. This study is an important step towards our understanding of molecular processes regulated by EHD1 proteins given the identification and characterization of several new interaction candidate genes.

11. Results

11.1 Bioinformatics analysis to identify potential EHD1 binding partners

In order to identify potential interaction partners of EHD, I mapped all human proteins in SwissProt database using a query set of 99 motif sequences. The query set consists of 7-mer custom-designed sequences taking into account NPF, DPF, and GPF ligands together with D/E/S/K at +1 to +4 positions (N/D/G-P-F-X-X-X-X-X, where X represents D/E/S/K). Acidic amino acid positions following the core NPF motif have been suggested to be important for EH-domain mediated EHD interaction selectivity. I have included serine and lysine in the extended list since phosphorylation or acetylation modifications, respectively, on these residues could alter the affinity of binding to EH domains within cellular environments where such modifications can take place. From this query, I identified a total of 2793 prospective candidate proteins/ORFs containing at least a single motif (Appendix A). Within this list, 776 proteins contained one or more NPF or extended NPF motifs. Furthermore, I found 790 proteins that contained at least one DPF or extended DPF motif and 984 proteins with at least one GPF or extended GPF motifs. A minor subset of 14 proteins contained all three motifs (Figure 4.1A).

Next, I used filtering parameters (details in Chapter 2) to narrow down the extensive list of 2793 proteins. As previously discussed, presence of multiple copies of NPF/DPF/GPF motifs is associated with stronger likelihood of interaction with an EH containing protein, as shown in the case of known interactor proteins for EHD1 including Rabensoyns 5 (seven motifs including six NPFs, one GPF), Rab11-Fip2 (four motifs including three NPFs, one DPF), Syndapins/Pacsins I (two NPFs), Syndapin II (three NPFs) and MICAL-L1 (three motifs including two NPFs, one GPF). I have focused my studies to include proteins that contained two or more NPF/DPF/GPF motifs. This resulted in the generation of a list containing 403 candidates. This list was then further filtered to remove secreted/extracellular proteins resulting in a total of 48 proteins containing at least a single NPF motif, 40

containing a single DPF and 68 containing at least one GPF motif. The list included 14 proteins that were positive for the presence of all three motifs (Figure 4.1B). Functional classification based tools were used to further select a subset of proteins within this list to synthesize a peptide library. Our final list was narrowed down to include 137 candidate proteins, including previously known EHD interaction partners. Within this candidate list, 23 proteins contained at least a single NPF motif, 13 proteins had DPF motifs and 20 contained GPF motifs. 6 proteins had all three motifs (Figure 4.1C).

A total of 333 individual peptides, corresponding to unique motifs identified in the final 137 proteins, were synthesized as 9-mer sequences to include the 7 amino acid motif identified by bioinformatics and two additional C-terminal residues (Appendix C). Within these putative EH domain ligands, 41% (135/333) corresponded to NPF, 31% (103/333) to DPF, and 29% (95/333) to GPF related motifs (Figure 4.1D).

11.2 Binding assay development & optimization for qHTS

To set up the peptide binding assay, two different GST EH-domain constructs incorporating the EH domain of EHD1 were purified and tested. EH1-A (residues 438-534) is an exclusive EH domain construct that includes a shorter linker region whereas, EH1-B (our lab designed construct) includes residues 400-534 for a complete linker region and EH domain. As a highly conserved tryptophan residue in the EH domain is important for binding to interaction partners (de Beer, 1998, 2000), I also generated a mutant construct designated EH1-B-W485A to further validate the EH domain-dependence of peptide binding in my assay. The GST-EH domain fusion proteins were purified by glutathione-sepharose affinity chromatography and purity assessed by coomassie staining of samples resolved on SDS-PAGE gels, as shown in Figure 4.2.

In three separate experiments, EH domain fusion proteins were titrated into FITC-βA-NPFEEEEED-[OH] (referred to as NPF1) peptide (100 nM determined by probe

standardization, data not shown). I observed a dose-dependent increase in the FP, indicating binding of FITC-labeled probe to purified GST-EH domain fusion proteins. The binding affinities (K_d), as determined by curve fitting the data, were very comparable for EH1-A (6.1 ± 0.1 μM) and EH1-B (7.1 ± 0.2 μM) constructs (Figure 4.3A). The EH1-B-W485A mutant on the other hand displayed markedly lower binding affinity (50 ± 5 μM), consistent with the critical role of the tryptophan 485 residue in mediating EH-NPF interactions. The GST protein, used as an internal control, displayed no apparent binding to the FITC-NPF1 peptide (Figure 4.3A). Since I did not observe much difference between the binding affinities of EH1-A and EH1-B fusion proteins, I utilized the EH1-B protein for all subsequent experiments described below.

To develop an assay suitable for a high throughput screening format, I set up a FP competitive binding assay and tested variables such as incubation time and DMSO concentration. To demonstrate competitive inhibition of EH1-ligand peptide interaction, I titrated the unlabeled –[H]-G-NPFEEEEED-[OH] peptide (referred to as NPF2) into a mixture of GST-EH1-B and FITC-NPF1 peptide. The IC_{50} value determined through curve fitting was 32.95 ± 2.3 μM and inhibition constant (K_i) was determined to be 13.68 μM (Figure 4.4). To rule out the possibility of nonspecific binding, I titrated another peptide that maintained the overall negative charge but lacked the critical NPF motif, -[H]-G-APAEEEEED-[OH] (referred to as APA3) (Figure 4.4). No decrease in FP values was observed with increasing concentrations of the APA3 peptide confirming that an intact NPF motif is a specific requirement for EH domain binding interaction with its ligands.

Next, I determined the stability of binding over time. Fluorescence polarization was measured at incubation periods of 5, 15, 30 or 60 min at room temperature. The K_d values were determined to be 14.9 ± 2.1, 23.4 ± 4.3, 20.3 ± 3.9 and 16.0 ± 4.3 at 5, 15, 30 and 60 min, respectively (Figure 4.5). The qHTS assay was therefore designed such that the plates

were set up at room temperature (25°C) and read immediately after the addition of all components.

I also determined the effect of DMSO on the FP values and total fluorescence (TF). Increasing concentrations of DMSO (0, 2.5, 5, 10 or 20%) were added to a master mix containing 100 nM NPF1 and 10 µM EH1-B. FP and TF values did not change with up to 10% DMSO (Figure 4.6). A final concentration of 5% DMSO was selected for the qHTS assay.

Finally, I determined the optimal protein concentration to be used in the qHTS screen. For this, a competition assay with 100 nM NPF1, 1 mM NPF2 and varying concentrations of EH1-B (2.5, 5, 7.5, 10 or 12.5 µM) were used (Figure 4.7). A concentration of 10 µM EH1-B gave an IC_{50} value of 33.2 ± 2.5 µM with a K_i of 13.8 µM.

Next, I determined a non-unit statistical parameter Z-score that reflects the reproducibility and reliability of qHTS assays. For this, I measured the FP values for 100 nM FITC-NPF1 alone, 100 nM NPF1 + 10 µM EH1-B, and 100 nM NPF1 + 10 µM EH1-B + 125 µM NPF2 in the presence of 5% DMSO. The average Z-score was 0.76, indicating that the assay is reproducible and suitable for a high throughput screen (Figure 4.8).

Based on these initial experiments, I determined the following conditions for my peptide screen: 10 µM EH1-B protein concentration, 100 nM FITC-NPF1, a final concentration of 5% DMSO, assay set up at room temperature and no further incubation period prior to reading the plates

11.3 Quantitative high-throughput assay to identify novel interactors

The screen was performed as illustrated in schematic Figure 2.2. The experiments were carried out on a Biomek FX platform and plates were read on a SpectraMax M5 plate reader as described in the methods section. The 333 peptides in the library were dissolved in DMSO at 100 mM concentration in 96 well plates. Each assay was carried out with 80

peptides at a time, including controls (NPF-1 alone, NPF-1 + EH1-B, NPF-1 + EH1-B + NPF-2). After measuring TF and FP values, the data were sorted and plots were generated on SigmPlot 11.0. Positive candidates were defined as peptides with a K_i value ≤ 200 μM. The average K_i value for the control peptide (NPF-2) was determined to be 42.9 μM. Minimum Significance ratio (MSR) was determined to be 1.66 for the control set. Based on the K_i values, positive candidates were grouped into three arbitrary groups in the order of their affinities for the EH domain of EHD1: Group I (K_i ≤ 50 μM), Group II (K_i ≤ 80 μM) and group III (K_i ≤ 200 μM) (Table 4.1). Each group included known interaction partners of EHD1 with Group I including most of these candidates. Of the eight known EHD1 interactor proteins tested in the screen, my screen detected seven of these, including Rabenosyn 5, SNAP-29, Rab11-Fip2, Syndapin I and II, MICAL-L1, and Fer-L15. The only protein whose competitive inhibition fell above the threshold of 200 μM was the Small conductance (KCa2.3) Ca^{2+}-activated K^+ Channel protein. KCa2.3 is a channel protein that associates with EHD1, however the exact mode of interaction is still uncharacterized. I included this candidate protein since it contained a single NPF tri-peptide motif.

My qHTS assay detected forty-two candidate proteins out of one hundred thirty seven selected candidates including seven proteins out of the eight known interactor proteins. Of the 34 new candidates, EHBP-1 was previously shown to bind with EHD2 (Guilherme et al., 2004). The screen detected four different protein families where multiple members were represented within my final list of candidates. These families are: 1) Secretory carrier-associated membrane proteins, 2) Arf-GAP domain and FG repeat-containing proteins, 3) Cadherin EGF LAG seven-pass G-type receptors, and 4) DnaJ homolog subfamily B members.

As expected, the binding affinities vary based on the motif sequence, with acidic residues following the NPF motif dictating the strongest interactors. Interestingly, serine/lysine residues were frequently observed in my novel target proteins at +1, +2, +3, +4

and +5 positions, indicating that acidic residues following phenylalanine is not the only requisite for effective EH-NPF binding.

As a further complement to my screen, I determined the docking affinities of each peptide from the selected candidate list using crystal structures of the EH domain of EHD1 obtained from PDB (Kieken et al., 2007). All but three of the peptides had a negative re-rank score, indicating an energetically favorable binding conformation (Table 4.2). The structures of peptides with the lowest re-rank score are depicted in Figure 4.9. Smoothened homolog peptide, corresponding to the sequence (-NPFCPEPSP) gave the lowest Molegro re-rank score suggesting strongest docking possibility. Smoothened homolog is a bona fide EHD1 interactor discovered in our laboratory (manuscript under review). The correlation R^2 between docking score and K_i was 0.002. We observed that there exists no correlation between the experimentally determined K_i values and the Molegro re-rank score, indicating the interaction between the candidate peptides and the EHD1 protein is far more complex than mere steric favorability and electrostatics.

11.4 Identification of Dnaja2 as a novel EHD1 interaction partner

I used yeast two-hybrid binding assay to confirm the association of EHD1 with a novel interactor, a member of the DnaJ/HSP40 family of proteins, using Hela cDNA library (Figure 4.10A). This family of evolutionary conserved proteins is known to play important roles in regulating molecular chaperone activity. DNAJ proteins include three distinct domains: an N-terminal J domain connected by a linker domain to a middle/C-terminal (MC) domain that contains two zinc finger motifs and a substrate-binding site (Qiu et al., 2006). The screen identified four clones that were sequence verified to be the DnaJ subfamily A member 2 (DnaJA2). DnaJA2 contains a single NPF motif present in its C-terminus. Next, I verified whether the interaction is mediated by the EH domain of EHD1 using GST pull-down experiments. To do this, I overexpressed HEK293 cells with DNAJA2-GFP and GFP-

Rabensoyn5 (as a positive control) and eGPF plasmid (as a negative control). Cell lysates were prepared from the transfected cells and incubated with glutathione-Sepharose beads coated with purified GST-fusion proteins of EH1-A, EH1-B, EH1-B W485A mutant and GST alone as a control. As expected, both GST-EH1-A and EH1-B pulled down DNAJA2 whereas EH1-B W485A mutant or GST alone vector did not pull down DNAJA2 protein (Figure 4.10B). As a control experiment, Rabenosyn5 was pulled down with both EH1-A, EH1-B and to a substantially lower extent with EH1-B W485A mutant. These results lead us to conclude that DNAJA2 is indeed a novel interaction partner of EHD1 and that this interaction is mediated through EH-NPF binding. The K_i of the peptide corresponding to this family member fell below the 200 nM threshold in my qHTS assay but multiple members of this family (DnaJ subfamily B members 1, 4 and 5) scored positive.

12. Discussion

Since the discovery of EHD proteins more than a decade ago, a number of interaction partners have been reported based on commonly used biochemical assays. I report the development and optimization of a FP based qHTS assay to identify novel interaction partners of EH domains, which I have tested using the EH domain of EHD1. FP is a solution-based assay that can detect the binding of a fluorescently labeled peptide to a protein of interest. The technique is based on the principle that the degree of polarization of a fluorescently labeled molecule is inversely proportional to its rate of molecular rotation when excited by polarized light. FP assays are widely used in monitoring enzyme-catalyzed hydrolysis, screening for inhibitors of protein-protein interaction and protein-nucleic acid interactions.

At the cellular and molecular level, it is anticipated that interactions of EHD1 and other EH domain-containing proteins with key target proteins provide a fundamental mechanism to regulate trafficking events. Many of these interactions are mediated through the EH domain-NPF motif binding. Though traditionally thought of as weak interactions, a tighter EH-NPF binding results from the influence of neighboring amino acid residues, as demonstrated by the strong positive impact of the presence of negatively charged residues following the NPF sequence (G. D. Henry et al., 2010). EH interactions are also mediated through DPF and GPF tri-peptide motifs. I employed these primary motifs together with negatively charged amino acids and serine/lysine residues to derive a list of motifs that were searched in the human protein databank. I identified a total of 2793 potential interaction partners that were filtered to select candidates based on subcellular localization and the presence of multiple motifs. As a pilot screen, I concentrated my efforts on a subset of these candidate motifs by concentrating on selected pathways, including vesicular trafficking, membrane transport, actin cytoskeleton and developmental pathways such as Dorso-ventral

axis formation, Axon guidance. The selected candidate list included 137 prospective EH domain interaction partner proteins within our peptide library.

I optimized the assay conditions and established the development of a high-throughput assay using the purified EH domain of EHD1. My screen detected a total of 42 positive candidates with an overall hit rate of 31%. I included eight candidate proteins that are already known and confirmed as interaction partners of EHD1. My assay detected all but one (KCa2.3), which is still uncharacterized in terms of its mode of EHD1 binding (Gao et al., 2010). Several of the identified EHD1 EH domain interactors are known to play a key role in vesicular trafficking including EH domain-binding protein, Epsin-2 and 3 (Salcini et al., 1999), AP2-associated protein kinase 1 (Conner and Schmid, 2002), Lysosomal-trafficking regulator (Barbosa et al., 1996), Synaptojanin-1, Disabled homolog 2 and Stonin-2 (Miliaras and Wendland, 2004).

My study identified several isoforms within a set of four important protein families. Each of these family members was represented multiple times in my screen. These candidate families include: 1) Secretory carrier-associated membrane protein (SCAMPs), 2) Arf-GAP domain and FG repeat-containing protein family (AGFGs), 3) Cadherin EGF LAG seven-pass G-type receptor family (CELSRs), and 4) DNAJ homolog subfamily members (DnaJs). Interestingly, DNAJ homolog subfamily A family member, DNAJA2 was identified and confirmed as a novel EHD1 target-using yeast two-hybrid and pull down assays. Separately, Smoothened, which was identified as a novel EHD1 interactor, was confirmed in pull-down assays (Manuscript under review). The high success rate in identifying binding motifs of high or moderate affinity among previously known EHD1 or other EHD interactors or interactors of EH domains of other endocytic proteins (EH domain-binding protein, Epsin-2 and 3, AP2-associated protein kinase 1 (Conner and Schmid, 2002), Lysosomal-trafficking regulator, Synaptojanin-1 (Montesinos et al., 2005), Disabled homolog 2, Stonin-2, Numb (Santolini et al., 2000), and the validation of examples of proteins newly identified in my

screen, together provide strong confidence that a majority of new EH domain interactors identified through our bioinformatics coupled with qHTS screen will emerge as genuine EH protein interactors. Importantly, the qHTS methodology developed here is suitable for expansion of this approach to other members of the EHD family as well as to other EH domains to help define the relative preferences of informatics-based motifs to various EH proteins to clearly define the hierarchy of EH domain-mediated protein-protein interactions within the endocytic system. As neighboring amino acid sequence and their post-translational modifications other than those considered here can positively or negatively impact the affinity of core NPF/DPF/GPF motifs to EH domains, future screens based on the approach defined here should help deepen our understanding of the endocytic traffic regulation through EH domain-dependent protein-protein interactions.

Secretory carrier membrane proteins (SCAMPs) 1-3 belong to a family of integral membrane proteins that play key roles in membrane trafficking. SCAMPs are components of secretory granules in exocrine glands, post-Golgi transport vesicles and synaptic vesicles. SCAMPs typically contain four transmembrane domains flanked by short cytosolic N- and C-termini. The N-terminus contains several tri-peptide that binds to EH domain proteins including, intersectin 1 and γ-synergin (Fernandez-Chacon et al., 1999; Fernandez-Chacon et al., 2000). SCAMPs participate as intrinsic membrane proteins of recycling vesicles that serve to recruit clathrin coats to the plasma membrane and the trans-Golgi network.

The family of Arf-GAP domain and FG repeat-containing proteins include regulators of intracellular traffic that nucleate the assembly of coat proteins at sites of carrier vesicle formation. AGFG1 acts as a cofactor for viral Rev, a step essential for HIV-1 replication (Yu et al., 2005).

The cadherin epidermal growth factor laminin G seven-pass G-type receptors (CELSRs) include a subgroup of adhesion G protein-coupled receptors that play roles in processes such as neuronal/endocrine cell differentiation, vessel valve formation, and

control of planar cell polarity during embryonic development. *Celsr* knockout animals exhibit several developmental defects and genetic mutations in humans are related to neural tube closure defects and cardiovascular diseases (X. J. Wang et al., 2014).

DnaJ/Hsp40 (heat shock 40) represents an evolutionary conserved protein family that plays important roles in protein transport across membranes, folding of newly synthesized proteins, refolding of misfolded proteins, and degradation, primarily by stimulating the ATPase activity of chaperone proteins, Hsp70s. The family of DnaJ/Hsp40 proteins includes 40 members in humans. DNAJ proteins contain three distinct domains: a conserved J domain (~ 70 amino acids) through which they bind to their partner Hsp70s, a glycine/phenylalanine (G/F)-rich region, and a cysteine-rich domain containing 4 motifs resembling a zing finger domain (Kampinga and Craig, 2010).

Future work is required to establish functional connection of EHD1 or other EH domain proteins with the new interaction partners, especially the protein families discussed above with multiple members identified in the screen.

Currently there are relatively limited chemical agents available to inhibit EH1-dependent vesicle trafficking pathways. The identified NPF peptides from my screen can be used to derive higher affinity binding ligands that could serve as biological probes or potential inhibitors with implications to investigate EHD1's role in cancer invasion and metastasis. The qHTS screen established here can also be directly used with small molecule chemical libraries to identify inhibitors of EH domain-target protein interaction.

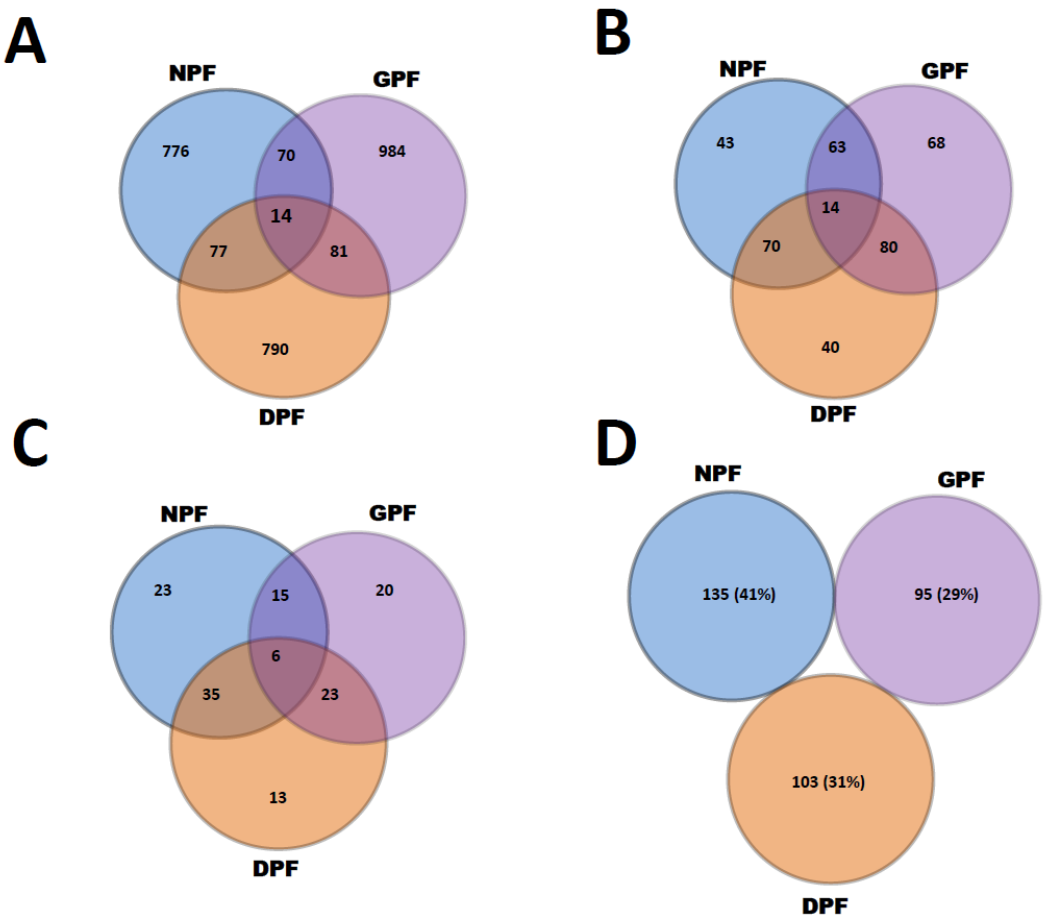

Figure 4.1 Venn Diagrams representing number of proteins containing NPF/DPF/GPF or combination motifs. A: Motif intersection from the complete list of 2973 candidate proteins. B: Motif intersection from the filtered list of 378 proteins containing two or more motifs. C: Motif intersection from the final candidate list of 137 proteins. D: Motif breakdown in our synthesized peptide library.

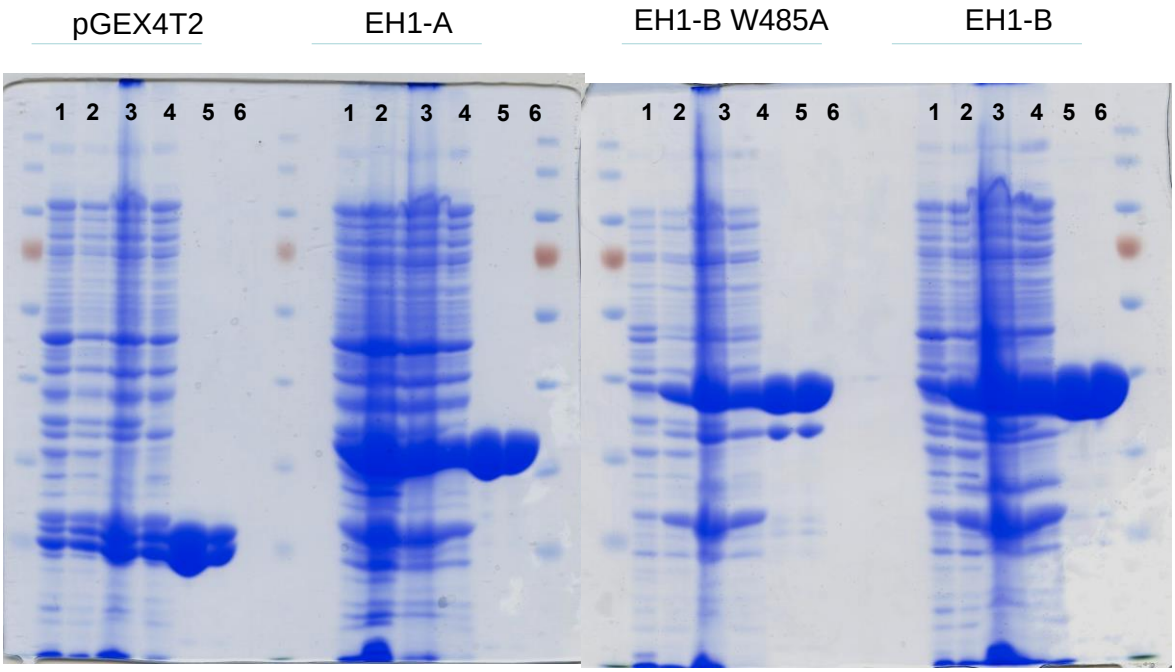

Figure 4.2 SDS-PAGE of samples from different EHD1-EH fusion proteins. Recombinant GST-EH1 (EH1-A), EH1-B, EH1-B W485A, and GST control proteins were expressed in bacteria and purified using Sepharose beads. The contents of each lane represents, 1- Pre Induction, 2- Post Induction, 3- Lysate after bacterial sonication, 4- Supernatant after centrifugation, 5- Eluted purified proteins, 6- Dialyzed purified proteins.

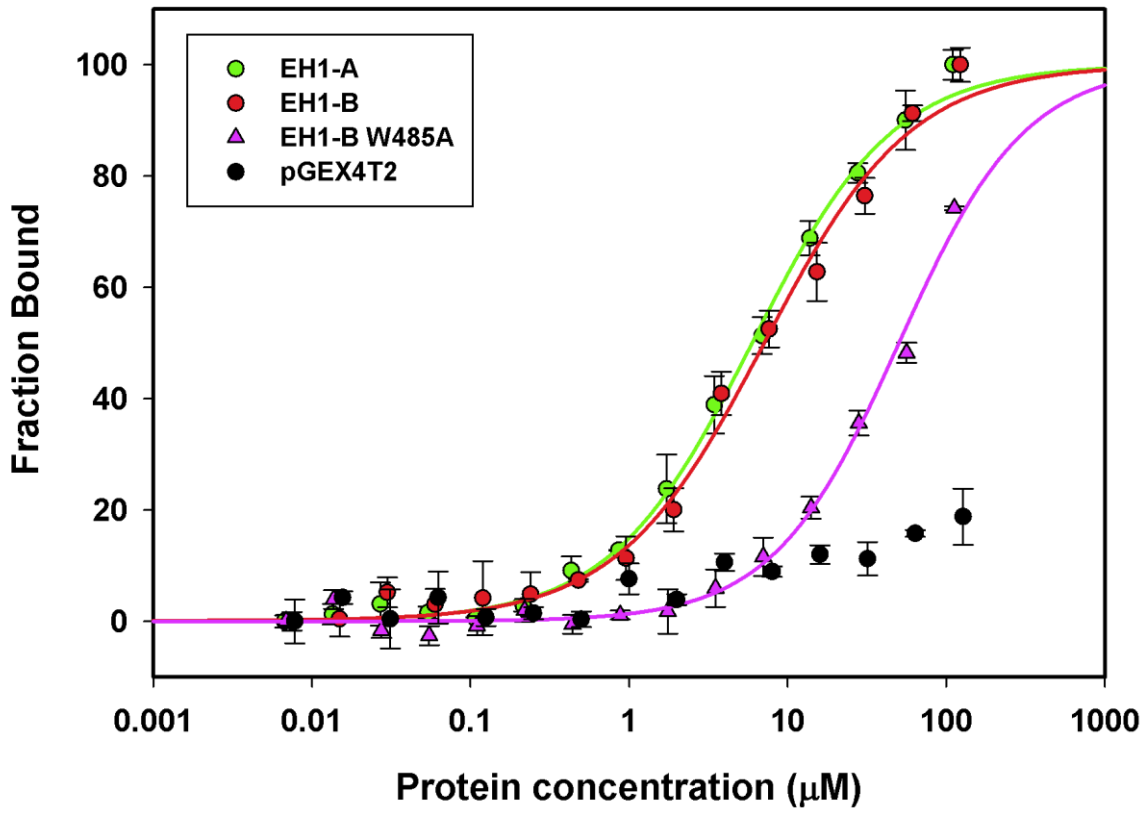

Figure 4.3 Direct binding assay of NPF2 probe with different GST-fusion proteins. K_d: EH1-A = 5.9 ± 0.2 μM; EH1-B = 7.1 ± 0.3 μM, EH1-B W485A = 50.3 ± 1.7 μM; and GST-vector alone. Error bars represent the standard deviation from three or more test replicates.

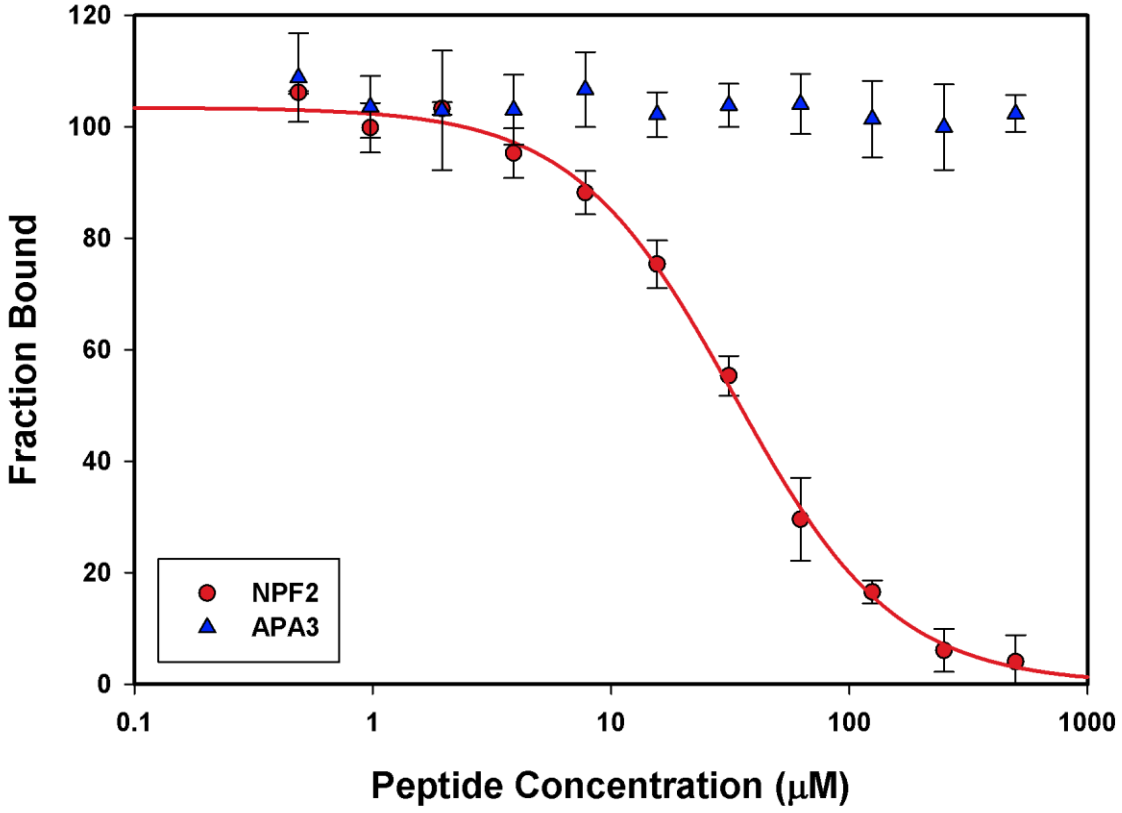

Figure 4.4 Competitive inhibition assay. Unlabeled NPF2 and APA3 peptides were titrated into a master mix of GST-EH1-A (10 μM) + 100 nM FITC-NPF1. IC_{50} = 32.95 ± 2.3 μM; K_i = 13.68 μM. Error bars represent the standard deviation from three or more test replicates.

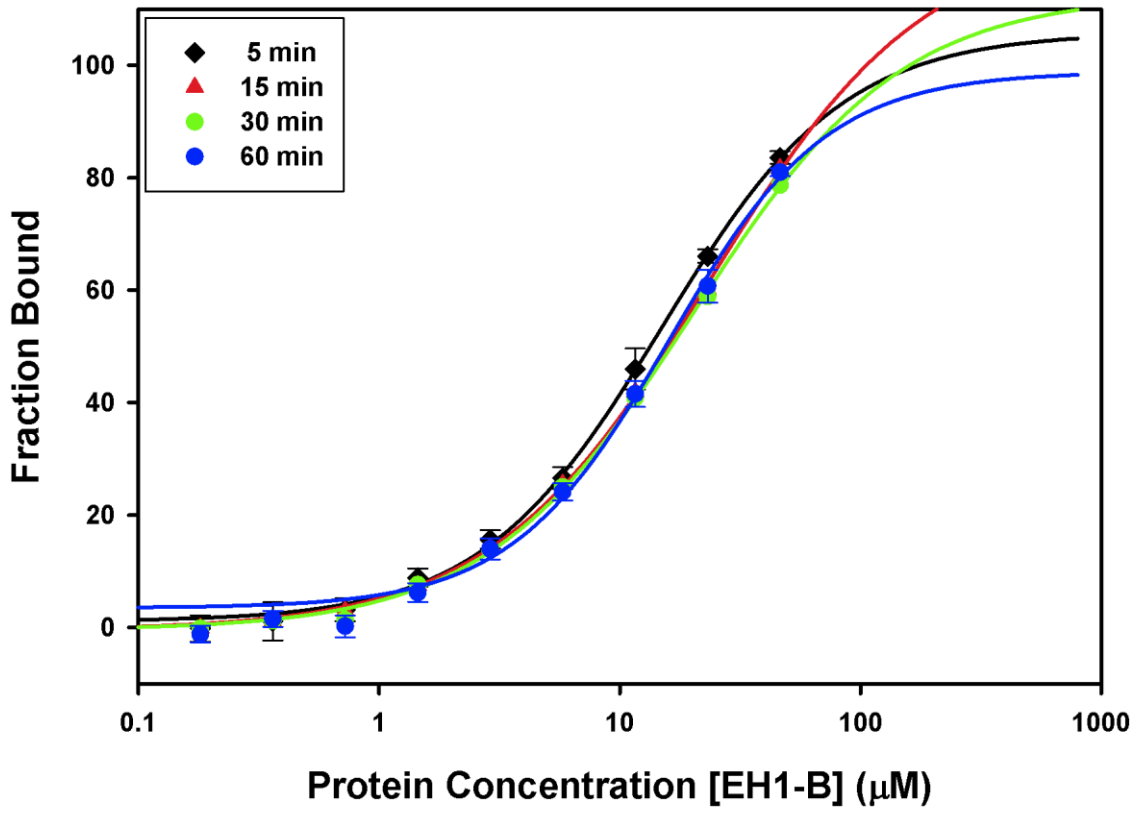

Figure 4.5 Binding reaction at different incubation time-points. 10 μM EH1-B incubated with 100 nM FITC-NPF1 at an interval of 5, 15, 30 and 60 minutes. K_d (5 min) = 14.9 ± 2.1 μM; K_d (15 min) = 23.4 ± 4.3 μM; K_d (30 min) = 20.3 ± 3.9 μM; K_d (60 min) = 16.0 ± 4.3 μM. Error bars represent the standard deviation from three or more test replicates.

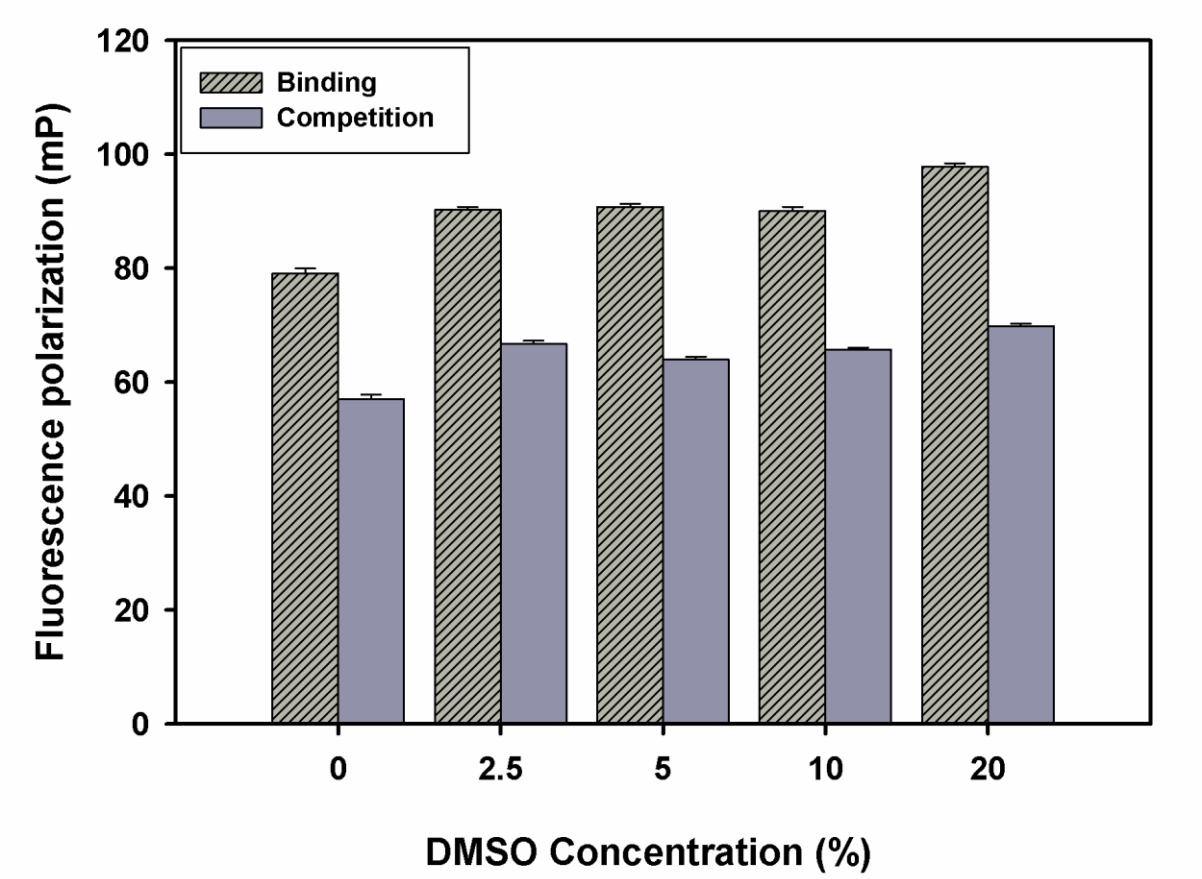

Figure 4.6 Stability of binding and competition assay with increasing DMSO concentration. For binding assay, increasing amounts of DMSO (0, 2.5, 5, 10, 20%) was added to EH1-B (10 M) and NPF1 (100 nM) and read immediately after setting up the reaction. For competition assay, increasing amounts of DMSO (0, 2.5, 5, 10, 20%) was added to EH1-B (10 μM), NPF1 (100 nM), NPF2 (100 μM) and read immediately after setting up the reaction.

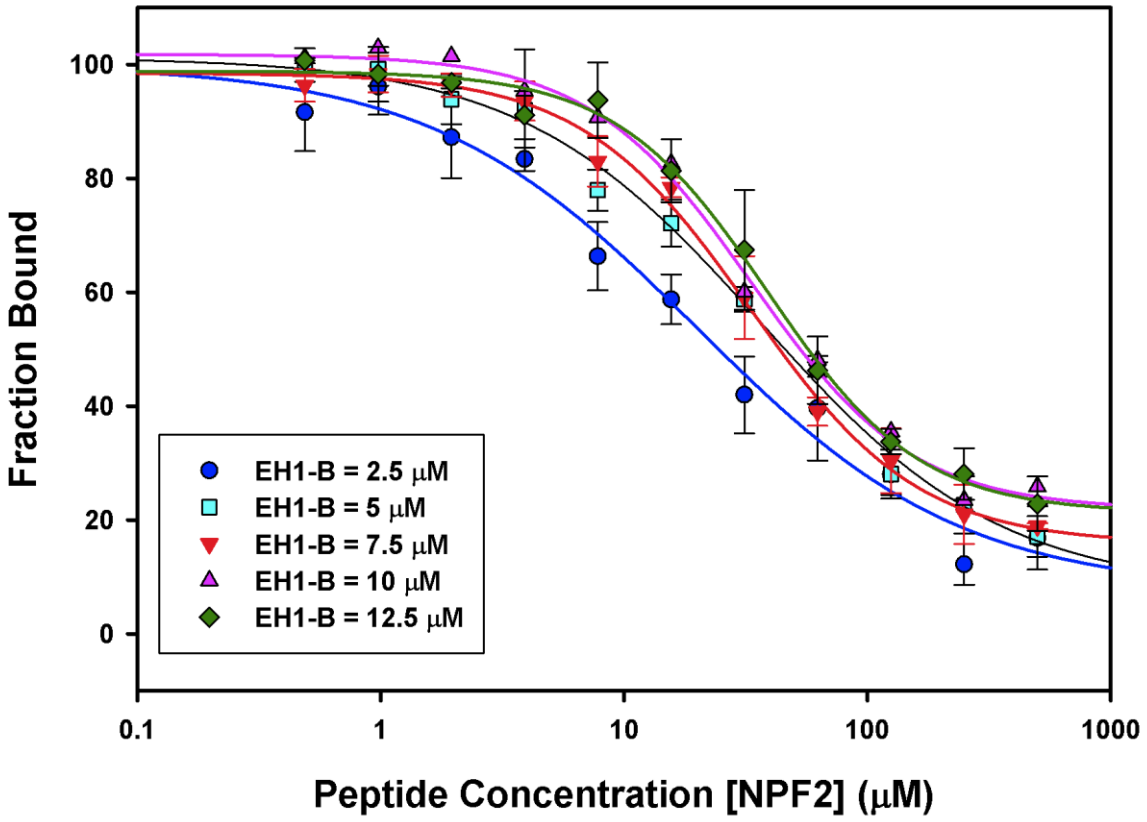

Figure 4.7 Effect of EH1-B protein concentration on an inhibition assay using NPF2 as a competing peptide. Displacement of FITC-NPF1 peptide from EH1-B by unlabeled NPF2 peptide in varying concentration of EH1-B. For 2.5 μM EH1-B (IC_{50} = 19.8 μM ; K_i = 8.2 μM); for 5 μM EH1-B (IC_{50} = 36.8 ± 5.9 μM ; K_i = 15.3 μM); for 7.5 μM EH1-B (IC_{50} = 32.9 ± 2.8 μM ; K_i = 13.7 μM); for 10 μM EH1-B (IC_{50} = 33.2 ± 2.5 μM ; K_i = 13.8 μM); for 20 μM (IC_{50} = 38.9 ± 4.0 μM ; K_i = 16.1 μM). Error bars represent the standard deviation from three or more test replicates.

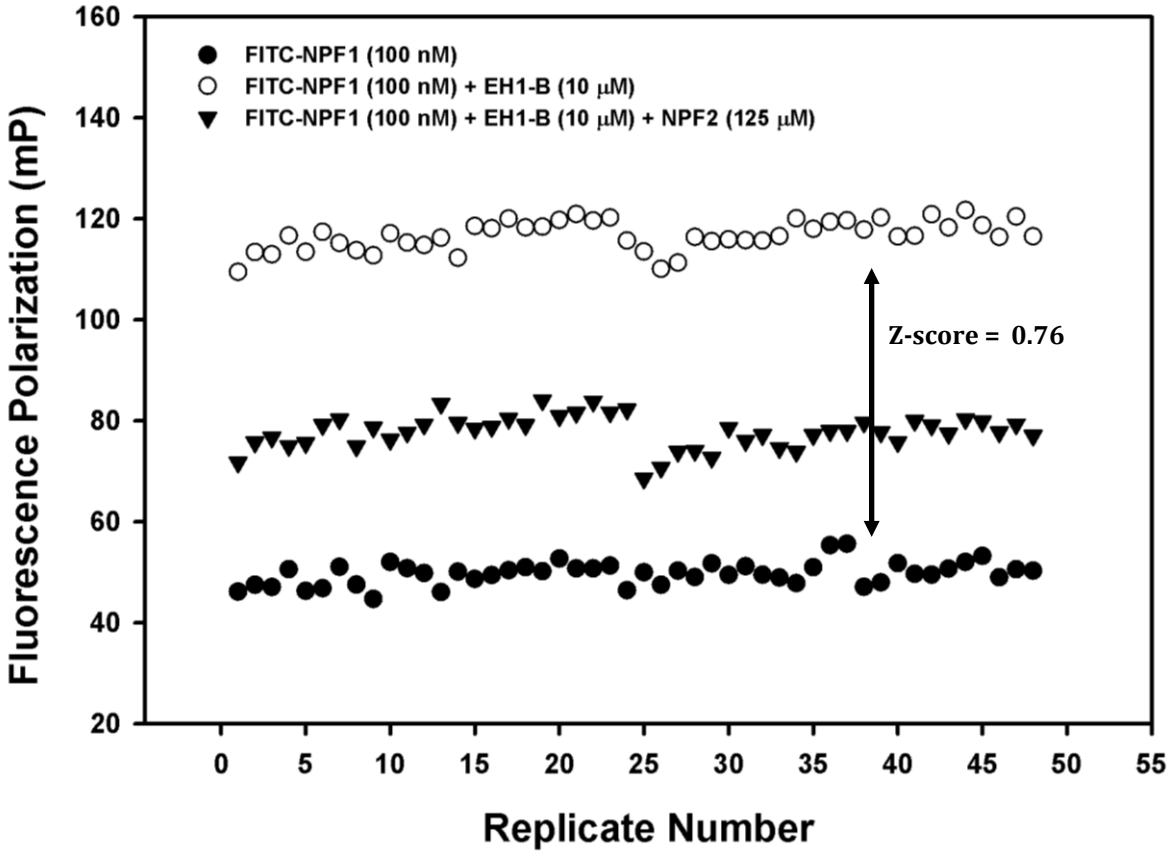

Figure 4.8 Z-score determination from a representative assay plate. The Z score was determined to be 0.76 in the test groups representing background signal (100 nM FITC-NPF1) versus assay signal (100 nM FITC-NPF1 + 10 μM EH1-B + 125 μM NPF2).

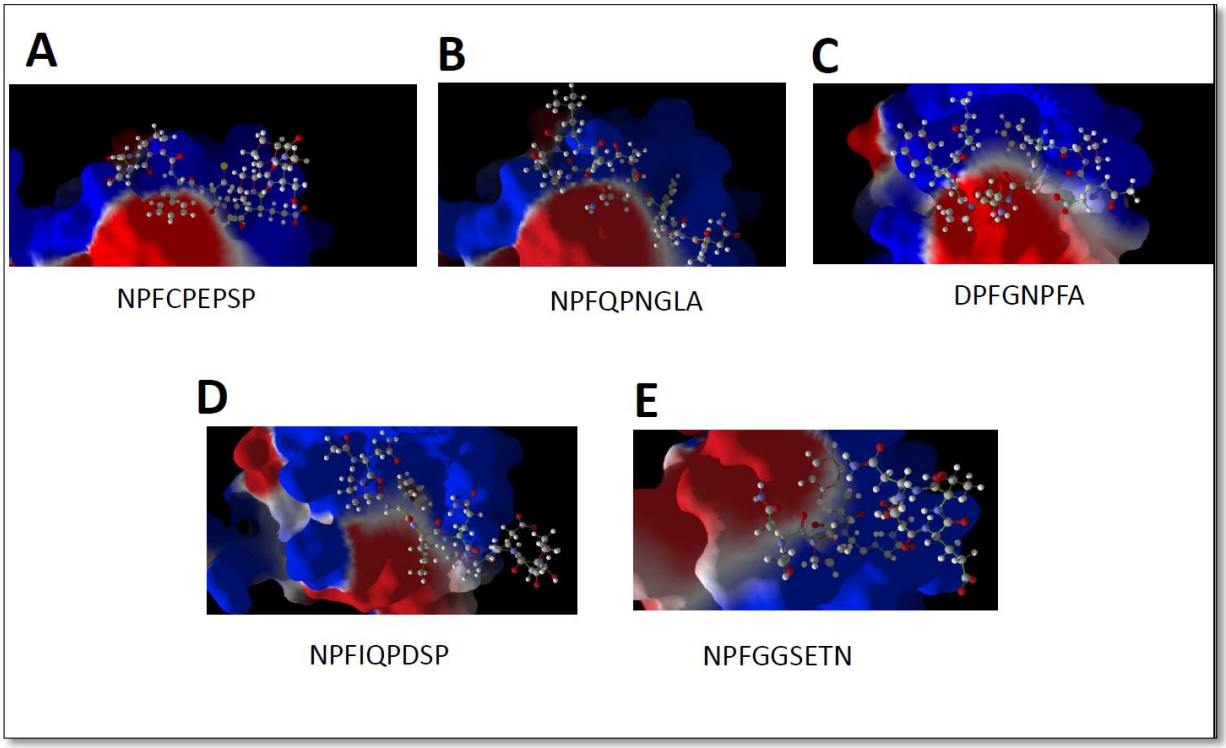

Figure 4.9 Docking affinities representing lowest energy structures of EHD1-EH domain in complex with peptides A) NPFCPEPSP, B) NPFQPNGLA, C) DPFGNPFA, D) NPFIQPDSP and E) NPFGGSETN. EH domain structure is color coded to represent; Red- partial negative charge, Blue- partial positive charge, and white- neutral charge.

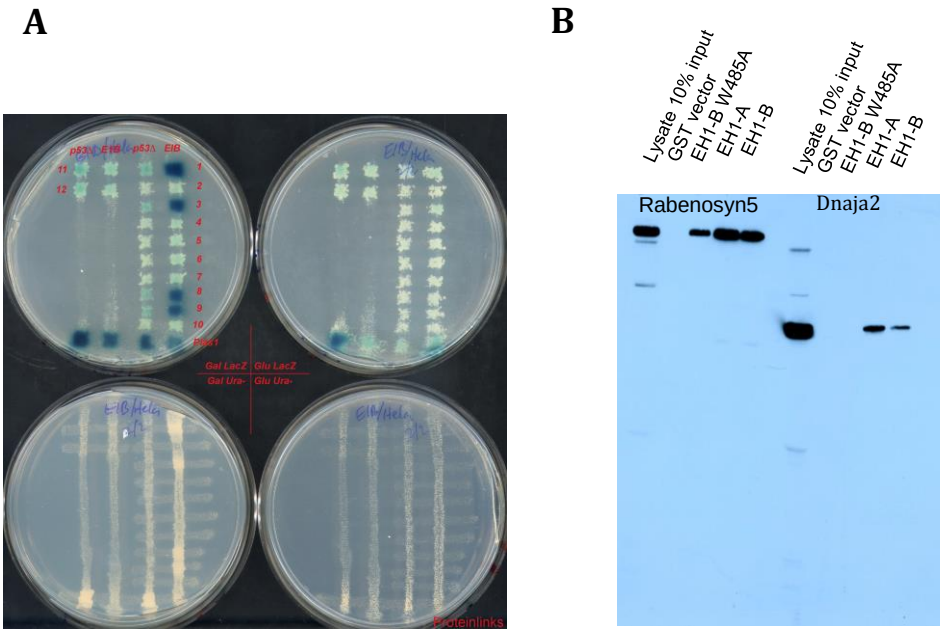

Figure 4.10 EHD1 and DNAJA2 are direct interacting partners. A) Yeast two hybrid studies were performed to assess EHD1 interaction partners using Hela cDNA library. **B) EH-1 DNAJA2 Interaction:** Recombinant GST-EH1-A, GST-EH1-B, GST-EH1-B W485A mutant and GST control proteins were expressed in bacteria and purified using Sepharose beads. 30 ug of purified protein was incubated with 500 mg of cell lysate expressing Rabenosyn5 and DNAJA2. Beads were washed and proteins were separated on 9% SDS-PAGE. EH1-DNAJA2 interaction was analyzed by immunoblotting with anti-GFP antibody. 73 KDa band corresponding to 46 KDa Dnaja2 + 27 KDa GFP is detected.

Protein ID	Protein/Gene Name	Motif Count	Motif Sequence	Ki [μM]
Group 1				
Q9H1K0	Rabenosyn-5	7	NPFEEEDEE	16.4
Q9UNF0	PACSIN2	3	NPFEDEDDT	20.4
O95721	SNAP-29	1	NPFDDDGED	29.6
P98161	Polycystin-1	2	NPFECDCGL	31.3
Q9H1K0	Rabenosyn-5	7	NPFDEEDLS	31.8
Q99698	LYST	4	NPFEETADG	38.6
Q8NDI1	EHBP1	5	NPFGDPDSE	40.5
Q9H1K0	Rabenosyn-5	7	NPFEEPTCI	40.6
Q8NDI1	EHBP1	5	NPFDDPDAA	45.3
Q9H1K0	Rabenosyn-5	7	NPFSEEDEH	50.0
Group 2				
Q7L804	Rab11Fip2	4	NPFEESSET	50.3
Q8NDI1	EHBP1	5	NPFDEPEAF	51.2
Q8N3F8	MICAL-L1	3	NPFEEEEED	51.3
O15127	SCAMP2	3	NPFADPVDV	52.5
Q9BY11	PACSIN1	2	NPFEDDSKG	52.6
O43424	GRID2	4	NPFERDSMY	55.1
Q9UNF0	PACSIN2	3	NPFDDDATS	56.2
Q8WZ42	Titin	12	NPFVVPDAP	57.3
O95081	AGFG2	5	NPFMTGPSS	57.9
O43426	Synaptojanin-1	5	NPFITGLTR	58.2
P98082	Disabled homolog 2	8	DPFGNPFA	59.6
Q2M2I8	AAK1	3	NPFDDDNFS	60.1
Q8WXE9	Stonin-2	2	NPFSAFFEE	62.3
O95081	AGFG2	5	NPFQPNGLA	64.3
P52594	AGFG11	4	NPFQTNARG	64.6
O43426	Synaptojanin-1	5	NPFSDRTAA	65.1
Q7L804	Rab11Fip2	4	NPFDATAGY	65.8
P25685	DNAJB1	2	NPFDTFFGQ	66.3
P98082	Disabled homolog 2	8	NPFLTNGIT	68.7
Q6V1P9	Protocadherin-23	2	NPFDVFLSP	70.8
O43424	GRID2	4	NPFQAVQEA	71.1
P52594	AGFG11	4	NPFMTGAPT	71.1
Q99698	LYST	4	NPFYFSQAM	73.2
Q8WZ42	Titin	12	NPFLAETNQ	73.3
Q9H1K0	Rabenosyn-5	7	NPFIQPDSP	74.2

Protein ID	Protein/Gene Name	Motif Count	Motif Sequence	K_i [μM]
Q9BY11	PACSIN1	2	NPFGGSETN	74.7
Q9H1K0	Rabenosyn-5	7	NPFEMDSDS	76.7
Q13639	HTR4	2	NPFLYAFLN	76.9
Q6V1P9	Protocadherin-23	2	NPFLIHPSF	76.9
Q9H201	Epsin-3	4	NPFLTGLSA	77.9
Q96JX3	Protein SERAC1	2	NPFADPFST	78.5
P35916	VEGFR3	2	NPFISVEWL	79.7
Group 3				
Q8WZ42	Titin	12	NPFALECVV	83.0
Q9UNF0	PACSIN2	3	NPFSSTDAN	83.5
Q8WXE9	Stonin-2	2	NPFLNETLQ	84.3
Q8N2Y8	Iporin	4	NPFCPPELG	84.6
Q6PFW1	PPIP5K1	2	NPFLINDLA	85.1
Q9NZM1	Myoferlin	2	NPFFDELFF	88.4
A0AVI2	Fer-1-like protein 5	3	NPFFNEIFF	91.3
Q96D09	GPRASP2	2	NPFSFWVGE	100.7
Q9UDY4	DNAJB4	2	NPFEIFFGR	103.8
Q99835	Smoothened homolog	2	NPFCPEPSP	107.3
O95081	AGFG2	5	NPFTAPAAQ	110.0
Q8WUH2	TGFBRAP1	2	NPFCEPVFV	112.2
O95208	Epsin-2	4	NPFLAPGAP	113.4
O14828	SCAMP3	3	NPFQDPAVI	125.4
P04629	NTRK1	2	NPFEFNPED	129.6
Q9H2D6	TRIOBP	3	NPFLLSLGV	130.4
Q9NYQ6	CELSR1	3	NPFAEVTTL	133.2
O75953	DNAJB5	2	NPFDIFFAS	137.8
O15126	SCAMP1	3	NPFADPDLN	152.5
Q9HCU4	CELSR2	2	NPFAEVTTN	154.4
O15127	SCAMP2	3	NPFSETNAA	178.1
O14828	SCAMP3	3	NPFETREPP	186.0
Q13492	PICALM	3	NPFGPVSGA	190.9

Table 4.1 K_i scores of positive candidate peptides

ProteinID	Protein/Gene Name	Motif sequence	Score	Crystal
Q99835	Smoothened homolog	NPFCPEPSP	-65.8899	2KFG
O95081	AGFG2	NPFQPNGLA	-63.7208	2KFG
P98082	Disabled homolog 2	DPFGNPFA	-63.0964	2KFG
Q9H1K0	Rabenosyn-5	NPFIQPDSP	-61.9542	2KFH
Q9BY11	PACSIN1	NPFGGSETN	-56.1623	2KFH
O43424	GRID2	NPFQAVQEA	-55.6069	2KFF
O95081	AGFG2	NPFMTGPSS	-55.419	2KFF
Q9UNF0	PACSIN2	NPFSSTDAN	-54.2612	2KFH
O95081	AGFG2	NPFTAPAAQ	-53.0713	2KFH
Q13492	PICALM	NPFGPVSGA	-52.2983	2KFF
Q13639	HTR4	NPFLYAFLN	-51.0078	2KFG
Q9BY11	PACSIN1	NPFEDDSKG	-50.6146	2KFF
Q9H201	Epsin-3	NPFLTGLSA	-48.7665	2KFH
O15127	SCAMP2	NPFADPVDV	-44.9722	2KFH
P98161	Polycystin-1	NPFECDCGL	-43.9035	2KFF
Q2M2I8	AAK1	NPFDDDNFS	-43.0607	2KFH
Q8NDI1	EHBP1	NPFDEPEAF	-42.2263	2KFG
Q8WUH2	TGFBRAP1	NPFCEPVFV	-41.7748	2KFG
Q9UNF0	PACSIN2	NPFEDEDDT	-41.7646	2KFH
O43426	Synaptojanin-1	NPFSDRTAA	-41.3235	2KFF
O95208	Epsin-2	NPFLAPGAP	-40.8927	2KFH
Q8NDI1	EHBP1	NPFGDPDSE	-39.5373	2KFF
Q9H1K0	Rabenosyn-5	NPFSEEDEH	-38.4706	2KFG
Q8N2Y8	Iporin	NPFCPPELG	-37.7525	2KFH
O75953	DNAJB5	NPFDIFFAS	-37.5281	2KFF
P35916	VEGFR3	NPFISVEWL	-36.9718	2KFF
P04629	NTRK1	NPFEFNPED	-36.2652	2KFH
Q96JX3	Protein SERAC1	NPFADPFST	-35.29	2KFG
Q9H1K0	Rabenosyn-5	NPFEEEDEE	-35.265	2KFH
Q8WZ42	Titin	NPFVVPDAP	-34.9619	2KFH
Q6V1P9	Protocadherin-23	NPFLIHPSF	-32.7565	2KFG
Q96D09	GPRASP2	NPFSFWVGE	-32.6678	2KFF
Q8WXE9	Stonin-2	NPFSAFFEE	-31.8959	2KFH
Q8WZ42	Titin	NPFLAETNQ	-31.7733	2KFF
O43426	Synaptojanin-1	NPFITGLTR	-31.6583	2KFG
Q9H1K0	Rabenosyn-5	NPFEEPTCI	-30.9027	2KFG
Q9NYQ6	CELSR1	NPFAEVTTL	-30.9007	2KFG
Q9H2D6	TRIOBP	NPFLLSLGV	-30.8731	2KFG

ProteinID	Protein/Gene Name	Motif sequence	Score	Crystal
Q7L804	RAB11FIP2	NPFDATAGY	-29.0738	2KFF
P52594	AGFG1	NPFMTGAPT	-28.0288	2KFH
Q9HCU4	CELSR2	NPFAEVTTN	-27.8897	2KFH
Q8WZ42	Titin	NPFALECVV	-27.2529	2KFF
O14828	SCAMP3	NPFETREPP	-26.8658	2KFF
Q99698	LYST	NPFYFSQAM	-26.769	2KFH
Q8N3F8	MICAL-like protein 1	NPFEEEEED	-26.4084	2KFF
Q8WXE9	Stonin-2	NPFLNETLQ	-25.3615	2KFF
O43424	GRID2	NPFERDSMY	-23.7501	2KFG
Q6V1P9	Protocadherin-23	NPFDVFLSP	-21.5522	2KFG
Q9UNF0	PACSIN2	NPFDDDATS	-21.2714	2KFH
Q99698	LYST	NPFEETADG	-21.1661	2KFG
O14828	SCAMP3	NPFQDPAVI	-20.5338	2KFG
P98082	Disabled homolog 2	NPFLTNGIT	-20.4701	2KFG
Q8NDI1	EHBP1	NPFDDPDAA	-19.7659	2KFG
Q9H1K0	Rabenosyn-5	NPFDEEDLS	-19.6919	2KFH
P25685	DNAJB1	NPFDTFFGQ	-17.1457	2KFF
Q9H1K0	Rabenosyn-5	NPFEMDSDS	-16.9562	2KFG
Q9NZM1	Myoferlin	NPFFDELFF	-16.2685	2KFH
Q9UDY4	DNAJB4	NPFEIFFGR	-14.5344	2KFG
O15127	SCAMP2	NPFSETNAA	-13.6633	2KFF
P52594	AGFG1	NPFQTNARG	-8.75694	2KFG
Q7L804	RAB11FIP2	NPFEESSET	-6.54745	2KFF
A0AVI2	Fer-1-like protein 5	NPFFNEIFF	-3.47441	2KFF
O95721	SNAP29	NPFDDDGED	N/A	
O15126	SCAMP1	NPFADPDLN	N/A	
Q6PFW1	PPIP5K1	NPFLINDLA	N/A	

Table 4.2 Molegro re-rank score for individual motifs

Chapter 5: Summary and Future directions

Summary

Recent studies have identified that members of the C-terminal Eps15 homology domain-containing (EHD) proteins play a key role in endocytic recycling, a fundamental cellular process that ensures the return of endocytosed membrane components and receptors back to the cell surface. In the studies discussed in this dissertation, I have characterized the ocular phenotypes observed in *Ehd1-null* mice. In addition, by utilizing the EH domain-NPF protein-protein interaction binding module, I have identified novel interaction partners of EHD1.

EHD1 is required for ocular lens development

Towards understanding the biological roles of mammalian EHD family proteins, we and others have begun to use mouse gene deletion models. These studies have started to reveal unique as well as redundant in vivo roles of EHD family members. Here, I provide genetic evidence for a critical role of the C-terminal Eps15 Homology Domain-containing protein 1 (EHD1), a regulator of endocytic recycling, for normal ocular development in mice.

To this aim, I have shown that *Ehd1* knockout mice generated in our laboratory displayed gross ocular phenotypes including anophthalmia, microphthalmia, and congenital cataracts. Alterations in ocular development of *Ehd1-null* mice were characterized using histological and immunohistochemical analyses. In comparison to the wild type (WT) embryos, hematoxylin and eosin (H&E) staining revealed defects in the *Ehd1* mutants that included smaller lenses, lack of lens, and persistence of the lens-stalk and the hyaloid vasculature. Together, these results indicate a requirement of EHD1 in normal eye development. To investigate whether these profound ocular defects in *Ehd1-null* mice resulted from its role in lens versus optic vesicle, I deleted *Ehd1* only in the presumptive lens ectoderm. To do this, I created tissue-specific deletion of *Ehd1* by mating Floxed-*Ehd1* mice to *Le-Cre* mice, which specifically deleted *Ehd1* from the lens and other ocular tissues

including cornea, conjunctiva, and eyelids. *Ehd1 CKO* adult mice recapitulated ocular phenotypes observed in *Ehd1-null* mice including, microphthalmia, congenital and juvenile cataracts. H&E staining revealed that *Ehd1 CKO* lenses were significantly smaller, the epithelial layer was noticeably thinner with sparse cells, and corneal endothelium appears disorganized.

The lens epithelial cells consist of actively proliferating cells that differentiate into fiber cells and thus give rise to the bulk of lens tissue. I determined the epithelial cell counts in *Ehd1* CKO as compared to the littermate cre- (or WT) controls. The *Ehd1* CKO lens epithelium showed significant ($p < 0.001$) reduction in the total number of epithelial cells throughout development suggesting a decline in size as the lens grew. Next, I examined the influence of EHD1 on the cell cycle, by carrying out BrdU incorporation assay. I found an overall trend of reduced BrdU incorporation in *Ehd1* CKO in all the developmental stages (embryonic day (E) 12.5, 14.5, 16.5) examined. Since, the overall number of epithelial cells and BrdU labeling Index decreased overtime in the lenses of *Ehd1* CKO, these findings led us to investigate the role of EHD1 in lens cell survival. I carried out TUNEL assay to detect apoptotic nuclei in serial sections of *Ehd1* CKO and control lens. TUNEL assay revealed a significant ($p < 0.01$) increase in the cell death in *Ehd1 CKO* lens epithelial and fiber cells in critical developmental time-points. These data together indicate that Ehd1 deletion results in decreased proliferation rate and increased cell death within the lens epithelium and thus contributes to the reduced epithelial cell count and lens growth. The differentiating lens fibre cells in *Ehd1 CKO* failed to align properly and were distorted as demonstrated by altered expression of tight junction marker ZO-1. In addition, the corneal endothelium exhibits marked abnormalities with failure to develop tight junctions with neighboring cells as demonstrated by discontinuous ZO-1 expression.

These results indicate that EHD1 regulates proliferation, survival and is thus required for overall development of the lens. The single gene model I have characterized here carries

substantial promise of elucidating novel mechanisms involved in ocular development with implications for understanding the pathogenesis of human ocular diseases such as cataracts, anophthalmia, and microphthalmia.

I speculate, EHD1 deficiency reflects a critical role of cell surface receptors whose endocytic recycling is EHD1-dependent in dictating spatio-temporal signaling events involved in coordinated cell fate, cell proliferation and morphogenetic decisions. Among such receptors, fibroblast growth factor (FGF) receptor signaling together with bone morphogenetic proteins (BMPs) are required for the proliferation and maintenance of lens placode and epithelial cells. Sustained FGF signaling is required for lens epithelial and fiber cells survival as demonstrated by the increased cell death in triple Fgfr mutant mice (MLR 10/ $Fgfr1^{flox/flox}$/$Fgfr2^{flox/flox}$/$Fgfr3^{-/-}$) (Zhao et al., 2008). Similarly, in Ehd1 CKO lenses, the lens epithelium underwent significantly increased apoptosis rate. Future studies will examine if these receptors are indeed direct or indirect targets of EHD1 and such studies will involve direct binding studies, cell biological analyses and mutagenesis.

During early embryogenesis, EHD1 expression is also observed in the developing the optic vesicle that differentiates into the neural retina. Further studies will need to determine if EHD1 function in the optic vesicle is essential for the inductive signaling that is necessary for lens development. This can be examined by deleting *Ehd1* in retinal progenitors of the optic vesicle using *Chx10-EGPF Cre* (Rowan and Cepko, 2004).

Collectively, the data presented in this study provide an essential role of the endocytic recycling pathway regulator EHD1, in regulating key ocular developmental decisions during mouse lens development.

Bioinformatics coupled with a high throughput screen identifies novel binding partners for EHD1 protein

The EH domain mediated EHD1 interactions are essential for their functions. I designed a set of motifs consisting of an extended interaction motif, -N/D/G-P-F-[D/E/S/K]-[D/E/S/K]-[D/E/S/K]-[D/E/S/K]. The resulting combinations of nighty-nine interaction motifs were searched in the human protein database, generating a total of two thousand seven hundred nighty-three prospective binding candidates. This list of candidate genes was filtered to finally obtain a peptide library of three hundred thirty-three 9-mer peptides. To identify novel interactional partners of EHD1, I expressed EH domain of EHD1 as a GST-fusion protein, and used it in a Fluorescence polarization (FP) based quantitative High throughput assay (qHTS). The screen identified forty-two potential candidates from a total of one hundred thirty seven proteins, a hit rate of 31%. The minimum significance ratio (MSR), a statistical parameter to characterize the reproducibility/reliability of the assay, was determined to be 1.66 (Inglese et al., 2006). I incorporated eight EHD1 known interaction partner proteins that contain N/D/G-P-F tri-peptide motifs including, Rabenosyn-5 (seven motifs; six NPFs, one GPF), Rab11Fip2 (four motifs; three NPFs, one DPF), MICAL-L1 (three motifs; two NPFs, one GPF), Fer1-L5 (three motifs; one NPF and two GPF), Syndapin II (three NPFs), Syndapin I (two NPFs), SNAP-29 (one NPF), and KCa2.3 (one NPF) (Naslavsky and Caplan, 2011). Except for KCa2.3, all proteins tested positive in my screen. The binding affinities of NPF peptides are strongest compared to the GPF/DPF motifs. From a total of 135 NPF peptides, 66 peptides demonstrated competitive binding that corresponds to 48.8% success rate. However, a single (DPF-G-N-P-F-A) peptide of Disabled homolog 2 displayed binding in this screen. Overall, the screen identified thirty-four candidate proteins and isoforms as potential EHD1-EH domain interaction partners.

Using yeast two hybrid screen, I identified a novel interaction partner DNAJA2 that belongs to the J family of co-chaperones. Multiple members of DNAJ/HSP-40 family were

represented within my positive candidate list from qHTS screen, validating the results using two different screens. To confirm this binding, DNAJA2, a single NPF motif protein, was precipitated using GST-EH1 fusion protein of EHD1.

My studies have led to the optimization of a FP based qHTS assay to identify novel interaction partners of EHD1. Future studies should address the validation and confirmation of these target proteins with an emphasis to define functions of EHD1 proteins in diverse cellular processes influenced by endocytic trafficking. It would be interesting to screen GST-EH domains of different EHD paralogs (EHD2-4) towards our peptide library to determine if they exhibit preferential binding. EHD proteins form homo-and hetero-oligomers that appear important for their localization and function. This association of EHD proteins might critically regulate cargo transport of specific interaction partner receptors/proteins. We have previously demonstrated that deletion of EHD genes leads to cellular compensation by up-regulation of other family members or its target proteins in specific mouse tissues (George et al., 2010; George et al., 2011; Mate et al., 2012). For example, loss of ankyrin-B in mouse heart tissue resulted in up-regulation of EHD3 protein. Ankyrin-B directly associates with EHD3 through their coiled-coil domain and EHD3 acts a novel trafficking protein to modulate membrane excitability in the absence of ankyrin-B (Gudmundsson et al., 2010). These results suggest functional relevance of EHD proteins with an important physiological implication in heart tissue. This could thus further help narrow down the likely functional targets in a tissue specific manner.

Together the studies above have contributed to establish a novel role of the endocytic recycling pathway regulators of the EHD family, with a focus on EHD1, in regulating key ocular developmental decisions and identify novel targets for this emerging family of regulatory proteins.

Chapter 6: Bibliography

References

Allaire, P.D., Marat, A.L., Dall'Armi, C., Di Paolo, G., McPherson, P.S., Ritter, B., 2010. The connecdenn DENN domain: A GEF for Rab35 mediating cargo-specific exit from early endosomes. Mol. Cell 37, 370-382.

Ashery-Padan, R., Gruss, P., 2001. Pax6 lights-up the way for eye development. Curr. Opin. Cell Biol. 13, 706-714.

Ashery-Padan, R., Marquardt, T., Zhou, X., Gruss, P., 2000. Pax6 activity in the lens primordium is required for lens formation and for correct placement of a single retina in the eye. Genes Dev. 14, 2701-2711.

Barbosa, M.D., Nguyen, Q.A., Tchernev, V.T., Ashley, J.A., Detter, J.C., Blaydes, S.M., Brandt, S.J., Chotai, D., Hodgman, C., Solari, R.C., Lovett, M., Kingsmore, S.F., 1996. Identification of the homologous beige and chediak-higashi syndrome genes. Nature 382, 262-265.

Bassnett, S., Kuszak, J.R., Reinisch, L., Brown, H.G., Beebe, D.C., 1994. Intercellular communication between epithelial and fiber cells of the eye lens. J. Cell. Sci. 107 (Pt 4), 799-811.

Baulmann, D.C., Ohlmann, A., Flugel-Koch, C., Goswami, S., Cvekl, A., Tamm, E.R., 2002. Pax6 heterozygous eyes show defects in chamber angle differentiation that are associated with a wide spectrum of other anterior eye segment abnormalities. Mech. Dev. 118, 3-17.

Beebe, D., Garcia, C., Wang, X., Rajagopal, R., Feldmeier, M., Kim, J.Y., Chytil, A., Moses, H., Ashery-Padan, R., Rauchman, M., 2004. Contributions by members of the TGFbeta superfamily to lens development. Int. J. Dev. Biol. 48, 845-856.

Beebe, D.C., Coats, J.M., 2000. The lens organizes the anterior segment: Specification of neural crest cell differentiation in the avian eye. Dev. Biol. 220, 424-431.

Benjamin, S., Weidberg, H., Rapaport, D., Pekar, O., Nudelman, M., Segal, D., Hirschberg, K., Katzav, S., Ehrlich, M., Horowitz, M., 2011. EHD2 mediates trafficking from the plasma membrane by modulating Rac1 activity. Biochem. J. 439, 433-442.

Benmerah, A., Lamaze, C., Begue, B., Schmid, S.L., Dautry-Varsat, A., Cerf-Bensussan, N., 1998. AP-2/Eps15 interaction is required for receptor-mediated endocytosis. J. Cell Biol. 140, 1055-1062.

Blixt, A., Mahlapuu, M., Aitola, M., Pelto-Huikko, M., Enerback, S., Carlsson, P., 2000. A forkhead gene, FoxE3, is essential for lens epithelial proliferation and closure of the lens vesicle. Genes Dev. 14, 245-254.

Bokel, C., Brand, M., 2014. Endocytosis and signaling during development. Cold Spring Harb Perspect. Biol. 6, 10.1101/cshperspect.a017020.

Bonanno, J.A., 2012. Molecular mechanisms underlying the corneal endothelial pump. Exp. Eye Res. 95, 2-7.

Bonifacino, J.S., Hurley, J.H., 2008. Retromer. Curr. Opin. Cell Biol. 20, 427-436.

Bottger, G., Nagelkerken, B., van der Sluijs, P., 1996. Rab4 and Rab7 define distinct nonoverlapping endosomal compartments. J. Biol. Chem. 271, 29191-29197.

Braun, A., Pinyol, R., Dahlhaus, R., Koch, D., Fonarev, P., Grant, B.D., Kessels, M.M., Qualmann, B., 2005. EHD proteins associate with syndapin I and II and such interactions play a crucial role in endosomal recycling. Mol. Biol. Cell 16, 3642-3658.

Brownell, I., Dirksen, M., Jamrich, M., 2000. Forkhead Foxe3 maps to the dysgenetic lens locus and is critical in lens development and differentiation. Genesis 27, 81-93.

Bucci, C., Parton, R.G., Mather, I.H., Stunnenberg, H., Simons, K., Hoflack, B., Zerial, M., 1992. The small GTPase rab5 functions as a regulatory factor in the early endocytic pathway. Cell 70, 715-728.

Caplan, S., Naslavsky, N., Hartnell, L.M., Lodge, R., Polishchuk, R.S., Donaldson, J.G., Bonifacino, J.S., 2002a. A tubular EHD1-containing compartment involved in the recycling of major histocompatibility complex class I molecules to the plasma membrane. EMBO J. 21, 2557-2567.

Caplan, S., Naslavsky, N., Hartnell, L.M., Lodge, R., Polishchuk, R.S., Donaldson, J.G., Bonifacino, J.S., 2002b. A tubular EHD1-containing compartment involved in the recycling of major histocompatibility complex class I molecules to the plasma membrane. EMBO J. 21, 2557-2567.

Chamberlain, C.G., McAvoy, J.W., 1987. Evidence that fibroblast growth factor promotes lens fibre differentiation. Curr. Eye Res. 6, 1165-1169.

Chen, Y., Doughman, Y.Q., Gu, S., Jarrell, A., Aota, S., Cvekl, A., Watanabe, M., Dunwoodie, S.L., Johnson, R.S., van Heyningen, V., Kleinjan, D.A., Beebe, D.C., Yang, Y.C., 2008. Cited2 is required for the proper formation of the hyaloid vasculature and for lens morphogenesis. Development 135, 2939-2948.

Chow, L.R., Lang, R.A., 2001. Early eye development in vertebrates. Annu. Rev. Cell Dev. Biol 17:255–96, .

Chung, H.J., Qian, X., Ehlers, M., Jan, Y.N., Jan, L.Y., 2009. Neuronal activity regulates phosphorylation-dependent surface delivery of G protein-activated inwardly rectifying potassium channels. Proc. Natl. Acad. Sci. U. S. A. 106, 629-634.

Confalonieri, S., Di Fiore, P.P., 2002. The Eps15 homology (EH) domain. FEBS Lett. 513, 24-29.

Conner, S.D., Schmid, S.L., 2002. Identification of an adaptor-associated kinase, AAK1, as a regulator of clathrin-mediated endocytosis. J. Cell Biol. 156, 921-929.

Coulombre, J.L., Coulombre, A.J., 1963. Lens development: Fiber elongation and lens orientation. Science 142, 1489-1490.

Curran, J., Makara, M.A., Little, S.C., Musa, H., Liu, B., Wu, X., Polina, I., Alecusan, J.S., Wright, P., Li, J., Billman, G.E., Boyden, P.A., Gyorke, S., Band, H., Hund, T.J., Mohler, P.J., 2014. EHD3-dependent endosome pathway regulates cardiac membrane excitability and physiology. Circ. Res. 115, 68-78.

Cvekl, A., Ashery-Padan, R., 2014. The cellular and molecular mechanisms of vertebrate lens development. Development 141, 4432-4447.

Cvekl, A., Duncan, M.K., 2007. Genetic and epigenetic mechanisms of gene regulation during lens development. Prog. Retin. Eye Res. 26, 555-597.

Daro, E., van der Sluijs, P., Galli, T., Mellman, I., 1996. Rab4 and cellubrevin define different early endosome populations on the pathway of transferrin receptor recycling. Proc. Natl. Acad. Sci. U. S. A. 93, 9559-9564.

Daumke, O., Lundmark, R., Vallis, Y., Martens, S., Butler, P.J., McMahon, H.T., 2007. Architectural and mechanistic insights into an EHD ATPase involved in membrane remodelling. Nature 449, 923-927.

de Beer, T., Hoofnagle, A.N., Enmon, J.L., Bowers, R.C., Yamabhai, M., Kay, B.K., Overduin, M., 2000. Molecular mechanism of NPF recognition by EH domains. Nat. Struct. Biol. 7, 1018-1022.

de Beer, T., Carter, R.E., Lobel-Rice, K.E., Sorkin, A., Overduin, M., 1998. Structure and asn-pro-phe binding pocket of the Eps15 homology domain. Science 281, 1357-1360.

de Iongh, R.U., Lovicu, F.J., Chamberlain, C.G., McAvoy, J.W., 1997. Differential expression of fibroblast growth factor receptors during rat lens morphogenesis and growth. Invest. Ophthalmol. Vis. Sci. 38, 1688-1699.

de Iongh, R.U., Lovicu, F.J., Hanneken, A., Baird, A., McAvoy, J.W., 1996. FGF receptor-1 (flg) expression is correlated with fibre differentiation during rat lens morphogenesis and growth. Dev. Dyn. 206, 412-426.

de Renzis, S., Sonnichsen, B., Zerial, M., 2002. Divalent rab effectors regulate the sub-compartmental organization and sorting of early endosomes. Nat. Cell Biol. 4, 124-133.

Doherty, G.J., McMahon, H.T., 2009. Mechanisms of endocytosis. Annu. Rev. Biochem. 78, 857-902.

Doherty, K.R., Demonbreun, A.R., Wallace, G.Q., Cave, A., Posey, A.D., Heretis, K., Pytel, P., McNally, E.M., 2008. The endocytic recycling protein EHD2 interacts with myoferlin to regulate myoblast fusion. J. Biol. Chem. 283, 20252-20260.

Donner, A.L., Lachke, S.A., Maas, R.L., 2006. Lens induction in vertebrates: Variations on a conserved theme of signaling events. Semin. Cell Dev. Biol. 17, 676-685.

Dudley, A.T., Robertson, E.J., 1997. Overlapping expression domains of bone morphogenetic protein family members potentially account for limited tissue defects in BMP7 deficient embryos. Dev. Dyn. 208, 349-362.

Dudley, A.T., Lyons, K.M., Robertson, E.J., 1995. A requirement for bone morphogenetic protein-7 during development of the mammalian kidney and eye. Genes Dev. 9, 2795-2807.

Dukes, J.D., Fish, L., Richardson, J.D., Blaikley, E., Burns, S., Caunt, C.J., Chalmers, A.D., Whitley, P., 2011. Functional ESCRT machinery is required for constitutive recycling of claudin-1 and maintenance of polarity in vertebrate epithelial cells. Mol. Biol. Cell 22, 3192-3205.

Duncan, M.K., Haynes, J.I.,2nd, Cvekl, A., Piatigorsky, J., 1998. Dual roles for pax-6: A transcriptional repressor of lens fiber cell-specific beta-crystallin genes. Mol. Cell. Biol. 18, 5579-5586.

Faber, S.C., Robinson, M.L., Makarenkova, H.P., Lang, R.A., 2002. Bmp signaling is required for development of primary lens fiber cells. Development 129, 3727-3737.

Faber, S.C., Dimanlig, P., Makarenkova, H.P., Shirke, S., Ko, K., Lang, R.A., 2001. Fgf receptor signaling plays a role in lens induction. Development 128, 4425-4438.

Fantes, J., Ragge, N.K., Lynch, S.A., McGill, N.I., Collin, J.R., Howard-Peebles, P.N., Hayward, C., Vivian, A.J., Williamson, K., van Heyningen, V., FitzPatrick, D.R., 2003. Mutations in SOX2 cause anophthalmia. Nat. Genet. 33, 461-463.

Fazioli, F., Minichiello, L., Matoskova, B., Wong, W.T., Di Fiore, P.P., 1993. Eps15, a novel tyrosine kinase substrate, exhibits transforming activity. Mol. Cell. Biol. 13, 5814-5828.

Feng, Y., Press, B., Wandinger-Ness, A., 1995. Rab 7: An important regulator of late endocytic membrane traffic. J. Cell Biol. 131, 1435-1452.

Fernandez-Chacon, R., Achiriloaie, M., Janz, R., Albanesi, J.P., Sudhof, T.C., 2000. SCAMP1 function in endocytosis. J. Biol. Chem. 275, 12752-12756.

Fernandez-Chacon, R., Alvarez de Toledo, G., Hammer, R.E., Sudhof, T.C., 1999. Analysis of SCAMP1 function in secretory vesicle exocytosis by means of gene targeting in mice. J. Biol. Chem. 274, 32551-32554.

Fletcher, S.J., Iqbal, M., Jabbari, S., Stekel, D., Rappoport, J.Z., 2014. Analysis of occludin trafficking, demonstrating continuous endocytosis, degradation, recycling and biosynthetic secretory trafficking. PLoS One 9, e111176.

Foley, K., Boguslavsky, S., Klip, A., 2011. Endocytosis, recycling, and regulated exocytosis of glucose transporter 4. Biochemistry 50, 3048-3061.

Furuta, Y., Hogan, B.L., 1998. BMP4 is essential for lens induction in the mouse embryo. Genes Dev. 12, 3764-3775.

Gage, P.J., Zacharias, A.L., 2009. Signaling "cross-talk" is integrated by transcription factors in the development of the anterior segment in the eye. Dev. Dyn. 238, 2149-2162.

Galperin, E., Benjamin, S., Rapaport, D., Rotem-Yehudar, R., Tolchinsky, S., Horowitz, M., 2002. EHD3: A protein that resides in recycling tubular and vesicular membrane structures and interacts with EHD1. Traffic 3, 575-589.

Gao, Y., Balut, C.M., Bailey, M.A., Patino-Lopez, G., Shaw, S., Devor, D.C., 2010. Recycling of the Ca2+-activated K+ channel, KCa2.3, is dependent upon RME-1, Rab35/EPI64C, and an N-terminal domain. J. Biol. Chem. 285, 17938-17953.

Garcia, C.M., Huang, J., Madakashira, B.P., Liu, Y., Rajagopal, R., Dattilo, L., Robinson, M.L., Beebe, D.C., 2011. The function of FGF signaling in the lens placode. Dev. Biol. 351, 176-185.

Garcia, C.M., Yu, K., Zhao, H., Ashery-Padan, R., Ornitz, D.M., Robinson, M.L., Beebe, D.C., 2005. Signaling through FGF receptor-2 is required for lens cell survival and for withdrawal from the cell cycle during lens fiber cell differentiation. Dev. Dyn. 233, 516-527.

George, M., Rainey, M.A., Naramura, M., Foster, K.W., Holzapfel, M.S., Willoughby, L.L., Ying, G., Goswami, R.M., Gurumurthy, C.B., Band, V., Satchell, S.C., Band, H., 2011. Renal thrombotic microangiopathy in mice with combined deletion of endocytic recycling regulators EHD3 and EHD4. PLoS One 6, e17838.

George, M., Rainey, M.A., Naramura, M., Ying, G., Harms, D.W., Vitaterna, M.H., Doglio, L., Crawford, S.E., Hess, R.A., Band, V., Band, H., 2010. Ehd4 is required to attain normal prepubertal testis size but dispensable for fertility in male mice. Genesis 48, 328-342.

George, M., Ying, G., Rainey, M.A., Solomon, A., Parikh, P.T., Gao, Q., Band, V., Band, H., 2007. Shared as well as distinct roles of EHD proteins revealed by biochemical and functional comparisons in mammalian cells and C. elegans. BMC Cell Biol. 8, 3.

Giridharan, S.S., Cai, B., Vitale, N., Naslavsky, N., Caplan, S., 2013. Cooperation of MICAL-L1, syndapin2, and phosphatidic acid in tubular recycling endosome biogenesis. Mol. Biol. Cell 24, 1776-90, S1-15.

Glaser, T., Jepeal, L., Edwards, J.G., Young, S.R., Favor, J., Maas, R.L., 1994. PAX6 gene dosage effect in a family with congenital cataracts, aniridia, anophthalmia and central nervous system defects. Nat. Genet. 7, 463-471.

Glaser, T., Walton, D.S., Maas, R.L., 1992. Genomic structure, evolutionary conservation and aniridia mutations in the human PAX6 gene. Nat. Genet. 2, 232-239.

Gokool, S., Tattersall, D., Seaman, M.N., 2007. EHD1 interacts with retromer to stabilize SNX1 tubules and facilitate endosome-to-golgi retrieval. Traffic 8, 1873-1886.

Gotoh, N., Ito, M., Yamamoto, S., Yoshino, I., Song, N., Wang, Y., Lax, I., Schlessinger, J., Shibuya, M., Lang, R.A., 2004. Tyrosine phosphorylation sites on FRS2alpha

responsible for Shp2 recruitment are critical for induction of lens and retina. Proc. Natl. Acad. Sci. U. S. A. 101, 17144-17149.

Govindarajan, V., Overbeek, P.A., 2001. Secreted FGFR3, but not FGFR1, inhibits lens fiber differentiation. Development 128, 1617-1627.

Grainger, R.M., 1992. Embryonic lens induction: Shedding light on vertebrate tissue determination. Trends Genet. 8, 349-355.

Grainger, R.M., Herry, J.J., Henderson, R.A., 1988. Reinvestigation of the role of the optic vesicle in embryonic lens induction. Development 102, 517-526.

Grant, B., Zhang, Y., Paupard, M.C., Lin, S.X., Hall, D.H., Hirsh, D., 2001. Evidence that RME-1, a conserved C. elegans EH-domain protein, functions in endocytic recycling. Nat. Cell Biol. 3, 573-579.

Grant, B.D., Donaldson, J.G., 2009. Pathways and mechanisms of endocytic recycling. Nat. Rev. Mol. Cell Biol. 10, 597-608.

Grant, B.D., Caplan, S., 2008. Mechanisms of EHD/RME-1 protein function in endocytic transport. Traffic 9, 2043-2052.

Graw, J., 2003. The genetic and molecular basis of congenital eye defects. Nat. Rev. Genet. 4, 876-888.

Grimm, C., Chatterjee, B., Favor, J., Immervoll, T., Loster, J., Klopp, N., Sandulache, R., Graw, J., 1998. Aphakia (ak), a mouse mutation affecting early eye development: Fine mapping, consideration of candidate genes and altered Pax6 and Six3 gene expression pattern. Dev. Genet. 23, 299-316.

Grosshans, B.L., Ortiz, D., Novick, P., 2006. Rabs and their effectors: Achieving specificity in membrane traffic. Proc. Natl. Acad. Sci. U. S. A. 103, 11821-11827.

Gudmundsson, H., Hund, T.J., Wright, P.J., Kline, C.F., Snyder, J.S., Qian, L., Koval, O.M., Cunha, S.R., George, M., Rainey, M.A., Kashef, F.E., Dun, W., Boyden, P.A., Anderson, M.E., Band, H., Mohler, P.J., 2010. EH domain proteins regulate cardiac membrane protein targeting. Circ. Res. 107, 84-95.

Guilherme, A., Soriano, N.A., Bose, S., Holik, J., Bose, A., Pomerleau, D.P., Furcinitti, P., Leszyk, J., Corvera, S., Czech, M.P., 2004. EHD2 and the novel EH domain binding protein EHBP1 couple endocytosis to the actin cytoskeleton. J. Biol. Chem. 279, 10593-10605.

Guilherme, A., Soriano, N.A., Furcinitti, P.S., Czech, M.P., 2004. Role of EHD1 and EHBP1 in perinuclear sorting and insulin-regulated GLUT4 recycling in 3T3-L1 adipocytes. J. Biol. Chem. 279, 40062-40075.

Hagstrom, S.A., Pauer, G.J., Reid, J., Simpson, E., Crowe, S., Maumenee, I.H., Traboulsi, E.I., 2005. SOX2 mutation causes anophthalmia, hearing loss, and brain anomalies. Am. J. Med. Genet. A. 138A, 95-98.

Haider, N.B., Searby, C., Galperin, E., Mintz, L., Horowitz, M., Stone, E.M., Sheffield, V.C., 1999. Evaluation and molecular characterization of EHD1, a candidate gene for bardet-biedl syndrome 1 (BBS1). Gene 240, 227-232.

Hardel, N., Harmel, N., Zolles, G., Fakler, B., Klocker, N., 2008. Recycling endosomes supply cardiac pacemaker channels for regulated surface expression. Cardiovasc. Res. 79, 52-60.

Heller, B., Adu-Gyamfi, E., Smith-Kinnaman, W., Babbey, C., Vora, M., Xue, Y., Bittman, R., Stahelin, R.V., Wells, C.D., 2010. Amot recognizes a juxtanuclear endocytic recycling compartment via a novel lipid binding domain. J. Biol. Chem. 285, 12308-12320.

Henry, G.D., Corrigan, D.J., Dineen, J.V., Baleja, J.D., 2010. Charge effects in the selection of NPF motifs by the EH domain of EHD1. Biochemistry 49, 3381-3392.

Henry, J.J., Grainger, R.M., 1987. Inductive interactions in the spatial and temporal restriction of lens-forming potential in embryonic ectoderm of xenopus laevis. Dev. Biol. 124, 200-214.

Hill, R.E., Favor, J., Hogan, B.L., Ton, C.C., Saunders, G.F., Hanson, I.M., Prosser, J., Jordan, T., Hastie, N.D., van Heyningen, V., 1991. Mouse small eye results from mutations in a paired-like homeobox-containing gene. Nature 354, 522-525.

Hogan, B.L., Horsburgh, G., Cohen, J., Hetherington, C.M., Fisher, G., Lyon, M.F., 1986. Small eyes (sey): A homozygous lethal mutation on chromosome 2 which affects the differentiation of both lens and nasal placodes in the mouse. J. Embryol. Exp. Morphol. 97, 95-110.

Inglese, J., Auld, D.S., Jadhav, A., Johnson, R.L., Simeonov, A., Yasgar, A., Zheng, W., Austin, C.P., 2006. Quantitative high-throughput screening: A titration-based approach that efficiently identifies biological activities in large chemical libraries. Proc. Natl. Acad. Sci. U. S. A. 103, 11473-11478.

Jones, M.C., Caswell, P.T., Norman, J.C., 2006. Endocytic recycling pathways: Emerging regulators of cell migration. Curr. Opin. Cell Biol. 18, 549-557.

Jovic, M., Naslavsky, N., Rapaport, D., Horowitz, M., Caplan, S., 2007. EHD1 regulates beta1 integrin endosomal transport: Effects on focal adhesions, cell spreading and migration. J. Cell. Sci. 120, 802-814.

Joyce, N.C., 2003. Proliferative capacity of the corneal endothelium. Prog. Retin. Eye Res. 22, 359-389.

Kamachi, Y., Uchikawa, M., Tanouchi, A., Sekido, R., Kondoh, H., 2001. Pax6 and SOX2 form a co-DNA-binding partner complex that regulates initiation of lens development. Genes Dev. 15, 1272-1286.

Kamachi, Y., Uchikawa, M., Collignon, J., Lovell-Badge, R., Kondoh, H., 1998. Involvement of Sox1, 2 and 3 in the early and subsequent molecular events of lens induction. Development 125, 2521-2532.

Kampinga, H.H., Craig, E.A., 2010. The HSP70 chaperone machinery: J proteins as drivers of functional specificity. Nat. Rev. Mol. Cell Biol. 11, 579-592.

Kao, W.W., Xia, Y., Liu, C.Y., Saika, S., 2008. Signaling pathways in morphogenesis of cornea and eyelid. Ocul. Surf. 6, 9-23.

Kidson, S.H., Kume, T., Deng, K., Winfrey, V., Hogan, B.L., 1999. The forkhead/winged-helix gene, Mf1, is necessary for the normal development of the cornea and formation of the anterior chamber in the mouse eye. Dev. Biol. 211, 306-322.

Kieken, F., Sharma, M., Jovic, M., Panapakkam Giridharan, S.S., Naslavsky, N., Caplan, S., Sorgen, P.L., 2010. Mechanism for the selective interaction of C-terminal Eps15 homology domain proteins with specific asn-pro-phe-containing partners. J. Biol. Chem. 285, 8687-8694.

Kieken, F., Jovic, M., Naslavsky, N., Caplan, S., Sorgen, P.L., 2007. EH domain of EHD1. J. Biomol. NMR 39, 323-329.

King, B.R., Vural, S., Pandey, S., Barteau, A., Guda, C., 2012. ngLOC: Software and web server for predicting protein subcellular localization in prokaryotes and eukaryotes. BMC Res. Notes 5, 351-0500-5-351.

Kreslova, J., Machon, O., Ruzickova, J., Lachova, J., Wawrousek, E.F., Kemler, R., Krauss, S., Piatigorsky, J., Kozmik, Z., 2007. Abnormal lens morphogenesis and ectopic lens formation in the absence of beta-catenin function. Genesis 45, 157-168.

Kuracha, M.R., Burgess, D., Siefker, E., Cooper, J.T., Licht, J.D., Robinson, M.L., Govindarajan, V., 2011. Spry1 and Spry2 are necessary for lens vesicle separation and corneal differentiation. Invest. Ophthalmol. Vis. Sci. 52, 6887-6897.

Lang, R.A., 2004. Pathways regulating lens induction in the mouse. Int. J. Dev. Biol. 48, 783-791.

Le, T.T., Conley, K.W., Brown, N.L., 2009. Jagged 1 is necessary for normal mouse lens formation. Dev. Biol. 328, 118-126.

Lee, D.W., Zhao, X., Scarselletta, S., Schweinsberg, P.J., Eisenberg, E., Grant, B.D., Greene, L.E., 2005. ATP binding regulates oligomerization and endosome association of RME-1 family proteins. J. Biol. Chem. 280, 17213-17220.

Lewis WH, 1904.
Experimental studies on the development of the eye in amphibia. I. on the origin of the lens

3:505–36. Rana Palustris. Am. J. 3:505-36, .

Lin, S.X., Grant, B., Hirsh, D., Maxfield, F.R., 2001. Rme-1 regulates the distribution and function of the endocytic recycling compartment in mammalian cells. Nat. Cell Biol. 3, 567-572.

Liu, W., Lagutin, O.V., Mende, M., Streit, A., Oliver, G., 2006. Six3 activation of Pax6 expression is essential for mammalian lens induction and specification. EMBO J. 25, 5383-5395.

Lovicu, F.J., McAvoy, J.W., de Iongh, R.U., 2011. Understanding the role of growth factors in embryonic development: Insights from the lens. Philos. Trans. R. Soc. Lond. B. Biol. Sci. 366, 1204-1218.

Lovicu, F.J., McAvoy, J.W., 2005. Growth factor regulation of lens development. Dev. Biol. 280, 1-14.

Lu, L., Hong, W., 2014. From endosomes to the trans-golgi network. Semin. Cell Dev. Biol. 31, 30-39.

Madakashira, B.P., Kobrinski, D.A., Hancher, A.D., Arneman, E.C., Wagner, B.D., Wang, F., Shin, H., Lovicu, F.J., Reneker, L.W., Robinson, M.L., 2012. Frs2alpha enhances fibroblast growth factor-mediated survival and differentiation in lens development. Development 139, 4601-4612.

Maddala, R., Reneker, L.W., Pendurthi, B., Rao, P.V., 2008. Rho GDP dissociation inhibitor-mediated disruption of rho GTPase activity impairs lens fiber cell migration, elongation and survival. Dev. Biol. 315, 217-231.

Maddala, R., Deng, P.F., Costello, J.M., Wawrousek, E.F., Zigler, J.S., Rao, V.P., 2004. Impaired cytoskeletal organization and membrane integrity in lens fibers of a rho GTPase functional knockout transgenic mouse. Lab. Invest. 84, 679-692.

Marg, A., Schoewel, V., Timmel, T., Schulze, A., Shah, C., Daumke, O., Spuler, S., 2012. Sarcolemmal repair is a slow process and includes EHD2. Traffic 13, 1286-1294.

Mate, S.E., Van Der Meulen, J.H., Arya, P., Bhattacharyya, S., Band, H., Hoffman, E.P., 2012. Eps homology domain endosomal transport proteins differentially localize to the neuromuscular junction. Skelet Muscle 2, 19-5040-2-19.

Maxfield, F.R., McGraw, T.E., 2004. Endocytic recycling. Nat. Rev. Mol. Cell Biol. 5, 121-132.

Mayor, S., Pagano, R.E., 2007. Pathways of clathrin-independent endocytosis. Nat. Rev. Mol. Cell Biol. 8, 603-612.

McMahon, H.T., Boucrot, E., 2011. Molecular mechanism and physiological functions of clathrin-mediated endocytosis. Nat. Rev. Mol. Cell Biol. 12, 517-533.

Medina-Martinez, O., Shah, R., Jamrich, M., 2009. Pitx3 controls multiple aspects of lens development. Dev. Dyn. 238, 2193-2201.

Medina-Martinez, O., Jamrich, M., 2007. Foxe view of lens development and disease. Development 134, 1455-1463.

Miliaras, N.B., Wendland, B., 2004. EH proteins: Multivalent regulators of endocytosis (and other pathways). Cell Biochem. Biophys. 41, 295-318.

Mintz, L., Galperin, E., Pasmanik-Chor, M., Tulzinsky, S., Bromberg, Y., Kozak, C.A., Joyner, A., Fein, A., Horowitz, M., 1999. EHD1--an EH-domain-containing protein with a specific expression pattern. Genomics 59, 66-76.

Montagnac, G., Echard, A., Chavrier, P., 2008. Endocytic traffic in animal cell cytokinesis. Curr. Opin. Cell Biol. 20, 454-461.

Montesinos, M.L., Castellano-Munoz, M., Garcia-Junco-Clemente, P., Fernandez-Chacon, R., 2005. Recycling and EH domain proteins at the synapse. Brain Res. Brain Res. Rev. 49, 416-428.

Moren, B., Shah, C., Howes, M.T., Schieber, N.L., McMahon, H.T., Parton, R.G., Daumke, O., Lundmark, R., 2012. EHD2 regulates caveolar dynamics via ATP-driven targeting and oligomerization. Mol. Biol. Cell 23, 1316-1329.

Mukherjee, S., Ghosh, R.N., Maxfield, F.R., 1997. Endocytosis. Physiol. Rev. 77, 759-803.

Naslavsky, N., Caplan, S., 2011. EHD proteins: Key conductors of endocytic transport. Trends Cell Biol. 21, 122-131.

Naslavsky, N., Rahajeng, J., Rapaport, D., Horowitz, M., Caplan, S., 2007. EHD1 regulates cholesterol homeostasis and lipid droplet storage. Biochem. Biophys. Res. Commun. 357, 792-799.

Naslavsky, N., Rahajeng, J., Sharma, M., Jovic, M., Caplan, S., 2006a. Interactions between EHD proteins and Rab11-FIP2: A role for EHD3 in early endosomal transport. Mol. Biol. Cell 17, 163-177.

Naslavsky, N., Rahajeng, J., Sharma, M., Jovic, M., Caplan, S., 2006b. Interactions between EHD proteins and Rab11-FIP2: A role for EHD3 in early endosomal transport. Mol. Biol. Cell 17, 163-177.

Naslavsky, N., Boehm, M., Backlund, P.S.,Jr, Caplan, S., 2004. Rabenosyn-5 and EHD1 interact and sequentially regulate protein recycling to the plasma membrane. Mol. Biol. Cell 15, 2410-2422.

Nikolovska-Coleska, Z., Wang, R., Fang, X., Pan, H., Tomita, Y., Li, P., Roller, P.P., Krajewski, K., Saito, N.G., Stuckey, J.A., Wang, S., 2004. Development and optimization of a binding assay for the XIAP BIR3 domain using fluorescence polarization. Anal. Biochem. 332, 261-273.

Ogino, H., Ochi, H., Reza, H.M., Yasuda, K., 2012. Transcription factors involved in lens development from the preplacodal ectoderm. Dev. Biol. 363, 333-347.

Olswang-Kutz, Y., Gertel, Y., Benjamin, S., Sela, O., Pekar, O., Arama, E., Steller, H., Horowitz, M., Segal, D., 2009. Drosophila Past1 is involved in endocytosis and is required for germline development and survival of the adult fly. J. Cell. Sci. 122, 471-480.

Pan, Y., Woodbury, A., Esko, J.D., Grobe, K., Zhang, X., 2006. Heparan sulfate biosynthetic gene Ndst1 is required for FGF signaling in early lens development. Development 133, 4933-4944.

Paoluzi, S., Castagnoli, L., Lauro, I., Salcini, A.E., Coda, L., Fre', S., Confalonieri, S., Pelicci, P.G., Di Fiore, P.P., Cesareni, G., 1998. Recognition specificity of individual EH domains of mammals and yeast. EMBO J. 17, 6541-6550.

Park, M., Penick, E.C., Edwards, J.G., Kauer, J.A., Ehlers, M.D., 2004. Recycling endosomes supply AMPA receptors for LTP. Science 305, 1972-1975.

Parton, R.G., Joggerst, B., Simons, K., 1994. Regulated internalization of caveolae. J. Cell Biol. 127, 1199-1215.

Patrakka, J., Xiao, Z., Nukui, M., Takemoto, M., He, L., Oddsson, A., Perisic, L., Kaukinen, A., Szigyarto, C.A., Uhlen, M., Jalanko, H., Betsholtz, C., Tryggvason, K., 2007. Expression and subcellular distribution of novel glomerulus-associated proteins dendrin, ehd3, sh2d4a, plekhh2, and 2310066E14Rik. J. Am. Soc. Nephrol. 18, 689-697.

Picciano, J.A., Ameen, N., Grant, B.D., Bradbury, N.A., 2003. Rme-1 regulates the recycling of the cystic fibrosis transmembrane conductance regulator. Am. J. Physiol. Cell. Physiol. 285, C1009-18.

Pohl, U., Smith, J.S., Tachibana, I., Ueki, K., Lee, H.K., Ramaswamy, S., Wu, Q., Mohrenweiser, H.W., Jenkins, R.B., Louis, D.N., 2000. EHD2, EHD3, and EHD4 encode novel members of a highly conserved family of EH domain-containing proteins. Genomics 63, 255-262.

Polo, S., Confalonieri, S., Salcini, A.E., Di Fiore, P.P., 2003. EH and UIM: Endocytosis and more. Sci. STKE 2003, re17.

Pontoriero, G.F., Smith, A.N., Miller, L.A., Radice, G.L., West-Mays, J.A., Lang, R.A., 2009. Co-operative roles for E-cadherin and N-cadherin during lens vesicle separation and lens epithelial cell survival. Dev. Biol. 326, 403-417.

Pontoriero, G.F., Deschamps, P., Ashery-Padan, R., Wong, R., Yang, Y., Zavadil, J., Cvekl, A., Sullivan, S., Williams, T., West-Mays, J.A., 2008. Cell autonomous roles for AP-2alpha in lens vesicle separation and maintenance of the lens epithelial cell phenotype. Dev. Dyn. 237, 602-617.

Posey, A.D.,Jr, Swanson, K.E., Alvarez, M.G., Krishnan, S., Earley, J.U., Band, H., Pytel, P., McNally, E.M., Demonbreun, A.R., 2014. EHD1 mediates vesicle trafficking required for normal muscle growth and transverse tubule development. Dev. Biol. 387, 179-190.

Posey, A.D.,Jr, Pytel, P., Gardikiotes, K., Demonbreun, A.R., Rainey, M., George, M., Band, H., McNally, E.M., 2011. Endocytic recycling proteins EHD1 and EHD2 interact with fer-1-like-5 (Fer1L5) and mediate myoblast fusion. J. Biol. Chem. 286, 7379-7388.

Qiu, X.B., Shao, Y.M., Miao, S., Wang, L., 2006. The diversity of the DnaJ/Hsp40 family, the crucial partners for Hsp70 chaperones. Cell Mol. Life Sci. 63, 2560-2570.

Rainey, M.A., George, M., Ying, G., Akakura, R., Burgess, D.J., Siefker, E., Bargar, T., Doglio, L., Crawford, S.E., Todd, G.L., Govindarajan, V., Hess, R.A., Band, V., Naramura, M., Band, H., 2010. The endocytic recycling regulator EHD1 is essential for spermatogenesis and male fertility in mice. BMC Dev. Biol. 10, 37.

Rajagopal, R., Huang, J., Dattilo, L.K., Kaartinen, V., Mishina, Y., Deng, C.X., Umans, L., Zwijsen, A., Roberts, A.B., Beebe, D.C., 2009. The type I BMP receptors, Bmpr1a and Acvr1, activate multiple signaling pathways to regulate lens formation. Dev. Biol. 335, 305-316.

Rapaport, D., Auerbach, W., Naslavsky, N., Pasmanik-Chor, M., Galperin, E., Fein, A., Caplan, S., Joyner, A.L., Horowitz, M., 2006. Recycling to the plasma membrane is delayed in EHD1 knockout mice. Traffic 7, 52-60.

Robinson, M.L., 2006. An essential role for FGF receptor signaling in lens development. Semin. Cell Dev. Biol. 17, 726-740.

Rotem-Yehudar, R., Galperin, E., Horowitz, M., 2001. Association of insulin-like growth factor 1 receptor with EHD1 and SNAP29. J. Biol. Chem. 276, 33054-33060.

Rowan, S., Conley, K.W., Le, T.T., Donner, A.L., Maas, R.L., Brown, N.L., 2008. Notch signaling regulates growth and differentiation in the mammalian lens. Dev. Biol. 321, 111-122.

Rowan, S., Cepko, C.L., 2004. Genetic analysis of the homeodomain transcription factor Chx10 in the retina using a novel multifunctional BAC transgenic mouse reporter. Dev. Biol. 271, 388-402.

Russell, P., Zigler, J.S.,Jr, Reddy, V., 1984. The development of a monoclonal antibody to a human gamma crystallin. Curr. Eye Res. 3, 1329-1335.

Saha, M.S., Spann, C.L., Grainger, R.M., 1989. Embryonic lens induction: More than meets the optic vesicle. Cell Differ. Dev. 28, 153-171.

Salcini, A.E., Chen, H., Iannolo, G., De Camilli, P., Di Fiore, P.P., 1999. Epidermal growth factor pathway substrate 15, Eps15. Int. J. Biochem. Cell Biol. 31, 805-809.

Salcini, A.E., Confalonieri, S., Doria, M., Santolini, E., Tassi, E., Minenkova, O., Cesareni, G., Pelicci, P.G., Di Fiore, P.P., 1997. Binding specificity and in vivo targets of the EH domain, a novel protein-protein interaction module. Genes Dev. 11, 2239-2249.

Santolini, E., Puri, C., Salcini, A.E., Gagliani, M.C., Pelicci, P.G., Tacchetti, C., Di Fiore, P.P., 2000. Numb is an endocytic protein. J. Cell Biol. 151, 1345-1352.

Santolini, E., Salcini, A.E., Kay, B.K., Yamabhai, M., Di Fiore, P.P., 1999. The EH network. Exp. Cell Res. 253, 186-209.

Saravanamuthu, S.S., Le, T.T., Gao, C.Y., Cojocaru, R.I., Pandiyan, P., Liu, C., Zhang, J., Zelenka, P.S., Brown, N.L., 2012. Conditional ablation of the Notch2 receptor in the ocular lens. Dev. Biol. 362, 219-229.

Sato, M., Sato, K., Liou, W., Pant, S., Harada, A., Grant, B.D., 2008. Regulation of endocytic recycling by C. elegans Rab35 and its regulator RME-4, a coated-pit protein. EMBO J. 27, 1183-1196.

Schedl, A., Ross, A., Lee, M., Engelkamp, D., Rashbass, P., van Heyningen, V., Hastie, N.D., 1996a. Influence of PAX6 gene dosage on development: Overexpression causes severe eye abnormalities. Cell 86, 71-82.

Schedl, A., Ross, A., Lee, M., Engelkamp, D., Rashbass, P., van Heyningen, V., Hastie, N.D., 1996b. Influence of PAX6 gene dosage on development: Overexpression causes severe eye abnormalities. Cell 86, 71-82.

Scheiblin, D.A., Gao, J., Caplan, J.L., Simirskii, V.N., Czymmek, K.J., Mathias, R.T., Duncan, M.K., 2014. Beta-1 integrin is important for the structural maintenance and homeostasis of differentiating fiber cells. Int. J. Biochem. Cell Biol. 50, 132-145.

Schneider, A., Bardakjian, T., Reis, L.M., Tyler, R.C., Semina, E.V., 2009. Novel SOX2 mutations and genotype-phenotype correlation in anophthalmia and microphthalmia. Am. J. Med. Genet. A. 149A, 2706-2715.

Scita, G., Di Fiore, P.P., 2010. The endocytic matrix. Nature 463, 464-473.

Sengupta, S., George, M., Miller, K.K., Naik, K., Chou, J., Cheatham, M.A., Dallos, P., Naramura, M., Band, H., Zheng, J., 2009. EHD4 and CDH23 are interacting partners in cochlear hair cells. J. Biol. Chem. 284, 20121-20129.

Servetnick, M., Grainger, R.M., 1991. Changes in neural and lens competence in xenopus ectoderm: Evidence for an autonomous developmental timer. Development 112, 177-188.

Shao, Y., Akmentin, W., Toledo-Aral, J.J., Rosenbaum, J., Valdez, G., Cabot, J.B., Hilbush, B.S., Halegoua, S., 2002. Pincher, a pinocytic chaperone for nerve growth factor/TrkA signaling endosomes. J. Cell Biol. 157, 679-691.

Sharma, M., Panapakkam Giridharan, S.S., Rahajeng, J., Naslavsky, N., Caplan, S., 2009. MICAL-L1 links EHD1 to tubular recycling endosomes and regulates receptor recycling. Mol. Biol. Cell 20, 5181-5194.

Sharma, M., Naslavsky, N., Caplan, S., 2008. A role for EHD4 in the regulation of early endosomal transport. Traffic 9, 995-1018.

Sigismund, S., Argenzio, E., Tosoni, D., Cavallaro, E., Polo, S., Di Fiore, P.P., 2008. Clathrin-mediated internalization is essential for sustained EGFR signaling but dispensable for degradation. Dev. Cell. 15, 209-219.

Smith, A.N., Miller, L.A., Song, N., Taketo, M.M., Lang, R.A., 2005. The duality of beta-catenin function: A requirement in lens morphogenesis and signaling suppression of lens fate in periocular ectoderm. Dev. Biol. 285, 477-489.

Smith, C.A., Dho, S.E., Donaldson, J., Tepass, U., McGlade, C.J., 2004. The cell fate determinant numb interacts with EHD/rme-1 family proteins and has a role in endocytic recycling. Mol. Biol. Cell 15, 3698-3708.

Sonnichsen, B., De Renzis, S., Nielsen, E., Rietdorf, J., Zerial, M., 2000. Distinct membrane domains on endosomes in the recycling pathway visualized by multicolor imaging of Rab4, Rab5, and Rab11. J. Cell Biol. 149, 901-914.

Spemann, H., 1901. Uber correlationen in der entwickelung des auges. Verh Anat Ges 15:61–79., .

Srinivas, S.P., 2010. Dynamic regulation of barrier integrity of the corneal endothelium. Optom. Vis. Sci. 87, E239-54.

Stenmark, H., 2012. The rabs: A family at the root of metazoan evolution. BMC Biol. 10, 68-7007-10-68.

Stoeber, M., Stoeck, I.K., Hanni, C., Bleck, C.K., Balistreri, G., Helenius, A., 2012. Oligomers of the ATPase EHD2 confine caveolae to the plasma membrane through association with actin. EMBO J. 31, 2350-2364.

Stolen, C.M., Griep, A.E., 2000. Disruption of lens fiber cell differentiation and survival at multiple stages by region-specific expression of truncated FGF receptors. Dev. Biol. 217, 205-220.

Stump, R.J., Ang, S., Chen, Y., von Bahr, T., Lovicu, F.J., Pinson, K., de Iongh, R.U., Yamaguchi, T.P., Sassoon, D.A., McAvoy, J.W., 2003. A role for wnt/beta-catenin signaling in lens epithelial differentiation. Dev. Biol. 259, 48-61.

Sugiyama, Y., Akimoto, K., Robinson, M.L., Ohno, S., Quinlan, R.A., 2009. A cell polarity protein aPKClambda is required for eye lens formation and growth. Dev. Biol. 336, 246-256.

Tomarev, S.I., Zinovieva, R.D., Chang, B., Hawes, N.L., 1998. Characterization of the mouse Prox1 gene. Biochem. Biophys. Res. Commun. 248, 684-689.

van Raamsdonk, C.D., Tilghman, S.M., 2000. Dosage requirement and allelic expression of PAX6 during lens placode formation. Development 127, 5439-5448.

Walseng, E., Bakke, O., Roche, P.A., 2008. Major histocompatibility complex class II-peptide complexes internalize using a clathrin- and dynamin-independent endocytosis pathway. J. Biol. Chem. 283, 14717-14727.

Walther, C., Gruss, P., 1991. Pax-6, a murine paired box gene, is expressed in the developing CNS. Development 113, 1435-1449.

Wang, X., Garcia, C.M., Shui, Y.B., Beebe, D.C., 2004. Expression and regulation of alpha-, beta-, and gamma-crystallins in mammalian lens epithelial cells. Invest. Ophthalmol. Vis. Sci. 45, 3608-3619.

Wang, X.J., Zhang, D.L., Xu, Z.G., Ma, M.L., Wang, W.B., Li, L.L., Han, X.L., Huo, Y., Yu, X., Sun, J.P., 2014. Understanding cadherin EGF LAG seven-pass G-type receptors. J. Neurochem. 131, 699-711.

Wawersik, S., Purcell, P., Rauchman, M., Dudley, A.T., Robertson, E.J., Maas, R., 1999. BMP7 acts in murine lens placode development. Dev. Biol. 207, 176-188.

Wigle, J.T., Chowdhury, K., Gruss, P., Oliver, G., 1999. Prox1 function is crucial for mouse lens-fibre elongation. Nat. Genet. 21, 318-322.

Wong, W.T., Schumacher, C., Salcini, A.E., Romano, A., Castagnino, P., Pelicci, P.G., Di Fiore, P.P., 1995. A protein-binding domain, EH, identified in the receptor tyrosine kinase substrate Eps15 and conserved in evolution. Proc. Natl. Acad. Sci. U. S. A. 92, 9530-9534.

Xu, Y., Shi, H., Wei, S., Wong, S.H., Hong, W., 2004. Mutually exclusive interactions of EHD1 with GS32 and syndapin II. Mol. Membr. Biol. 21, 269-277.

Yamada, R., Mizutani-Koseki, Y., Hasegawa, T., Osumi, N., Koseki, H., Takahashi, N., 2003. Cell-autonomous involvement of Mab21l1 is essential for lens placode development. Development 130, 1759-1770.

Yap, C.C., Lasiecka, Z.M., Caplan, S., Winckler, B., 2010. Alterations of EHD1/EHD4 protein levels interfere with L1/NgCAM endocytosis in neurons and disrupt axonal targeting. J. Neurosci. 30, 6646-6657.

Yu, Z., Sanchez-Velar, N., Catrina, I.E., Kittler, E.L., Udofia, E.B., Zapp, M.L., 2005. The cellular HIV-1 rev cofactor hRIP is required for viral replication. Proc. Natl. Acad. Sci. U. S. A. 102, 4027-4032.

Zavala, J., Lopez Jaime, G.R., Rodriguez Barrientos, C.A., Valdez-Garcia, J., 2013. Corneal endothelium: Developmental strategies for regeneration. Eye (Lond) 27, 579-588.

Zhang, Y., Overbeek, P.A., Govindarajan, V., 2007. Perinatal ablation of the mouse lens causes multiple anterior chamber defects. Mol. Vis. 13, 2289-2300.

Zhao, H., Yang, T., Madakashira, B.P., Thiels, C.A., Bechtle, C.A., Garcia, C.M., Zhang, H., Yu, K., Ornitz, D.M., Beebe, D.C., Robinson, M.L., 2008. Fibroblast growth factor receptor signaling is essential for lens fiber cell differentiation. Dev. Biol. 318, 276-288.

Chapter 7: Appendix

Appendix A: List of potential EHD1 binding partners

Protein ID	Protein	Count	Sequence length
Q9UBC2	EP15R	22	864
P42566	EPS15	15	896
Q8WZ42	TITIN	12	34350
P98082	DAB2	8	770
P98088	MUC5A	8	5030
Q9H1K0	RBNS5	7	784
Q9Y6R7	FCGBP	6	5405
O14686	KMT2D	6	5537
O95081	AGFG2	5	481
Q8NDI1	EHBP1	5	1231
Q6ZN28	MACC1	5	852
O43426	SYNJ1	5	1573
P22105	TENX	5	4289
P52594	AGFG1	4	562
Q9NSY1	BMP2K	4	1161
Q9P2D1	CHD7	4	2997
O95208	EPN2	4	641
Q9H201	EPN3	4	632
A9Z1Z3	FR1L4	4	1794
O43424	GRID2	4	1007
Q99698	LYST	4	3801
Q7L804	RFIP2	4	512
Q8N2Y8	RUSC2	4	1516
Q9Y493	ZAN	4	2812
Q2M2I8	AAK1	3	961
O43823	AKAP8	3	692
Q6UB99	ANR11	3	2663
O14497	ARI1A	3	2285
Q8NFD5	ARI1B	3	2236
Q13315	ATM	3	3056
Q8WXX7	AUTS2	3	1259
O75061	AUXI	3	913
Q9C0K0	BC11B	3	894
Q13191	CBLB	3	982
Q9H6E4	CC134	3	229
Q9NYQ6	CELR1	3	3014

Protein ID	Protein	Count	Sequence length
Q8IZA0	K319L	1	1049
Q92993	KAT5	1	513
Q92794	KAT6A	1	2004
Q86V97	KBTB6	1	674
Q8WVZ9	KBTB7	1	684
Q8NFY9	KBTB8	1	601
Q16322	KCA10	1	511
Q9UJ90	KCNE5	1	142
Q12791	KCMA1	1	1236
Q09470	KCNA1	1	495
P16389	KCNA2	1	499
P22001	KCNA3	1	575
P22459	KCNA4	1	653
P22460	KCNA5	1	613
P17658	KCNA6	1	529
P15382	KCNE1	1	129
Q12809	KCNH2	1	1159
Q9NS40	KCNH7	1	1196
Q9UGI6	KCNN3	1	736
O43526	KCNQ2	1	872
O43525	KCNQ3	1	872
A8MYU2	KCNU1	1	1149
P12532	KCRU	1	417
Q9Y597	KCTD3	1	815
Q7LBC6	KDM3B	1	1761
B2RXH2	KDM4E	1	506
Q9UGL1	KDM5B	1	1544
O15037	KHNYN	1	678
Q9H1H9	KI13A	1	1805
Q9NQT8	KI13B	1	1826
O95235	KI20A	1	890
Q7Z4S6	KI21A	1	1674
Q2KJY2	KI26B	1	2108
Q9P2E2	KIF17	1	1029
Q12756	KIF1A	1	1690
Q14807	KIF22	1	665

Q8TD26	CHD6	3	2715
Q96FN4	CPNE2	3	548
Q8TEH3	DEN1A	3	1009
Q9UPY3	DICER	3	1922
P25686	DNJB2	3	324
Q13217	DNJC3	3	504
O75417	DPOLQ	3	2590
Q9Y6I3	EPN1	3	576
Q9Y4C2	TCAF1	3	921
Q9HAH7	FBRS	3	460
Q9HCM7	FBSL	3	1045
Q9Y2H6	FND3A	3	1198
A0AVI2	FR1L5	3	2093
Q86XX4	FRAS1	3	4008
Q9UKJ3	GPTC8	3	1502
Q96JK4	HIPL1	3	782
Q92598	HS105	3	858
Q9BY89	K1671	3	1806
Q8NEZ4	KMT2C	3	4911
Q9UHV7	MED13	3	2174
Q8N3F8	MILK1	3	863
Q9UKN7	MYO15	3	3530
O60393	NOBOX	3	691
Q9Y6R0	NUMBL	3	609
P49757	NUMB	3	651
Q9UNF0	PACN2	3	486
Q96JQ0	PCD16	3	3298
Q9Y5E1	PCDB9	3	797
Q9UN67	PCDBA	3	800
Q13492	PICAL	3	652
Q9Y263	PLAP	3	795
Q92530	PSMF1	3	271
O95153	RIMB1	3	1857
O15126	SCAM1	3	338
O15127	SCAM2	3	329
O14828	SCAM3	3	347
Q9UI33	SCNBA	3	1791
Q9P0V3	SH3B4	3	963
O75094	SLIT3	3	1523

B7ZC32	KIF28	1	967
Q9Y496	KIF3A	1	699
Q8N5S9	KKCC1	1	505
Q96RR4	KKCC2	1	588
Q9BQ90	KLDC3	1	382
Q8NEP7	KLDC9	1	349
Q5JT82	KLF17	1	389
Q13351	KLF1	1	362
Q6PF15	KLH35	1	363
Q8WZ60	KLHL6	1	621
Q9P2G9	KLHL8	1	620
Q9UKR0	KLK12	1	248
Q8IZD2	KMT2E	1	1858
Q15139	KPCD1	1	912
Q9BZL6	KPCD2	1	878
Q05655	KPCD	1	676
Q04759	KPCT	1	706
Q05513	KPCZ	1	592
Q13601	KRR1	1	381
P43405	KSYK	1	635
P32004	L1CAM	1	1257
Q15334	L2GL1	1	1064
Q6P1M3	L2GL2	1	1020
A6NMS7	L37A1	1	1700
A6NM11	L37A2	1	1700
O60309	L37A3	1	1634
Q16787	LAMA3	1	3333
O15230	LAMA5	1	3695
P07942	LAMB1	1	1786
Q9Y6N6	LAMC3	1	1575
Q9NS86	LANC2	1	450
P42167	LAP2B	1	454
Q96RT1	LAP2	1	1412
O95461	LARGE	1	756
Q9Y4W2	LAS1L	1	734
Q6XYB7	LBX2	1	198
Q86VQ0	LCA5	1	697
A4D1U4	LCHN	1	455
O75112	LDB3	1	727

Q7Z7L1	SLN11	3	901
A2VEC9	SSPO	3	5147
Q9NY15	STAB1	3	2570
Q8WWQ8	STAB2	3	2551
Q9BSW7	SYT17	3	474
Q9H2D6	TARA	3	2365
Q9UMX0	UBQL1	3	589
Q9UHD9	UBQL2	3	624
O75385	ULK1	3	1050
Q6PJI9	WDR59	3	974
Q86UP3	ZFHX4	3	3567
Q13639	5HT4R	2	388
P78363	ABCA4	2	2273
O94911	ABCA8	2	1581
Q5T8D3	ACBD5	2	534
P21399	ACOC	2	889
P55198	AF17	2	1093
Q9UKA4	AKA11	2	1901
Q9H8T0	AKTIP	2	292
Q9UHK6	AMACR	2	382
P23109	AMPD1	2	780
P04745	AMY1	2	511
P19961	AMY2B	2	511
P04746	AMYP	2	511
O75179	ANR17	2	2603
Q96NW4	ANR27	2	1050
O60641	AP180	2	907
P51690	ARSE	2	589
P0C7U2	ASA2C	2	622
Q9NR71	ASAH2	2	780
P07307	ASGR2	2	311
Q674R7	ATG9B	2	924
P54259	ATN1	2	1190
Q6UX72	B3GN9	2	402
Q9UIF8	BAZ2B	2	2168
Q9H165	BC11A	2	835
Q5H9B9	BM2KL	2	411
P38398	BRCA1	2	1863
O60477	BRNP1	2	761

Q96DT0	LEG12	1	336
Q96B70	LENG9	1	501
Q8NES3	LFNG	1	379
Q8N135	LGI4	1	537
O75473	LGR5	1	907
Q9HBX8	LGR6	1	967
P48742	LHX1	1	406
Q6UY18	LIGO4	1	593
Q9UPQ0	LIMC1	1	1083
O75335	LIPA4	1	1185
Q8ND30	LIPB2	1	876
Q17RR3	LIPR3	1	467
Q05469	LIPS	1	1076
O75019	LIRA1	1	489
Q6PI73	LIRA6	1	481
O75022	LIRB3	1	631
P43034	LIS1	1	410
Q96S06	LMF1	1	567
Q8TE12	LMX1A	1	382
Q8IWU2	LMTK2	1	1503
O60663	LMX1B	1	402
O00370	LORF2	1	1275
Q99677	LPAR4	1	370
Q643R3	LPCT4	1	524
O94910	LPHN1	1	1474
O95490	LPHN2	1	1459
Q9P2M1	LR2BP	1	347
Q5SZI1	LRAD2	1	272
Q8N456	LRC18	1	261
Q8IZ02	LRC34	1	419
Q5VT99	LRC38	1	294
Q9H9A6	LRC40	1	602
Q8N309	LRC43	1	656
Q96FV0	LRC46	1	321
Q68CR7	LRC66	1	880
Q6ZNQ3	LRC69	1	347
Q9P244	LRFN1	1	771
Q6UXM1	LRIG3	1	1119
Q7Z4F1	LRP10	1	713

Q9C0B6	BRNP2	2	783
Q76B58	BRNP3	2	766
O43497	CAC1G	2	2377
O95180	CAC1H	2	2353
O75309	CAD16	2	829
Q9H251	CAD23	2	3354
Q8IXH8	CAD26	2	852
P19022	CADH2	2	906
Q9NS85	CAH10	2	328
O75493	CAH11	2	328
Q5T5Y3	CAMP1	2	1602
Q9Y6W3	CAN7	2	813
Q86VP6	CAND1	2	1230
P53634	CATC	2	463
Q7Z7H3	CATIP	2	387
Q8NA47	CCD63	2	563
Q13042	CDC16	2	620
A6H8M9	CDHR4	2	788
Q9BXF3	CECR2	2	1484
Q9HCU4	CELR2	2	2923
Q5SZD1	CF141	2	244
O14647	CHD2	2	1828
Q12873	CHD3	2	2000
Q14839	CHD4	2	1912
Q9HCK8	CHD8	2	2581
Q14008	CKAP5	2	2032
A5YKK6	CNOT1	2	2376
Q96NU0	CNT3B	2	1288
Q9P232	CNTN3	2	1028
Q9BZ76	CNTP3	2	1288
Q9C0A0	CNTP4	2	1308
Q8WYK1	CNTP5	2	1306
Q7Z7A1	CNTRL	2	2325
Q7Z449	CP2U1	2	544
Q9HB55	CP343	2	503
P08684	CP3A4	2	503
P24462	CP3A7	2	503
Q9BZB8	CPEB1	2	566
Q9UKF6	CPSF3	2	684

Q9NZR2	LRP1B	1	4599
Q07954	LRP1	1	4544
Q96NW7	LRRC7	1	1537
O43300	LRRT2	1	516
Q9UFC0	LRWD1	1	647
Q8ND56	LS14A	1	463
P22888	LSHR	1	699
Q9UK45	LSM7	1	103
Q9HCC9	LST2	1	887
Q8N2S1	LTBP4	1	1624
O60449	LY75	1	1722
Q9HBG7	LY9	1	655
P14151	LYAM1	1	372
P12980	LYL1	1	280
Q6UWN5	LYPD5	1	251
Q8N653	LZTR1	1	840
Q9BRK4	LZTS2	1	669
Q567V2	M17L2	1	206
Q99683	M3K5	1	1374
O95382	M3K6	1	1288
Q9H2W1	M4A6A	1	248
Q92918	M4K1	1	833
Q9Y4K4	M4K5	1	846
Q16706	MA2A1	1	1144
O00754	MA2B1	1	1011
Q9Y2E5	MA2B2	1	1009
Q9H063	MAF1	1	256
Q96QZ7	MAGI1	1	1491
Q9UJ55	MAGL2	1	529
Q9UDY8	MALT1	1	824
Q96JK9	MAML3	1	1134
Q9Y2U8	MAN1	1	911
P23368	MAOM	1	584
P78559	MAP1A	1	2803
P27816	MAP4	1	1152
Q9Y4F3	MARF1	1	1742
Q9P0N8	MARH2	1	246
P48740	MASP1	1	699
O00187	MASP2	1	686

Q5IJ48	CRUM2	2	1285
P61201	CSN2	2	443
P0CG12	CTF8A	2	524
O60494	CUBN	2	3623
O75140	DEPD5	2	1603
Q7L5Y6	DET1	2	550
Q7L7V1	DHX32	2	743
O95886	DLGP3	2	979
Q9Y485	DMXL1	2	3027
Q96M86	DNHD1	2	4753
Q96EY1	DNJA3	2	480
P25685	DNJB1	2	340
Q8WWF6	DNJB3	2	145
Q9UDY4	DNJB4	2	337
O75953	DNJB5	2	348
O75190	DNJB6	2	326
Q96HP0	DOCK6	2	2047
Q8TEK3	DOT1L	2	1739
Q5JSJ4	DX26B	2	861
Q8IVF4	DYH10	2	4471
Q9P2D7	DYH1	2	4330
Q9P225	DYH2	2	4427
Q8TE73	DYH5	2	4624
P43005	EAA3	2	524
Q9BQ95	ECSIT	2	431
Q5JVL4	EFHC1	2	640
Q9NZN4	EHD2	2	543
P28324	ELK4	2	431
Q9NRM1	ENAM	2	1142
Q9NX77	ENK13	2	482
P98073	ENTK	2	1019
P54760	EPHB4	2	987
P58107	EPIPL	2	5090
Q2NKX8	ERC6L	2	1250
Q7Z2Z2	ETUD1	2	1120
Q5T1H1	EYS	2	3165
Q9NZB2	F120A	2	1118
Q9P2D6	F135A	2	1515
Q05DH4	F16A1	2	1040

O60307	MAST3	1	1309
O15021	MAST4	1	2626
P43243	MATR3	1	847
Q9P267	MBD5	1	1494
Q96N66	MBOA7	1	472
A2RUH7	MBPHL	1	354
Q6VMQ6	MCAF1	1	1270
Q5U623	MCAF2	1	682
Q99705	MCHR1	1	422
Q9NXL9	MCM9	1	1143
P15529	MCP	1	392
P08235	MCR	1	984
Q6DN14	MCTP1	1	999
Q6DN12	MCTP2	1	878
Q9ULC4	MCTS1	1	181
Q71F56	MD13L	1	2210
Q8NFP4	MDGA1	1	955
Q9NU22	MDN1	1	5596
Q93074	MED12	1	2177
Q96RN5	MED15	1	788
Q9NVC6	MED17	1	651
A0JLT2	MED19	1	244
Q96HR3	MED30	1	178
O75586	MED6	1	246
Q7Z7M0	MEGF8	1	2845
Q5TIA1	MEI1	1	1274
Q14680	MELK	1	651
Q16820	MEP1B	1	701
Q9H9K5	MER34	1	563
A8MUP2	MET12	1	240
Q8IXQ9	MET20	1	262
Q86YR7	MF2L2	1	1114
O00587	MFNG	1	321
Q6NUT3	MFS12	1	480
Q8N468	MFSD4	1	514
Q6ZSS7	MFSD6	1	791
Q6UXD7	MFSD7	1	560
Q8IWI9	MGAP	1	3026
O43451	MGA	1	1857

Q8N612	F16A2	2	972
Q8IXR5	F178B	2	827
Q96MK2	FA65C	2	946
Q00597	FANCC	2	558
Q6V0I7	FAT4	2	4981
Q9Y613	FHOD1	2	1164
Q53EP0	FND3B	2	1204
Q8WW38	FOG2	2	1151
Q2WGJ9	FR1L6	2	1857
Q92945	FUBP2	2	711
P59646	FXYD4	2	89
O14976	GAK	2	1311
O60318	GANP	2	1980
Q75VX8	GAREL	2	874
Q96D09	GASP2	2	838
O14610	GBGT2	2	69
Q9NXP7	GIN1	2	522
P15104	GLNA	2	373
Q8WXG9	GPR98	2	6306
Q6UWM5	GPRL1	2	242
O95267	GRP1	2	797
Q7Z4H7	HAUS6	2	955
Q9H583	HEAT1	2	2144
A6NFD8	HELT	2	327
Q6UWX4	HIPL2	2	724
Q9UJY1	HSPB8	2	196
Q96N76	HUTU	2	676
Q7Z6Z7	HUWE1	2	4374
P01761	HV106	2	124
Q4G0P3	HYDIN	2	5121
Q9HBG6	IF122	2	1241
Q16666	IF16	2	785
Q8TDY8	IGDC4	2	1250
Q9ULG1	INO80	2	1556
Q9UL03	INT6	2	887
O14654	IRS4	2	1257
Q9HCM3	K1549	2	1950
Q5JYT7	K1755	2	1200
Q96RP8	KCNA7	2	456

P08493	MGP	1	103
Q5JRA6	MIA3	1	1907
Q8N344	MIER2	1	545
Q9NXC5	MIO	1	875
Q99797	MIPEP	1	713
Q8NDC0	MISSL	1	245
P03971	MIS	1	560
Q9HBH9	MKNK2	1	465
Q9UHC7	MKRN1	1	482
H3BPM6	MKROS	1	223
Q13434	MKRN4	1	485
P58340	MLF1	1	268
Q15773	MLF2	1	248
Q9HAP2	MLXIP	1	919
Q9H3L0	MMAD	1	296
Q99542	MMP19	1	508
P03956	MMP1	1	469
P14780	MMP9	1	707
Q96T76	MMS19	1	1030
Q96BX8	MOB3A	1	217
Q86VF5	MOGT3	1	341
Q8TE76	MORC4	1	937
Q7RTY0	MOT13	1	426
Q7RTX9	MOT14	1	510
O15374	MOT5	1	487
Q13163	MP2K5	1	448
Q00325	MPCP	1	362
Q9NZW5	MPP6	1	540
O60487	MPZL2	1	215
Q6DT37	MRCKG	1	1551
P49959	MRE11	1	708
Q8TDS7	MRGRD	1	321
Q86SM8	MRGRE	1	312
Q96AM1	MRGRF	1	343
Q86SM5	MRGRG	1	289
Q6ZUA9	MROH5	1	1318
Q68CQ1	MROH7	1	1323
P33527	MRP1	1	1531
O15439	MRP4	1	1325

Q9ULH0	KDIS	2	1771
O15550	KDM6A	2	1401
Q8IX03	KIBRA	2	1113
O60333	KIF1B	2	1816
Q9UMN6	KMT2B	2	2715
Q13753	LAMC2	2	1193
O43679	LDB2	2	373
P56470	LEG4	2	323
P53671	LIMK2	2	638
Q86W92	LIPB1	2	1011
Q96Q04	LMTK3	2	1460
O75197	LRP5	2	1615
Q8WUT4	LRRN4	2	740
Q16584	M3K11	2	847
P49641	MA2A2	2	1150
Q8IZL2	MAML2	2	1156
Q9Y2H9	MAST1	2	1570
Q6P0Q8	MAST2	2	1798
P04201	MAS	2	325
Q969V1	MCHR2	2	340
P49736	MCM2	2	904
Q9ULK4	MED23	2	1368
Q12866	MERTK	2	999
Q5VWP3	MLIP	2	458
Q16653	MOG	2	247
O75970	MPDZ	2	2070
Q92887	MRP2	2	1545
O15438	MRP3	2	1527
Q9Y4B5	MTCL1	2	1905
O95248	MTMR5	2	1867
Q7Z5P9	MUC19	2	6254
Q9HC84	MUC5B	2	5762
Q6PIF6	MYO7B	2	2116
Q9NZM1	MYOF	2	2061
Q86UW6	N4BP2	2	1770
Q9UK23	NAGPA	2	515
Q14934	NFAC4	2	902
Q08J23	NSUN2	2	767
Q96KG9	NTKL	2	808

O15440	MRP5	1	1437
Q96J65	MRP9	1	1359
Q7L0Y3	MRRP1	1	403
O15091	MRRP3	1	583
A6NI15	MSGN1	1	193
Q01726	MSHR	1	317
Q9HCI7	MSL2	1	577
Q8NHP6	MSPD2	1	518
Q4VC12	MSS51	1	460
Q9P289	STK26	1	416
P28360	MSX1	1	303
Q49AM1	MTEF2	1	385
Q99551	MTEF1	1	399
Q9Y4I5	MTL5	1	508
O43193	MTLR	1	412
Q13496	MTM1	1	603
Q13613	MTMR1	1	665
Q96EF0	MTMR8	1	704
Q9NXD2	MTMRA	1	777
Q86WG5	MTMRD	1	1849
Q9UKN1	MUC12	1	5478
Q8WXI7	MUC16	1	22152
Q8N307	MUC20	1	709
Q02817	MUC2	1	5179
Q14764	MVP	1	893
Q8IUG5	MY18B	1	2567
P23409	MYF6	1	242
Q9UKX3	MYH13	1	1938
Q15746	MYLK	1	1914
Q9HD67	MYO10	1	2058
Q96H55	MYO19	1	970
Q9UBC5	MYO1A	1	1043
Q12965	MYO1E	1	1108
O00160	MYO1F	1	1098
Q8NEV4	MYO3A	1	1616
Q8WXR4	MYO3B	1	1341
B2RTY4	MYO9A	1	2548
Q13459	MYO9B	1	2157
Q5VVJ2	MYSM1	1	828

P04629	NTRK1	2	796
O75694	NU155	2	1391
Q9P2P1	NYNRI	2	1898
Q8NGZ0	O2AJ1	2	328
Q9H488	OFUT1	2	388
P47890	OR1G1	2	313
Q8NH94	OR1L1	2	360
Q8NH93	OR1L3	2	324
Q8NGR8	OR1L8	2	309
Q8NHB8	OR5K2	2	316
Q8N148	OR6V1	2	313
Q12889	OVGP1	2	678
Q96KW2	P12L2	2	1035
Q8IZE3	PACE1	2	742
Q9BY11	PACN1	2	444
Q8TEW8	PAR3L	2	1205
Q8N6Y1	PCD20	2	951
Q6V1P9	PCD23	2	2916
Q9Y6V0	PCLO	2	5065
Q9GZU2	PEG3	2	1588
O00625	PIR	2	290
Q7Z442	PK1L2	2	2459
P98161	PKD1	2	4303
Q8NHP8	PLBL2	2	589
Q4KWH8	PLCH1	2	1693
Q8TEM1	PO210	2	1887
Q9Y520	PRC2C	2	2896
P57071	PRD15	2	1507
Q13029	PRDM2	2	1718
P06401	PRGR	2	933
Q8WUY3	PRUN2	2	3088
Q13332	PTPRS	2	1948
Q9BVG9	PTSS2	2	487
Q09MP3	R51A2	2	1159
Q9Y620	RA54B	2	910
O95294	RASL1	2	804
Q7Z6E9	RBBP6	2	1792
Q2PPJ7	RGPA2	2	1873
O14924	RGS12	2	1447

Q9UL68	MYT1L	1	1186
P28698	MZF1	1	734
O15049	N4BP3	1	544
Q9Y303	NAGA	1	409
Q9NX02	NALP2	1	1062
P59044	NALP6	1	892
Q7RTR0	NALP9	1	991
Q6IQ20	NAPEP	1	393
O96009	NAPSA	1	420
Q9H0A0	NAT10	1	1025
Q6IPT4	NB5R5	1	315
A2RRP1	NBAS	1	2371
Q14596	NBR1	1	966
Q15596	NCOA2	1	1464
Q13772	NCOA4	1	614
Q8NI08	NCOA7	1	942
P16435	NCPR	1	677
Q15784	NDF2	1	382
P29120	NEC1	1	753
P46934	NEDD4	1	1319
Q8WX92	NELFB	1	580
P18615	NELFE	1	380
Q8WTR8	NET5	1	489
Q8TDF5	NETO1	1	533
Q8NC67	NETO2	1	525
O76050	NEUL1	1	574
Q8WWR8	NEUR4	1	484
P21359	NF1	1	2839
O94856	NFASC	1	1347
Q12857	NFIA	1	509
Q12986	NFX1	1	1120
Q8NBF2	NHLC2	1	726
Q15599	NHRF2	1	337
Q86UT5	NHRF4	1	571
Q14112	NID2	1	1375
Q9Y2I1	NISCH	1	1504
Q9HAS0	NJMU	1	396
Q8IVV8	NKAI4	1	208
Q969F2	NKD2	1	451

Q9BYZ6	RHBT2	2	727
P47736	RPGP1	2	663
P04843	RPN1	2	607
Q5VT52	RPRD2	2	1461
Q13950	RUNX2	2	521
Q13761	RUNX3	2	415
Q8TE82	S3TC1	2	1336
Q6UVJ0	SAS6	2	657
Q14524	SCN5A	2	2016
Q9Y5Y9	SCNAA	2	1956
Q58EX2	SDK2	2	2172
O75533	SF3B1	2	1304
O95104	SFR15	2	1147
Q9H7N4	SFR19	2	1312
Q9Y566	SHAN1	2	2161
Q96IW2	SHD	2	340
O75093	SLIT1	2	1534
O94813	SLIT2	2	1529
Q9NTJ3	SMC4	2	1288
Q99835	SMO	2	787
Q9UM82	SPAT2	2	520
Q15772	SPEG	2	3267
Q6ZMY3	SPOC1	2	1216
Q96L03	SPT17	2	361
Q96JX3	SRAC1	2	654
Q8WXE9	STON2	2	905
P14410	SUIS	2	1827
Q9NSD9	SYFB	2	589
Q9UMS6	SYNP2	2	1093
Q9HCH5	SYTL2	2	934
Q5T011	SZT2	2	3432
Q14C87	T132D	2	1099
O75410	TACC1	2	805
O95359	TACC2	2	2948
Q8IZX4	TAF1L	2	1826
P21675	TAF1	2	1872
Q6P1X5	TAF2	2	1199
Q13207	TBX2	2	712
Q99593	TBX5	2	518

Q15270	NKX11	1	411
O95096	NKX22	1	273
Q8TAU0	NKX23	1	364
Q8NFZ4	NLGN2	1	835
Q8NA29	NLS1	1	543
P28336	NMBR	1	390
Q8TCU5	NMD3A	1	1115
O60391	NMD3B	1	1043
Q12879	NMDE1	1	1464
Q13224	NMDE2	1	1484
Q9GZQ4	NMUR2	1	415
Q9Y3T9	NOC2L	1	749
Q13823	NOG2	1	731
Q9BSC4	NOL10	1	688
Q76FK4	NOL8	1	1167
Q5C9Z4	NOM1	1	860
Q15155	NOMO1	1	1222
Q5JPE7	NOMO2	1	1267
P69849	NOMO3	1	1222
P78316	NOP14	1	857
Q86U38	NOP9	1	636
Q9Y314	NOSIP	1	301
P46531	NOTC1	1	2555
Q99466	NOTC4	1	2003
Q9Y5S8	NOX1	1	564
Q9HBY0	NOX3	1	568
Q9NPH5	NOX4	1	578
P55209	NP1L1	1	391
Q99457	NP1L3	1	506
Q99733	NP1L4	1	375
Q8IXF0	NPAS3	1	933
Q14207	NPAT	1	1427
P48145	NPBW1	1	328
P48146	NPBW2	1	333
O15118	NPC1	1	1278
Q9UHC9	NPCL1	1	1359
Q9BY65	NPCR1	1	106
Q7Z494	NPHP3	1	1330
Q8TAT6	NPL4	1	608

P57082	TBX4	2	545
O95947	TBX6	2	436
Q9UGU0	TCF20	2	1960
Q5HYJ1	TECRL	2	363
Q15569	TESK1	2	626
Q8WUH2	TGFA1	2	860
Q6YHU6	THADA	2	1953
Q5TEJ8	THMS2	2	643
Q8IVF5	TIAM2	2	1701
O15455	TLR3	2	904
Q8NE00	TM104	2	496
Q9H813	TM206	2	350
Q14106	TOB2	2	344
Q8N7U7	TPRX1	2	411
O60704	TPST2	2	377
Q96LD4	TRI47	2	638
Q9NQA5	TRPV5	2	729
Q9H1D0	TRPV6	2	725
P53804	TTC3	2	2025
Q9UNY4	TTF2	2	1162
Q6EMB2	TTLL5	2	1281
Q9H313	TTYH1	2	450
Q5TAX3	TUT4	2	1644
Q9UPX0	TUTLB	2	1349
O60294	TYW4	2	686
Q9H832	UBE2Z	2	354
Q14139	UBE4A	2	1066
O95155	UBE4B	2	1302
Q9NPG3	UBN1	2	1134
Q6ZU65	UBN2	2	1347
Q70CQ4	UBP31	2	1352
Q70CQ2	UBP34	2	3546
Q9H9J4	UBP42	2	1324
Q70EL4	UBP43	2	1123
Q9H347	UBQL3	2	655
Q9NRR5	UBQL4	2	601
Q8IYU4	UBQLN	2	475
Q5T4S7	UBR4	2	5183
Q5T124	UBX11	2	520

Q14916	NPT1	1	467
Q8N729	NPW	1	165
P25929	NPY1R	1	384
P50391	NPY4R	1	375
P15559	NQO1	1	274
O43847	NRDC	1	1150
P56975	NRG3	1	720
P48552	NRIP1	1	1158
O14786	NRP1	1	923
Q9NXE4	NSMA3	1	827
P30989	NTR1	1	418
Q16620	NTRK2	1	822
P49790	NU153	1	1475
Q5SRE5	NU188	1	1749
P03886	NU1M	1	318
Q92621	NU205	1	2012
P35658	NU214	1	2090
Q9NV35	NUD15	1	164
Q96RS6	NUDC1	1	583
Q8NFH4	NUP37	1	326
Q8NFH5	NUP53	1	326
Q7Z3B4	NUP54	1	507
Q99567	NUP88	1	741
P52948	NUP98	1	1817
O15504	NUPL2	1	423
Q9UBU9	NXF1	1	619
Q969Y0	NXPE3	1	559
Q8NGN2	O10S1	1	331
Q8NGC7	O11H6	1	330
P58182	O12D2	1	307
Q8NG84	O2AK2	1	335
Q8NGE2	O2AP1	1	309
Q8NGL6	O4A15	1	344
Q9Y5P0	O51B4	1	310
Q9H340	O51B6	1	312
Q8NGJ2	O52H1	1	320
Q8NH60	O52J3	1	311
P0C628	O5AC1	1	307
Q9NZP5	O5AC2	1	309

P22309	UD11	2	533
Q6BDS2	URFB1	2	1440
O75445	USH2A	2	5202
Q16572	VACHT	2	532
P35916	VGFR3	2	1363
Q6PFW1	VIP1	2	1433
Q5VIR6	VPS53	2	699
Q6ZS81	WDFY4	2	3184
Q8IZU2	WDR17	2	1322
Q8N5D0	WDTC1	2	677
O43895	XPP2	2	674
P52740	ZN132	2	706
O60281	ZN292	2	2723
Q14966	ZN638	2	1978
O60290	ZN862	2	1169
Q15942	ZYX	2	572
Q13362	2A5G	1	524
Q66LE6	2ABD	1	453
Q9NRA8	4ET	1	985
Q8WXA8	5HT3C	1	447
A5X5Y0	5HT3E	1	456
P34969	5HT7R	1	479
P05408	7B2	1	212
Q8IZ83	A16A1	1	802
P29274	AA2AR	1	412
Q9UDR5	AASS	1	926
O95477	ABCA1	1	2261
Q99758	ABCA3	1	1704
Q8WWZ7	ABCA5	1	1642
Q8N139	ABCA6	1	1617
Q8IZY2	ABCA7	1	2146
Q8WWZ4	ABCAA	1	1543
Q86UK0	ABCAC	1	2595
Q86UQ4	ABCAD	1	5058
Q9NUT2	ABCB8	1	735
Q09428	ABCC8	1	1581
O60706	ABCC9	1	1549
Q96J66	ABCCB	1	1382
P45844	ABCG1	1	678

A6NJZ3	O6C65	1	312
A6NIJ9	O6C70	1	312
A6NL08	O6C75	1	312
A6NCV1	O6C74	1	312
Q6IFN5	O7E24	1	339
A6NM76	O6C76	1	312
P04181	OAT	1	439
Q9BQT8	ODC	1	299
O75665	OFD1	1	1012
Q9Y2G5	OFUT2	1	429
Q8N543	OGFD1	1	542
Q6UX06	OLFM4	1	510
Q6U736	OPN5	1	354
P04001	OPSG	1	364
P04000	OPSR	1	364
Q9P1Q5	OR1A1	1	309
Q9Y585	OR1A2	1	309
Q15619	OR1C1	1	314
Q8NGR6	OR1B1	1	318
P34982	OR1D2	1	312
P47884	OR1D4	1	311
P58170	OR1D5	1	312
P30953	OR1E1	1	314
P47887	OR1E2	1	323
Q8WZA6	OR1E3	1	343
O43749	OR1F1	1	312
Q8NHA8	OR1FC	1	337
O60431	OR1I1	1	355
Q8NGS3	OR1J1	1	322
Q8NGS2	OR1J2	1	313
Q8NGS1	OR1J4	1	313
Q8NGR5	OR1L4	1	311
Q8NGR2	OR1L6	1	347
Q8NGA1	OR1M1	1	313
Q8NGS0	OR1N1	1	311
Q8NGR9	OR1N2	1	330
Q8NH06	OR1P1	1	330
Q15612	OR1Q1	1	314
Q8NH92	OR1S1	1	325

Q9H222	ABCG5	1	651
Q96SE0	ABHD1	1	405
Q8WTS1	ABHD5	1	349
Q9NYB9	ABI2	1	513
O14639	ABLM1	1	778
Q8N0Z2	ABRA	1	381
Q13085	ACACA	1	2346
O00763	ACACB	1	2458
P49748	ACADV	1	655
P11230	ACHB	1	501
Q07912	ACK1	1	1038
Q9Y615	ACL7A	1	435
Q99798	ACON	1	780
Q86TX2	ACOT1	1	421
P49753	ACOT2	1	483
Q8N9L9	ACOT4	1	421
Q9NR19	ACSA	1	701
Q9ULC5	ACSL5	1	683
Q9UKU0	ACSL6	1	697
Q53FZ2	ACSM3	1	586
P0C7M7	ACSM4	1	580
Q01718	ACTHR	1	297
Q03154	ACY1	1	408
O14672	ADA10	1	748
O43184	ADA12	1	909
P78536	ADA17	1	824
P25100	ADA1D	1	572
O43506	ADA20	1	726
Q99965	ADAM2	1	735
Q8NI60	ADCK3	1	647
Q96D53	ADCK4	1	544
Q5VUY2	ADCL4	1	407
P40145	ADCY8	1	1251
P35611	ADDA	1	737
P35612	ADDB	1	726
Q9UEY8	ADDG	1	706
Q6IQ32	ADNP2	1	1131
Q3LIE5	ADPRM	1	342
Q9Y6U3	ADSV	1	715

Q8NGQ3	OR1S2	1	325
Q5JQS5	OR2BB	1	317
P0C604	OR4A8	1	315
Q8NGL9	OR4CG	1	310
Q8NGC2	OR4E2	1	313
Q8NGI9	OR5A2	1	324
Q8NHB7	OR5K1	1	308
A6NET4	OR5K3	1	321
A6NMS3	OR5K4	1	321
O95007	OR6B1	1	311
Q96RD1	OR6C1	1	312
Q9NZP2	OR6C2	1	312
Q8NGE1	OR6C4	1	309
A6NF89	OR6C6	1	314
Q9NZP0	OR6C3	1	311
Q8NGZ6	OR6F1	1	308
Q8NGC5	OR6J1	1	347
Q8NGM8	OR6M1	1	313
Q8NGY5	OR6N1	1	312
Q8NH40	OR6S1	1	331
Q8NGN1	OR6T1	1	323
Q8NH79	OR6X1	1	312
Q15622	OR7A5	1	319
Q8NGA2	OR7A2	1	310
O76100	OR7AA	1	309
O14581	OR7AH	1	309
O76099	OR7C1	1	320
O60412	OR7C2	1	319
Q8NG98	OR7D4	1	312
Q96RA2	OR7D2	1	312
Q8NGA0	OR7G1	1	311
Q8NG99	OR7G2	1	324
Q8NGT5	OR9A2	1	310
Q8NGU2	OR9A4	1	314
Q9BXB4	OSB11	1	747
Q969R2	OSBP2	1	916
Q9UJX0	OSGI1	1	560
Q99650	OSMR	1	979
P39656	OST48	1	456

Q8IUX7	AEBP1	1	1158
P55197	AF10	1	1068
P43652	AFAM	1	599
P51825	AFF1	1	1210
P51816	AFF2	1	1311
Q5BKT4	AG10A	1	473
Q5I7T1	AG10B	1	473
Q9H9G7	AGO3	1	860
O00468	AGRIN	1	2067
P50052	AGTR2	1	363
Q09666	AHNK	1	5890
P35869	AHR	1	848
Q9NZD4	AHSP	1	102
Q9BRQ8	AIFM2	1	373
Q9Y4K1	AIM1	1	1723
Q96IF1	AJUBA	1	538
P14550	AK1A1	1	325
Q9Y2D5	AKAP2	1	859
Q5JQC9	AKAP4	1	854
Q5T2L2	AKCL1	1	129
Q9P2G1	AKIB1	1	1089
Q12802	AKP13	1	2813
Q9ULX6	AKP8L	1	646
Q8N8R7	AL14E	1	260
P47895	AL1A3	1	512
P30837	AL1B1	1	517
P05091	ALDH2	1	517
Q2TAA5	ALG11	1	492
Q9BVK2	ALG8	1	526
Q13686	ALKB1	1	389
Q9UM73	ALK	1	1620
O95076	ALX3	1	343
Q5JTC6	AMER1	1	1135
Q86SJ2	AMGO2	1	522
Q4VCS5	AMOT	1	1084
P49418	AMPH	1	695
Q6ZTN6	AN13D	1	518
Q9BXX2	AN30B	1	1392
Q9P2R3	ANFY1	1	1169

Q86UW1	OSTA	1	340
Q7RTW8	OTOAN	1	1153
Q9HC10	OTOF	1	1997
Q01804	OTUD4	1	1114
Q8WZ82	OVCA2	1	227
Q7RTY7	OVCH1	1	1134
Q96RQ9	OXLA	1	567
Q15072	OZF	1	292
A8CG34	P121C	1	1229
Q8N7R1	P1L12	1	296
Q5VU65	P210L	1	1888
Q06190	P2R3A	1	1150
P56373	P2RX3	1	397
Q99571	P2RX4	1	388
Q86VZ1	P2RY8	1	359
Q9H244	P2Y12	1	342
P04054	PA21B	1	148
Q9UP65	PA24C	1	541
Q68DD2	PA24F	1	849
Q9UQ80	PA2G4	1	394
P39877	PA2G5	1	138
Q8N7B6	PACRL	1	248
Q9Y2J8	PADI2	1	665
Q99487	PAFA2	1	392
Q9ULR5	PAI2B	1	123
Q9BPZ3	PAIP2	1	127
Q8NC51	PAIRB	1	408
Q9NP74	PALMD	1	551
Q9BZ23	PANK2	1	570
Q96RD6	PANX2	1	677
Q9NVV4	PAPD1	1	582
P55085	PAR2	1	397
O00254	PAR3	1	374
Q96RI0	PAR4	1	385
Q8TEW0	PARD3	1	1356
Q9NWS1	PARI	1	579
Q9Y6F1	PARP3	1	533
Q96RG2	PASK	1	1323
Q02962	PAX2	1	417

Q9UNK9	ANGE1	1	670
O95841	ANGL1	1	491
Q86XS5	ANGL5	1	388
Q01484	ANK2	1	3957
Q12955	ANK3	1	4377
Q8IWZ3	ANKH1	1	2542
Q9P2S6	ANKY1	1	941
Q9NQW6	ANLN	1	1124
P55345	ANM2	1	433
Q9BYT9	ANO3	1	981
Q6IWH7	ANO7	1	933
P20594	ANPRB	1	1047
Q6UB98	ANR12	1	2062
Q8N8A2	ANR44	1	993
Q8NB46	ANR52	1	1076
Q92625	ANS1A	1	1134
Q7Z6G8	ANS1B	1	1248
P28039	AOAH	1	575
P27338	AOFB	1	520
O43747	AP1G1	1	822
O75843	AP1G2	1	785
O14617	AP3D1	1	1153
Q9H0R1	AP5M1	1	490
Q9NUS5	AP5S1	1	200
Q8NCL9	APCDL	1	501
Q9UBZ4	APEX2	1	518
P35414	APJ	1	380
Q8IXF9	AQ12A	1	295
A6NM10	AQ12B	1	295
P29972	AQP1	1	269
Q3SXY8	AR13B	1	428
Q8WWN8	ARAP3	1	1544
P25098	ARBK1	1	689
P35626	ARBK2	1	688
Q8N6H7	ARFG2	1	521
A6NJG6	ARGFX	1	315
Q8TER5	ARH40	1	1519
Q92974	ARHG2	1	986
O94989	ARHGF	1	841

Q9Y5B6	PAXB1	1	917
Q6ZW49	PAXI1	1	1069
Q86U86	PB1	1	1689
Q9BYU1	PBX4	1	374
Q8NF37	PCAT1	1	534
Q7L5N7	PCAT2	1	544
P05166	PCCB	1	539
Q96QU1	PCD15	1	1955
Q9Y5E7	PCDB2	1	798
Q9Y5E6	PCDB3	1	796
Q9Y5E5	PCDB4	1	795
Q9Y5E4	PCDB5	1	795
Q9Y5E3	PCDB6	1	794
Q9Y5E2	PCDB7	1	793
Q9UN66	PCDB8	1	801
Q9Y5F2	PCDBB	1	797
Q9Y5F1	PCDBC	1	795
Q9Y5E9	PCDBE	1	798
Q9Y5E8	PCDBF	1	787
Q9NRJ7	PCDBG	1	776
Q9H158	PCDC1	1	963
O60245	PCDH7	1	1069
Q4G0U5	PCDP1	1	840
Q96NT5	PCFT	1	459
Q5JVF3	PCID2	1	399
P35558	PCKGC	1	622
Q16822	PCKGM	1	640
Q15154	PCM1	1	2024
Q96MG8	PCMD1	1	357
Q9NV79	PCMD2	1	361
Q6UW60	PCSK4	1	755
Q92824	PCSK5	1	1860
Q96RV3	PCX1	1	2341
Q63HM2	PCX4	1	1172
Q8N8D1	PDCD7	1	485
Q9Y233	PDE10	1	779
Q13370	PDE3B	1	1112
P35913	PDE6B	1	854
O76083	PDE9A	1	593

Q6ZSZ5	ARHGI	1	1173
Q9Y4B4	ARIP4	1	1467
Q8NEN0	ARMC2	1	867
Q9P291	ARMX1	1	453
Q7L311	ARMX2	1	632
Q6P1M9	ARMX5	1	558
Q7Z6K5	ARPIN	1	226
Q8N5I2	ARRD1	1	433
Q8TBH0	ARRD2	1	407
P15289	ARSA	1	507
P51689	ARSD	1	593
Q96EG1	ARSG	1	525
O00192	ARVC	1	962
Q9HBK9	AS3MT	1	375
Q13510	ASAH1	1	395
Q495Z4	ASAS1	1	193
Q8WXK1	ASB15	1	588
Q8N3C0	ASCC3	1	2202
Q7RTU5	ASCL5	1	278
Q9Y294	ASF1A	1	204
Q92484	ASM3A	1	453
Q92485	ASM3B	1	455
P17405	ASM	1	629
Q9Y2G3	AT11B	1	1177
Q8NB49	AT11C	1	1132
Q9H7F0	AT133	1	1226
Q4VNC1	AT134	1	1196
Q4VNC0	AT135	1	1218
P24539	AT5F1	1	256
Q14CW9	AT7L3	1	347
P15336	ATF2	1	505
Q2TAZ0	ATG2A	1	1938
Q6UY14	ATL4	1	1074
P54710	ATNG	1	66
Q5TC12	ATPF1	1	328
Q6RW13	ATRAP	1	159
Q8WXE1	ATRIP	1	791
Q9H324	ATS10	1	1103
Q8WXS8	ATS14	1	1223

Q15120	PDK3	1	406
Q96HC4	PDLI5	1	596
Q29RF7	PDS5A	1	1337
Q9NTI5	PDS5B	1	1447
P52945	PDX1	1	283
Q8NEN9	PDZD8	1	1154
Q9H792	PEAK1	1	1746
Q5VY43	PEAR1	1	1037
P36955	PEDF	1	418
P11678	PERE	1	715
P22079	PERL	1	712
O75420	PERQ1	1	1035
Q6Y7W6	PERQ2	1	1299
Q8IYB4	PEX5R	1	626
P17858	PFKAL	1	780
Q9H720	PG2IP	1	699
Q75T13	PGAP1	1	922
Q9NXJ5	PGPI	1	209
P21810	PGS1	1	368
P07585	PGS2	1	359
P53611	PGTB2	1	331
Q8IZ21	PHAR4	1	702
O94880	PHF14	1	888
P15735	PHKG2	1	406
Q9P1Y6	PHRF1	1	1649
Q8N3S3	PHTF2	1	785
O14813	PHX2A	1	284
Q99453	PHX2B	1	314
Q5UE93	PI3R6	1	754
Q15735	PI5PA	1	1006
Q9H5I5	PIEZ2	1	2752
P37287	PIGA	1	484
Q8TEQ8	PIGO	1	1089
Q9Y237	PIN4	1	131
Q9BXM7	PINK1	1	581
Q8TC59	PIWL2	1	973
Q8TDX9	PK1L1	1	2849
Q7Z443	PK1L3	1	1732
Q9P0L9	PK2L1	1	805

Q8TE56	ATS17	1	1095
O95450	ATS2	1	1211
O15072	ATS3	1	1205
Q9UKP5	ATS6	1	1117
Q9UBB4	ATX10	1	475
Q8WWM7	ATX2L	1	1075
O15265	ATX7	1	892
Q13825	AUHM	1	339
Q9H7T9	AUNIP	1	357
O43521	B2L11	1	198
O75752	B3GL1	1	331
Q7Z7M8	B3GN8	1	397
Q67FW5	B3GNL	1	361
O96024	B3GT4	1	378
Q9Y2C3	B3GT5	1	310
Q8NHY0	B4GN2	1	566
Q9UBV7	B4GT7	1	327
P56817	BACE1	1	501
Q9Y5Z0	BACE2	1	518
Q9P281	BAHC1	1	2608
O14514	BAI1	1	1584
O60241	BAI2	1	1585
Q9UQB8	BAIP2	1	552
O94812	BAIP3	1	1187
Q6ZNE5	BAKOR	1	492
Q8WY36	BBX	1	941
Q6ZUJ8	BCAP	1	805
P41182	BCL6	1	706
Q6W2J9	BCOR	1	1755
Q8NFC6	BD1L1	1	3051
A6H8Y1	BDP1	1	2624
O76090	BEST1	1	585
Q8NFU1	BEST2	1	509
Q8N1M1	BEST3	1	668
Q8NFU0	BEST4	1	473
Q9UHR4	BI2L1	1	511
Q6UXY1	BI2L2	1	529
Q5TH69	BIG3	1	2177
O00499	BIN1	1	593

P42338	PK3CB	1	1070
Q9ULU4	PKCB1	1	1186
Q9NTG1	PKDRE	1	2253
Q9HAU0	PKHA5	1	1116
P08F94	PKHD1	1	4074
O94827	PKHG5	1	1062
Q9ULM0	PKHH1	1	1364
Q86WI1	PKHL1	1	4243
Q9Y4G2	PKHM1	1	1056
Q8IWE5	PKHM2	1	1019
Q69YJ1	PKHMP	1	520
Q16512	PKN1	1	942
Q53H76	PLA1A	1	456
Q5JTB6	PLAC9	1	97
Q6DJT9	PLAG1	1	500
Q9NQ66	PLCB1	1	1216
Q00722	PLCB2	1	1185
Q01970	PLCB3	1	1234
Q15147	PLCB4	1	1175
P19174	PLCG1	1	1290
P16885	PLCG2	1	1265
O75038	PLCH2	1	1416
P08567	PLEK	1	350
Q99541	PLIN2	1	437
O60664	PLIN3	1	434
Q96Q06	PLIN4	1	1357
Q00G26	PLIN5	1	463
O00168	PLM	1	92
Q8IY17	PLPL6	1	1366
O60733	PLPL9	1	806
A0PG75	PLS5	1	271
Q8NAT1	PMGT2	1	580
Q8N490	PNKD	1	385
Q9NVS9	PNPO	1	261
Q8TCS8	PNPT1	1	783
Q8WVV4	POF1B	1	589
Q9UBT6	POLK	1	870
Q5K4E3	POLS2	1	855
Q9Y244	POMP	1	141

Q86UB2	BIVM	1	503
Q9NR09	BIRC6	1	4857
P55107	GDF10	1	478
P36894	BMR1A	1	532
Q1RMZ1	BMT2	1	405
Q01954	BNC1	1	994
Q6PGQ7	BORA	1	559
P17213	BPI	1	487
O15178	BRAC	1	435
Q5PSV4	BRM1L	1	323
P32247	BRS3	1	399
Q6RI45	BRWD3	1	1802
Q3C1V8	BSH	1	233
O00481	BT3A1	1	513
P78410	BT3A2	1	334
O00478	BT3A3	1	584
Q9NY30	BTG4	1	223
Q7Z6A9	BTLA	1	289
O60566	BUB1B	1	1050
O43684	BUB3	1	328
Q7L1Q6	BZW1	1	419
P11586	C1TC	1	935
Q6UB35	C1TM	1	978
Q4AC94	C2CD3	1	2353
Q86YS7	C2CD5	1	1000
Q6DHV5	C2D2B	1	322
Q16581	C3AR	1	482
Q6ZMU1	C3P1	1	363
Q6P1W5	CA094	1	598
Q8N9H9	CA127	1	656
Q5T5A4	CA194	1	169
B1AJZ1	CA196	1	125
Q9Y6J0	CABIN	1	2220
Q9NZU7	CABP1	1	370
O75952	CABYR	1	493
O60840	CAC1F	1	1977
Q9P1Z2	CACO1	1	691
Q9Y6N8	CAD10	1	788
P55287	CAD11	1	796

Q15165	PON2	1	354
Q99575	POP1	1	1024
Q96QC0	PP1RA	1	940
Q8TF05	PP4R1	1	950
Q9P1A2	PP4RL	1	415
Q9NPH0	PPA6	1	428
Q5VZY2	PPC1A	1	271
P10619	PPGB	1	480
O43447	PPIH	1	177
Q9H2H8	PPIL3	1	161
Q8WUA2	PPIL4	1	492
Q5T8A7	PPR26	1	1209
Q5R3F8	PPR29	1	820
Q7Z5V6	PPR32	1	425
Q6ZSY5	PPR3F	1	799
Q5VV67	PPRC1	1	1664
Q5THK1	PR14L	1	2151
A6NEV1	PR23A	1	266
Q9H4Q4	PRD12	1	367
Q9GZV8	PRD14	1	571
Q9NQX1	PRDM5	1	630
Q9NQX0	PRDM6	1	595
Q5JRX3	PREP	1	1037
Q9UBK2	PRGC1	1	798
Q86YN6	PRGC2	1	1023
P49642	PRI1	1	420
P78527	PRKDC	1	4128
P51817	PRKX	1	358
O43930	PRKY	1	277
P49683	PRLHR	1	370
O43490	PROM1	1	865
Q8N271	PROM2	1	834
P27918	PROP	1	469
O60508	PRP17	1	579
Q6P2Q9	PRP8	1	2335
B1ATL7	PRR32	1	298
P85299	PRR5	1	388
C9JH25	PRRT4	1	899
Q2VWP7	PRTG	1	1150

P55289	CAD12	1	794
P55290	CAD13	1	713
Q13634	CAD18	1	790
Q9HBT6	CAD20	1	801
Q86UP0	CAD24	1	819
P12830	CADH1	1	882
P22223	CADH3	1	829
P55283	CADH4	1	916
P55285	CADH6	1	790
Q9ULB5	CADH7	1	785
P55286	CADH8	1	799
Q9ULB4	CADH9	1	789
P00915	CAH1	1	261
O75155	CAND2	1	1236
Q9BXL7	CAR11	1	1154
Q9BX69	CARD6	1	1037
Q86X55	CARM1	1	608
Q92851	CASPA	1	521
Q13948	CASP	1	678
P41180	CASR	1	1078
P04040	CATA	1	527
Q8WUQ7	CATIN	1	758
Q96KX2	CAZA3	1	299
Q6UXQ4	CB066	1	117
Q53S99	CB083	1	150
P22681	CBL	1	906
Q8N4T0	CBPA6	1	437
Q9UPW5	CBPC1	1	1226
Q8NEM8	CBPC3	1	1001
Q5JPI3	CC038	1	329
Q96JG6	CC132	1	964
Q8IY82	DRC7	1	874
A2VCL2	CC162	1	907
Q9NV96	CC50A	1	361
Q3MIR4	CC50B	1	351
Q49A88	CCD14	1	953
Q8N5R6	CCD33	1	958
Q494V2	CCD37	1	611
Q6ZN84	CCD81	1	652

Q9BQI7	PSD2	1	771
Q9NYI0	PSD3	1	1048
Q8NDX1	PSD4	1	1056
Q9Y248	PSF2	1	185
Q9UQ74	PSG8	1	426
Q16401	PSMD5	1	504
P26599	PTBP1	1	531
O95758	PTBP3	1	552
Q9Y6C5	PTC2	1	1203
O14684	PTGES	1	152
Q3KNS1	PTHD3	1	767
Q4JDL3	PTN20	1	420
Q9Y2R2	PTN22	1	807
P54829	PTN5	1	565
P35236	PTN7	1	360
P43378	PTN9	1	593
Q15257	PTPA	1	358
A2A3K4	PTPC1	1	754
P10586	PTPRF	1	1907
P23470	PTPRG	1	1445
Q9HD43	PTPRH	1	1115
Q9UMZ3	PTPRQ	1	2332
O14522	PTPRT	1	1441
P23471	PTPRZ	1	2315
P48651	PTSS1	1	473
Q14671	PUM1	1	1186
P22102	PUR2	1	1010
Q13610	PWP1	1	501
Q15269	PWP2	1	919
Q92626	PXDN	1	1479
Q7Z7A4	PXK	1	578
Q9Y6I8	PXMP4	1	212
Q9Y3Y4	PYGO1	1	419
Q9BRQ0	PYGO2	1	406
P27708	PYR1	1	2225
Q9NXS2	QPCTL	1	382
Q2KHR3	QSER1	1	1735
Q9Y2K5	R3HD2	1	976
Q9ULC3	RAB23	1	237

P78396	CCNA1	1	465
P32248	CCR7	1	378
O75794	CD123	1	336
P08571	CD14	1	375
O95400	CD2B2	1	341
P16671	CD36	1	472
O43866	CD5L	1	347
P06127	CD5	1	495
P48960	CD97	1	835
P30260	CDC27	1	824
O75419	CDC45	1	566
Q9BYE9	CDHR2	1	1310
O94921	CDK14	1	469
Q9BWU1	CDK19	1	502
Q6NVV7	CDPF1	1	123
Q92903	CDS1	1	461
O95674	CDS2	1	445
Q49AR2	CE022	1	442
Q9H799	CE042	1	3197
Q8N8E3	CE112	1	955
Q03701	CEBPZ	1	1054
Q9HC77	CENPJ	1	1338
Q8TCT0	CERK1	1	537
Q9HA82	CERS4	1	394
Q6UXA7	CF015	1	325
Q9H6K1	CF106	1	298
Q8NEG2	CG057	1	295
A5D8W1	CFA69	1	941
A4D263	CG072	1	438
Q99674	CGRE1	1	301
Q99675	CGRF1	1	332
Q8N9H6	CH031	1	132
Q15782	CH3L2	1	390
Q6NUI6	CHADL	1	762
Q86WJ1	CHD1L	1	897
O14646	CHD1	1	1710
Q8TDI0	CHD5	1	1954
Q3L8U1	CHD9	1	2897
Q8IWX8	CHERP	1	916

Q15276	RABE1	1	862
Q92878	RAD50	1	1312
P04049	RAF1	1	648
P15918	RAG1	1	1043
Q7Z5J4	RAI1	1	1906
Q5U651	RAIN	1	963
C9J798	RAS4B	1	803
P20936	RASA1	1	1047
Q14644	RASA3	1	834
O43374	RASL2	1	803
O75884	RBBP9	1	186
Q9H2M9	RBGPR	1	1393
Q5T481	RBM20	1	1227
Q96EV2	RBM33	1	1170
P78332	RBM6	1	1123
P53805	RCAN1	1	252
Q7Z4M0	RE114	1	266
O95072	REC8	1	547
O94762	RECQ5	1	991
Q01201	RELB	1	579
Q04864	REL	1	619
P51606	RENBP	1	427
Q96D71	REPS1	1	796
Q6NUM9	RETST	1	610
Q8N1G1	REXO1	1	1221
Q96IC2	REXON	1	774
P35251	RFC1	1	1148
Q6WKZ4	RFIP1	1	1283
Q2KHR2	RFX7	1	1363
Q6GYQ0	RGPA1	1	2036
P0DJD1	RGPD2	1	1756
P0DJD0	RGPD1	1	1748
Q8NE09	RGS22	1	1264
P49802	RGS7	1	495
A5PLK6	RGSL	1	1076
O94844	RHBT1	1	696
P0C7M4	RHF2B	1	288
Q13017	RHG05	1	1502
Q96QB1	RHG07	1	1528

Q13231	CHIT1	1	466
O00533	NCHL1	1	1208
Q9P2E5	CHPF2	1	772
O43529	CHSTA	1	356
Q9NRB3	CHSTC	1	414
Q9NPF2	CHSTB	1	352
Q9NZ63	CI078	1	289
Q5VXU9	CI084	1	1444
Q9Y375	CIA30	1	327
Q99828	CIB1	1	191
O75838	CIB2	1	187
Q96Q77	CIB3	1	187
A0PJX0	CIB4	1	185
Q96RK0	CIC	1	1608
Q969X6	CIR1A	1	686
Q8IVU9	CJ107	1	208
Q8N5U0	CK042	1	333
Q9H0W9	CK054	1	315
Q9BRQ4	CK070	1	267
Q96SN8	CK5P2	1	1893
Q8IXR9	CL056	1	622
P0C7M8	CLC2L	1	214
A8K7I4	CLCA1	1	914
P09496	CLCA	1	248
P51800	CLCKA	1	687
P51801	CLCKB	1	687
P35523	CLCN1	1	988
P51788	CLCN2	1	898
P51790	CLCN3	1	818
P51793	CLCN4	1	760
P51795	CLCN5	1	746
Q96JQ2	CLMN	1	1002
Q9HAW4	CLSPN	1	1339
Q5EBM0	CMPK2	1	449
Q8N3K9	CMYA5	1	4069
Q9H972	CN093	1	538
Q9BXV9	CN142	1	100
Q15021	CND1	1	1401
P42695	CNDD3	1	1498

Q8N264	RHG24	1	748
Q2M1Z3	RHG31	1	1444
O14559	RHG33	1	1287
Q9NRY4	RHG35	1	1499
Q9BQY4	RHXF2	1	288
Q4ADV7	RIC1	1	1423
Q9NPQ8	RIC8A	1	531
A6NNM3	RIM3B	1	1639
Q9UFD9	RIM3A	1	1639
A6NJZ7	RIM3C	1	1639
O15034	RIMB2	1	1052
O14730	RIOK3	1	519
Q13546	RIPK1	1	671
Q7LG56	RIR2B	1	351
P31350	RIR2	1	389
Q15835	RK	1	563
P61313	RL15	1	204
Q9UNX3	RL26L	1	145
P61254	RL26	1	145
Q9BYD6	RM01	1	325
Q5T653	RM02	1	305
Q6P1L8	RM14	1	145
Q9BYC8	RM32	1	188
O94763	RMP	1	535
Q6ZNA4	RN111	1	994
Q96D59	RN183	1	192
Q9NXI6	RN186	1	227
Q5TA31	RN187	1	235
Q63HN8	RN213	1	5207
Q2M238	RN3P1	1	152
Q969K3	RNF34	1	372
O94941	RNF37	1	541
Q9H0F5	RNF38	1	515
Q68DV7	RNF43	1	783
P19474	RO52	1	475
O75116	ROCK2	1	1388
Q04912	RON	1	1400
P08922	ROS1	1	2347
Q9Y2J0	RP3A	1	694

Q86XI2	CNDG2	1	1143
Q6IBW4	CNDH2	1	605
Q6P9H4	CNKR3	1	555
Q9NRU3	CNNM1	1	951
Q9H8M5	CNNM2	1	875
Q8NE01	CNNM3	1	707
Q6P4Q7	CNNM4	1	775
Q9UKZ1	CNO11	1	510
O95628	CNOT4	1	575
Q12860	CNTN1	1	1018
Q8IWV2	CNTN4	1	1026
O94779	CNTN5	1	1100
Q8N8G6	CO054	1	183
Q2T9L4	CO059	1	293
A8K5M9	CO062	1	175
P01024	CO3	1	1663
P53420	CO4A4	1	1690
Q14031	CO4A6	1	1691
P05997	CO5A2	1	1499
P25940	CO5A3	1	1745
Q9GZY4	COA1	1	146
P12107	COBA1	1	1806
Q99715	COCA1	1	3063
Q8WTW3	COG1	1	980
Q9UP83	COG5	1	839
Q07092	COGA1	1	1604
P39060	COIA1	1	1754
Q96P44	COLA1	1	957
Q8NFW1	COMA1	1	1626
P49747	COMP	1	757
P53621	COPA	1	1224
Q9Y678	COPG1	1	874
Q9UBF2	COPG2	1	871
Q9NZJ6	COQ3	1	369
Q92828	COR2A	1	525
Q9UQ03	COR2B	1	480
P57737	CORO7	1	925
Q2UY09	COSA1	1	1125
Q12887	COX10	1	443

Q2QD12	RPEL1	1	228
Q96AT9	RPE	1	228
Q92565	RPGF5	1	580
P49247	RPIA	1	311
Q9BUL9	RPP25	1	199
Q9NQL2	RRAGD	1	400
Q9UI43	MRM2	1	246
Q9NYV6	RRN3	1	651
Q14684	RRP1B	1	758
P56182	RRP1	1	461
P62266	RS23	1	143
P61247	RS3A	1	264
Q5VWQ0	RSBN1	1	802
P51398	RT29	1	398
Q9NZ71	RTEL1	1	1219
Q92541	RTF1	1	710
A6NKG5	RTL1	1	1358
O75298	RTN2	1	545
Q9NQC3	RTN4	1	1192
Q96C34	RUND1	1	613
Q01196	RUNX1	1	453
Q9UJJ7	RUSD1	1	312
A8MWD9	RUXGL	1	76
P62308	RUXG	1	76
P34925	RYK	1	604
P21817	RYR1	1	5038
Q15413	RYR3	1	4870
Q9Y666	S12A7	1	1083
Q16348	S15A2	1	729
Q8N697	S15A4	1	577
Q6NT16	S18B1	1	456
Q9H228	S1PR5	1	398
Q9H015	S22A4	1	551
O76082	S22A5	1	557
Q9Y694	S22A7	1	548
Q9Y6Y8	S23IP	1	1000
Q8NG04	S2610	1	563
P40879	S26A3	1	764
O43511	S26A4	1	780

Q9Y6N1	COX11	1	276
Q9BSU1	CP070	1	422
Q8WTQ4	CP078	1	265
O43303	CP110	1	1012
Q16678	CP1B1	1	543
Q6UW02	CP20A	1	462
Q07973	CP24A	1	514
Q02318	CP27A	1	531
P20813	CP2B6	1	491
P33261	CP2CJ	1	490
P05181	CP2E1	1	493
P20815	CP3A5	1	502
Q02928	CP4AB	1	519
P78329	CP4F2	1	520
Q08477	CP4F3	1	520
P98187	CP4F8	1	520
Q9HBI6	CP4FB	1	524
Q9HCS2	CP4FC	1	524
Q8N118	CP4X1	1	509
Q86W10	CP4Z1	1	505
Q8N1L4	CP4Z2	1	340
O75881	CP7B1	1	506
Q7Z5Q1	CPEB2	1	589
Q8IZJ3	CPMD8	1	1885
Q99829	CPNE1	1	537
Q96A23	CPNE4	1	557
Q9HCH3	CPNE5	1	593
Q9UBL6	CPNE7	1	633
O95741	CPNE6	1	557
Q86YQ8	CPNE8	1	564
Q8IYJ1	CPNE9	1	553
Q9BRF8	CPPED	1	314
Q9P2I0	CPSF2	1	782
Q16630	CPSF6	1	551
P31327	CPSM	1	1500
P23786	CPT2	1	658
Q9H3G5	CPVL	1	476
Q96SM3	CPXM1	1	734
Q96N68	CR015	1	181

P58743	S26A5	1	744
Q9Y2P4	S27A6	1	619
Q14542	S29A2	1	456
Q6ZUB1	S31E1	1	1445
Q969S0	S35B4	1	331
Q99624	S38A3	1	504
Q8NBI5	S43A3	1	491
Q9UMX9	S45A2	1	530
Q86VL8	S47A2	1	602
P61619	S61A1	1	476
Q9H9S3	S61A2	1	476
P48065	S6A12	1	614
Q9NSD5	S6A13	1	602
Q9UN76	S6A14	1	642
Q8TBB6	S7A14	1	771
O43865	SAHH2	1	530
Q96HN2	SAHH3	1	611
P23526	SAHH	1	432
Q9BXA9	SALL3	1	1300
Q8N6K7	SAMD3	1	520
Q9Y3Z3	SAMH1	1	626
Q9NSI8	SAMN1	1	373
O94885	SASH1	1	1247
O75995	SASH3	1	380
Q96F10	SAT2	1	170
P43007	SATT	1	532
P0C263	SBK2	1	348
A3KN83	SBNO1	1	1393
O95486	SC24A	1	1093
O95487	SC24B	1	1268
O94979	SC31A	1	1220
Q9NQW1	SC31B	1	1179
Q9Y289	SC5A6	1	635
Q9GZV3	SC5A7	1	580
Q9Y345	SC6A5	1	797
P31641	SC6A6	1	620
Q9UPN6	SCAF8	1	1271
Q99590	SCAFB	1	1463
Q9BY12	SCAPE	1	1400

Q70SY1	CR3L2	1	520
A6NIL9	CRAS1	1	109
Q8IUH2	CREG2	1	290
P24387	CRHBP	1	322
Q9NZV1	CRIM1	1	1036
O75462	CRLF1	1	422
Q96RY5	CRML	1	1269
H7BZ55	CROL3	1	2252
Q8N1N5	CRPAK	1	446
P02741	CRP	1	224
P02489	CRYAA	1	173
Q5T4H9	CSC10	1	136
P07333	CSF1R	1	972
Q8WXD9	CSKI1	1	1431
O14936	CSKP	1	926
Q96S65	CSRN1	1	589
Q12996	CSTF3	1	717
O94985	CSTN1	1	981
Q8NHU2	CFA61	1	1237
Q9Y5B0	CTDP1	1	961
Q16619	CTF1	1	201
Q96RT6	CTGE2	1	745
Q8IX94	CTGE4	1	777
O15320	CTGE5	1	804
Q86UF2	CTGE6	1	777
P0CG41	CTGE8	1	777
A4FU28	CTGE9	1	777
A4D2H0	CTGEF	1	777
Q86XM0	CTSRD	1	798
Q8WZ74	CTTB2	1	1663
C9J442	CV046	1	243
Q6UX04	CWC27	1	472
P36382	CXA5	1	358
P13498	CY24A	1	195
P04839	CY24B	1	570
Q15438	CYH1	1	398
Q99418	CYH2	1	400
O43739	CYH3	1	400
Q6ZMK1	CYHR1	1	362

Q8WVM8	SCFD1	1	642
P13521	SCG2	1	617
P35498	SCN1A	1	2009
Q99250	SCN2A	1	2005
Q9NY46	SCN3A	1	2000
P35499	SCN4A	1	1836
Q01118	SCN7A	1	1682
Q9UQD0	SCN8A	1	1980
Q15858	SCN9A	1	1988
Q6R2W3	SCND3	1	1325
P51170	SCNNG	1	649
O75880	SCO1	1	301
Q9BYC2	SCOT2	1	517
Q14160	SCRIB	1	1630
Q6P3W7	SCYL2	1	929
Q9NVU7	SDA1	1	687
Q96C92	SDCG3	1	435
P21912	SDHB	1	280
P57772	SELB	1	596
Q9BVL4	SELO	1	669
P62341	SELT	1	195
Q13214	SEM3B	1	749
Q99985	SEM3C	1	751
Q13275	SEM3F	1	785
Q9NS98	SEM3G	1	782
O95754	SEM4F	1	770
Q13591	SEM5A	1	1074
Q9P283	SEM5B	1	1151
Q7Z6J9	SEN54	1	526
P50454	SERPH	1	418
Q9UPS6	SET1B	1	1966
Q8NE22	SETD9	1	299
Q7Z333	SETX	1	2677
Q86YV5	SG223	1	1402
Q16586	SGCA	1	387
Q92629	SGCD	1	289
Q13326	SGCG	1	291
Q8NE28	STKL1	1	680
Q5FBB7	SGOL1	1	561

Q5M775	CYTSB	1	1068
Q6NUT2	D19L2	1	758
Q6NXN4	D19P1	1	242
Q8N9W5	DAAF3	1	541
Q9Y4D1	DAAM1	1	1078
O75553	DAB1	1	588
Q96NX9	DACH2	1	599
Q96B18	DACT3	1	629
Q9P219	DAPLE	1	2028
Q8TCX1	DC2L1	1	351
A2VCK2	DCD2B	1	349
A8MYV0	DCD2C	1	355
Q9UHG0	DCDC2	1	476
P59894	DCDC1	1	354
Q6ZRR9	DCDC5	1	648
Q8IZD4	DCP1B	1	617
Q5T1A1	DCST2	1	773
Q5TDH0	DDI2	1	399
Q9NUL7	DDX28	1	540
Q86TM3	DDX53	1	631
Q6ZN54	DEFI8	1	512
Q9H6A0	DEN2D	1	471
Q6IQ26	DEN5A	1	1287
Q6ZUT9	DEN5B	1	1274
Q8IWF6	DEN6A	1	608
Q8NEG7	DEN6B	1	585
Q8N2C3	DEPD4	1	294
P15924	DESP	1	2871
P60981	DEST	1	165
O76075	DFFB	1	338
Q96DF8	DGC14	1	476
Q8WYQ5	DGCR8	1	773
Q16760	DGKD	1	1214
P52429	DGKE	1	567
Q86XP1	DGKH	1	1220
Q5KSL6	DGKK	1	1271
P52824	DGKQ	1	942
Q6UX07	DHR13	1	377
Q9BTZ2	DHRS4	1	278

Q96HU1	SGSM3	1	749
Q5HYK7	SH319	1	790
Q15464	SHB	1	509
Q7M4L6	SHF	1	423
Q92835	SHIP1	1	1189
Q9BZQ2	SHP1L	1	725
Q6PI26	SHQ1	1	577
Q9Y274	SIA10	1	331
Q11206	SIA4C	1	333
Q8NDV1	SIA7C	1	305
O15466	SIA8E	1	376
Q9HAT2	SIAE	1	523
Q9NXL6	SIDT1	1	827
P57059	SIK1	1	783
Q9BPZ7	SIN1	1	522
Q96FS4	SIPA1	1	1042
Q8IXJ6	SIR2	1	389
Q9NTG7	SIR3	1	399
Q9P1W8	SIRPG	1	387
O75563	SKAP2	1	359
P12755	SKI	1	728
P48764	SL9A3	1	834
Q9Y2E8	SL9A8	1	581
Q96A28	SLAF9	1	289
Q9P270	SLAI2	1	581
Q68D06	SLN13	1	897
P0C7P3	SLN14	1	912
Q499Z3	SLNL1	1	407
Q9BQ83	SLX1	1	275
Q9NZC9	SMAL1	1	954
Q9UHJ3	SMBT1	1	866
Q5VUG0	SMBT2	1	894
Q14683	SMC1A	1	1233
Q8NDV3	SMC1B	1	1235
Q9UQE7	SMC3	1	1217
Q8IY18	SMC5	1	1101
Q96SB8	SMC6	1	1091
P51532	SMCA4	1	1647
Q8ND04	SMG8	1	991

Q96HY7	DHTK1	1	919
O43143	DHX15	1	795
Q7Z478	DHX29	1	1369
Q7L2E3	DHX30	1	1194
Q14147	DHX34	1	1143
Q9H2U1	DHX36	1	1008
Q96C10	DHX58	1	678
Q9BTC0	DIDO1	1	2240
Q68CQ4	DIEXF	1	756
P59910	DJB13	1	316
O75165	DJC13	1	2243
Q6Y2X3	DJC14	1	702
Q15700	DLG2	1	870
O14490	DLGP1	1	977
Q15398	DLGP5	1	846
O00548	DLL1	1	723
P11532	DMD	1	3685
Q9Y5R5	DMRT2	1	561
Q8IXT2	DMRTD	1	367
Q8TDJ6	DMXL2	1	3036
Q9GZS0	DNAI2	1	605
Q8IYX4	DND1	1	353
O60884	DNJA2	1	412
Q7Z6W7	DNJB7	1	309
Q8NHS0	DNJB8	1	232
O75937	DNJC8	1	253
P49916	DNLI3	1	1009
Q9Y6K1	DNM3A	1	912
Q9UBC3	DNM3B	1	853
Q9UJW3	DNM3L	1	386
P26358	DNMT1	1	1616
Q8IZD9	DOCK3	1	2030
Q8N1I0	DOCK4	1	1966
Q18PE1	DOK7	1	504
Q9UPQ8	DOLK	1	538
Q9NYP3	DONS	1	566
Q9Y3R5	DOP2	1	2298
Q9UKG1	DP13A	1	709
Q8NEU8	DP13B	1	664

Q8N5G0	SMI20	1	168
Q9H4F8	SMOC1	1	434
Q92925	SMRD2	1	531
Q9HCE7	SMUF1	1	757
Q9HAU4	SMUF2	1	748
Q53HV7	SMUG1	1	270
O95721	SNP29	1	258
Q13487	SNPC2	1	334
Q13573	SNW1	1	536
Q9Y5W8	SNX13	1	968
Q9Y5W7	SNX14	1	946
Q9NRS6	SNX15	1	342
P57768	SNX16	1	344
Q9H2Y9	SO5A1	1	848
P18583	SON	1	2426
Q9UPU3	SORC3	1	1222
P57073	SOX8	1	446
P48436	SOX9	1	509
Q9H0E3	SP130	1	1048
Q3ZLR7	SP201	1	823
P0C7V6	SP202	1	817
Q3SY56	SP6	1	376
Q9BVQ7	SPA5L	1	753
A1X283	SPD2B	1	911
Q9NRA0	SPHK2	1	654
O43278	SPIT1	1	529
O95149	SPN1	1	360
Q8TCT8	SPP2A	1	520
Q8NCJ5	SPRY3	1	442
Q7Z572	SPT21	1	469
Q96JI7	SPTCS	1	2443
Q8N5C6	SRBD1	1	995
Q6ZRS2	SRCAP	1	3230
Q9C0H9	SRCN1	1	1055
A1L4H1	SRCRL	1	1573
P61011	SRP54	1	504
P78362	SRPK2	1	688
Q9UQ35	SRRM2	1	2752
P81877	SSBP2	1	361

Q9H2P9	DPH5	1	285
Q14181	DPOA2	1	598
P49005	DPOD2	1	469
Q07864	DPOE1	1	2286
P56282	DPOE2	1	527
P09884	DPOLA	1	1462
Q9NY33	DPP3	1	737
Q5T2R2	DPS1	1	415
Q12882	DPYD	1	1025
Q8TE96	DQX1	1	717
Q6PKH6	DR4L2	1	230
Q8N682	DRAM1	1	238
P21918	DRD5	1	477
A6NNA5	DRGX	1	263
Q9UII6	DS13B	1	198
Q08554	DSC1	1	894
Q02487	DSC2	1	901
Q14574	DSC3	1	896
Q14126	DSG2	1	1118
Q96FN9	DTD2	1	168
Q9NRD9	DUOX1	1	1551
Q9NRD8	DUOX2	1	1548
O77932	DXO	1	396
Q96DT5	DYH11	1	4523
Q9C0G6	DYH6	1	4158
Q96JB1	DYH8	1	4490
Q9NYC9	DYH9	1	4486
Q8NCM8	DYHC2	1	4307
Q7RTS9	DYM	1	669
Q05193	DYN1	1	864
Q9Y463	DYR1B	1	629
O75923	DYSF	1	2080
Q03001	DYST	1	7570
Q9NVP4	DZAN1	1	752
Q86YF9	DZIP1	1	867
Q9NZJ5	E2AK3	1	1116
Q9P2K8	E2AK4	1	1649
O00716	E2F3	1	465
Q96AV8	E2F7	1	911

Q76I76	SSH2	1	1423
Q6IMI4	ST6B1	1	303
Q92783	STAM1	1	540
O75886	STAM2	1	525
Q9P2P6	STAR9	1	4700
Q9Y2K9	STB5L	1	1186
Q687X5	STEA4	1	459
Q8IWL8	STH	1	128
Q15468	STIL	1	1287
P31948	STIP1	1	543
Q8N2I9	STK40	1	435
Q6ZVD7	STOX1	1	989
Q9H6E5	STPAP	1	874
A6NGW2	STRCL	1	1772
Q7RTU9	STRC	1	1775
O60499	STX10	1	249
O43752	STX6	1	255
Q9Y6J8	STYL1	1	313
P53597	SUCA	1	346
Q96I99	SUCB2	1	432
Q9HAC7	SUCHY	1	445
Q8IWU5	SULF2	1	870
O75486	SUPT3	1	399
Q9UGT4	SUSD2	1	822
O60279	SUSD5	1	629
Q8IYB8	SUV3	1	786
Q86Y97	SV422	1	462
Q9HCS7	SYF1	1	855
O15056	SYNJ2	1	1496
Q8IV01	SYT12	1	421
O43581	SYT7	1	403
Q9BW92	SYTM	1	718
Q86TM6	SYVN1	1	617
Q9BVX2	T106C	1	250
Q8N4U5	T11L2	1	519
A2VDJ0	T131L	1	1609
Q14DG7	T132B	1	1078
Q8N3T6	T132C	1	1108
Q6IEE7	T132E	1	984

Q9H329	E41LB	1	900
P43004	EAA2	1	574
P48664	EAA4	1	564
Q9BY08	EBPL	1	206
P40939	ECHA	1	763
Q08426	ECHP	1	723
Q92611	EDEM1	1	657
Q3B7T1	EDRF1	1	1238
Q7L9B9	EEPD1	1	569
P26641	EF1G	1	437
P13639	EF2	1	858
P60507	EFC1	1	584
P18146	EGR1	1	543
P11161	EGR2	1	476
Q8N3D4	EH1L1	1	1523
Q9H4M9	EHD1	1	534
Q9NZN3	EHD3	1	535
Q9H223	EHD4	1	541
P41567	EIF1	1	113
O60739	EIF1B	1	113
O15371	EIF3D	1	548
O00303	EIF3F	1	357
Q15717	ELAV1	1	326
Q12926	ELAV2	1	359
Q14576	ELAV3	1	367
P26378	ELAV4	1	380
P78545	ELF3	1	371
P0C7U0	ELFN1	1	828
P15502	ELN	1	786
Q9H9T3	ELP3	1	547
P50402	EMD	1	254
Q04743	EMX2	1	252
Q04741	EMX1	1	257
A6NNW6	ENO4	1	628
P06733	ENOA	1	434
P13929	ENOB	1	434
P09104	ENOG	1	434
Q13822	ENPP2	1	863
Q9Y6X5	ENPP4	1	453

Q86VY9	T200A	1	491
Q9Y3Q8	T22D4	1	395
Q96DZ7	T4S19	1	209
Q96RJ0	TAAR1	1	339
Q9P1P5	TAAR2	1	351
Q8N5C8	TAB3	1	712
Q8N9U0	TAC2N	1	490
O75478	TAD2A	1	443
Q15573	TAF1A	1	450
Q15572	TAF1C	1	869
Q5VWG9	TAF3	1	929
Q8N103	TAGAP	1	731
Q13885	TBB2A	1	445
Q9BVA1	TBB2B	1	445
P04350	TBB4A	1	444
P68371	TBB4B	1	445
P07437	TBB5	1	444
Q9BUF5	TBB6	1	446
Q3ZCM7	TBB8	1	444
A6NNZ2	TBB8L	1	444
Q9P2M4	TBC14	1	693
Q9NUY8	TBC23	1	699
Q3MII6	TBC25	1	688
Q9Y2I9	TBC30	1	924
Q66K14	TBC9B	1	1250
Q9NVR7	TBCC1	1	557
Q86TI0	TBCD1	1	1168
Q9BYX2	TBD2A	1	928
Q9UPU7	TBD2B	1	963
Q16650	TBR1	1	682
O75333	TBX10	1	385
Q96SF7	TBX15	1	602
O60806	TBX19	1	448
O95935	TBX18	1	607
Q9UL17	TBX21	1	535
Q9Y458	TBX22	1	520
Q9UMR3	TBX20	1	447
O43435	TBX1	1	398
O15119	TBX3	1	743

O75355	ENTP3	1	529
Q9NQZ7	ENTP7	1	604
O95936	EOMES	1	686
Q96L91	EP400	1	3159
Q9H2F5	EPC1	1	836
P21709	EPHA1	1	976
P54764	EPHA4	1	986
P54762	EPHB1	1	984
P29323	EPHB2	1	1055
P54753	EPHB3	1	998
Q7L775	EPMIP	1	607
Q15303	ERBB4	1	1308
Q6P6B1	ERIC5	1	374
P11474	ERR1	1	423
Q9NQ30	ESM1	1	184
Q6ZVH7	ESPNL	1	1005
Q6UWW8	EST3	1	571
Q5XG92	EST4A	1	561
A0FGR9	ESYT3	1	886
P38117	ETFB	1	255
Q6ZN32	ETV3L	1	361
Q9Y603	ETV7	1	341
Q8IYI6	EXOC8	1	725
Q01780	EXOSX	1	885
Q8NEV8	EXPH5	1	1989
O43909	EXTL3	1	919
Q8NFI4	F10A5	1	369
A6NFQ2	TCAF2	1	919
Q86V42	F124A	1	546
Q6P0A1	F180B	1	224
A6NE01	F186A	1	2351
Q9H8M7	F188A	1	445
P81408	F189B	1	668
Q6ZSG2	F196A	1	479
Q8TCP9	F200A	1	573
P0CF97	F200B	1	657
Q6ZU69	F205A	1	1335
Q63HN1	F205B	1	556
P0C875	F228B	1	321

Q9H3H9	TCAL2	1	227
Q969E4	TCAL3	1	200
Q96EI5	TCAL4	1	215
Q5H9L2	TCAL5	1	206
Q6IPX3	TCAL6	1	200
Q7Z6L1	TCPR1	1	1165
Q92526	TCPW	1	530
P40227	TCPZ	1	531
Q8IZJ6	TDH	1	230
B5MCY1	TDR15	1	1934
O60522	TDRD6	1	2096
Q8NDG6	TDRD9	1	1382
Q9NZ01	TECR	1	308
Q96QE5	TEFM	1	360
Q9NT68	TEN2	1	2774
Q9P273	TEN3	1	2699
Q6N022	TEN4	1	2769
Q68CZ2	TENS3	1	1445
Q16473	TENXA	1	311
Q99973	TEP1	1	2627
Q8NA31	TERB1	1	727
Q96S53	TESK2	1	571
Q6N021	TET2	1	2002
O43151	TET3	1	1660
Q12789	TF3C1	1	2109
Q04206	TF65	1	551
Q8WVM0	TFB1M	1	346
P19532	TFE3	1	575
O95379	TFIP8	1	198
O95932	TGM3L	1	706
Q7Z6K1	THAP5	1	395
P24557	THAS	1	533
P05543	THBG	1	415
Q8N1K5	THMS1	1	641
P00734	THRB	1	622
P01266	THYG	1	2768
O95411	TIAF1	1	115
Q13009	TIAM1	1	1591
P35590	TIE1	1	1138

Q6NXP2	F71F2	1	309
Q86YD7	F90A1	1	464
Q658T7	F90A2	1	463
A6NKC0	F90A7	1	464
A8MXJ8	F90A5	1	464
A6NJQ4	F90A8	1	464
A6NDY2	F90AA	1	464
A6NNJ1	F90A9	1	464
P0C7W9	F90AE	1	464
A6NEW6	F90AG	1	464
P0C7W8	F90AD	1	464
A6NE21	F90AI	1	464
A8MX19	F90AC	1	464
P0C7V4	F90AJ	1	464
A8MXZ1	F90AN	1	464
A6NIJ5	F90AK	1	464
P0C7X0	F90AO	1	464
A6NNH2	F90AR	1	459
A8MWA6	F90AM	1	464
P00742	FA10	1	488
Q641Q2	FA21A	1	1341
Q9Y4E1	FA21C	1	1318
Q5SRD0	FA21D	1	308
Q8N5C1	FA26E	1	309
Q86UY5	FA83A	1	434
Q9BQN1	FA83C	1	747
Q9UBU6	FA8A1	1	413
P16930	FAAA	1	419
Q6GMR7	FAAH2	1	532
Q8WVX9	FACR1	1	515
Q13158	FADD	1	208
O60427	FADS1	1	444
Q53R41	FAKD1	1	847
Q8IZU1	FAM9A	1	332
Q8NB91	FANCB	1	859
Q14296	FASTK	1	549
Q14517	FAT1	1	4588
Q9NYQ8	FAT2	1	4349
Q8TDW7	FAT3	1	4589

P35625	TIMP3	1	211
Q9BVW5	TIPIN	1	301
Q07352	TISB	1	338
Q9H0I9	TKTL2	1	626
P29401	TKT	1	623
Q9UKI8	TLK1	1	766
O43897	TLL1	1	1013
Q9BXR5	TLR10	1	811
Q15399	TLR1	1	786
O60602	TLR5	1	858
Q9Y2C9	TLR6	1	796
Q9NR97	TLR8	1	1041
Q6UXF1	TM108	1	575
B3SHH9	TM114	1	223
Q8N3G9	TM130	1	435
Q5U3C3	TM164	1	297
Q9H0V1	TM168	1	697
Q9P2C4	TM181	1	612
Q6ZVM7	TM1L2	1	507
A6NML5	TM212	1	194
A6NGB7	TM221	1	291
A0PJW6	TM223	1	202
C9JQI7	TM232	1	657
A6NFC5	TM235	1	223
Q9NWD8	TM248	1	314
Q8TBM7	TM254	1	123
Q9UK28	TM59L	1	342
Q9NS93	TM7S3	1	570
Q8TDI8	TMC1	1	760
Q8TDI7	TMC2	1	906
Q7Z5M5	TMC3	1	1100
Q7Z404	TMC4	1	712
Q6UXY8	TMC5	1	1006
Q7Z403	TMC6	1	805
Q7Z402	TMC7	1	723
P49755	TMEDA	1	219
Q9Y2B1	TMEM5	1	443
Q6ZUK4	TMM26	1	368
P28289	TMOD1	1	359

Q5TGI0	FAXC	1	409
A6NHQ2	FBLL1	1	333
P23142	FBLN1	1	703
Q12805	FBLN3	1	493
P22087	FBRL	1	321
Q5XX13	FBW10	1	1052
Q6X9E4	FBW12	1	464
Q8IX29	FBX16	1	292
Q9UKT7	FBXL3	1	428
Q96RD9	FCRL5	1	977
Q86WN1	FCSD1	1	690
Q99581	FEV	1	238
O14843	FFAR3	1	346
O95750	FGF19	1	216
P55075	FGF8	1	233
Q2V2M9	FHOD3	1	1422
Q9BXR6	FHR5	1	569
Q92562	FIG4	1	907
P02751	FINC	1	2386
Q14315	FLNC	1	2725
P36888	FLT3	1	993
Q9NZ56	FMN2	1	1722
Q4ZHG4	FNDC1	1	1894
Q8IX07	FOG1	1	1006
P53539	FOSB	1	338
A8MTJ6	FOXI3	1	420
Q08050	FOXM1	1	763
O15353	FOXN1	1	648
Q0VG06	FP100	1	881
O14772	FPGT	1	594
Q5H8C1	FREM1	1	2179
Q5SZK8	FREM2	1	3169
P0C091	FREM3	1	2139
Q5JV73	FRPD3	1	1810
Q9P0K9	FRS1L	1	344
O94915	FRYL	1	3013
Q5TBA9	FRY	1	3013
P23945	FSHR	1	695
Q5CZC0	FSIP2	1	6907

Q9NZR1	TMOD2	1	351
Q9NYL9	TMOD3	1	352
Q6ZT21	TMPPE	1	453
Q8IU80	TMPS6	1	811
Q8IUR5	TMTC1	1	882
Q8NDV7	TNR6A	1	1962
P50616	TOB1	1	345
O60784	TOM1	1	492
Q92547	TOPB1	1	1522
Q96KB5	TOPK	1	322
Q12888	TP53B	1	1972
Q8WVT3	TPC12	1	735
P0DI81	TPC2A	1	140
P0DI82	TPC2B	1	140
Q9UL33	TPC2L	1	140
P17752	TPH1	1	444
Q9Y296	TPPC4	1	219
Q96Q05	TPPC9	1	1148
Q9Y3C4	TPRKB	1	175
Q4KMQ1	TPRN	1	711
O60507	TPST1	1	370
Q309B1	TR16L	1	348
O95361	TRI16	1	564
Q9UPN9	TRI33	1	1127
Q9UPQ4	TRI35	1	493
Q8NG06	TRI58	1	486
O15016	TRI66	1	1216
Q6ZTA4	TRI67	1	783
Q92519	TRIB2	1	343
Q9C037	TRIM4	1	500
Q9BZR9	TRIM8	1	551
Q15643	TRIPB	1	1979
Q7Z4G4	TRM11	1	463
Q7Z2T5	TRM1L	1	733
Q32P41	TRM5	1	509
O75762	TRPA1	1	1119
Q9UBN4	TRPC4	1	977
Q9Y210	TRPC6	1	931
Q9HCF6	TRPM3	1	1732

Q8N475	FSTL5	1	847
P19526	FUT1	1	365
Q9Y231	FUT9	1	359
Q96ME1	FXL18	1	805
Q6PCT2	FXL19	1	694
Q96DB9	FXYD5	1	178
Q9H0Q3	FXYD6	1	95
P58549	FXYD7	1	80
P58550	FXYD8	1	94
Q9Y2I7	FYV1	1	2098
Q13467	FZD5	1	585
Q9H461	FZD8	1	694
O14556	G3PT	1	408
P04406	G3P	1	335
Q96RP7	G3ST4	1	486
P34059	GALNS	1	522
Q14435	GALT3	1	633
Q8TET4	GANC	1	914
Q5JY77	GASP1	1	1395
Q9BWX5	GATA5	1	397
P43694	GATA4	1	442
Q92908	GATA6	1	595
P61952	GBG11	1	73
P50151	GBG10	1	68
Q9UBI6	GBG12	1	72
Q9P2W3	GBG13	1	67
P63211	GBG1	1	74
P59768	GBG2	1	71
P50150	GBG4	1	75
P63215	GBG3	1	75
P63218	GBG5	1	68
O60262	GBG7	1	68
Q9UK08	GBG8	1	70
P48169	GBRA4	1	554
Q96CN9	GCC1	1	775
Q92947	GCDH	1	438
Q9NP62	GCM1	1	436
O75603	GCM2	1	506
Q92616	GCN1L	1	2671

Q96QT4	TRPM7	1	1865
Q9UHF7	TRPS1	1	1281
Q9Y4A5	TRRAP	1	3859
Q8WWH5	TRUB1	1	349
Q8TE23	TS1R2	1	839
Q92574	TSC1	1	1164
P16473	TSHR	1	764
Q96NA8	TSNA1	1	513
Q2NL82	TSR1	1	804
Q9UJK0	TSR3	1	312
Q6SA08	TSSK4	1	328
Q9NQE7	TSSP	1	514
Q86WT1	TT30A	1	665
Q8N4P2	TT30B	1	665
Q6IQ55	TTBK2	1	1244
Q8TAM2	TTC8	1	541
Q6ZVT0	TTL10	1	673
Q9BTX7	TTPAL	1	342
Q9BSA4	TTYH2	1	534
Q9C0H2	TTYH3	1	523
O00295	TULP2	1	520
Q5VYS8	TUT7	1	1495
Q9P2J2	TUTLA	1	1179
O14907	TX1B3	1	124
Q9NUW8	TYDP1	1	608
Q06418	TYRO3	1	890
Q8TBC4	UBA3	1	463
Q9NZ09	UBAP1	1	502
Q15386	UBE3C	1	1083
Q7Z6J8	UBE3D	1	389
P51784	UBP11	1	963
Q9Y4E8	UBP15	1	981
O94966	UBP19	1	1318
Q9UPT9	UBP22	1	525
O75604	UBP2	1	605
Q8NFA0	UBP32	1	1604
Q8NB14	UBP38	1	1042
Q9Y6I4	UBP3	1	520
Q70EL2	UBP45	1	814

Q5T4J0	GCNT6	1	391
Q9BSJ2	GCP2	1	902
Q02153	GCYB1	1	619
Q9NZC3	GDE1	1	331
P35573	GDE	1	1532
O14793	GDF8	1	375
Q8WTR4	GDPD5	1	605
P06396	GELS	1	782
Q8TEQ6	GEMI5	1	1508
Q9UJ14	GGT7	1	662
Q04446	GLGB	1	702
P01215	GLHA	1	116
P08151	GLI1	1	1106
Q92990	GLMN	1	594
Q16775	GLO2	1	308
Q9H4A5	GLP3L	1	285
O94925	GLSK	1	669
Q9UI32	GLSL	1	602
Q86SR1	GLT10	1	603
Q49A17	GLTL6	1	601
Q9NZD2	GLTP	1	209
Q6IB77	GLYAT	1	296
Q969I3	GLYL1	1	302
Q8WU03	GLYL2	1	294
Q5SZD4	GLYL3	1	288
Q9Y5P6	GMPPB	1	360
Q6P2S7	GNN	1	1318
Q9UJJ9	GNPTG	1	305
Q9H2G9	GO45	1	400
Q5T7V8	GORAB	1	394
Q8IZF2	GP116	1	1346
Q86SQ6	GP123	1	560
Q8NGU9	GP150	1	434
Q6NV75	GP153	1	609
Q9UJ42	GP160	1	338
Q14439	GP176	1	515
Q86V85	GP180	1	440
P32249	GP183	1	361
P07359	GP1BA	1	652

Q96K76	UBP47	1	1375
Q13107	UBP4	1	963
P35125	UBP6	1	1406
Q8IWV7	UBR1	1	1749
Q8IWV8	UBR2	1	1755
O95071	UBR5	1	2799
Q8TF42	UBS3B	1	649
P0C7P4	UCRIL	1	283
P47985	UCRI	1	274
Q9HAW8	UD110	1	530
P35504	UD15	1	534
Q9HAW7	UD17	1	530
Q9HAW9	UD18	1	530
O60656	UD19	1	530
Q3SY77	UD3A2	1	523
Q70J99	UN13D	1	1090
Q8IWX7	UN45B	1	931
Q6UXZ4	UNC5D	1	953
Q9H9P5	UNKL	1	680
Q9C0B0	UNK	1	810
Q9UKP6	UR2R	1	389
Q14146	URB2	1	1524
Q15853	USF2	1	346
Q93008	USP9X	1	2570
O00507	USP9Y	1	2555
Q13336	UT1	1	389
Q15849	UT2	1	920
Q5T230	UTF1	1	341
O75691	UTP20	1	2785
O14607	UTY	1	1347
Q08AM6	VAC14	1	782
Q9P0L0	VAPA	1	249
O95292	VAPB	1	243
Q6EMK4	VASN	1	673
Q9UI12	VATH	1	483
P52735	VAV2	1	878
P15498	VAV	1	845
Q8N8G2	VGLL2	1	317
P09327	VILI	1	827

Q8N158	GPC2	1	579
O75487	GPC4	1	556
Q9Y625	GPC6	1	555
P43304	GPDM	1	727
Q86YW7	GPHB5	1	130
P0CG08	GPHRB	1	455
B7ZAQ6	GPHRA	1	455
Q9H9Y4	GPN2	1	310
P49685	GPR15	1	360
Q8NDV2	GPR26	1	337
O75388	GPR32	1	356
O15354	GPR37	1	613
O15529	GPR42	1	346
Q9BZJ8	GPR61	1	451
Q9BZJ7	GPR62	1	368
O95800	GPR75	1	540
Q96P69	GPR78	1	363
Q9NYM4	GPR83	1	423
P60893	GPR85	1	370
P40197	GPV	1	560
P18283	GPX2	1	190
O15544	GR6	1	149
P49863	GRAK	1	264
Q13322	GRB10	1	594
Q14449	GRB14	1	540
Q14451	GRB7	1	532
Q3V6T2	GRDN	1	1871
Q4ZG55	GREB1	1	1949
Q9ULK0	GRID1	1	1009
Q16099	GRIK4	1	956
Q16478	GRIK5	1	980
P30550	GRPR	1	384
Q9NZM4	GSCR1	1	1560
Q9BYG8	GSDMC	1	508
Q14687	GSE1	1	1217
P78417	GSTO1	1	241
Q8IYK4	GT252	1	626
Q9NYZ3	GTSE1	1	720
Q9UBP9	GULP1	1	304

O43314	VIP2	1	1243
P54219	VMAT1	1	525
Q05940	VMAT2	1	514
Q96RL7	VP13A	1	3174
Q7Z7G8	VP13B	1	4022
Q709C8	VP13C	1	3753
Q5THJ4	VP13D	1	4388
Q96AX1	VP33A	1	596
Q9H267	VP33B	1	617
Q9Y4B6	VPRBP	1	1507
Q96QK1	VPS35	1	796
Q86VN1	VPS36	1	386
Q8IV63	VRK3	1	474
Q96IQ7	VSIG2	1	327
Q7Z5K2	WAPL	1	1190
Q2M389	WASH7	1	1173
Q96G27	WBP1	1	269
O75717	WDHD1	1	1129
Q9BZH6	WDR11	1	1224
Q9C0J8	WDR33	1	1336
O15213	WDR46	1	610
Q5VTH9	WDR78	1	848
Q562E7	WDR81	1	1941
Q6UXN9	WDR82	1	313
A4D1P6	WDR91	1	747
P30291	WEE1	1	646
P0C1S8	WEE2	1	567
Q8IUA0	WFDC8	1	241
Q8NEX5	WFDC9	1	89
Q9P202	WHRN	1	907
Q5T9L3	WLS	1	541
Q9BYP7	WNK3	1	1800
Q96J92	WNK4	1	1243
Q96S55	WRIP1	1	665
P19544	WT1	1	449
Q9GZV5	WWTR1	1	400
Q9UPY5	XCT	1	501
P47989	XDH	1	1333
A4UGR9	XIRP2	1	3374

Q5JVS0	HABP4	1	413
O43593	HAIR	1	1189
P54257	HAP1	1	671
O00165	HAX1	1	279
Q96EW2	HBAP1	1	488
Q99714	HCD2	1	261
Q16836	HCDH	1	314
P51610	HCFC1	1	2035
Q9Y5Z7	HCFC2	1	792
Q9H0R4	HDHD2	1	259
Q9H8Q6	HEAS1	1	139
Q86Y56	DAAF5	1	855
Q86WZ0	HEAT4	1	1026
Q9Y5Z4	HEBP2	1	205
Q9NRZ9	HELLS	1	838
Q8TDG4	HELQ	1	1101
Q9BYK8	HELZ2	1	2649
P42694	HELZ	1	1942
P13716	HEM2	1	330
P05981	HEPS	1	417
Q9HCC6	HES4	1	221
Q1W209	ESRG	1	222
Q04756	HGFA	1	655
O14964	HGS	1	777
Q5SR56	HIAL1	1	506
Q96MC6	HIAT1	1	490
Q14526	HIC1	1	733
A8MVS5	HIDE1	1	230
Q16665	HIF1A	1	826
Q9Y2N7	HIF3A	1	669
O00291	HIP1	1	1037
Q86Z02	HIPK1	1	1210
Q9H2X6	HIPK2	1	1198
Q9H422	HIPK3	1	1215
P10072	HKR1	1	659
P01893	HLAH	1	362
Q96RW7	HMCN1	1	5635
Q92619	HMHA1	1	1136
P52272	HNRPM	1	730

O43592	XPOT	1	962
P18887	XRCC1	1	633
P13010	XRCC5	1	732
M0R1G4	YA044	1	241
P46937	YAP1	1	504
Q6UXU1	YC002	1	168
Q6ZUG5	YC006	1	572
A8MPS7	YDJC	1	323
Q9Y548	YIPF1	1	306
Q9BWQ6	YIPF2	1	316
Q6ZSR9	YJ005	1	355
Q8NDZ9	YJ017	1	215
Q6ZUT4	YL014	1	128
A6NCN8	YL021	1	305
P49750	YLPM1	1	1951
Q96TA2	YMEL1	1	773
Q86U90	YRDC	1	279
Q9H6S0	YTDC2	1	1430
Q9BTK2	YX002	1	45
Q6N043	Z280D	1	979
Q96KM6	Z512B	1	892
Q9C0D4	Z518B	1	1074
Q6ZN79	Z705A	1	300
P0CH99	Z705D	1	300
P0CI00	Z705B	1	300
A8MVS1	Z705F	1	300
A8MWA4	Z705E	1	302
A8MUZ8	Z705G	1	300
Q9BTP6	ZBED2	1	218
Q49AG3	ZBED5	1	693
Q8IZ13	ZBED8	1	594
Q5SVQ8	ZBT41	1	909
O15062	ZBTB5	1	677
Q53FD0	ZC21C	1	456
Q7Z2W4	ZCCHV	1	902
Q86VM9	ZCH18	1	953
Q96GR4	ZDH12	1	267
Q8WVZ1	ZDH19	1	309
Q9C0B5	ZDHC5	1	715

Q96IR7	HPDL	1	371
Q969F9	HPS3	1	1004
O14792	HS3S1	1	307
P34932	HSP74	1	840
P04792	HSPB1	1	205
P57058	HUNK	1	714
P01744	HV104	1	147
P31260	HXA10	1	410
Q92826	HXB13	1	284
Q9GZZ0	HXD1	1	328
Q12794	HYAL1	1	435
Q8NFM7	I17RD	1	739
Q7Z5L9	I2BP2	1	587
Q9NZ38	IDAS1	1	188
P22304	IDS	1	550
P35475	IDUA	1	653
Q9Y6M1	IF2B2	1	599
O00425	IF2B3	1	579
P78344	IF4G2	1	907
O43432	IF4G3	1	1585
Q9BYX4	IFIH1	1	1025
P09914	IFIT1	1	478
Q6WRI0	IGS10	1	2623
Q9BYH8	IKBZ	1	718
O15111	IKKA	1	745
Q13422	IKZF1	1	519
Q9UKT9	IKZF3	1	509
Q9H2S9	IKZF4	1	585
Q9H5V7	IKZF5	1	419
Q14005	IL16	1	1332
Q9UHF5	IL17B	1	180
P31785	IL2RG	1	369
P29218	IMPA1	1	277
Q17R60	IMPG1	1	797
Q53TQ3	IN80D	1	878
P48551	INAR2	1	515
P38484	INGR2	1	337
Q96PE3	INP4A	1	977
Q14641	INSL4	1	139

Q9NXF8	ZDHC7	1	308
Q9ULC8	ZDHC8	1	765
O60315	ZEB2	1	1214
Q86XD8	ZFAN4	1	727
Q15911	ZFHX3	1	3703
Q96KR1	ZFR	1	1074
P17010	ZFX	1	805
Q7Z3T8	ZFY16	1	1539
Q68DK2	ZFY26	1	2539
P08048	ZFY	1	801
Q9UKY1	ZHX1	1	873
Q15915	ZIC1	1	447
O60481	ZIC3	1	467
Q9H091	ZMY15	1	742
Q9UBW7	ZMYM2	1	1377
Q8NC26	ZN114	1	417
P52736	ZN133	1	654
O75362	ZN217	1	1048
Q14584	ZN266	1	549
Q9Y2X9	ZN281	1	895
Q8WUU4	ZN296	1	475
A6NFI3	ZN316	1	1004
Q5BKZ1	ZN326	1	582
Q9H4Z2	ZN335	1	1342
Q8N895	ZN366	1	744
Q9H8N7	ZN395	1	513
Q96IQ9	ZN414	1	312
O94892	ZN432	1	652
Q8N8Z8	ZN441	1	693
Q8N0Y2	ZN444	1	327
P59923	ZN445	1	1031
Q9Y4E5	ZN451	1	1061
Q96JG9	ZN469	1	3925
Q8WTR7	ZN473	1	871
Q5JVG2	ZN484	1	852
Q8TB69	ZN519	1	540
Q8TF50	ZN526	1	670
Q8N988	ZN557	1	423
Q8TC21	ZN596	1	504

Q01101	INSM1	1	510
Q96T92	INSM2	1	566
Q6P9B9	INT5	1	1019
Q9ULD6	INTU	1	942
Q92813	IOD2	1	273
Q8NFU5	IPMK	1	416
Q5JU85	IQEC2	1	1478
P48200	IREB2	1	963
Q14653	IRF3	1	427
Q92985	IRF7	1	503
Q9NZN1	IRPL1	1	696
Q6UXK2	ISLR2	1	745
O14498	ISLR	1	428
P56199	ITA1	1	1179
P26006	ITA3	1	1051
P23229	ITA6	1	1130
P05107	ITB2	1	769
P16144	ITB4	1	1822
P18084	ITB5	1	799
Q9H0X4	ITFG3	1	552
Q6UXV1	IZUM2	1	221
P23458	JAK1	1	1154
Q96AA8	JKIP2	1	810
Q96JJ6	JPH4	1	628
Q14667	K0100	1	2235
Q92628	K0232	1	1395
Q5VV43	K0319	1	1072
Q2KHM9	K0753	1	967
Q8IV33	K0825	1	1275
Q8NCT3	K0895	1	520
Q7Z7F0	K0907	1	614
Q6NV74	K121L	1	962
Q9P260	K1468	1	1216
Q9C0D2	CE295	1	2601

Q9ULD9	ZN608	1	1512
Q5T7W0	ZN618	1	954
Q7L945	ZN627	1	461
Q9UEG4	ZN629	1	869
O15015	ZN646	1	1829
Q5HYK9	ZN667	1	610
P17019	ZN708	1	499
Q9Y462	ZN711	1	761
Q9BY31	ZN717	1	904
A8MTY0	ZN724	1	619
Q6NUN9	ZN746	1	644
Q6IQ21	ZN770	1	691
Q8N393	ZN786	1	782
Q5FWF6	ZN789	1	425
Q5JPB2	ZN831	1	1677
P0CJ78	ZN865	1	1059
P17038	ZNF43	1	809
Q9UC06	ZNF70	1	446
P17098	ZNF8	1	575
Q8ND25	ZNRF1	1	227
Q9ULT6	ZNRF3	1	936
Q6NXT4	ZNT6	1	461
P60852	ZP1	1	638
Q05996	ZP2	1	745
Q6X784	ZPBP2	1	338
O75312	ZPR1	1	459
Q5FWF4	ZRAB3	1	1079
Q9UGI0	ZRAN1	1	708
Q6NSZ9	ZSC25	1	544
Q8NBB4	ZSCA1	1	408
Q9H7M6	ZSWM4	1	989
Q9P217	ZSWM5	1	1185
Q9H900	ZWILC	1	591
Q9C0D3	ZY11B	1	744
Q8IYH5	ZZZ3	1	903

Appendix B: Selected candidate proteins for peptide library construction

Protein ID	Protein Name	Count	Motif positions	Sequence length	Motif
Q8WZ42	TITIN	12	DPF (15825-15827)	34350	DPFGPPDAP
Q8WZ42	TITIN	12	GPF (17626-17628)	34350	GPFVETSEA
Q8WZ42	TITIN	12	GPF (18319-18321)	34350	GPFVETPKP
Q8WZ42	TITIN	12	NPF (21383-21385)	34350	NPFGTKVEH
Q8WZ42	TITIN	12	NPF (23659-23661)	34350	NPFVVPDAP
Q8WZ42	TITIN	12	NPF (24741-24743)	34350	NPFVLPGPP
Q8WZ42	TITIN	12	DPF (26905-26907)	34350	DPFTVPSPP
Q8WZ42	TITIN	12	GPF (28076-28078)	34350	GPFSEPSEF
Q8WZ42	TITIN	12	DPF (31353-31355)	34350	DPFDKPSQP
Q8WZ42	TITIN	12	NPF (32372-32374)	34350	NPFLAETNQ
Q8WZ42	TITIN	12	GPF (4785-4787)	34350	GPFEISWFK
Q8WZ42	TITIN	12	NPF (7587-7589)	34350	NPFALECVV
P98082	DAB2	8	NPF (253-255)	770	NPFLTNGIT
P98082	DAB2	8	DPF (293-295)	770	DPFRDDPFT
P98082	DAB2	8	DPF (298-300)	770	DPFTQPDQS
P98082	DAB2	8	NPF (396-398)	770	NPFVGSPPK
P98082	DAB2	8	NPF (592-594)	770	NPFQSNIFP
P98082	DAB2	8	NPF (736-738)	770	NPFFKDSFG
P98082	DAB2	8	DPF (763-765)	770	DPFGNPFA
Q9H1K0	RBNS5	7	GPF (555-557)	784	GPFQLEPSR
Q9H1K0	RBNS5	7	NPF (626-628)	784	NPFDEEDLS
Q9H1K0	RBNS5	7	NPF (662-664)	784	NPFEEEDEE
Q9H1K0	RBNS5	7	NPF (677-679)	784	NPFIQPDSP
Q9H1K0	RBNS5	7	NPF (688-690)	784	NPFSEEDEH
Q9H1K0	RBNS5	7	NPF (709-711)	784	NPFEEPTCI
Q9H1K0	RBNS5	7	NPF (718-720)	784	NPFEMDSDS
O43426	SYNJ1	5	DPF (1323-1325)	1573	DPFEDLSFN
O43426	SYNJ1	5	NPF (1394-1396)	1573	NPFITGLTR
O43426	SYNJ1	5	NPF (1404-1406)	1573	NPFSDRTAA
O43426	SYNJ1	5	NPF (1415-1417)	1573	NPFRAKSEE
O43426	SYNJ1	5	DPF (1555-1557)	1573	DPFTTLASK
O95081	AGFG2	5	DPF (232-234)	481	DPFAAPQMA
O95081	AGFG2	5	NPF (366-368)	481	NPFTAPAAQ
O95081	AGFG2	5	NPF (381-383)	481	NPFQPNGLA
O95081	AGFG2	5	NPF (459-461)	481	NPFMTGPSS
Q8NDI1	EHBP1	5	NPF (268-270)	1231	NPFDDPDAA

Q8NDI1	EHBP1	5	NPF (279-281)	1231	NPFGDPDSE
Q8NDI1	EHBP1	5	NPF (309-311)	1231	NPFKEVQTP
Q8NDI1	EHBP1	5	NPF (321-323)	1231	NPFDEPEAF
Q8NDI1	EHBP1	5	NPF (370-372)	1231	NPFYEPKST
A9Z1Z3	FR1L4	4	DPF (1066-1068)	1794	DPFLAEAGI
A9Z1Z3	FR1L4	4	GPF (1573-1575)	1794	GPFALEEAE
A9Z1Z3	FR1L4	4	DPF (16-18)	1794	DPFQVSRAQ
A9Z1Z3	FR1L4	4	DPF (783-785)	1794	DPFARVLIS
O43424	GRID2	4	DPF (314-316)	1007	DPFAQNMEI
O43424	GRID2	4	NPF (697-699)	1007	NPFERDSMY
O43424	GRID2	4	NPF (74-76)	1007	NPFQAVQEA
O43424	GRID2	4	GPF (963-965)	1007	GPFRHRAPN
O95208	EPN2	4	DPF (488-490)	641	DPFESQPLT
O95208	EPN2	4	NPF (537-539)	641	NPFLAPGAP
O95208	EPN2	4	NPF (552-554)	641	NPFQVNQPQ
P52594	AGFG1	4	NPF (434-436)	562	NPFVAAAGP
P52594	AGFG1	4	NPF (449-451)	562	NPFQTNARG
P52594	AGFG1	4	NPF (540-542)	562	NPFMTGAPT
Q7L804	RFIP2	4	DPF (302-304)	512	DPFTNVTAS
Q7L804	RFIP2	4	NPF (323-325)	512	NPFEESSET
Q7L804	RFIP2	4	NPF (406-408)	512	NPFTAKFRA
Q7L804	RFIP2	4	NPF (440-442)	512	NPFDATAGY
Q8N2Y8	RUSC2	4	NPF (101-103)	1516	NPFLLQEGV
Q8N2Y8	RUSC2	4	NPF (43-45)	1516	NPFCPPELG
Q8N2Y8	RUSC2	4	GPF (787-789)	1516	GPFGPSTDS
Q8N2Y8	RUSC2	4	DPF (963-965)	1516	DPFSLTEKP
Q99698	LYST	4	NPF (2699-2701)	3801	NPFQKEIFT
Q99698	LYST	4	DPF (372-374)	3801	DPFAPRQKK
Q99698	LYST	4	NPF (422-424)	3801	NPFYFSQAM
Q99698	LYST	4	NPF (531-533)	3801	NPFEETADG
Q9H201	EPN3	4	DPF (423-425)	632	DPFAKPPES
Q9H201	EPN3	4	NPF (524-526)	632	NPFLTGLSA
Q9H201	EPN3	4	NPF (537-539)	632	NPFGAGEPG
Q9Y493	ZAN	4	DPF (1191-1193)	2812	DPFFRVTAK
Q9Y493	ZAN	4	GPF (1363-1365)	2812	GPFETCLLH
Q9Y493	ZAN	4	GPF (1750-1752)	2812	GPFSQCHQV
Q9Y493	ZAN	4	GPF (2555-2557)	2812	GPFAACHQT
A0AVI2	FR1L5	3	GPF (1125-1127)	2093	GPFIRVVFL
A0AVI2	FR1L5	3	GPF (1623-1625)	2093	GPFRWRDQM

A0AVI2	FR1L5	3	NPF (206-208)	2093	NPFFNEIFF
O14828	SCAM3	3	NPF (19-21)	347	NPFQDPAVI
O14828	SCAM3	3	NPF (42-44)	347	NPFETREPP
O14828	SCAM3	3	NPF (9-11)	347	NPFAEPSEL
O15126	SCAM1	3	NPF (16-18)	338	NPFKDPSVT
O15126	SCAM1	3	NPF (38-40)	338	NPFSDSRTP
O15126	SCAM1	3	NPF (7-9)	338	NPFADPDLN
O15127	SCAM2	3	NPF (16-18)	329	NPFQDPSVT
O15127	SCAM2	3	NPF (38-40)	329	NPFSETNAA
O15127	SCAM2	3	NPF (7-9)	329	NPFADPVDV
O75061	AUXI	3	DPF (582-584)	913	DPFGAPSKP
O75061	AUXI	3	DPF (608-610)	913	DPFLQPTRS
O75061	AUXI	3	DPF (677-679)	913	DPFADLGTL
O75385	ULK1	3	GPF (419-421)	1050	GPFSSSRCG
O75385	ULK1	3	GPF (668-670)	1050	GPFHGQPLG
O75385	ULK1	3	GPF (687-689)	1050	GPFGRSFST
P25686	DNJB2	3	DPF (111-113)	324	DPFAELFDD
P25686	DNJB2	3	GPF (121-123)	324	GPFSELQNR
P25686	DNJB2	3	GPF (135-137)	324	GPFFTFSSS
P49757	NUMB	3	DPF (343-345)	651	DPFSSAPMT
P49757	NUMB	3	NPF (637-639)	651	NPFSSDLQK
Q13191	CBLB	3	DPF (424-426)	982	DPFDPRDEG
Q13191	CBLB	3	DPF (440-442)	982	DPFGMPMLD
Q13191	CBLB	3	DPF (857-859)	982	DPFVDLASG
Q13217	DNJC3	3	NPF (476-478)	504	NPFHRSWNS
Q13217	DNJC3	3	NPF (489-491)	504	NPFSSGGPF
Q13217	DNJC3	3	GPF (495-497)	504	GPFRFKFHF
Q13492	PICAL	3	DPF (420-422)	652	DPFSATVDA
Q13492	PICAL	3	NPF (437-439)	652	NPFLTKSSG
Q13492	PICAL	3	NPF (639-641)	652	NPFGPVSGA
Q2M2I8	AAK1	3	NPF (696-698)	961	NPFDDDNFS
Q2M2I8	AAK1	3	DPF (777-779)	961	DPFIPLQVP
Q2M2I8	AAK1	3	DPF (812-814)	961	DPFGSTSDA
Q8N3F8	MILK1	3	GPF (232-234)	863	GPFSQPKQQ
Q8N3F8	MILK1	3	NPF (425-427)	863	NPFEEEEED
Q8N3F8	MILK1	3	NPF (633-635)	863	NPFNRKPSP
Q8TEH3	DEN1A	3	NPF (832-834)	1009	NPFVPSMPA
Q8TEH3	DEN1A	3	GPF (853-855)	1009	GPFGAPPAS
Q8TEH3	DEN1A	3	DPF (972-974)	1009	DPFEDLLQK

Q96JQ0	PCD16	3	DPF (2320-2322)	3298	DPFSVGRYG
Q96JQ0	PCD16	3	GPF (303-305)	3298	GPFSIDAHT
Q96JQ0	PCD16	3	GPF (608-610)	3298	GPFGLLSYS
Q9BSW7	SYT17	3	DPF (358-360)	474	DPFVKIQLV
Q9BSW7	SYT17	3	DPF (385-387)	474	DPFYNESFS
Q9BSW7	SYT17	3	GPF (51-53)	474	GPFPAQTPP
Q9H2D6	TARA	3	DPF (1036-1038)	2365	DPFPFFPEP
Q9H2D6	TARA	3	DPF (1083-1085)	2365	DPFPFLPDT
Q9H2D6	TARA	3	NPF (1761-1763)	2365	NPFLLSLGV
Q9NYQ6	CELR1	3	NPF (2038-2040)	3014	NPFAEVTTL
Q9NYQ6	CELR1	3	NPF (2527-2529)	3014	NPFLCTVVA
Q9NYQ6	CELR1	3	GPF (2694-2696)	3014	GPFVLLFHC
Q9UI33	SCNBA	3	GPF (113-115)	1791	GPFNSIRSL
Q9UI33	SCNBA	3	DPF (576-578)	1791	DPFTELAIT
Q9UI33	SCNBA	3	DPF (82-84)	1791	DPFYRNHKT
Q9UKJ3	GPTC8	3	GPF (1450-1452)	1502	GPFTFHPVP
Q9UKJ3	GPTC8	3	GPF (259-261)	1502	GPFTAVQIT
Q9UKJ3	GPTC8	3	GPF (535-537)	1502	GPFFPVLSK
Q9UKN7	MYO15	3	GPF (297-299)	3530	GPFDPGYTY
Q9UKN7	MYO15	3	GPF (804-806)	3530	GPFQPPFLP
Q9UKN7	MYO15	3	NPF (962-964)	3530	NPFLQLLGP
Q9UN67	PCDBA	3	DPF (112-114)	800	DPFQIYRAE
Q9UN67	PCDBA	3	GPF (732-734)	800	GPFPGHLVD
Q9UN67	PCDBA	3	NPF (295-297)	800	NPFSGEIFL
Q9UNF0	PACN2	3	NPF (362-364)	486	NPFEDEDDT
Q9UNF0	PACN2	3	NPF (405-407)	486	NPFSSTDAN
Q9UNF0	PACN2	3	NPF (417-419)	486	NPFDDDATS
Q9Y2H6	FND3A	3	GPF (744-746)	1198	GPFSEKCDI
Q9Y2H6	FND3A	3	GPF (838-840)	1198	GPFSEVVAC
Q9Y2H6	FND3A	3	GPF (937-939)	1198	GPFSHMIKL
Q9Y6I3	EPN1	3	NPF (502-504)	576	NPFLPGGGP
Q9Y6I3	EPN1	3	NPF (518-520)	576	NPFQPAPPA
Q9Y6R0	NUMBL	3	GPF (468-470)	609	GPFDAAPAQ
Q9Y6R0	NUMBL	3	NPF (595-597)	609	NPFSGDLQK
Q9Y6R0	NUMBL	3	DPF (575-577)	609	DPFEAQWAA
A6H8M9	CDHR4	2	GPF (179-181)	788	GPFSINEQG
A6H8M9	CDHR4	2	GPF (613-615)	788	GPFWPEQPR
O14654	IRS4	2	DPF (1049-1051)	1257	DPFSECCMD
O14654	IRS4	2	NPF (813-815)	1257	NPFRSSPLG

O14924	RGS12	2	GPF (1297-1299)	1447	GPFCTPQSP
O14924	RGS12	2	GPF (474-476)	1447	GPFCPDPEG
O43497	CAC1G	2	NPF (329-331)	2377	NPFKGAINF
O43497	CAC1G	2	GPF (798-800)	2377	GPFGYIKNP
O60494	CUBN	2	GPF (677-679)	3623	GPFARIHFH
O60494	CUBN	2	GPF (726-728)	3623	GPFTHTRQC
O60641	AP180	2	DPF (402-404)	907	DPFAPEPTP
O60641	AP180	2	DPF (478-480)	907	DPFAPSEGS
O75140	DEPD5	2	GPF (1422-1424)	1603	GPFALPSYL
O75140	DEPD5	2	NPF (599-601)	1603	NPFAPSRMP
O75179	ANR17	2	GPF (1925-1927)	2603	GPFPVRPLS
O75179	ANR17	2	GPF (2252-2254)	2603	GPFSTLFEN
O75190	DNJB6	2	DPF (108-110)	326	DPFSFDFFE
O75190	DNJB6	2	DPF (117-119)	326	DPFEDFFGN
O75197	LRP5	2	GPF (1420-1422)	1615	GPFPHEYVS
O75197	LRP5	2	GPF (1446-1448)	1615	GPFTGIACG
O75309	CAD16	2	GPF (278-280)	829	GPFEVNAEG
O75309	CAD16	2	GPF (67-69)	829	GPFAMDPDS
O75445	USH2A	2	DPF (4123-4125)	5202	DPFTLYTLT
O75445	USH2A	2	DPF (591-593)	5202	DPFPFEHFR
O75953	DNJB5	2	NPF (106-108)	348	NPFDIFFAS
O75953	DNJB5	2	DPF (136-138)	348	DPFGAFGRF
O75970	MPDZ	2	NPF (1268-1270)	2070	NPFADSLQI
O75970	MPDZ	2	GPF (1809-1811)	2070	GPFHSERRP
O94911	ABCA8	2	DPF (1192-1194)	1581	DPFFRISPR
O94911	ABCA8	2	DPF (608-610)	1581	DPFSRHQVW
O95180	CAC1H	2	DPF (2279-2281)	2353	DPFLDGSHS
O95180	CAC1H	2	NPF (287-289)	2353	NPFICSSRR
O95248	MTMR5	2	DPF (1440-1442)	1867	DPFYRTLEG
O95248	MTMR5	2	NPF (39-41)	1867	NPFPQGIEL
O95886	DLGP3	2	GPF (285-287)	979	GPFCLEGPD
O95886	DLGP3	2	GPF (97-99)	979	GPFDTCEDC
P04629	NTRK1	2	NPF (365-367)	796	NPFGQASAS
P04629	NTRK1	2	NPF (381-383)	796	NPFEFNPED
P07307	ASGR2	2	NPF (229-231)	311	NPFNTWIGL
P07307	ASGR2	2	NPF (37-39)	311	NPFLKGPPP
P19022	CADH2	2	GPF (174-176)	906	GPFPQELVR
P19022	CADH2	2	GPF (635-637)	906	GPFAFDLPL
P25685	DNJB1	2	NPF (110-112)	340	NPFDTFFGQ

P25685	DNJB1	2	DPF (129-131)	340	DPFSGFPMG
P35916	VGFR3	2	NPF (218-220)	1363	NPFLVHITG
P35916	VGFR3	2	NPF (330-332)	1363	NPFISVEWL
P43005	EAA3	2	NPF (312-314)	524	NPFRFAMGM
P43005	EAA3	2	NPF (483-485)	524	NPFALESTI
P54760	EPHB4	2	GPF (516-518)	987	GPFGQEHHS
P54760	EPHB4	2	DPF (592-594)	987	DPFTYEDPN
P78363	ABCA4	2	NPF (1868-1870)	2273	NPFHWDLIG
P78363	ABCA4	2	DPF (729-731)	2273	DPFILFLFL
P98161	PKD1	2	NPF (125-127)	4303	NPFECDCGL
P98161	PKD1	2	NPF (2832-2834)	4303	NPFPFGYIS
Q13042	CDC16	2	DPF (261-263)	620	DPFHASCLP
Q13042	CDC16	2	DPF (401-403)	620	DPFVMHEVG
Q13639	5HT4R	2	DPF (282-284)	388	DPFIDYTVP
Q13639	5HT4R	2	NPF (308-310)	388	NPFLYAFLN
Q14008	CKAP5	2	NPF (476-478)	2032	NPFLADVDK
Q14008	CKAP5	2	NPF (991-993)	2032	NPFLRQELL
Q14524	SCN5A	2	DPF (716-718)	2016	DPFTDLTIT
Q14524	SCN5A	2	DPF (84-86)	2016	DPFYSTQKT
Q15942	ZYX	2	DPF (162-164)	572	DPFKARVSS
Q15942	ZYX	2	NPF (37-39)	572	NPFRPGDSE
Q16572	VACHT	2	GPF (143-145)	532	GPFIDRMSY
Q16572	VACHT	2	GPF (516-518)	532	GPFDACEDD
Q16653	MOG	2	DPF (146-148)	247	DPFYWVSPG
Q2PPJ7	RGPA2	2	DPF (1331-1333)	1873	DPFLPLANV
Q2PPJ7	RGPA2	2	GPF (1599-1601)	1873	GPFYFCRLL
Q2WGJ9	FR1L6	2	DPF (848-850)	1857	DPFAKVTFL
Q4KWH8	PLCH1	2	NPF (719-721)	1693	NPFSGDPLP
Q4KWH8	PLCH1	2	DPF (760-762)	1693	DPFVEVEII
Q5IJ48	CRUM2	2	GPF (432-434)	1285	GPFCGQNTT
Q5IJ48	CRUM2	2	GPF (761-763)	1285	GPFRGCLQD
Q5JVL4	EFHC1	2	DPF (286-288)	640	DPFPLLMNR
Q5JVL4	EFHC1	2	DPF (348-350)	640	DPFTRRYYK
Q5VIR6	VPS53	2	NPF (383-385)	699	NPFLEDEPT
Q5VIR6	VPS53	2	NPF (415-417)	699	NPFHGIVSK
Q674R7	ATG9B	2	GPF (253-255)	924	GPFHSKVTL
Q674R7	ATG9B	2	GPF (407-409)	924	GPFSLFRGG
Q6P0Q8	MAST2	2	DPF (1545-1547)	1798	DPFPSRDPR
Q6P0Q8	MAST2	2	NPF (569-571)	1798	NPFVVSMFC

Q6PFW1	VIP1	2	NPF (1142-1144)	1433	NPFSPPRTL
Q6PFW1	VIP1	2	NPF (129-131)	1433	NPFLINDLA
Q6PIF6	MYO7B	2	NPF (106-108)	2116	NPFQVLPLY
Q6PIF6	MYO7B	2	GPF (1163-1165)	2116	GPFCAERLR
Q6UVJ0	SAS6	2	NPF (129-131)	657	NPFKHLTHL
Q6UVJ0	SAS6	2	DPF (53-55)	657	DPFFLYNLV
Q6V0I7	FAT4	2	DPF (2672-2674)	4981	DPFISEILE
Q6V0I7	FAT4	2	GPF (3542-3544)	4981	GPFTYYLLS
Q6V1P9	PCD23	2	NPF (1103-1105)	2916	NPFLIHPSF
Q6V1P9	PCD23	2	NPF (1586-1588)	2916	NPFDVFLSP
Q75VX8	GAREL	2	NPF (631-633)	874	NPFSGPAYP
Q75VX8	GAREL	2	DPF (702-704)	874	DPFELGQGS
Q7Z442	PK1L2	2	DPF (1385-1387)	2459	DPFAQYHYL
Q7Z442	PK1L2	2	DPF (574-576)	2459	DPFTTVTLG
Q7Z4H7	HAUS6	2	DPF (531-533)	955	DPFQKEQDH
Q7Z4H7	HAUS6	2	NPF (573-575)	955	NPFLTRNQI
Q7Z7A1	CNTRL	2	DPF (1135-1137)	2325	DPFKRRGYW
Q7Z7A1	CNTRL	2	GPF (2214-2216)	2325	GPFEEKLNF
Q7Z7H3	CATIP	2	GPF (352-354)	387	GPFDPWRPS
Q7Z7H3	CATIP	2	NPF (371-373)	387	NPFRSLEPE
Q8IVF4	DYH10	2	GPF (1454-1456)	4471	GPFLQTVHK
Q8IVF4	DYH10	2	DPF (522-524)	4471	DPFSIKSSQ
Q8IXH8	CAD26	2	DPF (532-534)	852	DPFTFELDN
Q8IXH8	CAD26	2	GPF (69-71)	852	GPFPKLIGE
Q8IZL2	MAML2	2	DPF (338-340)	1156	DPFNIDLGQ
Q8IZL2	MAML2	2	GPF (473-475)	1156	GPFGQEKIP
Q8N6Y1	PCD20	2	GPF (473-475)	951	GPFRLSPYK
Q8N6Y1	PCD20	2	GPF (54-56)	951	GPFSCLGSY
Q8TE73	DYH5	2	GPF (3532-3534)	4624	GPFNQEFRD
Q8TE73	DYH5	2	GPF (4384-4386)	4624	GPFQPMNIF
Q8TEW8	PAR3L	2	GPF (1153-1155)	1205	GPFRQDVPP
Q8TEW8	PAR3L	2	GPF (978-980)	1205	GPFGYPRDG
Q8WUH2	TGFA1	2	DPF (132-134)	860	DPFCVEVCI
Q8WUH2	TGFA1	2	NPF (823-825)	860	NPFCEPVFV
Q8WWF6	DNJB3	2	DPF (108-110)	145	DPFSFDLLG
Q8WWF6	DNJB3	2	DPF (85-87)	145	DPFEYVFSF
Q8WXE9	STON2	2	NPF (313-315)	905	NPFLNETLQ
Q8WXE9	STON2	2	NPF (329-331)	905	NPFSAFFEE
Q8WXG9	GPR98	2	DPF (1237-1239)	6306	DPFGVFILD

Q8WXG9	GPR98	2	GPF (708-710)	6306	GPFNGSVLF
Q92887	MRP2	2	DPF (1396-1398)	1545	DPFNNYSDE
Q92887	MRP2	2	GPF (1526-1528)	1545	GPFYFMAKE
Q969V1	MCHR2	2	NPF (2-4)	340	NPFHASCWN
Q969V1	MCHR2	2	NPF (302-304)	340	NPFLYILLS
Q96D09	GASP2	2	NPF (290-292)	838	NPFSFWVGE
Q96D09	GASP2	2	DPF (610-612)	838	DPFIHEISK
Q96EY1	DNJA3	2	GPF (267-269)	480	GPFVMRSTC
Q96EY1	DNJA3	2	NPF (75-77)	480	NPFICTASF
Q96JX3	SRAC1	2	NPF (115-117)	654	NPFADPFST
Q96JX3	SRAC1	2	DPF (119-121)	654	DPFSTVDIE
Q96M86	DNHD1	2	GPF (3452-3454)	4753	GPFPPLRRQ
Q96M86	DNHD1	2	GPF (958-960)	4753	GPFMDPTQD
Q96NW4	ANR27	2	NPF (11-13)	1050	NPFYLALQK
Q96NW4	ANR27	2	DPF (131-133)	1050	DPFSLKTIE
Q96RP8	KCNA7	2	GPF (184-186)	456	GPFPAPLNG
Q96RP8	KCNA7	2	DPF (207-209)	456	DPFFVVETL
Q99835	SMO	2	NPF (735-737)	787	NPFCPEPSP
Q99835	SMO	2	DPF (746-748)	787	DPFLPSAPA
Q9BVG9	PTSS2	2	GPF (115-117)	487	GPFSRPHPA
Q9BVG9	PTSS2	2	DPF (184-186)	487	DPFHNIWDK
Q9BY11	PACN1	2	NPF (367-369)	444	NPFGGSETN
Q9BY11	PACN1	2	NPF (379-381)	444	NPFEDDSKG
Q9H251	CAD23	2	GPF (1750-1752)	3354	GPFEVTEGQ
Q9H251	CAD23	2	DPF (3134-3136)	3354	DPFCRNLEL
Q9H313	TTYH1	2	NPF (309-311)	450	NPFQQRLTL
Q9H313	TTYH1	2	DPF (433-435)	450	DPFNPQESK
Q9HBG6	IF122	2	DPF (1148-1150)	1241	DPFTAKLSF
Q9HBG6	IF122	2	DPF (964-966)	1241	DPFSVHRPE
Q9HCH5	SYTL2	2	NPF (160-162)	934	NPFNSSKLP
Q9HCH5	SYTL2	2	NPF (548-550)	934	NPFSHPDKL
Q9HCU4	CELR2	2	NPF (1959-1961)	2923	NPFAEVTTN
Q9HCU4	CELR2	2	GPF (2602-2604)	2923	GPFIFLSYV
Q9NQA5	TRPV5	2	GPF (476-478)	729	GPFTIMIQK
Q9NQA5	TRPV5	2	GPF (423-425)	729	GPFHVIIIT
Q9NZM1	MYOF	2	DPF (396-398)	2061	DPFVEVSFA
Q9NZM1	MYOF	2	NPF (238-240)	2061	NPFFDELFF
Q9NZN4	EHD2	2	NPF (126-128)	543	NPFGNTFLN
Q9NZN4	EHD2	2	GPF (420-422)	543	GPFVERGPD

Q9P225	DYH2	2	DPF (2897-2899)	4427	DPFRNWIRQ
Q9P225	DYH2	2	GPF (3322-3324)	4427	GPFLTNYRD
Q9P2D7	DYH1	2	GPF (3227-3229)	4330	GPFTGQYRT
Q9P2D7	DYH1	2	GPF (804-806)	4330	GPFYINTDN
Q9UDY4	DNJB4	2	NPF (106-108)	337	NPFEIFFGR
Q9UDY4	DNJB4	2	DPF (130-132)	337	DPFSAFGFS
Q9UKA4	AKA11	2	NPF (1064-1066)	1901	NPFPHSHTF
Q9UKA4	AKA11	2	DPF (1316-1318)	1901	DPFILSLPP
Q9UMS6	SYNP2	2	DPF (251-253)	1093	DPFLRSSKI
Q9UMS6	SYNP2	2	GPF (826-828)	1093	GPFKGPQAA
Q9Y2H9	MAST1	2	DPF (333-335)	1570	DPFPDVVHL
Q9Y2H9	MAST1	2	NPF (431-433)	1570	NPFVVGMFC
Q9Y4B5	MTCL1	2	GPF (1531-1533)	1905	GPFPTSRAR
Q9Y4B5	MTCL1	2	DPF (1777-1779)	1905	DPFQKGLRA
Q9Y566	SHAN1	2	DPF (2048-2050)	2161	DPFAPVFVP
Q9Y566	SHAN1	2	GPF (952-954)	2161	GPFNPGSGG
Q9Y613	FHOD1	2	DPF (27-29)	1164	DPFACANFP
Q9Y613	FHOD1	2	GPF (596-598)	1164	GPFPPPPPL
Q9Y6V0	PCLO	2	NPF (174-176)	5065	NPFDLISDS
Q9Y6V0	PCLO	2	DPF (4600-4602)	5065	DPFVKVYLL
O60884	DNJA2	1	NPF (322-324)	412	NPFEKGDLY
O95721	SNP29	1	NPF (9-11)	258	NPFDDDGED
Q9UGI6	KCNN3	1	NPF (173-175)	736	NPFTEIAMS

Appendix C: List of synthesized peptides

Peptide Sequence	Molecular Weight	Purity (%)
GPFQLEPSR	1030.16	99.07
NPFDEEDLS	1065.07	99.32
NPFEEEDEE	1137.09	99.52
NPFIQPDSP	1014.11	97.33
NPFSEEDEH	1103.08	97.77
NPFEEPTCI	1049.17	96.75
NPFEMDSDS	1041.07	98.89
DPFTNVTAS	951.01	97.55
NPFEESSET	1039.03	95.69
NPFTAKFRA	1051.22	96.18
NPFDATAGY	955	97.74
GPFSQPKQQ	1016.13	95.39
NPFEEEEED	1137.09	97.86
NPFNRKPSP	1056.2	95.52
NPFEDEDDT	1081.02	98.08
NPFSSTDAN	951.95	95.56
NPFDDDATS	980.95	98.74
NPFGGSETN	921.93	97.92
NPFEDDSKG	1008.02	95.09
NPFDDDGED	1022.94	97.77
DPFGPPDAP	911.97	99.55
GPFVETSEA	935.99	98.85
GPFVETPKP	971.13	99.64
NPFGTKVEH	1028.14	99.11
NPFVVPDAP	955.09	99.48
NPFVLPGPP	937.12	98.89
DPFTVPSPP	956.07	99.26
GPFSEPSEF	996.05	99.77
DPFDKPSQP	1030.11	98.72
NPFLAETNQ	1033.11	98.54
GPFEISWFK	1110.29	96.75
NPFALECVV	991.17	96.47
NPFLTNGIT	976.11	99.96
DPFRDDPFT	1109.17	97.59
DPFTQPDQS	1034.06	97.64
NPFVGSPPK	942.09	99.57

Peptide Sequence	Molecular Weight	Purity (%)
GPFDTCEDC	986.04	97.48
DPFPDVVHL	1038.18	99.19
NPFVVGMFC	1013.25	95.38
DPFTFELDN	1097.16	96.82
GPFPKLIGE	957.15	97.55
GPFRLSPYK	1064.26	98.58
GPFSCLGSY	930.05	97.52
GPFEVTEGQ	963.02	96.37
DPFCRNLEL	1106.27	97.22
NPFGQASAS	877.92	96.96
NPFEFNPED	1108.14	99.42
NPFGNTFLN	1023.12	99.411
GPFVERGPD	973.06	98.84
GPFGQEHHS	995.03	99.53
DPFTYEDPN	1097.11	96.84
DPFSECCMD	1046.15	96.22
NPFRSSPLG	974.09	98.09
DPFFRISPR	1134.31	96.78
DPFSRHQVW	1171.29	99.83
GPFEVNAEG	918.97	97.49
GPFAMDPDS	936.02	95.92
DPFGVFILD	1022.18	95.7
GPFNGSVLF	937.07	97.66
NPFHASCWN	1075.17	96.4
NPFLYILLS	1079.31	98.67
NPFAEVTTN	992.06	96
GPFIFLSYV	1042.25	96.77
DPFIDYTVP	1066.19	98.07
NPFLYAFLN	1098.28	98.13
NPFADSLQI	1004.12	97.6
GPFHSERRP	1082.02	97.87
GPFPQELVR	1042.21	96.58
GPFAFDLPL	976.15	95.62
NPFLVHITG	997.17	96.45
NPFISVEWL	1104.28	98.22
NPFFDELFF	1175.32	96.63

NPFQSNIFP	1063.19	95.21	DPFTLYTLT	1070.22	97.63
NPFFKDSFG	1058.17	97.28	DPFPFEHFR	1191.32	98.54
DPFGNPFA	863.93	99.71	DPFAPVFVP	988.16	99.17
DPFEDLSFN	1083.13	98.85	GPFNPGSGG	788.82	99.26
NPFITGLTR	1018.19	96.79	DPFCVEVCI	1024.22	96.41
NPFSDRTAA	978.04	99.66	NPFCEPVFV	1051.23	99.48
NPFRAKSEE	1077.17	99.24	NPFLNETLQ	1075.2	99.39
DPFTTLASK	979.11	99.76	NPFSAFFEE	1087.16	96.9
NPFDDPDAA	960.96	97.64	NPFSGDPLP	943.03	98.94
NPFGDPDSE	976.96	99.11	DPFVEVEII	1060.22	98.04
NPFKEVQTP	1059.2	96.62	NPFDTFFGQ	1072.15	98.58
NPFDEPEAF	1065.11	96.8	DPFSGFPMG	954.08	99.56
NPFYEPKST	1082.19	99.3	DPFLPLANV	985.16	97.32
DPFAAPQMA	947.09	95.02	GPFYFCRLL	1115.36	99.68
NPFTAPAAQ	916.01	99.63	GPFPVRPLS	969.16	99.71
NPFQPNGLA	957.06	96.49	GPFSTLFEN	1011.11	98.94
NPFMTGPSS	937.05	98.02	DPFPSRDPR	1086.18	99.29
DPFAQNMEI	1064.19	99.77	NPFVVSMFC	1043.27	95.81
NPFERDSMY	1158.26	99.73	GPFLQTVHK	1026.21	98.08
NPFQAVQEA	1003.19	97.61	DPFSIKSSQ	1008.1	99.09
GPFRHRAPN	1051.18	97.19	DPFRNWIRQ	1231.39	97.74
DPFFRVTAK	1080.26	99.18	GPFLTNYRD	1082.19	97.73
GPFETCLLH	1016.18	97.69	GPFTGQYRT	1026.13	96.17
GPFSQCHQV	1002.12	98.58	GPFYINTDN	1040.11	96.52
GPFAACHQT	931.04	99.09	GPFNQEFRD	1109.17	95.93
DPFESQPLT	1033.11	97.93	GPFQPMNIF	1050.25	98.57
NPFLAPGAP	883.02	96.94	DPFKRRGYW	1224.4	95.04
NPFQVNQPQ	1071.17	98.3	GPFEEKLNF	1080.22	99.9
DPFAKPPES	987.09	96.55	NPFLADVDK	1018.14	95.95
NPFLTGLSA	919.05	98.25	NPFLRQELL	1129.33	99.34
NPFGAGEPG	844.89	96.15	DPFHASCLP	986.11	97.43
NPFQKEIFT	1123.28	98.3	DPFVMHEVG	1030.18	97.76
DPFAPRQKK	1086.27	98.66	NPFKHLTHL	1106.3	95.44
NPFYFSQAM	1104.26	96.1	DPFFLYNLV	1127.32	96.38
NPFEETADG	978.98	95.98	DPFQKEQDH	1143.19	99.54
NPFLLQEGV	1016.17	97.52	NPFLTRNQI	1102.27	98.04
NPFCPPELG	973.12	97.15	GPFALPSYL	964.14	97.53
GPFGPSTDS	863.89	96.96	NPFAPSRMP	1016.2	95.27
DPFSLTEKP	1033.16	95.5	NPFSPPRTL	1028.19	98.07

DPFLAEAGI	932.05	96.29	NPFLINDLA	1016.17	97.51
GPFALEEAE	962.03	99.3	DPFSFDFFE	1150.22	96.42
DPFQVSRAQ	1047.14	95.23	DPFEDFFGN	1087.12	95.05
DPFARVLIS	1017.2	96.11	NPFEIFFGR	1126.29	95.09
NPFVAAAGP	842.96	99.17	DPFSAFGFS	974.05	97.83
NPFQTNARG	1004.08	97.79	DPFTAKLSF	1025.18	96.03
NPFMTGAPT	935.07	97.29	DPFSVHRPE	1083.18	95.42
GPFIRVVFL	1047.32	98.86	NPFPHSHTF	1083.18	98.94
GPFRWRDQM	1192.27	98.66	DPFILSLPP	998.2	97.09
NPFFNEIFF	1174.33	96.95	DPFACANFP	981.1	96.15
NPFDDDNFS	1070.05	95.6	GPFPPPPPL	918.11	99.9
DPFIPLQVP	1025.22	96.79	DPFKARVSS	1006.14	98.88
DPFGSTSDA	895.89	95.18	NPFRPGDSE	1018.06	99.37
DPFSVGRYG	997.08	97.79	NPFYLALQK	1093.3	99.57
GPFSIDAHT	944.02	98.25	DPFSLKTIE	1049.2	99.38
GPFGLLSYS	940.07	96.56	GPFHSKVTL	985.16	99.53
NPFAEVTTL	991.12	96.18	GPFSLFRGG	937.07	99.75
NPFLCTVVA	963.16	97.27	GPFRQDVPP	1012.14	97.33
GPFVLLFHC	1032.27	97.34	GPFGYPRDG	965.04	99.8
GPFDPGYTY	1016.08	99.24	GPFSRPHPA	965.09	99.08
GPFQPPFLP	999.19	98.8	DPFHNIWDK	1171.29	95.05
NPFLQLLGP	998.2	98.08	GPFARIHFH	1081.25	99.77
NPFLPGGGP	854.97	95.1	GPFTHTRQC	1046.17	99.22
NPFQPAPPA	938.06	99.39	NPFLEDEPT	1061.12	99.59
GPFDAAPAQ	872.94	99.36	NPFHGIVSK	998.16	99.39
NPFSGDLQK	1005.1	99.16	DPFYWVSPG	1067.18	98.71
DPFDPRDEG	1047.05	97.3	GPFCGQNTT	924	95.44
DPFGMPMLD	1022.22	97.84	GPFRGCLQD	992.12	96.51
DPFVDLASG	919.99	98.35	NPFNSSKLP	1003.13	95.83
GPFSSSRCG	896.98	96.35	NPFSHPDKL	1054.18	96.86
GPFHGQPLG	809.02	97.25	GPFPTSRAR	988.2	98.91
GPFGRSFST	955.05	97.98	DPFQKGLRA	1031.19	96.95
NPFVPSMPA	959.14	95.63	GPFPAPLNG	869	98.15
GPFGAPPAS	799.89	96.9	DPFFVVETL	1066.23	97.68
DPFEDLLQK	1104.23	98.46	NPFHWDLIG	1098.24	97.96
NPFHRSWNS	1144.22	97.42	DPFILFLFL	1124.4	95.8
NPFSSGGPF	908.97	97.93	DPFTDLTIT	1022.13	96.68
GPFRFKFHF	1182.4	98.03	DPFYSTQKT	1086.18	97.07
GPFSEKCDI	995.12	95.93	NPFECDCGL	997.11	95.85

GPFSEVVAC	908.04	96.6	NPFPFGYIS	1041.18	97.33
GPFSHMIKL	1029.28	95.85	NPFCPEPSP	987.1	98.34
NPFKDPSVT	1004.12	99.03	DPFLPSAPA	914.03	97.27
NPFSDSRTP	1020.07	99.16	DPFAQYHYL	1153.27	95.57
NPFADPDLN	1002.06	95.49	DPFTTVTLG	950.06	96.67
NPFQDPSVT	1004.07	96.18	DPFAKVTFL	1037.23	97.83
NPFSETNAA	949.98	99.18	NPFLIHPSF	1071.25	96.63
NPFADPVDV	973.06	99.01	NPFDVFLSP	1035.17	96.24
GPFNSIRSL	990.4	99.44	NPFADPFST	995.07	98.34
DPFTELAIT	1006.13	98.1	DPFSTVDIE	1022.09	95.61
DPFYRNHKT	1177.29	99.33	GPFSINEQG	948.01	95.8
DPFVKIQLV	1058.3	98.48	GPFWPEQPR	1113.25	96.51
DPFYNESFS	1105.13	99.04	DPFISEILE	1062.19	98.06
GPFPAQTPP	911.03	98.31	GPFTYYLLS	1060.22	96.94
DPFSATVDA	921.97	99.44	NPFKGAINF	1007.17	95.22
NPFLTKSSG	950.07	99.72	GPFGYIKNP	992.15	95.89
NPFGPVSGA	844.93	98.71	DPFLDGSHS	974	96.09
NPFQDPAVI	1000.13	99.04	NPFICSSRR	1079.25	95.7
NPFETREPP	1086.18	97.76	NPFRFAMGM	1070.31	99.98
NPFAEPSEL	1003.09	98.92	NPFALESTI	991.12	99.39
DPFSSAPMT	952.06	99.53	GPFIDRMSY	1085.26	98.85
NPFSSDLQK	1035.13	99.06	GPFDACEDD	967.96	99.08
DPFPFFPEP	1092.23	99.52	GPFPHEYVS	1032.13	99.17
DPFPFLPDT	1048.17	98.94	GPFTGIACG	821.95	97.53
NPFLLSLGV	959.16	99.76	NPFNTWIGL	1061.22	98.03
DPFGAPSKP	915.02	99.39	NPFLKGPPP	966.16	96.73
DPFLQPTRS	1060.18	98.83	GPFVMRSTC	997.2	99.66
DPFADLGTL	948.05	99.44	NPFICTASF	999.15	98.5
DPFAELFDD	1068.11	95.52	DPFLRSSKI	1062.24	99.46
GPFSELQNR	1047.14	97.07	GPFKGPQAA	872	99.65
GPFFTFSSS	976.06	98.97	GPFCTPQSP	933.05	98.44
GPFTFHPVP	998.16	99.12	GPFCPDPEG	917.99	97.91
GPFTAVQIT	933.08	99.72	GPFDPWRPS	1058.17	99.8
GPFFPVLSK	991.21	98.38	NPFRSLEPE	1088.19	99.54
DPFEAQWAA	1034.1	97.03	DPFYRTLEG	1097.2	97.26
DPFQIYRAE	1138.26	97.48	NPFPQGIEL	1014.16	97.2
GPFPGHLVD	938.06	96.86	DPFNIDLGQ	1018.1	95.27
NPFSGEIFL	1023.16	97.92	GPFGQEKIP	972.12	96.52
DPFVEVSFA	1010.12	98.13	DPFSFDLLG	1010.12	96.62

GPFTIMIQK	1034.06	97.04	DPFEYVFSF	1150.26	95.08
NPFQVLPLY	1090.03	98.35	NPFDIFFAS	1057.18	95.82
GPFCAERLR	1048.23	96.58	DPFGAFGRF	1013.13	97.23
DPFNNYSDE	1100.07	96.89	DPFPLLMNR	1102.33	97.94
GPFYFMAKE	1089.29	96.85	DPFTRRYYK	1245.41	99.53
GPFHVIIIT	996.23	95.88	NPFSFWVGE	1082.19	95.844
NPFDLISDS	1007.07	97.42	DPFIHEISK	1085.23	98.94
DPFVKVYLL	1093.34	98.46	GPFPPLRRQ	1067.27	95.86
DPFAPEPTP	970.06	95.36	GPFMDPTQD	1007.09	98.07
DPFAPSEGS	905.92	98.96	NPFSGPAYP	949.04	97.37
NPFQQRLTL	1116.3	99.29	DPFELGQGS	948.99	95.24
DPFNPQESK	1061.13	99.24	NPFTEIAMS	1009.15	96.86
GPFCLEGPD	934.04	97.84	NPFEKGDLY	1082.19	99.66